STUDY ON RIVERBANK STABILITY UNDER HYDRAULIC AND STATIC LOAD CONDITION USING LIMIT EQUILIBRIUM METHOD AND FINITE ELEMENT METHOD

A THESIS SUBMITTED TO THE

DEPARTMENT OF WATER RESOURCES ENGINEERING

In partial fulfilment of the requirement for the degree of

MASTER OF SCIENCE IN WATER RESOURCES ENGINEERING

BY

MD. SHAHIDUL ISLAM
Student ID: 0417162032(F)

DEPARTMENT OF WATER RESOURCES ENGINEERING

BANGLADESH UNIVERSITY OF ENGINEERING AND TECHNOLOGY

DHAKA 1000, BANGLADESH

The thesis titled **"STUDY ON RIVER BANK STABILITY UNDER HYDRAULIC AND STATIC LOAD CONDITION USING LIMIT EQUILIBRIUM METHOD AND FINITE ELEMENT METHOD"** submitted by **Md. Shahidul Islam**, Roll No.: **0417162032(F)**, Session: **April 2017**, to the Department of Water Resources Engineering, Bangladesh University of Engineering and Technology, has been accepted as satisfactory in partial fulfillment of the requirement for the degree of MASTER OF SCIENCE IN WATER RESOURCES ENGINEERING on **December 30, 2020**.
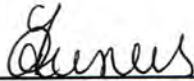
BOARD OF EXAMINERS

Dr. Md. Abdul Matin
Professor
Department of Water Resources Engineering,
BUET, Dhaka-1000

Chairman
(Supervisor)

Dr. Anika Yunus
Professor and Head
Department of Water Resources Engineering,
BUET, Dhaka-1000

Member
(Ex-Officio)

Dr. A T M Hasan Zobeyer
Professor
Department of Water Resources Engineering,
BUET, Dhaka-1000

Member

Dr. G. M. Tarekul Islam
Professor
Institute of Water and Flood Management,
BUET, Dhaka-1000

Member
(External)

DECLARATION

This is to certify that this thesis entitled "**Study on Riverbank Stability under Hydraulic and Static Load Condition using Limit Equilibrium Method and Finite Element Method**" has been done by me under the supervision of Dr. Md. Abdul Matin, Professor, Department of Water Resources Engineering, Bangladesh University of Engineering and Technology, Dhaka. It is hereby declared that this thesis work or any part of it has not been submitted elsewhere for the award of any degree or diploma from any institution.

Dr. Md. Abdul Matin

Countersigned by the Supervisor

Md. Shahidul Islam

Signature of the Candidate

ACKNOWLEDGEMENT

ABSTRACT

The present study deals with the riverbank stability analysis in order to find out the reasons for failures of the selected reach of Jamuna river of Bangladesh. Various scenarios considering the hydraulic and static load condition have been applied in this study. These load conditions are hydraulic shear stress, surcharge load, pore water pressure, toe scouring, river water fluctuations and slope protection load. Limit equilibrium method (LEM) and finite element method (FEM) of slope stability analysis have been applied for stability analysis for various load condition. Two types of bank materials range from very fine clay soil of median size 0.028mm to coarse sand of size 0.167 mm, have been used in this study. The hydraulic load was determined by applying SMS & SRH-2D depth-averaged numerical model using a highly refined mesh. Erosion rate was evaluated from the excess shear stress model, based on critical shear stress, τ_c and erodibility co-efficient, k_d. The stability of the riverbank was analyzed with the limit equilibrium method in the SLOPE/W module and the finite element method in Optum G2. The limit equilibrium method (LEM) used in this study was the Morgenstern-Price technique, while the strength reduction technique was used in FEM. In both cases, Mohr-Coulomb failure criteria were chosen for analysis. A total of seven scenarios of various load conditions have been used to assess the slope stability of the riverbank. Among these, the water level drawdown of water level, bed scouring, pore water pressure etc. and various static loads are incorporated in the model run. Also, the base material of the riverbank consists of clay with mica (30%), silt and sand layers were taken into consideration for a separate scenario. A sensitivity analysis was performed in SLOPE/W to obtain a range of design data that could be used in the design of riverbank protection works. Results from the hydrodynamic model analysis reveal that hydraulic shear stress at the toe of the riverbank was found as 10 to12 Pa compared to that of critical shear stress 6.34 to 8.91 Pa, which clearly indicates the vulnerability of bank stability under the hydraulic action. Therefore, soil erosion at the toe has to be considered as the most critical fluvial riverbank erosion. Erosion rates have been determined from the excess shear stress obtained from the model analysis, which ranges between 20 mm/hr to 160 mm/hr depending on the lower and upper soil layer of the bank. Erodibility co-efficient obtained from the present analysis found to range between 3.1 to 3.64 cm3/N-s of Jamuna riverbank material, which indicates a very erodible soil particle. It is also found that the stability of the riverbank fails when scour depth attained more than seven meters under the given bank

slope. The effect of surcharge load was found to be very significant for the slope failure mechanism. It is found that more than 60 KPa surcharge loads made the riverbank unstable without any scour. With an existing scour depth of five meters, only 45 KPa surcharge loads were needed to make the riverbank fail. The layer with clay and mica (30%) showed more resistant to erosion than the layer with sandy silt and silty sand as obtained from the present analysis. Furthermore, a sensitivity analysis was carried out using slope/w to obtain design soil parameters for stable riverbank against surcharge and slope protection loads. Results obtained from LEM and FEM are compared and found the higher safety factor with LEM than FEM. Finally, a field study was carried out with similar data collected from the Jamuna river near Chauhali, Sirajganj. Results from the field study also compared with the results as obtained from previous scenario analysis and found satisfactory as far as slope stability concerned. It is hoped that the study will be helpful for understanding the design methodology of riverbank training work and bank protection works of rivers of Bangladesh.

Table of Contents

LIST OF FIGURES

LIST OF TABLES

LIST OF ABBREVIATION

ACRONYM	ELABORATION
HFL	Highest flood level
LWL	Low water level
PWD	Public works department
FOS	Factor of safety
BWDB	Bangladesh Water Development Board
SMS	Surface Water Modeling System
SRH-2D	Sedimentation and River Hydraulics
LEM	Limit equilibrium method
FEM	Finite element method
BSTEM	Bank Stability and Toe Erosion Model
CAD	Computer-aided design
WSE	Water surface elevation
ADCP	Acoustic Doppler current profiler
GBM	Ganges-Brahmaputra-Meghna
JNA	Joint Needs Assessment

LIST OF NOTATIONS

τ_c	Critical shear stress (N/m^2)
τ_a	Hydraulic shear stress (N/m^2)
ε	Erosion rate (mm/hr)
k_d	Erodibility co-efficient (Cm^3/N-s)
c	Cohesion (Kn/m^2)
γ	Unit weight (KN/m3)
φ	Angle of internal friction (°)
d_{50}	Median soil diameter (mm)
SC	Silt-clay content (%)
P$_C$	Clay percentage
n	Porosity (%)
Q	Discharge (m^3/s)
v	Velocity (m/s)
σ	Effective stress (KN/m^2)
τ	Frictional shearing resistance (KN/m^2)
k	Hydraulic conductivity (m/s)
γ_{dry}	Dry unit weight (KN/m3)
γ_{sat}	Saturated unit weight (KN/m3)

CHAPTER ONE
INTRODUCTION

1.1   General

Riverbank erosion in Bangladesh refers to an endemic and recurrent natural hazard. It is estimated that presently, about 5 per cent of Bangladesh's total floodplain is affected by erosion. Some researchers have already reported that erosion of riverbanks is taking place in about 94 out of 492 Upazilas of Bangladesh. This major natural disaster causes untold misery every year to thousands of people living along the bank of rivers.

According to Joint Needs Assessment (JNA) identified that, among 28 districts affected by the floods, the most severely affected districts are: Jamalpur, Sirajgonj, Tangail, Kurigram, Gaibandha, Sylhet, Sunamganj, Bogura, Bandarban. In those districts, 85% of the overall displacement occurred equivalent to 261,499 persons, including 57406 school-age children (29407 boys and 28,002 girls). Around the displaced population, 239387 persons are still living in makeshift shelters or on embankments, and some returned as water started to increase in their areas.

It is apprehended that there are mostly two processes behind river bank instability. One is lateral erosion which increases the bed width of the channel and results in steepening of the bank, which reduces its stability. Another is bed lowering which increases bank height and causes bank erosion which applied directly on the river bank. Hydraulic parameters directly affecting riverbank failure such as discharge condition, water level, velocity, shear stress, wave action, seepage and piping, soil parameters such as bank material size, gradation and cohesion inherently affects riverbank erosion.

1.2   Background

The rivers of Bangladesh are composed of alluvial deposits. The banks of rivers are subjected to erosion due to complex soil-water interaction. In early times, a different probabilistic approach is used to determine the stability of the riverbank. Rivers with wide variability in flow, velocity, sediment gradation have some challenges to determine their erosion properly. Enhanced

technologies are developed with the development of the different computerized model to determine erosion and channel change.

1.3 Present state of the problem

Hydraulic parameters are vital for slope stability analysis of riverbank where discharge and velocity of water are comparatively higher. In recent years, tension crack, pore water pressure, bank-toe erosion, seepage, weathering and weakening, fluvial erosion, and mass failure are becoming the main consideration for determining bank retreat. Several models are developed considering these factors. Coupled models with bank erosion and slope stability are used in different studies. Nowadays, the finite element method is widely used for hydraulic modelling. Finite element seepage properties are used for finding out the seepage properties. Most of these models account for the geotechnical properties of the bank material, including soil shear strength (cohesion, angle of internal friction, and unit weight), positive and negative pore water pressure and confining pressure exerted by the flow. Deterministic bank stability and toe erosion model (BSTEM) is used for coupling with a two-dimensional model (SRH-2D) in a recent study. In this study, an attempt will be made3 to carry out riverbank stability analysis under hydraulic and static load condition.

1.4 Objectives of the study

Specific objectives of this study can be set as follows:

    i)   To apply the hydrodynamic model for the generation of hydraulic load along the riverbank of the selected reach of river Jamuna.

    ii)   To analyse the riverbank stability due to various hydraulic load and static load condition.

    iii)   To perform a case study which involves an investigation of riverbank stability of Jamuna river at Chauhali Upazila, Sirajganj.

    iv)   To suggest the riverbank stability parameter for the safe design of riverbank protection from the results as obtained from the study.

1.5   Thesis overview

This thesis is divided into five chapters. Chapter one describes the background, present state and objectives of the study. In chapter two, previous works and general terminology have been discussed related to this study. In chapter three, the methodology of performing this thesis work has been described. Chapter four shows the development of a 2D morphological model using SMS-SRH 2D and a discussion about results. Chapter five shows conclusions drawn from this study and recommendation for further research.

CHAPTER TWO
LITERATURE REVIEW

2.1 General

Riverbank erosion is a natural geomorphic process occurring in all alluvium bed channels. It is an endemic and recurrent mechanism by which a river adjusts its size, shape, slope and other morphological properties. Thus, it conveys sediment and the discharge obtained from the upstream catchment. Most numerical methods do not take into account bank erosion explicitly and therefore have limitations for studying the geomorphic response of river. The purpose of this section is to give a general description of the related theories about bank erosion processes. Some notable works performed by different researchers have also been discussed at the end of this chapter.

2.2 Review of existing literature related to the riverbank erosion process

High rates of riverbank erosion are of great concern because bank erosion causes serious problems, including the loss of fertile land, damage to flood mitigation structures, downstream sedimentation, and the loss of life (Mosselman et al., 1995; Muramoto & Fujita, 1992; Tingsanchali & Chinnarasri, 1997). It is well documented that bank failure contributes a significant amount, up to 80% of sediment, to the total sediment load of rivers ((Bull & Kirkby, 1997; Evans et al., 2006; Sekely et al., 2002; Simon & Darby, 1999). Understanding the mechanism behind riverbank erosion, therefore, is essential in the design of appropriate and cost-effective bank protection. So, a clear understanding of the bank erosion process is necessary for river utilization and management.

The bank erosion, especially composite river banks, is very complex as the banks are associated with many controlling variables. Since these controlling variable are associated with uncertainty in their measurements, therefore, it is difficult to model bank erosion in a large river (Karmaker & Dutta, 2009). Normally, in the alluvial river bed, the lower layer of composite banks is composed of cohesionless materials and the top layer of the bank is composed of fine soil with vegetation cover. Banks of the alluvial river reaches are mostly composed of stratified soil layers, grain sizes of which vary from fine to course one (Dutta & Karmakar, 2015).

Composite banks are composed of alternate layers of cohesive and non-cohesive strata. The nature of the erosion in a riverbank is dependent on soil characteristics. The erosion in cohesionless soil is because of the loss of individual particles. By contrast, in a cohesive soil, the erosion occurs after the removal of aggregates from the soil because they are bound tightly by electrochemical forces (Buffington & Montgomery, 1997; Lawler et al., 1997; Shields, 1936).

Riverbank erosion is a result of complex combinations of several processes. These processes are well studied (Abidin et al., 2017; Darby et al., 2010; Davis & Harden, 2014; Julian & Torres, 2006; Lawler, 1992; Lawler et al., 1999; Lawler, 1993; R. Grove et al., 2013; Semmad & Chalermyanont, 2018; Thorne, 1982; Yu et al., 2019) and are described below.

Subaerial processes are climate-related phenomena that reduce soil strength, inducing direct erosion and making the bank more susceptible to fluvial erosion by desiccation, cracking, slaking, piping, sapping etc.(Thorne, 1982). Such processes occur on the riverbank surface in contact with air, and therefore, exclude processes during periods of inundation. In those settings, these processes can directly erode the bank material (Couper & Maddock, 2001), but more commonly, they act to lower the shear strength of the bank surface (subaerial preparation) such that other bank erosion processes are enhanced (Wynn et al., 2008).

Subaerial processes, which include wetting and drying of the riverbank, are commonly thought of as 'preparatory' rather than erosive processes (Duijsings, 1987; Green et al., 1999; Lawler et al., 1997; THORNE, 1990; Wolman, 1959). Controlled mainly by climatic conditions, subaerial processes are largely independent of flow. They dominate streambank retreat in the upper reaches of river systems, delivering soil directly to the stream channel and making the banks more vulnerable to flow erosion by reducing the packing density of soils and destroying imbrication (Abernethy & Rutherfurd, 1998; Thorne & Tovey, 1981). They weaken the surface of the bank prior to fluvial erosion, thus increasing the efficacy of the latter.

Although subaerial 'weakening and weathering' of the soil can occur in a number of ways, all are associated with moisture conditions within the material (Dietrich & Gallinatti, 1991; Osman & Thorne, 1988; Thorne, 1992) found that the highest rates of bank retreat occur as a result of high flows during prolonged wet period rather than simply the largest storms or floods. The dynamics of soil moisture and soil composition play a key role at weakening and weathering of bank materials when subaerial processes erode riverbank.

Based on past researches, two major components of erosion were found: wind and water (Musa et al., 2010). Water erodes soil and transports soil particles from higher altitudes and deposits them in low lying areas. Water has been identified as a major cause of soil erosion problems, compared to the wind (Singer & Munns, 2006).

Fluvial bank erosion is a very common phenomenon in alluvial rivers, and almost all the rivers in the world is facing a severe threat of bank erosion (Dutta & Karmakar, 2015). The direct removal of sediment by the river is termed fluvial erosion, which is the result of the shear stress of the water exceeding the shear strength of the sediment (Julian & Torres, 2006). This is the lower limit of bank erosion, represents the entrainment of individual soil grains or flocs (Figure 2.1) from the bank face due to the hydrodynamic streamflow (Gaskin et al., 2003; Lawler, 1993).

Riverbank erosion is a cyclic process initiated by the fluvial erosion of the river bed and/or toe, which makes a geotechnically unstable riverbank. This instability causes riverbank failure and deposition of failed materials at the bank toe. Recurrent floods remove that failed material. This erosion cycle is repeated until the channel widens enough to reduce the boundary shear stress to non-cohesive levels (Thorne, 1982). The boundary shear stress, which controls the incipient motion and deposition of sediment, plays a fundamental role in the bank erosion process and is interlinked with fluvial erosion (Blanckaert & Graf, 2001; Kim et al., 2000; Papanicolaou et al., 2007; Yu et al., 2019).
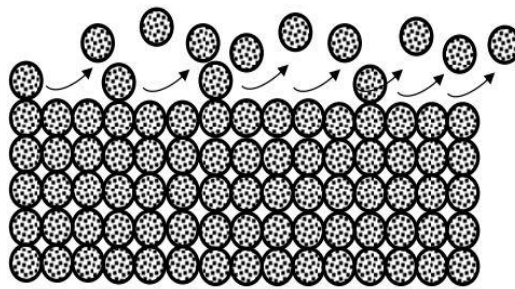
Figure 2.1: Fluvial erosion (Sutarto, 2014)

Mass erosion is a quasi-continuous process (Vermeyen, 1995). It requires a higher magnitude hydrodynamic shear stress than fluvial erosion (Huang et al., 2006). Mass erosion proceeds at a higher rate of erosion. It causes larger retreats of the bank soil due to the higher shear forces,

comparatively to fluvial erosion but smaller retreats for mass failure. It is classified as "intermediate amplitude" erosional process (Gaskin et al., 2003). Retreat length for fluvial erosion is usually in millimetres, whereas mass erosion is in centimetres and for mass failure in meters (Figure 2.2).
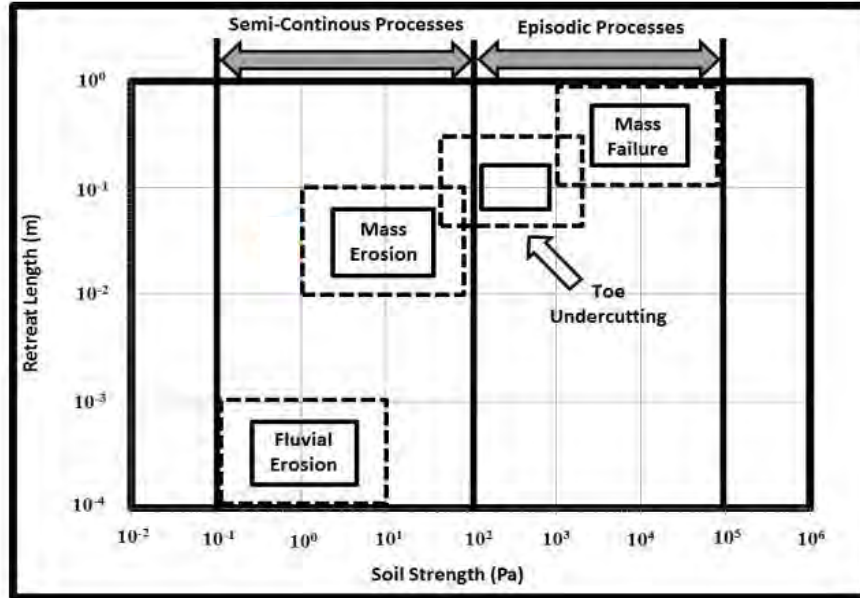
Figure 2.2: A conceptual figure showing different modes of bank erosion (Sutarto, 2014)

Illustration of the sequence of occurrence of fluvial (red circled marked line) and mass failure (blue squared-marked line) as a function of the shear stress magnitude is shown in a conceptual schematic, in Figure 2.3. Clearly, with the increase of shear stress, a regime change is found in the mode of bank erosion from fluvial to mass erosion and exceeds a threshold value for the onset of mass erosion, which is called mass erosional strength, $\tau_{c,m}$. The threshold value for fluvial erosion is indicated by $\tau_{c,f}$.

7
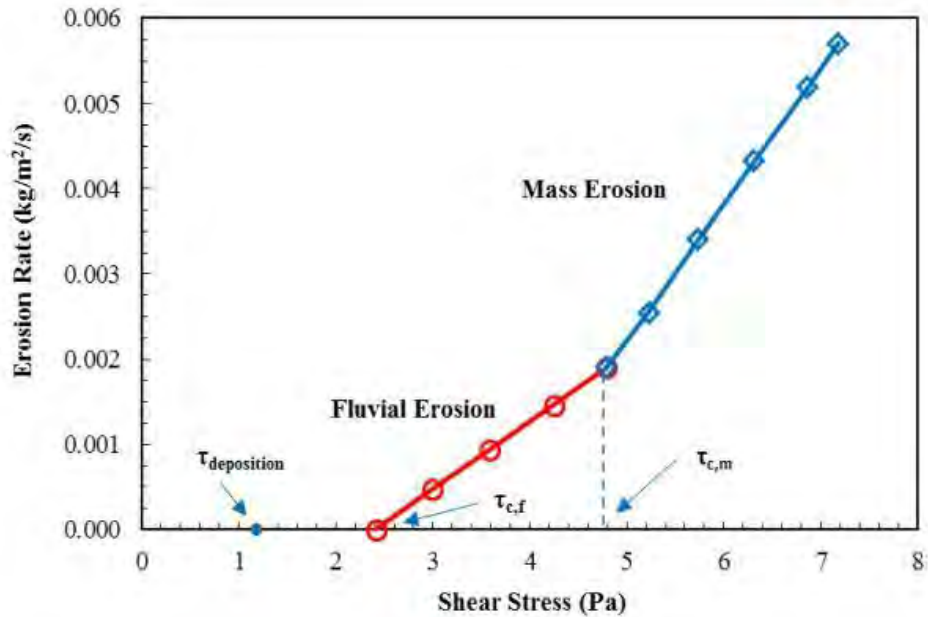
Figure 2.3: An idealistic illustration of fluvial and mass erosion ((Sutarto, 2014)). Fluvial erosion (red circle-marked line) occurs at the lower range of shear stress while mass erosion (blue square-marked line) ensues at the upper range of shear stress.

Due to the higher rate of erosion, the retreat manifests as the detachment of the soil chunks or clods (Figure 2.4) from the bank profile or with the removal of soil layers in the form of 'thin sheets' (Gaskin et al., 2003; Huang et al., 2006; Mazurek et al., 1999; Winterwerp et al., 2012; Winterwerp & Van Kesteren, 2004).
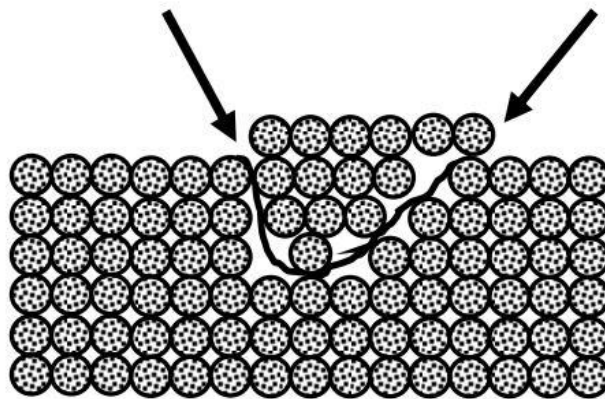
Figure 2.4: Mass erosion ((Sutarto, 2014)

8

The downslope movement of a sediment unit to the internal strength becoming lower than gravitationally induced stresses is referred to as mass movement/failure/wasting. It exceeds the shear strength of the soil by increasing the weight of the overlying material, such as by vegetation growth or increased water content may be quantified using the factor of safety (Parker et al., 2008). Mass failure indicates the upper limit of bank retreat, which is considered a "high amplitude" erosion process regarding its contributions to the instream sediment budget (Darby et al., 2007). Mass failure usually occurs with the collapse or slumping of soil blocks along an embedded plane (Planer failure) due to different but often interrelated mechanisms, such as the development of positive pore water pressure within the bank profile (Millar & Quick, 1998; Pizzuto, 1984; Simon & Collison, 2002; Simon & Rinaldi, 2000; Thorne, 1982); the water level drawdown of water stage (Langendoen, 2010; Langendoen, 2000); the occurrence of high seepage gradient force (Chu-Agor et al., 2009; Fox & Felice, 2014; Midgley et al., 2012). In addition to slumping, there are other forms of mass failure, such as rotational, piping or sapping (Langendoen, 2000; Thorne, 1982), all of which occur at discrete times and more often during later stages of a runoff event (Lawler et al., 1997; Rinaldi et al., 2008).

Relation among fluvial erosion, mass erosion and mass failure: Fluvial erosion and mass failures are often interlinked (Darby et al., 2007; Rinaldi & Darby, 2007) with the basal undercutting of a riverbank lowering FOS so that riverbanks with an excess basal capacity (Thorne & Osman, 1988) are likely to become unstable. Riverbanks with composite structures, such as cohesive sediment overlying a gravel layer, are susceptible to undercutting and can result in overhangs that produce cantilever failure (Langendoen & Simon, 2008; Thorne & Tovey, 1981). These failures usually occur after periods of flood entrainment when the confining pressure of the water channel has been removed on the falling limb ((Luppi et al., 2009) often leaving characteristics blocks resting at the bank toe. Notably, in the middle and lower reaches of drainage basins, bank erosion is likely to be driven by a combination of the hydraulic forces of flow, and mass failure caused by gravity (Figure 2.5).
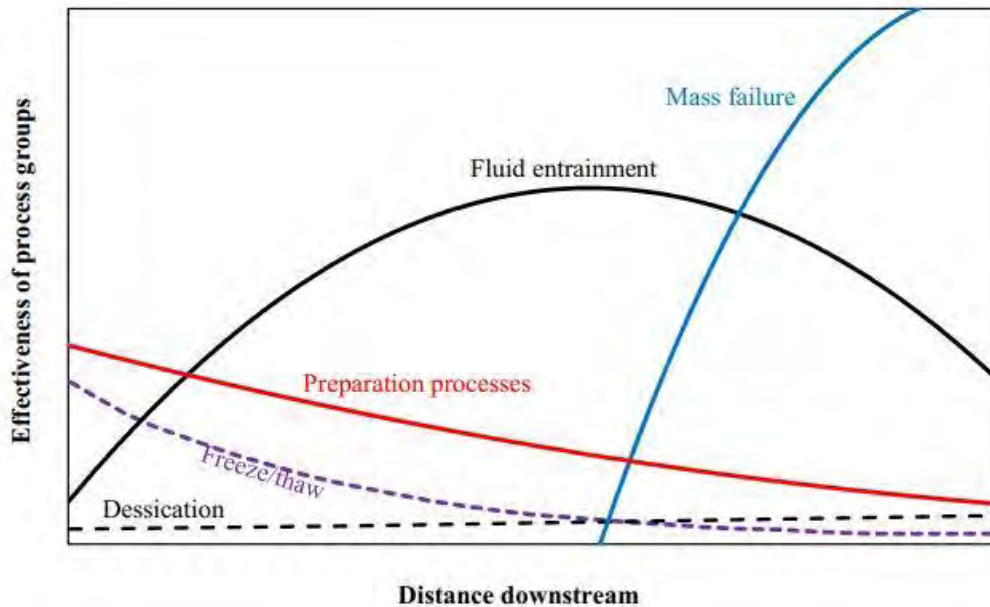
Figure 2.5: Conceptual model of erosional process dominance at the watershed scale (Lawler, 1992; Rinaldi & Darby, 2007)

Generally, mass failure will most likely dominate bank erosion in the lower reaches of a catchment where the critical bank height is more often exceeded (ASCE Task Committee on Hydraul. & Adjust., 1998). On the other hand, fluvial and mass erosion will dominate in the middle reaches of a watershed where the stream power, therefore, the shearing action of flow is highest (Lawler, 1992). This conceptual figure provides some general insight into the dominant bank erosion process and the potential interaction among those different modes at a different location in a catchment. Although this conception is not always valid as many other factors such as soil composition, seepage, groundwater dynamics, and the presence of roots may dictate the dominant mode of erosion at certain locations within a catchment, the figure provides a good representation of the relationship between different processes along a river continuum (Sutarto, 2014).

One or a combination of these processes is responsible for the riverbank erosion. The bank erosion for a homogeneous bank is mainly dominated by a single process. For example, in a cohesive soil, slip circle failure often takes place, whereas in sandy cohesionless, planer failure is the reason behind the erosion process(Dutta & Karmakar, 2015). Mass wasting is often triggered by hydraulically controlled bank erosion, and it is widely accepted that the long-term bank erosion

10

rate is, therefore, controlled by the rate of hydraulic erosion at the toe (Darby et al., 2010; Rinaldi & Darby, 2007; Thorne, 1982).

Riverbank retreat derives from a complex combination of the various process where a key role is played by the interactions of groundwater and surface water. Seepage flow determines an important control on bank instability by two processes: hydraulic gradient forces, causing possible mass failure or liquefaction; and seepage erosion and undercutting, eventually inducing a collapse of the upper bank (Rinaldi & Nardi, 2013). Seepage undercutting has been demonstrated to be an important instability process(Cancienne et al., 2008; Chu-Agor, Wilson, et al., 2008). Though fluvial erosion is the most common bank erosion process in many rivers, sometimes the actual bank failure occurs long after the high flow period, which is not affected by fluvial erosion (Hagerty, 1991b). This indicates that other processes, like seepage induced erosion of riverbanks, are also significant criteria for bank failure (Crosta & Prisco, 1999; Darby & Thorne, 1996; Fox et al., 2010; Rinaldi & Casagli, 1999; Rinaldi & Nardi, 2013).

One process that inmates mass failure of riverbanks is seepage erosion of non-cohesive sediment by groundwater flow, whereby lateral groundwater emerges from the bank and undercuts the bank by removing soil particles (Fox et al., 2006; Fox et al., 2007; Wilson et al., 2007). The most critical factors contributing to seepage erosion are the presence of the exfiltration face, source of water which can create sufficient water head, removal of failed or displaced material from the bank toe and a sufficient hydraulic gradient (Hagerty, 1991a). A composite riverbank often provides an exfiltration face. During the rising phases of the stage hydrograph, the water from the river infiltrates through the bank face and stores as bank storage (Fox et al., 2006). Seepage gradient has a dominating effect on the time taken to develop undercuts that lead to bank collapse (Karmaker & Dutta, 2013). Seepage erosion by liquefaction was evaluated by Dunne (1990) using the balance of forces acting on a volume of soil. Chu-Agor, Fox, et al. (2008) investigated tension or "pop-out" failure due to seepage forces exceeding the soil strength by computing the factor of safety of cohesive slopes. Recent research study on bank erosion model emphasizes on the fluvial erosion and finite element-based seepage analysis due to the variation of pore water pressure (Darby et al., 2007; Duong Thi & Do Minh, 2019; Rinaldi et al., 2004; Rinaldi & Darby, 2007).

2.3   Review of previous works on riverbank stability

Riverbank erosion is a complex process involving subaerial erosion, fluvial erosion, seepage erosion and mass failure. Most of the related researches are performed coupling two or more factors either through in-situ testing (Al-Madhhachi et al., 2011; Casagli et al., 1999; Das et al., 2019; Fox et al., 2007; Karmaker & Dutta, 2011, 2015; Lindow et al., 2009; Semmad & Chalermyanont, 2018) or computer-aided numerical modelling (Chang et al., 2020; Darby et al., 2002; Darby et al., 2007; Darby & Thorne, 1996; Lai et al., 2012; Lai & Wu, 2014; Mohammed-Ali et al., 2020; Nagata et al., 2000) to determine bank erosion rate, as individual acts of these factors are not capable of capturing reason behind bank failure. Subaerial erosion, fluvial erosion and seepage erosion cause basal toe erosion, which eventually lead to overhanging failure in the upper bank in the form of mass wasting. The rate of bank erosion is regulated fluvially, although the upper bank failure mechanism is not directly fluvial in nature. The process has significant implications for river engineering, channel changes and sediment movement through fluvial systems. (Karmaker & Dutta, 2013; Patsinghasanee et al., 2015; Thorne & Tovey, 1981).

Riverbank erosion is the integrated product of different morphological processes. Affuso et al. (2000) modelled unsaturated flow and monitored effects on stream bank failures using finite element seepage analysis with limit equilibrium method and compared measurement with computed values of pore water pressure. Couper and Maddock (2001) showed subaerial erosion as an important mechanism responsible for riverbank erosion. Julian and Torres (2006) examined hydraulic bank erosion by separating estimated bank shear stress into four properties: magnitude, duration, event peak, and variability. Chu-Agor et al. (2009) predicted erosion by subsurface flow or seepage, developing an empirical sediment transport function that was able to predict seepage erosion and undercutting. Veihe et al. (2011) determined the magnitude of bank erosion on a cohesive streambank within a small channelized stream using a photoelectric erosion pin (PEEP) sensor. Midgley et al. (2013) showed seepage erosion to be an essential mechanism of streambank failure combined with fluvial erosion processes. R. Grove et al. (2013) demonstrated the process and volume of riverbank erosion using multi-temporal LiDar and high-resolution imagery. Karmaker and Dutta (2013) developed a functional relationship between seepage erosion rate and its controlling variables using lysimeter experiments. Fox and Felice (2014) evaluated seepage failure mechanisms using varying hydraulic conditions across various soil types. Abidin et al.

(2017) focused on the subaerial erosion process, which mainly depended on the combination of rainfall intensity and the ability of the soil to withstand raindrop effects. Patsinghasanee et al. (2017) coupled fluvial erosion and cantilever failure for cohesive riverbanks using experimental flumes. Arai et al. (2018) conducted a series of bank erosion experiments in a soil box to explore cohesionless bank failure by focusing on the influence of sand type. Salem and Rennie (2017) introduced a practical procedure and test device designed to allow a fast and accurate determination of the critical shear stress of cohesive and non-cohesive soils both in laboratory sample and in the field. Dunne et al. (2019) presented an instrument, provisionally called the "Mudbluster", that was capable of reproducibly determining τ_c for submerged cohesive and non-cohesive sediments in-situ. Duong Thi and Do Minh (2019) estimated river bank erosion using shear stress and erosion rate curve from laboratory experiments. Also, they assessed riverbank stability under river water level change using slope/w and seep/w from Geo-slope product. In another of their research, tension crack and soil erosion were seen factors causing instability of Red river (Toan, 2020). Mohammed-Ali et al. (2020) investigated riverbank instability from the fluctuation of water level downstream from riverbanks due to hydropower flow releases. Several studies were performed by different researchers to estimate excess shear stress parameters, critical shear stress (τ_c) and erodibility co-efficient (k_d) based on in-situ jet testing to evaluate fluvial erosion (Al-Madhhachi et al., 2011; Al-Madhhachi et al., 2013; Clark & Wynn, 2007; Cossette et al., 2017; Daly et al., 2013; Daly et al., 2015; Dutta & Karmakar, 2015; Enlow et al., 2017; Karamigolbaghi et al., 2016; Karmaker & Dutta, 2011; Semmad et al., 2019; Simon & Collison, 2001).

Different river bank erosion processes can be quantified with the help of computer-aided numerical modelling or hydrodynamic modelling. Darby et al. (2002) performed numerical modelling coupling a two-dimensional depth-averaged model of flow and bed topography with a mechanistic model of bank erosion and compared it with two flume experiments. The bank stability model used by Simon et al. (2003) incorporated pore-water pressure distributions, layering, confining pressures, reinforcement effects of riparian vegetation and bank geometries to solve for the factor of safety. The effects of bank-toe erosion on stability were investigated by rerunning the model using iterated bank profiles by the Bank and Toe-Erosion Model. Results indicate that streambank failure is possible when bank-toe erosion is accounted for. Rinaldi and Darby (2007) combined fluvial erosion and mass wasting by developing a simulation modelling approach in which the hydraulic erosion, finite element seepage, and limit equilibrium stability models, for the first time,

fully coupled. Rinaldi et al. (2008) developed a model of fluvial bank erosion with groundwater flow and bank stability analyses to account for the influence of hydraulic erosion on the mass failure process using detailed hydrodynamic simulation. Luppi et al. (2009) performed bank simulations by linking hydrodynamic, fluvial erosion, groundwater flow and bank stability model, understanding the factors influencing bank changes and process at a seasonal scale. Darby et al. (2010) quantified hydraulic bank erosion using an excess shear stress model where a cohesive strength meter was used to determine bank erodibility parameters. Simon and Rinaldi (2006) developed an enhanced Bank Stability and Toe Erosion Model, which was originally developed at National Sedimentation Laboratory by Simon et al. (1999), to predict bank toe erosion and undercutting by hydraulic shear. Lai and Greimann (2010) presented numerical formulations applicable to arbitrarily shaped cells for the 2D depth-averaged equation and implemented it into a numerical model, SRH-2D. Lai and Wu (2013) used their two dimensional (2D) mobile bed model SRH-2D with its bank erosion capability to simulate a 16.7 Kilometer reach on the Chosui river. Karmaker and Dutta (2015) developed a bank erosion model in a river bend by coupling several bank erosion processes, including fluvial erosion, seepage erosion, and cantilever mass failure, with an existing hydrodynamic and morphological model. Klavon et al. (2017) reviewed one of the most comprehensive streambank retreat models, the Bank Stability and Toe Erosion Model (BSTEM), involving subaerial process, fluvial erosion, seepage erosion, and geotechnical failure. Zong et al. (2017) improved BSTEM (5.4) to predict riverbank retreat by inputting a dynamic water table and calculated the distribution of dynamic pore water pressure, and considered the depositional form of the failed blocks, which was based on triangular distributions. Semmad and Chalermyanont (2018) analyzed the riverbank erosion process, including subaerial process, fluvial erosion, and bank failure and also estimated erodibility parameters of riverbank soil using empirical formulae and submerged jet test incorporating Bank Stability and Toe Erosion Model with a lumped adjustment factor. Ashraf and Shakir (2018) predicted riverbank erosion by coupling the output from the two dimensional numerical model to the excess shear stress approach and compared that erosion from Landsat Imagery. Chang et al. (2020) proposed a methodology to predict riverbank failure caused by bend scour, integrating a one-dimension (1D) hydraulic model, a two-dimensional hydrodynamic finite volume model of bend scour prediction.

In many studies, it is believed that riverbank erosion initiates with basal toe erosion. Subaerial erosion, fluvial erosion, seepage erosion, any of these factors can be responsible for toe erosion. It

is very difficult to determine the reason for bank toe erosion, which leads to cantilever failure. In this study, the riverbank erosion process is assessed involving fluvial erosion, mass failure and the impact of surcharge load on the river bank. At first, the bank erosion rate is estimated using the excess shear stress model. Applied shear stress on the river bank is quantified by two-dimensional hydrodynamic modelling, SRH-2D (pre and postprocessing by SMS) and critical shear stress is measured by empirical formulae. Slope/w package from Geoslope product is used to determine geotechnical failure considering undercutting and surcharge load.

CHAPTER THREE
THEORETICAL BACKGROUND ON BANK EROSION AND STABILITY ANALYSIS

3.1 General

Many researchers had conducted studies relevant to riverbank stability analysis. Literature related to these works has been reviewed in the previous chapter. This chapter describes the theoretical backgrounds of riverbank stability and analysis relevant to the present study. These are mainly on different riverbank erosion mechanisms, hydrodynamic fluvial process, bank erosion rate, factors affecting bank erosion, hydrodynamic analysis, slope stability analysis, the factor of safety etc. Besides, various mathematical equations and formula of SRH-2D are also explained in this chapter. Terminologies, theories and mechanism of riverbank erosion have also been briefly described.

3.2 Mechanisms of riverbank erosion

The fundamental process related with riverbank movement is bank erosion, failure of bank material to resist erosion, mass failure causing bank instability, the effect of vegetation, seepage effects, surface erosion of banks, bank augmentation etc.

In an alluvial river, flowing water exerts drag and lift forces on the boundaries that tend to separate and entrain surface particles. Boundary sediment must provide an internally derived force capable of resisting erosive forces to maintain in place by the flow. This resisting force depends on grain size, size distribution and particles electromechanical bonding. Bank erodibility may vary the distance to distance along the reach. For non-cohesive bank materials, resisting forces to erosion are generated due to the immersed weight of soil particles.

3.2.1 Failures of bank material to resist erosion

Bank erosion can be increased by the process of weakening and weathering of bank materials. The mechanisms responsible for weakening and separating grains and aggregates are closely associated with soil moisture condition at and beneath the bank surface. Changes in moisture can significantly influence the erodibility of the riverbank. Repetition of wetting and drying can cause swelling and shrinkage of soil and contribute to cracking that significantly increases erosion and decrease soil

16

strength. When this weakening process occurs, bank erosion may vary from time to time. It means that the effectiveness of a given flow which erodes the bank depends on both the magnitude and direction of the particular event and also on antecedent condition.

3.2.2 Mass failure causing bank instability

Flowing water causes bank erosion, directly removing material from the bank face. It also hampers bank stability by mass failure. When there is a difference in the balance between gravitational forces, mass failure occurs. These forces tend to move soil down the slope, and forces of friction and cohesion, which resist movement. Failure of bank occurs when bank height is increased due to scour of the bed beneath the bank toe, or bank angle is increased due to undercutting.

3.2.3 Surface erosion of banks

The main impacts responsible for surface erosion of river banks are:

i) Current induced shear stress.

ii) Wave loads (wind-generated waves; ship and boat generated waves).

iii) Seepage (excessive pore pressure).

iv) Surface run-off.

v) Mechanical action (desiccation, ship impact, activities of humans and animals).
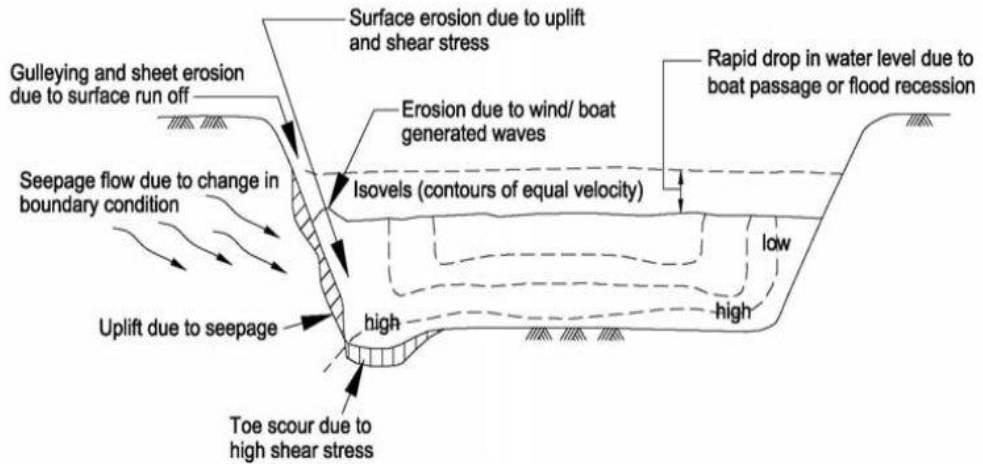
Figure 3.1: Processes of surface erosion (Hemphill & Bramley, 1989).

The main factor of bank erosion is the shear stress induced by current flow. Typical shear stress-induced distribution in a trapezoidal cross-section of a straight channel is shown in the following Figure 3.2:
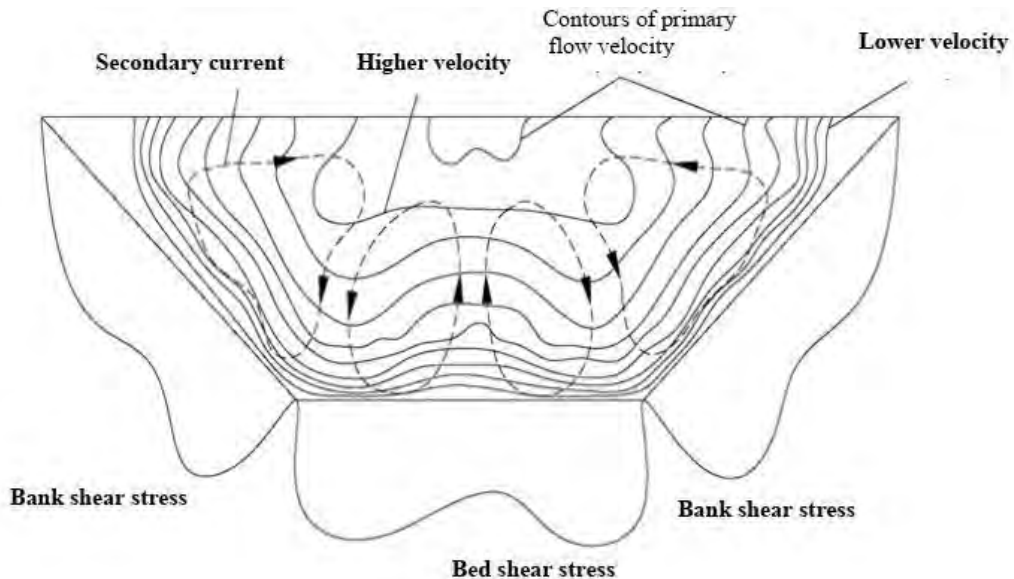
Figure 3.2: Contours of primary and secondary flows as well as the shear stress distribution in a trapezoidal channel (Hemphill & Bramley, 1989)

3.2.4 **Hydraulic fluvial process**

Gravitational mass failures often occur after hydraulic fluvial erosion. Hydraulic fluvial erosion is also responsible for the transport of the sediment deposits produced by mass failures. If there is a difference or imbalance between hydraulic shear stress and bank material resistance strength, hydraulic fluvial erosion occurs. Where the shear stress exceeds bank material strength, an erosion process will be initiated. In general, shear stress increases as flow increases, while bank strength typically reduces, e.g., when the bank becomes saturated. Hydraulically induced failure may be of three types: bed degradation(vertical), basal cleanout, and undercutting.

3.2.5 **Bed degradation**

Bed degradation occurs when the erosive power of flowing water increases to the point that it moves and erodes sediment6s on a channel bed. This is usually in the vertical direction and increases bank height and steepens bank slope, making the bank susceptible to undercutting and mass failure.

3.2.6 **Toe erosion**

The process of removing supportive or protective materials at the bank toe is toe erosion. This usually occurs when discharge is high. The protective material may cause mass failure. The repeated cycle of the basal cleanout, undercutting, mass failure, and bank toe accumulation plays an important role in controlling the erosion rate of the riverbank.

3.2.7 **Undercutting**

The direct removal of bank materials laterally by running water is undercutting. Local effects such as vegetation, presence of debris, bank soil characteristics such as poor drainage, and/or presence of a layer of non-cohesive materials. It often occurs on the outside bend of a meandering river. Undercutting is a fundamental process for the initiation of mass failure with the cohesive bank materials.

3.2.8 Mass failure process

Gravitation is one of the main reasons for mass failure. The different classification has been done so far. One classification is, according to Watson and Basher (2006), who classified mass failure into six categories as given below:

3.2.9 Shallow slide

In this process, a layer of material moves along a plane parallel to the bank surface (**Figure 3.3**). This type of failure occurs when cohesion of bank material is low, and angles are steep, and when bank angle, due to hydraulic fluvial erosion, exceeds the angle of internal friction of the bank material. Shallow slide failure often occurs as a secondary failure following a rotational and/ or slab failure (Thorne, 1998).
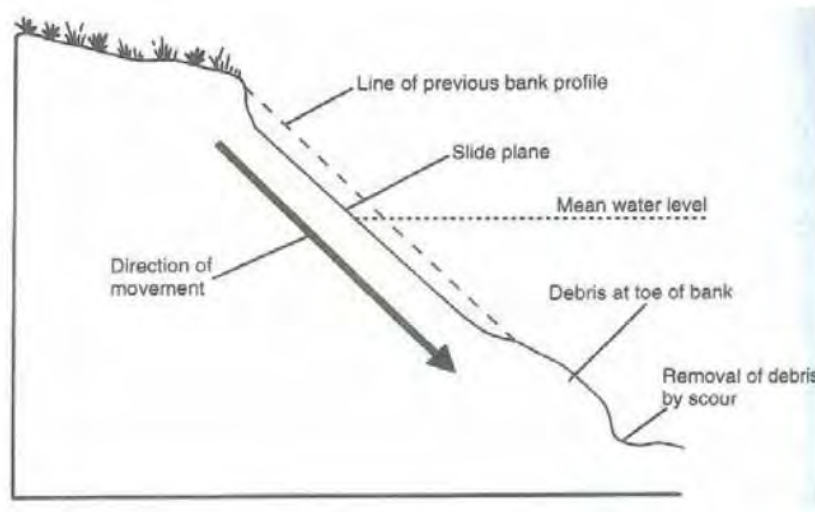
Figure 3.3: Schematic of shallow slide (Source: Watson and Basher, 2006)

3.2.10 Rotational failure

Rotational failure is a deep-seated movement of a layer of material both downward and outward along a curved slip surface. After failure, the upper slope of the slipped block is typically tilted inward the bank. The failure causes the formation of the tensile crack along the vertical direction and/ or high pore water pressure in the bank material (Figure 3.4). It often occurs during water level drawdown after high flow events on banks. Rotational failure generally occurs on the

cohesive bank with a tall bank and shallow profile. It generates more significant sediment discharge than planer failure (Dapporto et al., 2003).
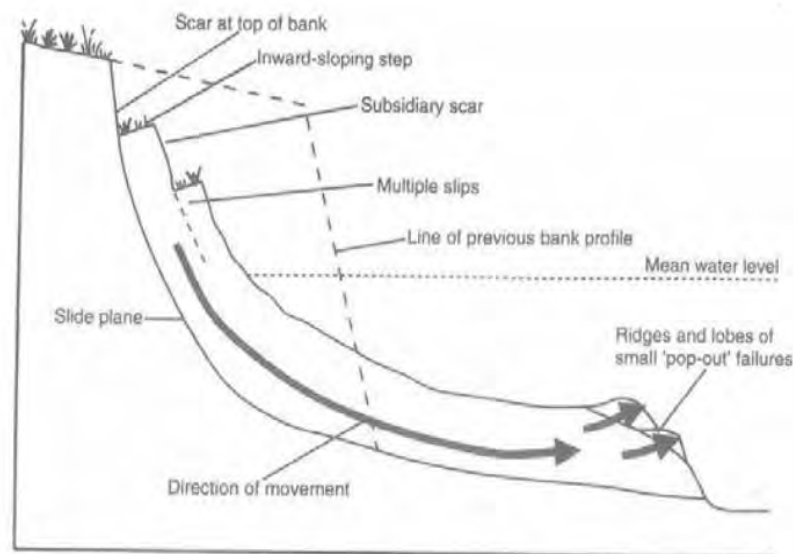
Figure 3.4: Schematic of rotational failure (Source: Watson and Basher, 2006)

3.2.11 Planer or slab failure

In this process, the deep-seated material of the bank slides and topples forward into the channel. Behind this process, different factors such as scour at the bank toe, high pore pressure in the bank material, and the development of tension cracks at banks play a key role (Figure 3.5). Failed materials accumulate at the lower section of the bank temporarily. Vertical tension cracks often cause planer failure. Desiccation and tension can develop water levelly, and cracks develop due to the release of stress. Tension cracks decrease the potential failure and hence decrease bank stability. Planer failure occurs on fine-grained, low height, steep cohesive banks, which is seen during lower flow conditions.

Tension cracks

Slip plane

Bare, exposed bank

Line of previous slope profile

'Slab' of soil

Direction of movement

Mean water level

Soil debris at toe of bank

Steepening of toe by scour
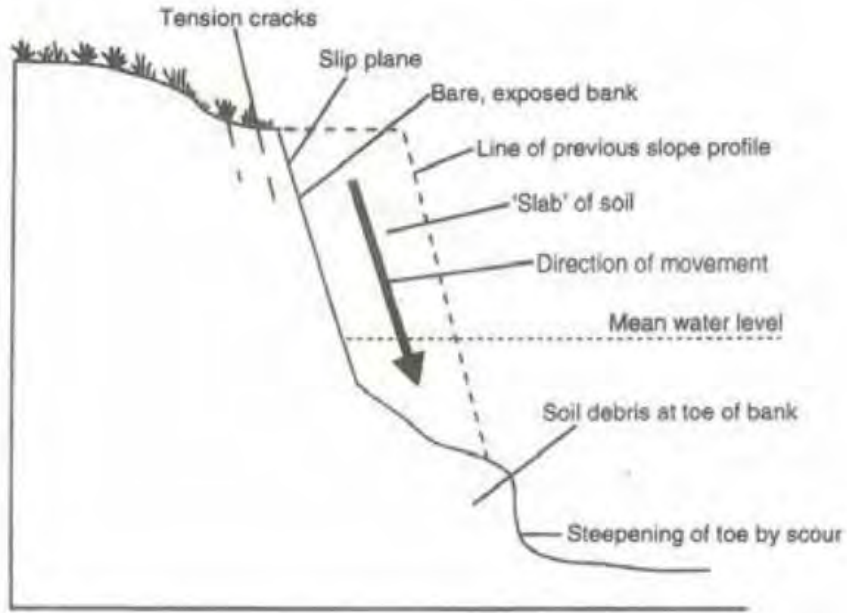
Figure 3.5: Schematic of planar failure (Source: Watson and Basher, 2006)

3.2.12 Cantilever failure

In this process, an overhanging block collapses into the river. Cantilever failure tends to occur on banks with composition layers of fine/ coarse and/or cohesive/non-cohesive materials and is the result of significant undercutting. Cantilever failure is more active under low flow condition (Figure 3.6).
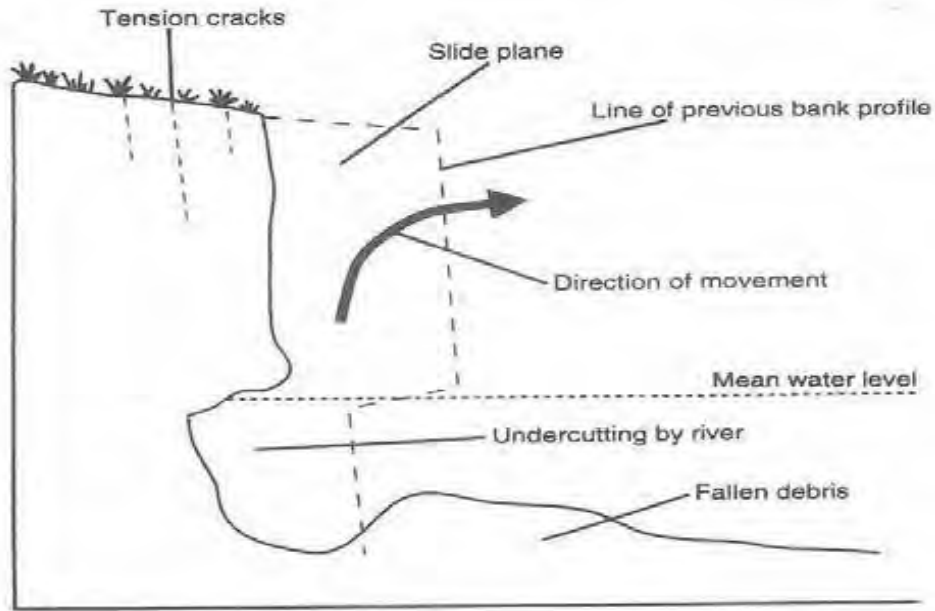
Figure 3.6: Schematic of cantilever failure (Source: Watson and Basher, 2006)
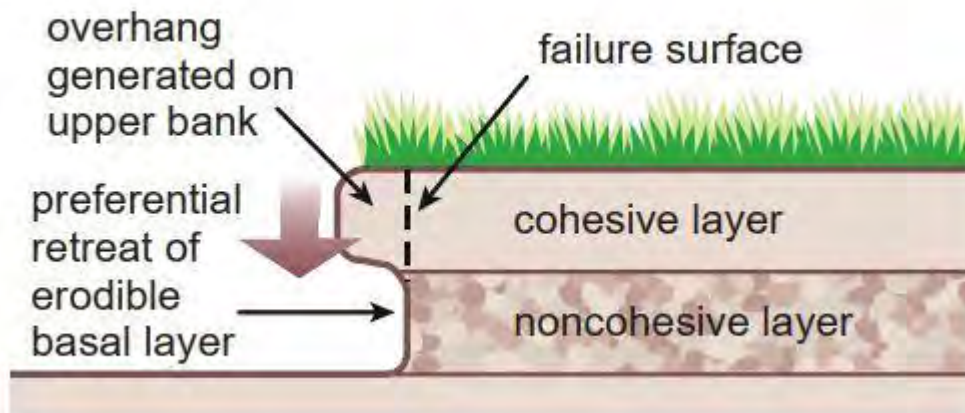
Figure 3.7: An illustration of a cantilever failure (Source: BSTEM (2009))

23

3.2.13 **Wet Earthflow**

In this process, the soil of a bank flows as a highly viscous liquid. The material flows down the bank to form lobes of material at the toe (Figure 3.8). This material is very weak and can be easily removed by the flow of water, even at lower flows (Thorne, 1998). Saturation and increased bank height cause wet earthflow, which results in loss of strength on a section of a bank. Wet earthflow occurs on a low bank angle and bank subjected to intense seepage and poor drainage. It is typically caused by waterlogging associated with high rainfall or water level drawdown of water in the channel.
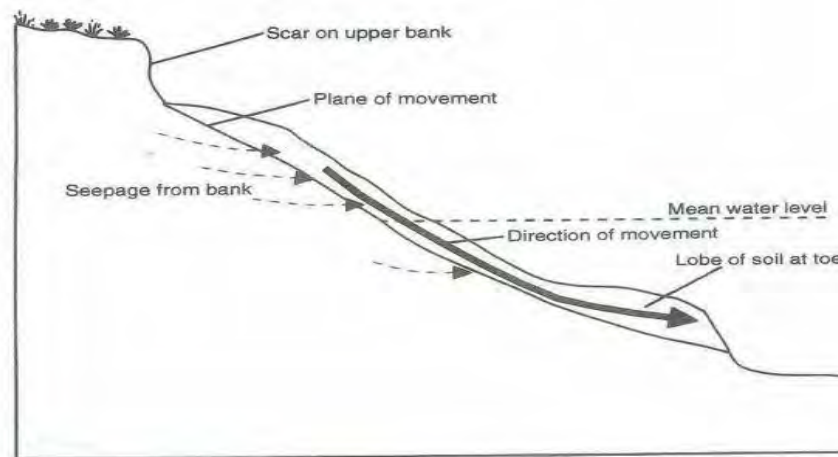
Figure 3.8: Schematic of wet earthflow (Source: Watson and Basher, 2006)

3.2.14 **Piping failure**

Simon (BSTEM, 2009) added another failure mood: piping failure, which needs separate discussion, as described below:

High groundwater seepage pressures and seepage flows causes selective removal of sections of the bank and results in the collapse of part of the bank. The failure is the result of groundwater flow along with layers of saturated river banks, with sand and coarser material sandwiched between layers of finer coarser material (Figure 3.9). Where river stage and/or groundwater seepage changes, flow is induced in more permeable layers. If the flow magnitude through the permeable layers is capable of dislodging and transporting particles, the material is slowly removed. This can

lead to undermining of portions of the cohesive upper bank leading to planer or cantilever failures (Thorne, 1998).
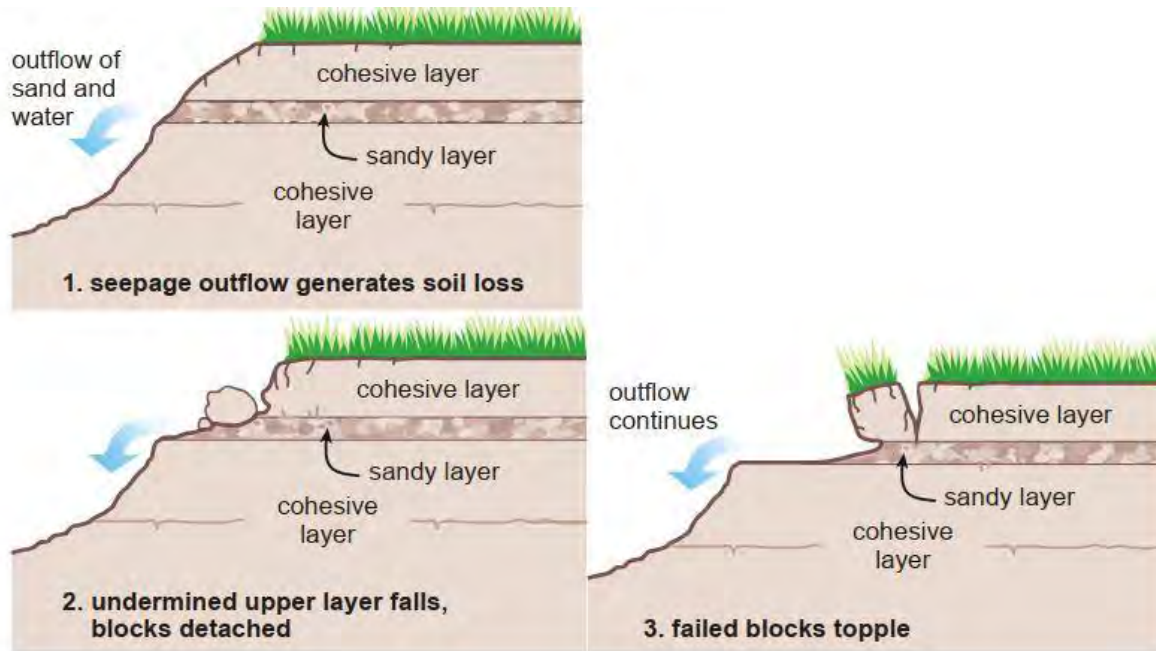
Figure 3.9: An illustration of piping failure (Source: BSTEM, 2009)

3.3 Bank erosion rate

Normally, the erosion rate of the soil is approximated using the excess shear stress equation. It is widely accepted that the rate of fluvial bank erosion can be quantified using an excess shear stress formula such as (Arulanandan et al., 1980; Partheniades, 1965)

$$\varepsilon = K_d(\tau - \tau_c)^a \qquad\qquad (3.1)$$

where $\varepsilon(m/s)$ is the fluvial bank-erosion rate per unit time and unit bank area. τ(Pa) is the boundary shear stress applied by the flow, K_d (m²s/kg) and τ_c(Pa) are erodibility parameters, and a (dimensionless) is an empirically derived exponent commonly assumed to be unity (Hanson, 1990a, 1990b; Hanson & Cook, 2004). If the boundary shear stresses are below the critical shear stress (shear stress at which erosion begins), the erosion rate is assumed to remain zero (Hanson,

25

1990a; Osman & Thorne, 1988). Erosion occurs when the boundary shear stress exceeds the critical shear stress(Semmad et al., 2019).

3.3.1 Methods of finding soil erodibility

Soil erodibility parameters (τ_c and K_d) are very difficult to quantify (Grissinger, 1982). There are many approaches to measuring the erodibility parameters. Once τ_c is determined, K_d can be determined from empirical formulae and erosion rate can be obtained from excess shear stress model (Cossette et al.; Daly et al., 2013; Hanson & Simon, 2001; Semmad & Chalermyanont, 2018; Simon et al., 2011; Wynn et al., 2004; Yagisawa et al., 2019).

Numerous studies have determined τ_c and K_d using different methods. A submerged jet test (JET-Jet Erosion Test) apparatus is one of the methods which is used by many researchers (Al-Madhhachi et al., 2011; Hanson, 1990b; Hanson & Cook, 1997, 2004; Hanson et al., 2002; Hanson & Simon, 2001; Hanson & Hunt, 2007). The original jet device was developed by Hanson (1990b). The submerged Jet test is the most widely used method of the in-situ test(Hanson & Cook, 2004). A jet device is convenient and portable for testing in the field. This apparatus is capable of testing of varied soil under varied conditions (Figure 3.10). The jet device has three important components: submergence tank, jet tube, and point gauge. The device distributes a circular Jet through the nozzle at a constant velocity. The Jet water diffuses radially generating shear stress on the bank soil (Semmad et al., 2019). Thus, a scour hole is created and is evaluated at regular intervals throughout the test. Time series of shear stress and scour depth are measured to determine erosion variables.
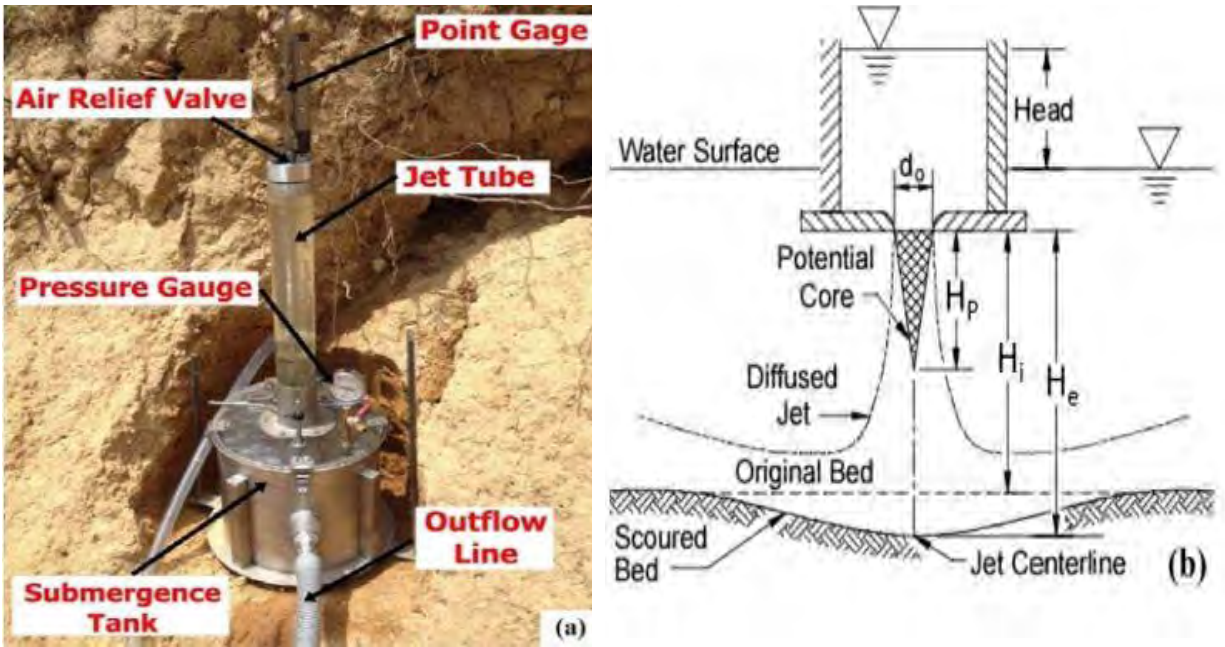
Figure 3.10: Schematic representation of a) submerged jet device b) diffuse jet producing boundary shear stress on the bank soil(taken from Hanson and Cook (2004))

A new miniature version of the JET device, which is referred to as the "mini" JET, was developed by Hanson in 2009. The mini-Jet device is smaller and lighter than the original JET device. The mini-Jet device can be more easily used in the field as well as in the laboratory. The mini Jet device was first used by Simon et al. (2010), who conducted 279 tests using the "mini" jet to measure τ_c and K_d.

3.4 Salient factors affecting the bank erosion

Knighton (1998) provided detailed information on factors influencing bank erosion processes. Some important factors are discussed below:

3.4.1 Flow properties

Fluvial shear stress is the dominant factor causing the bank erosion process. Good knowledge of flow and shear stress is necessary. The removal of bank material by hydraulic action is closely related to near-bank velocity and its gradient close to the bank. High flows remove both bank material and also scour the base, steepens the bank and lead to subsequent mass failure. Important

flow properties are magnitude, frequency and duration of discharge, magnitude and distribution of stream velocity and, shear stress and level of turbulence.

3.4.2 Channel geometry

Width, depth, the slope of the channel, and stream curvature (concave, convex, straight) are related to channel geometry. Channel geometry affects the hydraulic forces causing bank erosion and is important when the distribution of bank erosion along a channel reach is considered. For example, high rates of erosion commonly associated with river curvature result from the higher velocity gradients and hence higher shear stress against the outer banks of channel bends. Several channel geomorphic units (e.g., pools, riffles, runs) are related with different flow velocity and channel gradient, and hence shear stress on the banks and bed. The geometry of the channel cross-section is a good indication of the potential riverbank instability.

3.4.3 Bank geometry

Bank geometry is characterized by height, slope length, profile and shape. Bank height and slope are critical parameters when assessing river bank erosion potential, particularly when dealing with cohesive bank material (Dapporto et al., 2003; Rosgen, 1996). When the erosion of the bank and channel bed adjacent to the bank have increased the bank's height and steepness to a point where it reaches a condition of limiting stability, failures occur. Mechanics of failure depend on the properties of bank material and geometry of the bank at the point of collapse.

3.4.4 Bank material

It is characterized by size, gradation, cohesiveness and stratification of bank materials. A bank can be broadly classified as non-cohesive, cohesive, and stratified. Non-cohesive bank materials are relatively coarser and are usually well-drained. As a result, pore water pressure is a significant problem (Thorne & Tovey, 1981). The type of erosion occurs, grain by grain, in the form of dry granular flow. Cohesive banks are eroded less by grain-by-grain, but gravity and positive pore water pressure cause mass movement. Since cohesive materials are more likely to be poorly drained, positive pore water pressure can develop, particularly during the water level drawdown in the channel (Thorne & Tovey, 1981). The presence of a tension crack also causes bank instability. Tension cracks can extend a considerable portion of bank height, therefore weakening the stability of the slope. Weakening is further enhanced because cracks form paths for water to

28

move downward from the surface to lubricate a potential slide plane (Morgan et al., 1999). The stratified bank consists of layers of material of differing size, permeability and cohesion and non-cohesive materials (Group, 1998; Simons & Li, 1982). The non-cohesive layers are eroded more quickly, producing a stepped bank with more resistant material. Piping is also common in stratified alluvial banks.

3.4.5 Bank soil-moisture condition

Soil moisture content, seepage, pore water pressure and piping are related to bank soil-moisture conditions. The process of weakening and weathering reduces the strength of bank material and decreases stability. Swelling and shrinkage of soil due to cycles of wetting and drying lead to the growth of fissures and tension cracks which encourage failure. Seepage forces can reduce the cohesion of bank material by removing clay particles and may promote the development of soil pipes in the lower bank (Knighton, 1998). Cohesive river bank material is generally in a condition of partial saturation.

Consequently, it is subject to negative pore water pressures (suctions) that produce an increase in apparent cohe4sion of the bank material. Rainfall, variation in river flow and evapotranspiration of the bank's vegetation causes fluctuation in negative pore-water pressures in river banks. Bank failures are likely to occur mainly during the water level drawdown when the bank material is still at or near saturation and as the confining pressure of the water approaches zero (Casagli et al., 1999; Simon & Collison, 2001). In stratified banks with lenses of sand and coarser material sandwiched between layers by river stage changes (Simons & Li, 1982). If the flow through the permeable layers is capable of dislodging and transporting particles, the material is slowly removed. This can lead to the undermining of properties of the cohesive upper bank leading to gravitation induced block failures.

3.5 Hydrodynamic Modeling Tools

A numerical model is a powerful tool to predict and obtain information about water levels, current velocities, waves and sediment transport in a situation where field measurements are rarely done. There is different software available to simulate flow and sediment transport with bed level changes in river systems. They are mainly HEC-RAS, SMS, MIKE 11, MIKE 21C, DELFT 3D etc.

3.5.1 Surface water modelling system (SMS)

SMS (Surface-water modelling system) is a computer program for building and simulating surface water models. It is a graphical user interface and analysis tool that allows engineers and scientists to visualize, manipulate, analyze, and understand numerical data and associated measurements. Many of the devices in SMS are generic. They are designed to facilitate the establishment and operation of numerical models of river, coasts, inlets, bays, estuaries, and lakes. It features 1d and 2d modelling and a unique conceptual model approach. Some of the currently supported models in SMS include ADCIRC, BOUSS-2D, SRH-2D, CGWAVE, CMS-FLOW, CMS-WAVE (WABED), FESWMS, Gencode, PTM, STWAVE, TABS and TUFLOW.

3.5.2 SRH-2D

SRH-2D, Sedimentation and River Hydraulics- Two-Dimensional model, two-dimensional hydraulic sediment, temperature and vegetation model for river systems is used for the current modelling study. It was developed at the technical service centre, Bureau of Reclamation (Lai, 2008). This hydraulic flow model documented by(Lai, 2008; Lai & Greimann, 2010), has been widely used by internal and external users.

Some of the unique features of SRH-2D have been discussed by Lai (2008) :

  i)   A primary feature is the use of a flexible mesh.
  ii)   The arbitrarily shaped element method of Lai et al. (2003) is adopted for geometry representation.
  iii) This allows the use of most existing meshes available: structured, quadrilateral mesh, purely triangular mesh, finite element mesh, cartesian mesh, or hybrid mesh.
  iv)   Relatively stable numerical algorithm used with very few stability-ensuring parameters and ease of use of the model.

SRH-2d is particularly useful for problems where 2D effects are taken into consideration. For example, flows with in-stream structures such as weirs, diversion dams, release gates, cofferdams, etc.; bends and point bars; perched rivers; and multi-threaded streams. 2D models are required to simulate some features such as flow circulation and eddies, lateral variations, overtopping over

banks and levees, differential flow shears on river banks, and interactions between the main channel; vegetation areas and floodplain (Lai et al., 2003).

3.5.2.1 Capabilities of SRH-2D

SRH-2D is capable of analyzing following hydrodynamic processes (Lai, 2008):

    i)   2D depth-averaged governing equations with the dynamic wave (shallow water) approximation for flow hydraulics;

    ii)   An implicit solution scheme for time advancement;

    iii)   Unstructured meshes with arbitrary mesh cell shapes. In most applications, a combination of quadrilateral and triangular meshes is recommended;

    iv)   Steady or unsteady flows;

    v)   Subcritical and supercritical flow regimes;

    vi)   Time-accurate, non-equilibrium modelling of sediment transport;

    vii)   Multi-size-class sediment transports with bed sorting and armouring;

    viii)   Effects of gravity and secondary flows;

    ix)   A unified formulation for suspended load, bedload and mixed load;

    x)   Non-cohesive or cohesive sediments; and

    xi)   Coupled mobile-bed and bank erosion modelling.

SRH-2D may be applied in the following fields (Lai, 2008):

    i)   Flow in one or multiple streams covering the main channel, side channels, and floodplains;

    ii)   Flood routing and inundation mapping over any terrain;

    iii)   Flow around in-stream structures such as weirs, diversion dams, release gates, coffer dams, etc.;

    iv)   Flow over-spill over banks and levees;

    v)   Flow over vegetated areas and interaction with main channel flows;

    vi)   Flow in reservoirs with known flow release; and

    vii)   Morphological assessment of bed erosion potential.

3.5.2.2 Governing Equations

Most open channel flows are relatively shallow, and the effect of vertical motions is negligible. As a result, the most general flow equations, the three-dimensional Navier-Stokes equations, may be vertically averaged to obtain a set of depth-averaged two-dimensional equations, leading to the following well known 2D St. Venant equations:

$$\frac{\partial h}{\partial t} + \frac{\partial hU}{\partial x} + \frac{\partial hV}{\partial y} = e \tag{3.2}$$

$$\frac{\partial hU}{\partial t} + \frac{\partial hUU}{\partial x} + \frac{\partial hVU}{\partial y} = \frac{\partial hT_{xx}}{\partial x} + \frac{\partial hT_{xy}}{\partial y} - gh\frac{\partial z}{\partial x} - \frac{\tau_{bx}}{\rho} + D_{xx} + D_{xy} \tag{3.3}$$

$$\frac{\partial hV}{\partial t} + \frac{\partial hUV}{\partial x} + \frac{\partial hVV}{\partial y} = \frac{\partial hT_{xy}}{\partial x} + \frac{\partial hT_{yy}}{\partial y} - gh\frac{\partial z}{\partial y} - \frac{\tau_{by}}{\rho} + D_{yx} + D_{yy} \tag{3.4}$$

In the above, t is time, x and y are horizontal Cartesian coordinates, h is water depth, U and V are depth-averaged velocity components in x and y directions, respectively, e is excess rainfall rate, g is gravitational acceleration, T_{xx}, T_{xy} and T_{yy} are depth-averaged turbulent stresses, D_{xx}, D_{xy}, D_{yx}, D_{yy} are dispersion terms due to depth averaging, $z=z_b +h$ is water surface elevation, zb is bed elevation, ρ is water density, and τ_{bx}, τ_{by} are the bed shear stresses (friction). Bed friction is calculated using Manning's roughness equation as follows:

$$\begin{pmatrix} \tau_{bx} \\ \tau_{by} \end{pmatrix} = \rho C_f \begin{pmatrix} U \\ V \end{pmatrix} \sqrt{U^2 + V^2}; \qquad C_f = \frac{gn^2}{h^{1/3}} \tag{3.5}$$

where n is the Manning's roughness coefficient.

Turbulence stresses are based on the Boussinesq equations as:

$$T_{xx} = 2(\upsilon + \upsilon_t)\frac{\partial U}{\partial x} - \frac{2}{3}k$$

$$T_{xy} = (\upsilon + \upsilon_t)(\frac{\partial U}{\partial y} + \frac{\partial V}{\partial x}) \qquad \textbf{(3.6)}$$

$$T_{yy} = 2(\upsilon + \upsilon_t)\frac{\partial V}{\partial y} - \frac{2}{3}k$$

Where υ is the kinematic viscosity of water, υt is turbulent eddy viscosity, and k is turbulent kinetic energy.

A turbulence model is used to compute the turbulent eddy viscosity. Two turbulence models may be used Rodi (1993): the depth-averaged parabolic model and the two-equation k-ε model. With the parabolic model, $\upsilon_t = C_t\, U*h$ in which $U*$ is the bed frictional velocity. The model constant C_t ranges from 0.3 to 1.0, and a default value of Ct =0.7 is used by SRH-2D.

If the k-ε model is used, turbulent viscosity is calculated with $\upsilon_t = C_\mu k^2 /\epsilon$. Two additional equations are solved as follows:

$$\frac{\partial hk}{\partial t} + \frac{\partial hUk}{\partial x} + \frac{\partial hVk}{\partial y} = \frac{\partial}{\partial x}(\frac{h\upsilon_t}{\sigma_k}\frac{\partial k}{\partial x}) + \frac{\partial}{\partial y}(\frac{h\upsilon_t}{\sigma_k}\frac{\partial k}{\partial y}) + P_h + P_{kb} - h\varepsilon \qquad \textbf{(3.7)}$$

$$\frac{\partial h\varepsilon}{\partial t} + \frac{\partial hU\varepsilon}{\partial x} + \frac{\partial hV\varepsilon}{\partial y} = \frac{\partial}{\partial x}(\frac{h\upsilon_t}{\sigma_\varepsilon}\frac{\partial \varepsilon}{\partial x}) + \frac{\partial}{\partial y}(\frac{h\upsilon_t}{\sigma_\varepsilon}\frac{\partial \varepsilon}{\partial y}) + C_{\varepsilon1}\frac{\varepsilon}{k}P_h + P_{\varepsilon b} - C_{\varepsilon2}h\frac{\varepsilon^2}{k}$$

$$\textbf{(3.8)}$$

The following definitions and coefficients are used Rodi (1993),

$$P_h = h\upsilon_t \left[2\left(\frac{\partial U}{\partial x}\right)^2 + 2\left(\frac{\partial V}{\partial y}\right)^2 + \left(\frac{\partial U}{\partial y} + \frac{\partial V}{\partial x}\right)^2 \right] \tag{3.9}$$

$$P_{kb} = C_f^{-1/2} U_*^3; \quad P_{\varepsilon b} = C_{\varepsilon \Gamma} C_{\varepsilon 2} C_\mu^{1/2} C_f^{-3/4} U_*^4 / h \tag{3.10}$$

$$C_\mu = 0.09, C_{\varepsilon 1} = 1.44, C_{\varepsilon 2} = 1.92, \sigma_k = 1, \sigma_\varepsilon = 1.3, C_{\varepsilon \Gamma} = 1.8 \sim 3.6 \tag{3.11}$$

The terms and are added to account for the generation of turbulent energy and dissipation due to bed friction for uniform flows.

The dispersion terms arise due to the depth averaging process and may become necessary when secondary flows are present Flokstra (1976). It was shown by Mihn Duc (1996) that the effect of the secondary flow might be accounted for indirectly by increasing the coefficient of momentum exchange in the horizontal plane.

Some discussion of Manning's roughness coefficient is in order. With SRH-2D, the Manning's coefficient is a local constant that does not change with the flow; but it may be spatially distributed depending on bed types. In addition to Manning's coefficient, another representation of flow roughness is also convenient with the equivalent roughness height of the bed. For a loose bed, the equivalent roughness height and Manning's coefficient should include both effects of the bed material grain size and bed form.

3.6 Slope stability analysis

Slope stability analysis is very important for investigating the condition of the river bank by determining the factor of safety. This factor of safety can be obtained by two methods: limit equilibrium method and finite element method.

3.6.1 Limit equilibrium method (LEM) of analysis

Most of the slope stability analyses are currently done by limit equilibrium analysis due to their accuracy and simplicity. These methods include cutting the slope into fine slices and apply appropriate equilibrium equations (equilibrium of the forces and/or moments). Many alternatives' methods exist, such as the Bishop and Fellenius methods, according to the assumption made on

the efforts between the slices and the equilibrium equations considered. In most of the cases, they give similar results. For example, Duncan (1996) reported that the difference between various methods is less than 6.

3.6.2 Basics of the limit equilibrium method

Over the years, many different methods have been developed to determine the stability of earth slopes. All are very close to each other. The differences between methods depend on:

    i)   What equations of statics are included and satisfied;

    ii)   Which interslice forces are included;

    iii)   What is the assumed relationship between the interslice shear and normal forces;

Figure 3.11 shows a typical sliding mass discretized into slices and the possible forces on the slice. Normal and shear forces act on the slice side and the slice base.
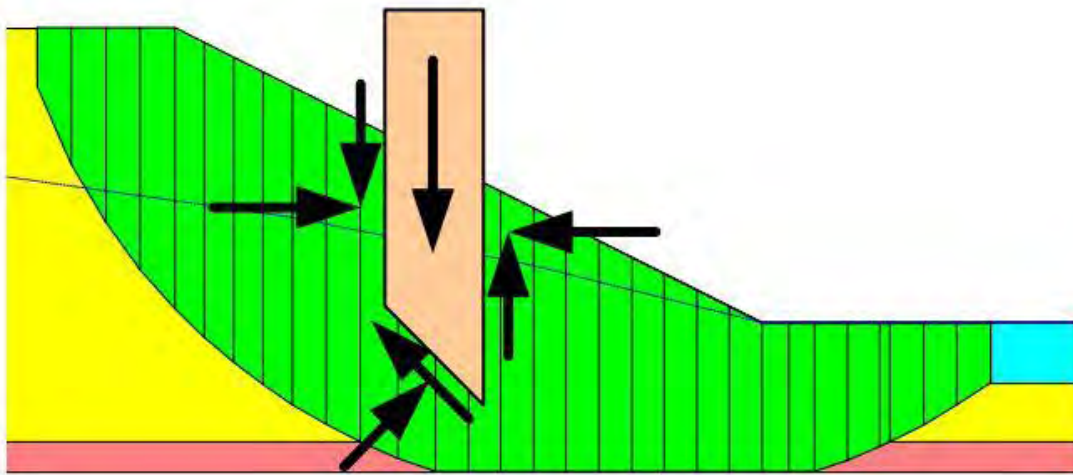
Figure 3.11: Slice discretization and slice forces in a slide mass

3.6.3 Method of slices

The most common method currently used to determine the stability of the slope is the method of slices. This is because many inexpensive programs use this method. In addition to that, the method is accepted by most geotechnical engineers. In these programs, the user can change failure surface geometries, soil parameters, and pore water pressure condition easily.

The theoretical basis for the method of slices is that the normal stress acting at a point on a potential sliding surface should be affected mainly by the weight of the soil lying above the point (Lambe & Whitman, 1969). The potential slide mass then divided vertically into slices, and the equilibrium of each slice is determined considering forces and moments.

Examples of different solutions are ordinary, simplified Bishop, Janbu simplified, Spencer and Morgenstern-Price. All use assumptions when it comes to interslice forces. Thus, the factor of safety varies among the methods slightly by + or – 10 percentage. The ordinary method may vary as much as 60 per cent (Whitman & Bailey, 1967) and should be used carefully.

3.6.3.1 Ordinary method of slices

This method fails to satisfy the force equation for the slide mass as well as individual slices and neglects all interslice forces. However, this is the simplest method among the method of slices(Fellenius, 1936). A circular slip surface is assumed in this method which is also known as the Swedish method of slices or the Fellanious method.

3.6.3.2 Simplified Bishop

This method assumes that the vertical interslice shear force does not exist, and the resultant interslice force is horizontal(Bishop, 1955). It satisfies the equilibrium of the moment but not forces.

3.6.3.3 Janbu Simplified Method

This method depends on the horizontal forces equilibrium equation to obtain the factor of safety and does not consider interslice forces. It assumes a correction factor related to cohesion, angle of internal friction and the shape of the failure surface (Janbu et al., 1956).

3.6.3.4 Spencer method

This is a very accurate method. It satisfies both equilibria of forces and moments. It works for any shape of the slip surface. This method assumes that the inclination of the side forces is the same for all slices.

3.6.3.5 Morgenstern-Price

The method proposed by Morgenstern and price is similar to spencer's method, except that the inclination of the resultant interslice force is assumed to vary according to a part of an arbitrary function. This method allows for different types of interslice force functions (Morgenstern & Price, 1965).

3.6.3.6 General limit equilibrium

This method considers either force or moment equilibrium. It uses the assumptions of various methods and may be used to analyze circular and noncircular failure surface ((Fredlund et al., 1981).

Table 3.1: Methods of slope stability analysis (MO et al., 2006)

Method	Factor of safety (FS)		Interslice force assumption (H=Horizontal, V=Vertical)
	Force Equilibrium	Moment equilibrium	
Ordinary (Swedish)	-	Yes	Ignore both H, V
Bishop's Simplified	-	Yes	V ignored; H considered
Janbu's simplified	Yes	-	V ignored; H considered
Janbu's Generalized	Yes	-	Both H, V considered
Spencer	Yes	Yes	Both H, V considered
Morgenstern-Price	Yes	Yes	Both H, V considered
Lowe-Karafiath	Yes	-	Both H, V considered
Corps of Engineers	Yes	-	Both H, V considered

3.6.4   Factor of safety

The factor of safety is defined as the ratio of the summation of resisting forces and moments to the summation of driving forces and moments which bring the slope in an equilibrium condition along a slip surface according to equation 13.

$$\text{Factor of safety} = \frac{\sum resisting\ forces, moments}{\sum driving\ forces, moment} \tag{3.12}$$

Theoretically, a factor of safety means that the failure mass is on the verge of sliding (Gofar & Kassim, 2007). It is essential to provide a reasonable value for the factor of safety that satisfies both safety and economic conditions.

3.6.5   Design Factor of Safety

A minimum factor of safety as low as 1.25 is used for highway embankment side slopes. This value of the safety factor should be increased to a minimum of 1.30 to 1.50 for slopes whose failure would cause significant damage, such as end slopes beneath bridge abutments, major retaining structures and major roadways such as regional routes interstates, etc. The selection of the design safety factor for a particular project depends on (Samtani & Nowatzki, 2006):

    i)   The method of stability analysis used.

    ii)   The method used to determine the shear strength

    iii)   The degree of confidence in the reliability of subsurface data.

    iv)   The consequences of a failure

    v)   How critical the application is.

Table 3. 2 presents the minimum values of the factor of safety proposed by different authors. A long-term factor of safety equal to 1.5 is often recommended in the literature.

Table 3. 2: Factor of safety proposed by different authors

Factor of safety	Significance	References
Less than 1	Failure	Cheng and Lau (2014)
1.0-1.2	Questionable safety	
1.3-1.4	Satisfactory for cuts questionable for dams	
1.5-1.75	Safe for dams	
FS < 1.07	Unstable slope	Bowles (1984)
1.07 < FS < 1.25	Critical slope	
FS > 1.25	Stable slope	
FS < 1	unstable	Modified from Ray and De Smedt (2009)
1 < FS < 1.25	Quasi-stable	
1.25 < FS < 1.5	Moderately stable	
FS > 1.5	Theoretically stable	

3.6.6 Multi-Stage Method for analysing the effect of water level drawdown

Stability analysis during water level drawdown is an essential consideration in the design of riverbank protection works. The stabilizing effect of the water on the upstream face is lost during water level drawdown, but the riverbank's pore-water pressures may remain high. As a result, the stability of the upstream front of the bank can be significantly reduced. The dissipation of pore-water pressure in the bank is mostly influenced by the river materials' permeability and storage characteristics. Highly porous materials drain quickly during the water level drawdown, but low permeability materials take a long time to drain.

Duncan et al. (1990) proposed a three-stage approach for modelling staged water level drawdown. The first stage involves the stability analysis of the riverbank before drawdown. The pore-water pressures are at their maximum values (piezometric line before drawdown). The useful strength parameters for all materials are used to determine the effective normal and shear stresses at each slice base. At the end of the first stage, the effective normal stress and effective shear stress along the slip surface are used to determine the undrained shear strength for materials that do not drain freely. The second stage involves the stability analysis of the riverbank after drawdown when the water level is low, and the pore-water pressure in the materials is at a steady-state condition (piezometric line after drawdown). In this second stage, the effective strength parameters for the

freely drained materials are used, and the undrained shear strengths determined from the result of Stage 1 are used for materials that do not drain freely. In the third stage, the effective normal stress obtained from stage two, together with the effective strength parameters, is used to compute all slices' drained strength along the slip surface. For materials that do not drain freely, the drained strength at the base of each slice is compared with the undrained strength, and the smaller strength is chosen. In other words, the effective strength may be used if it is smaller than the undrained strength for materials that do not drain freely. This is needed to avoid using undrained strengths that are higher than drained strengths, which cannot be mobilized if cavitation or drainage occurs (Duncan et al., 1990). The computed factor of safety from the first and second stages is ignored. Only the factor of safety calculated from the third stage analysis is used to represent the stability after water level drawdown. In stage drawdown analysis, drawdown may occur immediately or after several month of reaching high flood level.

3.7 Finite Element Method (FEM) of analysis

As the computer program has improved, the application of finite element analysis in geotechnical analysis has become popular. These methods offer several advantages: to model slope with a degree of very high practical condition (complex geometry, sequences of loading, presence of material for reinforces, the action of water, laws for complex soil behaviour) and to represent the deformation of soils better. To analyze slopes, the strength reduction method is applied. This method is based on the reduction of the cohesion(C) and the tangent of the friction angle (tanϕ) of the soil. The parameters are reduced in steps until the soil mass fails.

3.7.1 Determination of FOS by finite element method

The finite element algorithm computes the factor of safety, FOS, based on the mean values of the shear strength parameters using the strength reduction method (Matsui & San, 1992). The factor of safety of a slope is defined as the factor that the original shear strength parameters must be divided by in order to bring the slope to the point of failure. The strength parameters at the point of failure c_f and φ_f, are therefore given by,

$$c_f = \frac{c}{FOS} \tag{3.13}$$

and

$$\varphi_f = \arctan\left(\frac{tan\phi}{FOS}\right) \qquad\qquad\qquad \textbf{(3.14)}$$

The definition of the factor of safety is essentially the same as that used in limit equilibrium methods, which is the ratio of shear strength of soil to shear stress required for equilibrium(Duncan, 1996). Validation studies conducted by Griffiths and Lane (1999) indicate good relation between the FOS computed by finite element method and that obtained from the stability charts developed by Taylor (1937) and Bishop and Morgenstern and Price (1965).

3.8 Effects of water on slope stability

Very soft, saturated foundation soils or groundwater generally play a prominent role in geotechnical failures in general. They are certainly significant factors in cut slope stability and in the stability of fill slopes involving both "internal" and "external" slope failures. The effect of water on cut and fill slope stability is briefly discussed below (Samtani & Nowatzki, 2006).

3.8.1 Effects of Water on bank soil stability

Next to gravity, water is the most important factor in slope stability. The effect of gravity is known; therefore, water is the key factor in assessing slope stability.

3.8.1.1 Effect on Cohesionless Soils

In cohesionless soils, water does not affect the angle of internal friction (φ). The effect of water on cohesionless soils below the water table is to decrease the intergranular (effective) stress between soil grains ($\sigma'n$), which decreases the frictional shearing resistance (τ').

3.8.1.2 Effect on Cohesive Soils

Routine seasonal fluctuations in the groundwater table do not usually influence either the amount of water in the pore spaces between soil grains or the cohesion. The attractive forces between soil particles prevent water absorption unless external forces such as pile driving, disrupt the grain structure. However, certain clay minerals react to the presence of water and cause volume changes of the clay mass.

An increase in absorbed moisture is a significant factor in the decrease in strength of cohesive soils. Water absorbed by clay minerals causes increased water contents that decrease the cohesion of clayey soils. These effects are amplified if the clay mineral happens to be expansive, e.g., montmorillonite.

3.8.2 **Cutting and filling on underlaying soil material**

Excess pore-water pressures are created when fills are placed on clay or silt. Provided the applied loads do not cause the undrained shear strength of the clay or silt to be exceeded, as the excess pore water pressure dissipates, consolidation occurs, and the shear strength of the clay or silt increases with time. For this reason, the factor of safety increases with time under the load of the fill.

As a cut is made in clay, the effective stress is reduced. This reduction will allow the clay to expand and absorb water, which will lead to a decrease in the clay strength with time. For this reason, the factor of safety of a cut slope in clay may decrease with time. Cut slopes in clay should be designed by using useful strength parameters and the effective stresses that will exist in the soil after the cut are made.

Soil properties, model description, the methodology of stability analysis and theories have been used in this study, these are described in the subsequent chapter.

CHAPTER FOUR
DATA COLLECTION AND METHODOLOGY

4.1   General

To perform hydrodynamic modelling, various types of data, e.g., morphological, bathymetry and hydraulic data, need to be collected. Data collection is an important step for conducting research work to represent the field condition in a realistic model. For this analysis, two types of data are collected for hydrodynamic and slope stability modelling, respectively. For hydrodynamic modelling, bathymetry, water level and discharge data are collected, and for slope stability analysis, soil strata information, soil properties and grain size of bank and bed material are collected. Also, a satellite image of the study area is collected for hydrodynamic analysis. This chapter describes a brief discussion about the collection of data and methods for performing the work.

4.2   Data collection

Quality data are a prerequisite for reliable model setup, model results, and understanding to understand the existing physical process. To determine the present hydraulic conditions and to develop a mathematical model of Jamuna river near Chauhali, various data have been collected. With proper care, data are gathered to make the result more realistic. A brief description of data collection is given below:

4.2.1   Data collection for hydraulic modelling

4.2.1.1   Satellite image

A satellite image of the study area was collected from the Bangladesh water Development Board. The satellite image of the Jamuna river near Chauhali, Sirajganj, was captured during the year 2017, and the image was georeferenced. This image is used to find out the exact position of planform changes after performing modelling and helps to analysis without any confusion. The satellite image is shown in the following figure which shows the study area at Chauhali along the left bank of Jamuna river in Sirajganj district (Figure 4.1).
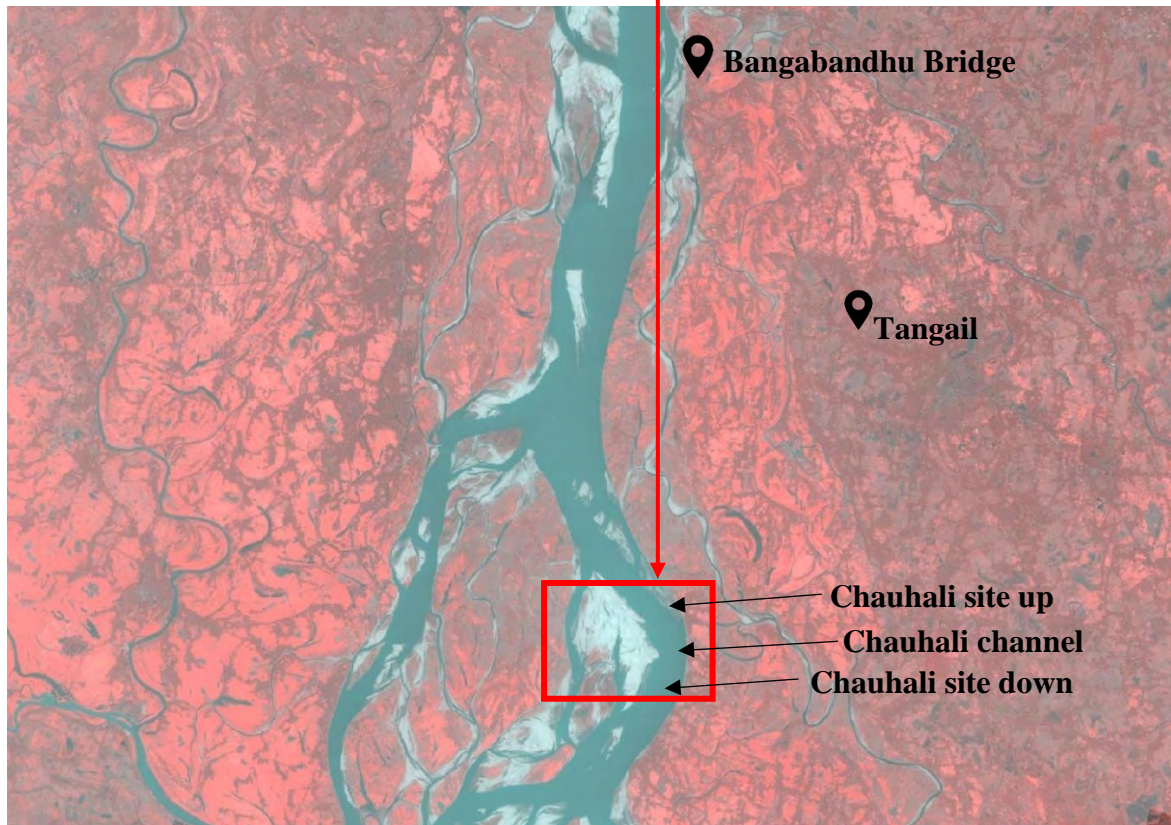
Figure 4.1: Study area

4.2.1.2 Water level data

Water level data at different locations are required for calculating the river slope considering the water level of different locations as well as providing boundary of the two-dimensional model and also to calibrate the model. Water level data at Chauhali site up, Chauhali channel and Chauhali site down of Jamuna river have been collected and analyzed to get an idea about the amount of water flowing at this location. The location, duration and source of data are illustrated in Table 4.1. Data of Chauhali site up and down have been used for providing boundary conditions of model and data of Chauhali channel have been used for calibration purpose. Table 4.2 shows water level data at Chauhali site up and down. For calibration purpose, the water level of Chauhali channel at Jamuna river during August 2017 has been used. Measured water level data collection of Chauhali channel has been plotted, as shown in Figure 4.2.

Table 4.1: Location, time and source of the water level data collection

Monitoring station	Station co-ordinate				Duration	Source
	Start		End			
	Lat	Long	Lat	Long		
Chauhali site up	24° 12.694000' N	89° 47.114500' E	24° 12.667900' N	89° 45.258400' E	01/08/2017 To 25/08/2017	BWDB
Chauhali channel	24° 10.391500' N	89° 48.429000' E	24° 10.631200' N	89° 45.863400' E	12/11/2016 To 13/10/2017	BWDB
Chauhali site down	24° 6.563600' N	89° 47.152100' E	24° 7.833900' N	89° 44.461700' E	01/08/2017 To 25/08/2017	BWDB

Table 4.2 : Water level data (in mPWD)

Date / Location	01-08-2017	15-08-2017	18-08-2017	25-08-2017
Chauhali site up	10.44	12.21	12.66	11.66
Chauhali site down	10.05	11.81	12.13	11.14

45
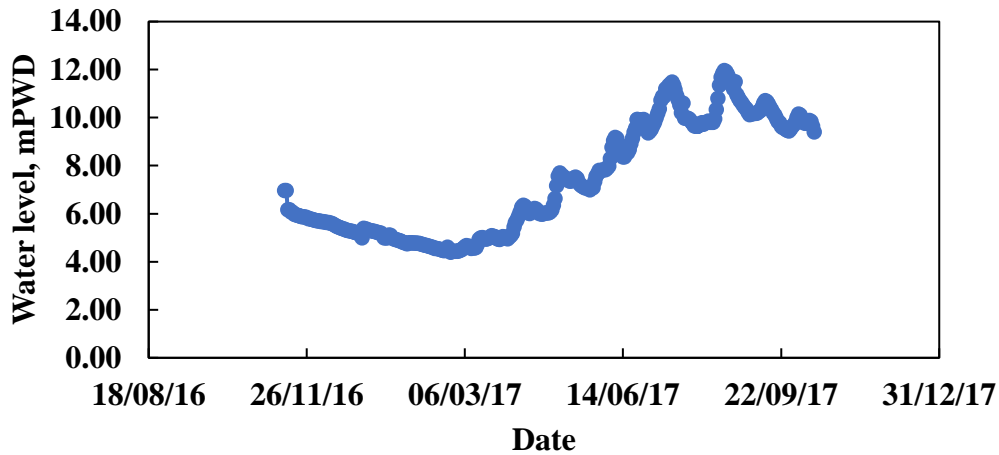
Figure 4.2: Measured water level data at Chauhali channel of Jamuna river.

4.2.1.3 **Discharge Data**

Discharge data are needed to investigate the hydrological characteristics of the river and to provide boundary for the two-dimensional morphological model. The data are given briefly in the following Table 4.3. Discharge data of Chauhali site up and down have been used for providing boundary condition and data of Chauhali channel have been used for calibration purpose. Source and locations of these data has been shown in Table 4.1.

Table 4.3: Discharge data at Chauhali channel

		Discharge (m^3/s) in different dates of August 2017			
Location	Measurement	01-08-2017	15-08-2017	18-08-2017	25-08-2017
Chauhali Site up	Left to Right	30639	43727	51821	32125
	Right to left	29936	43372	51791	32339
	Average	30288	43549	51806	32232
Chauhali channel	Left to Right	23434	41157	51331	30242
	Right to left	23815	41027	51193	30388
	Average	23625	41092	51262	30315
Chauhali site down	Left to Right	28553	47386	54752	32549
	Right to left	28693	47622	54525	32704
	Average	28623	47504	54639	32627

4.2.1.4 **Bathymetry data**

The post-monsoon 2017 bathymetry data of the Jamun river have been collected from BWDB. These surveyed bathymetry data covers the entire 8.210 Km reach of Jamuna river from Chauhali site up and down. Figure 4.3 shows the cross-section lines of bathymetry data within this reach. The spacing between the cross-sections is about 1Km. For the purpose of the study, the left channel of Jamuna river near Chauhali was considered. Figure 4.4 shows the cross-sections of the channel.
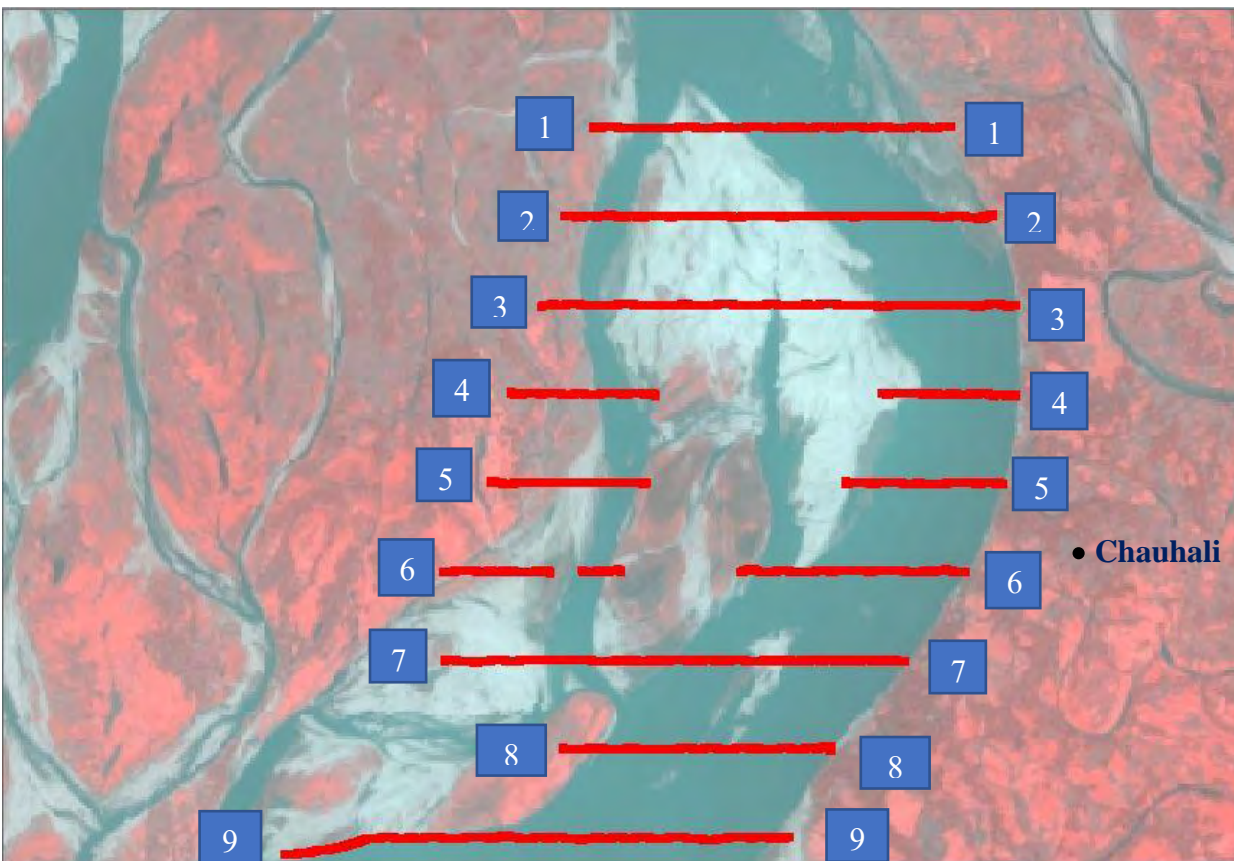
Figure 4.3: Cross section line of bathymetric survey for the study area in Jamuna river.

Cross section 4-4

Left bank

Right bank

Depth (m)

Distance (m)

Cross section 5-5

Left bank

Right bank

Depth (m)

Distance (m)
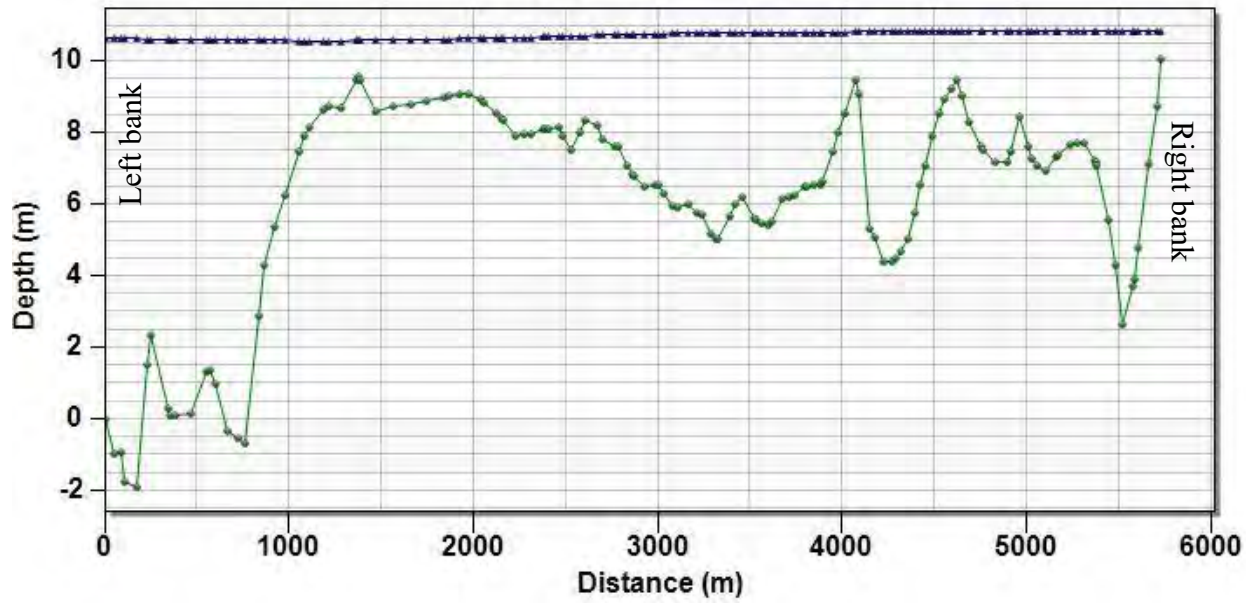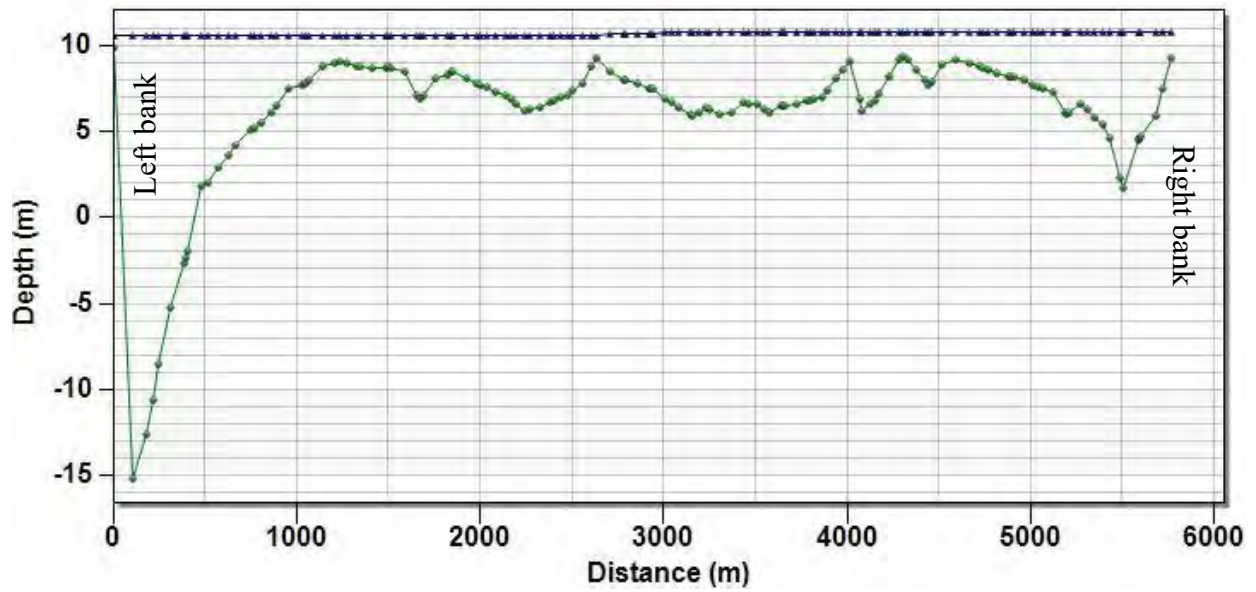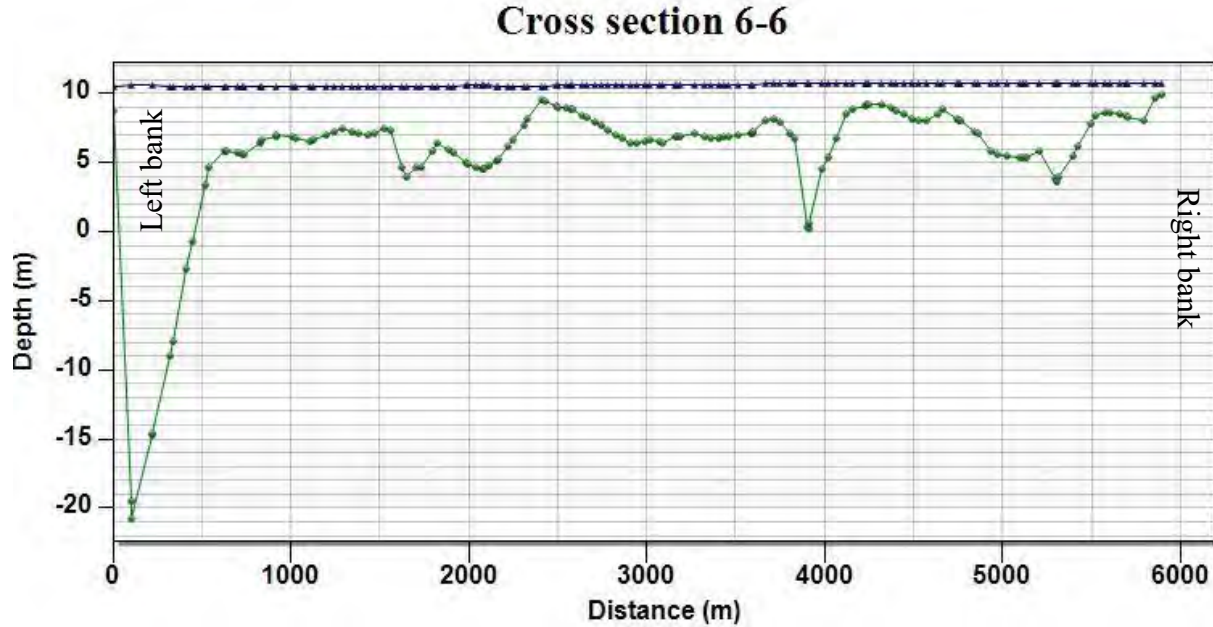
Figure 4.4: Demonstration of the cross-section in the Chauhali channel of Jamuna river

4.2.2 Data for slope stability analysis

To perform slope stability analysis, different data are required to find out the right outcome. Information about the soil layer near the bank and geotechnical properties of soil done by laboratory testing are collected.

4.2.2.1 Soil strata information

The formation of different bank strata and their properties is necessary data for slope stability analysis. Data are collected from BWDB. Borehole test and sieve analysis were performed to know the layer information. Soil properties such as cohesion and angle of internal friction are obtained from laboratory testing. The direct shear test is one of the methods to find out the shear strength parameters of soil. These soil properties are summarized in Table 4.5.

Table 4.4: Summary of laboratory test results of soil at 6m depth

Type of soil	Percentage retained on defined sieve	USCS Classification	D50	Angle of internal friction (°)	Cohesion (KPa)	Unit weight (gm/cc)
Gravel	0.00					
Coarse sand	0.13					
Medium sand	1.88	Sandy silt (ML)	0.028	29	6	1.66
Fine sand	31.31					
Silt size	49.96					
Clay size	16.72					
Colloid	0.00					

Table 4.5: Summary of laboratory test results of soil at 7.5m depth

Type of soil	Percentage retained on defined sieve	USCS Classification	D50	Angle of internal friction (°)	Cohesion (KPa)	Unit weight (gm/cc)
Gravel	0.00					
Coarse sand	0.03					
Medium sand	1.86	Silty sand (SM)	0.167	28	6	1.66
Fine sand	56.11					
Silt size	42.00					
Clay size	0.00					
Colloid	0.00					

4.3 Application of SMS and SRH-2D model for hydrodynamic analysis

Surface water modelling system (SMS) and SRH-2D are used for hydrodynamic modelling. The model uses SMS as pre-processor and post-processor and SRH-2D as a solver. SRH-2D is a two-dimensional sedimentation and river hydraulics module which is included in the SMS program. This software can generate flexible and hybrid mesh.
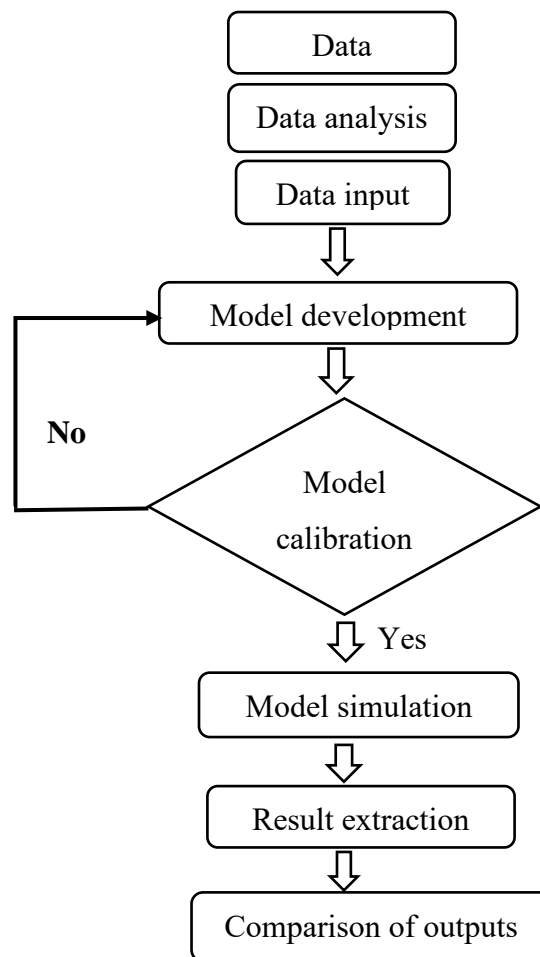
Figure 4.5 : Flow chart of hydrodynamic modeling

4.3.1 **Model setup**

There are many ways to build models in SMS. The process may vary with each project, but a suggested process is to:

i)   Import background images and data;

ii)   Setting up model domain;

iii)   Generate geometries such as mesh or grid;

iv)   Set up model parameters and simulation;

v)   Run the model simulation;

vi)   Analyze the simulation results.
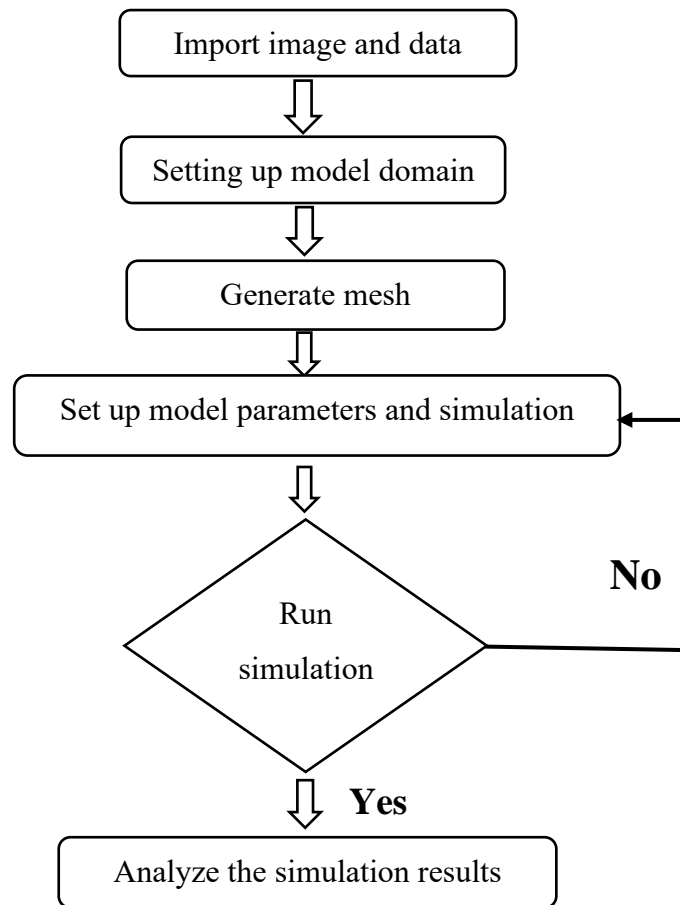
Figure 4.6 : Flow chart for building models in SMS

4.3.1.1 Use of satellite image as the background of the model domain

A good way to visualize the model is to import a digital image of the site for this study. A satellite image of Chauhali is used as a background image as a JPEG file. The image was georeferenced, or it can be done by SMS interface. Once the image is inside SMS, it is displayed in plan view behind all other data, or it can be mapped as a texture onto a finite element mesh or triangulated scatter point surface.

4.3.1.2 Setting up the Conceptual model domain

A conceptual model consists of a vector-based representation (lines and curves) of the situation being modelled. This includes the geometric extents, geometric feature definition such as channel definition such as channels or banks, the location of local forcing functions acting on the domain (such as inflow or water level boundary conditions). It does not include numerical details like elements. This conceptual model is usually constructed over a background image using feature objects in the map module.

- **Feature objects:** Feature objects in SMS include points, nodes, arcs, and polygons. Feature objects are grouped into sets called "coverages". One coverage is active at a time. The active coverage is displayed in a bolder font in the project explorer window, and objects in this coverage are displayed with specified display attribute. These objects can be selected and edited in the graphics window (Figure 4.7).
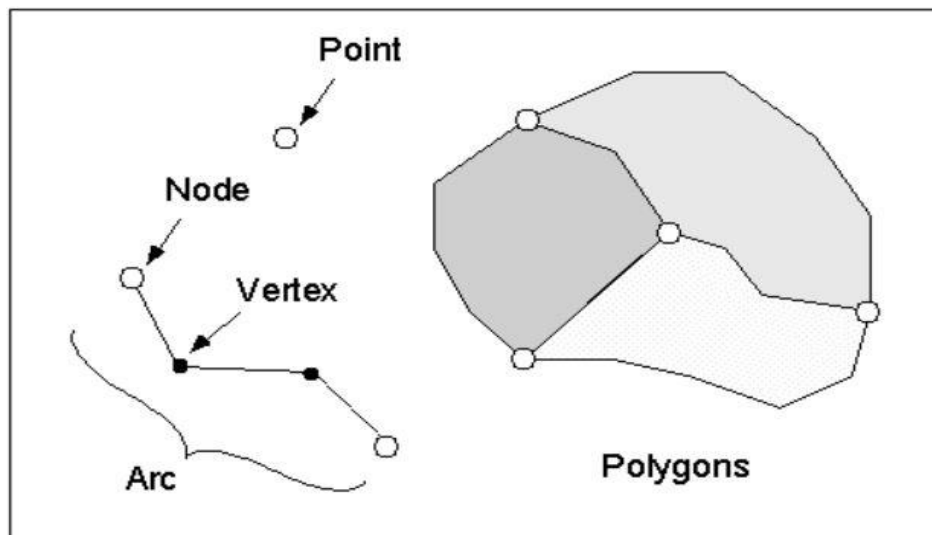
Figure 4.7: Feature objects

- **Creating feature arc:** A set of feature objects can be created to define topographically important features such as river channels and material region boundaries. Feature objects can be digitized directly inside SMS, converted from an existing CAD file (such as DXF or DWG), or they can be extracted from survey data (Figure 4.8).

4.3.1.3 Bathymetry data within the model domain

SMS includes a tool to work with, edit, view, and use surfaces. Most commonly, these surfaces represent physical surfaces such as the topographic land surface or a bathymetric surface beneath a water body. Such surfaces are created from surveys or observations and are stored either as unstructured points or regular grids. Scatter points are used to interpolate bathymetric data onto a grid for numerical analysis.

The model domain has been drawn with available scatter data, and the boundary of this domain has been demarcated using boundary values of these data. The lower portion of the model domain had been narrowed as there were an insufficiency of available data. Figure 4.8 illustrates the model domain with bathymetric data showing different boundary conditions.
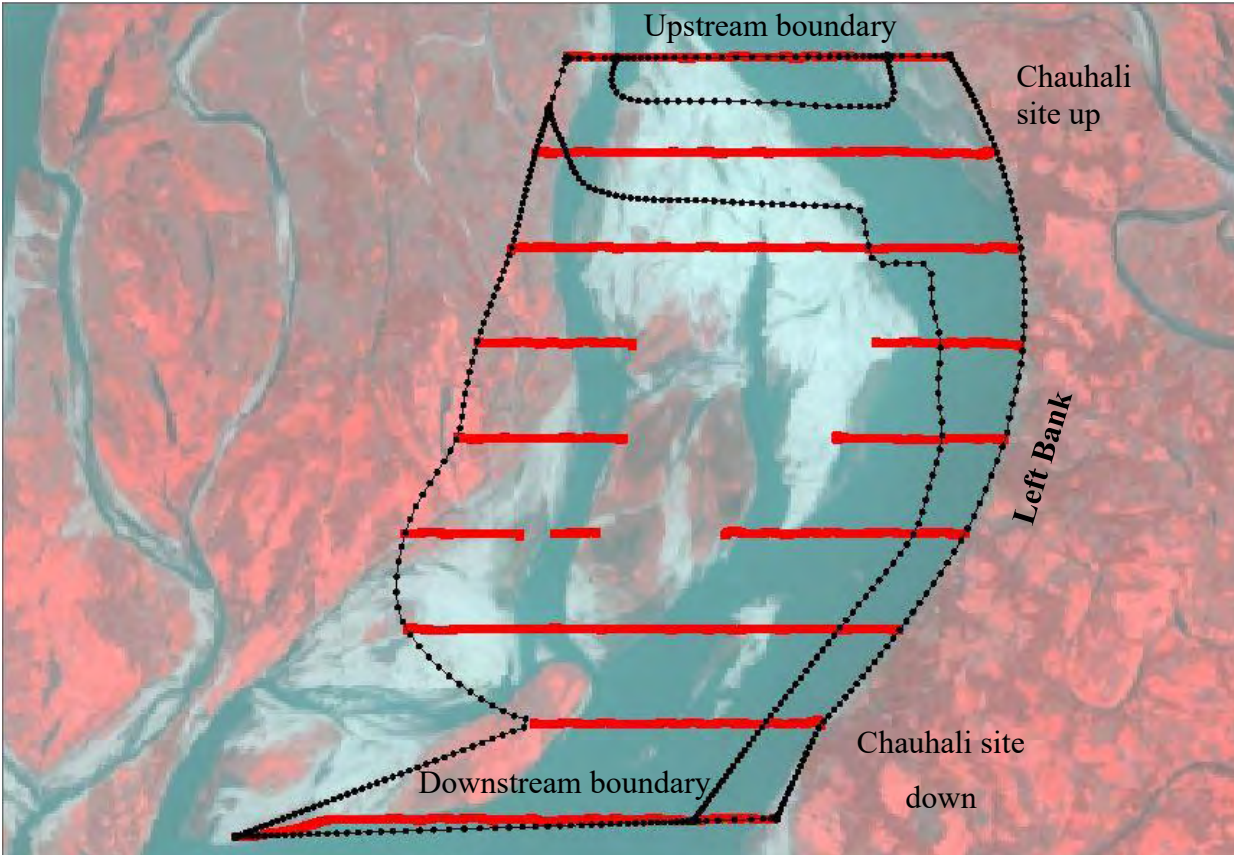
Figure 4.8: Hydrodynamic model domain

4.3.1.4 Mesh generation

A mesh consists of nodes that are grouped together to form elements. These nodes and elements define the computational domain of the numerical model. A numerical simulation required a geometric definition of its domain. For many geometric analysis codes, this geometric definition is a mesh (Figure 4.9).
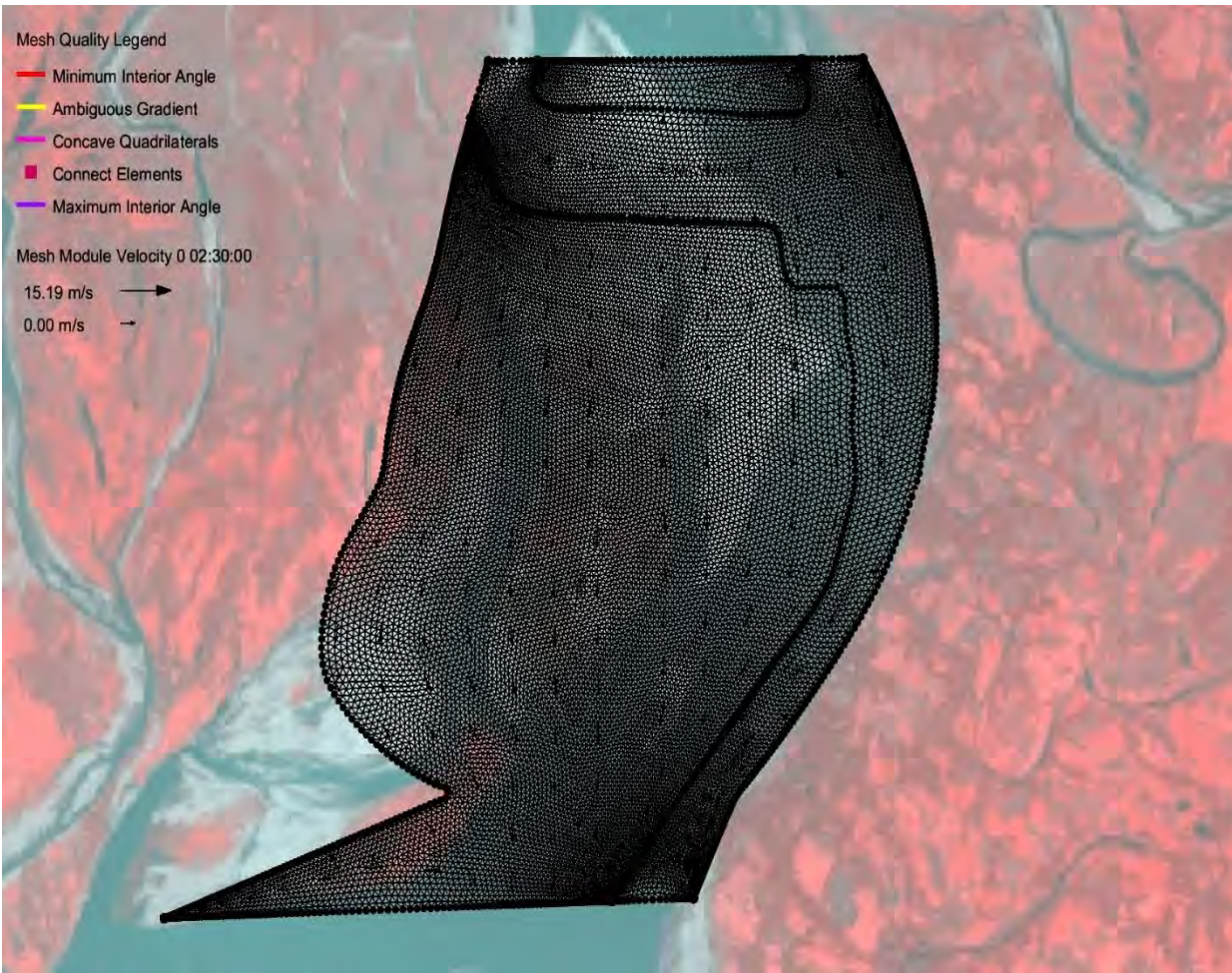
Figure 4.9: Generated model mesh for selected domain

4.3.1.5 **Mesh properties**

Automated mesh generation was preferred both for mesh generation as well as mesh revision to ensure the mesh generation can be replicated and preserved. A mesh consists of randomly spaced and positioned nodes connected to form elements or cells with three or four sides. The sides can be linear or quadratic. A quadratic form of mesh has been generated in this study. A mesh could also be referred to as an unstructured grid. The paving method was applied to generate the mesh. This method principally creates a triangle of various size based on the vertex distribution of the boundary arcs. SMS supports a patching approach for the generation of cells or elements in a region. The patch mesh method was applied to generate three- or four-sided regions to be created. Then, the mesh was edited by changing the meshing parameter in the conceptual model. The

number of elements in the mesh was 14810. The number of nodes was 7607. The model domain has a distance of about 8.210 km along the river bank. The number of triangular elements in the mesh was 14810. The unstructured grid is shown in the following Figure 4.10:
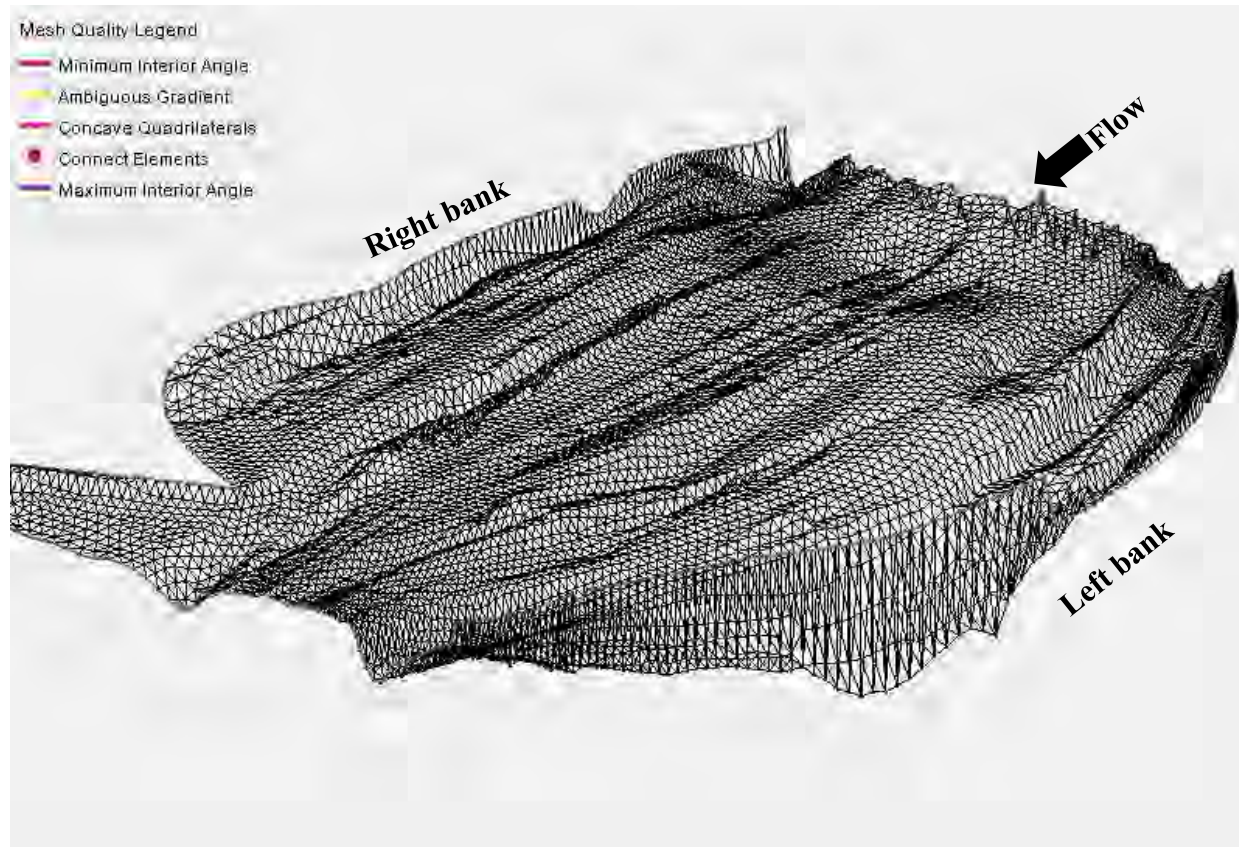
Figure 4.10: Mesh quality as unstructured grid

4.3.1.6 Saving file

When a file is saved, separate files are created for the map, scatter data, and data for numerical analysis. The project file(*.sms) is a binary file in HDF5 format that references the individual data file.

4.3.2 Boundary condition

It is necessary to use hydrological data at the model boundaries to simulate the hydrodynamic model. Boundary hydrographs at the Chauhali site up and down are shown in **Figure 4.11** and **Figure 4.12**. For this model, time-series data of discharge has been used as an upstream boundary condition, and the rating curve has been used as the downstream boundary condition (Figure 4.13).
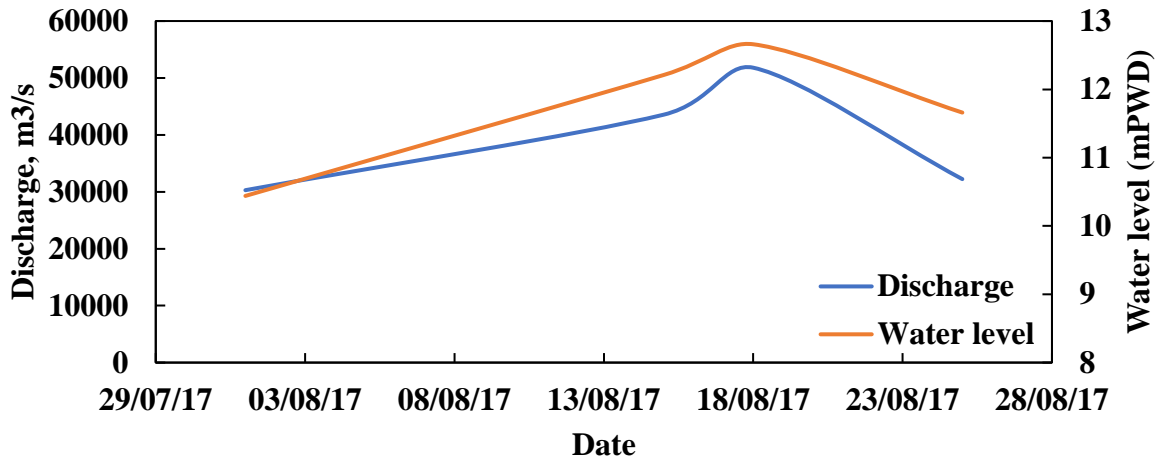
Figure 4.11: Discharge and water level boundary at Chauhali site up
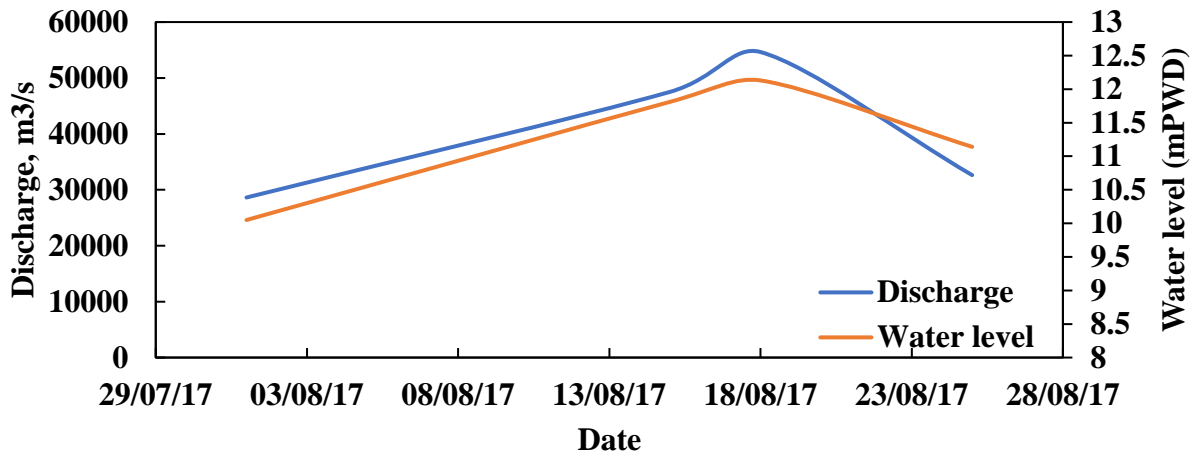
Figure 4.12: Discharge and water level boundary at Chauhali site down
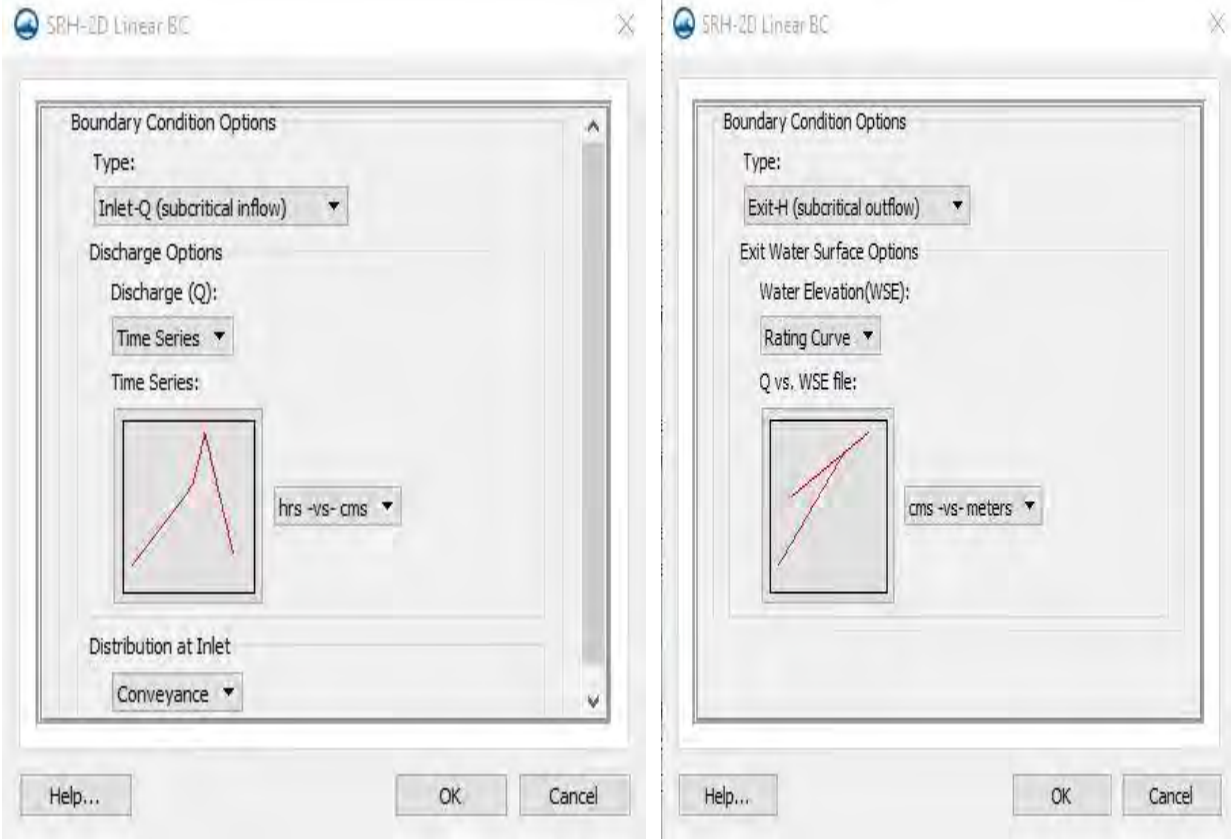
Figure 4.13 : Inflow and outflow boundary condition

4.3.3 **SRH 2D model control**

The model is simulated for a specified period. To determine the highest value of bank shear stress during the flow event, a short period of time of 720 hours was considered. The hydrodynamic time step has been set to 5 seconds for the simulations. The initial condition was automatic in SMS interface. Rigid bed simulation was done. Result output frequency was 0.1. In all the simulations, the parabolic turbulence factor is 0.7 for Jamuna river. The parameters used in the model domain shown in following Table 4.6:

Table 4.6: SRH-2D model control parameter

Simulation Description	Start time (hours)	Time step (seconds)	End time (hours)	Initial condition	Parabolic Turbulence	Result output frequency
Rigid_bed	0	5	720	Automatic	0.7	1

4.4 Empirical equations for estimation of Bank erosion rate

The evaluation of critical shear stress and erodibility is of primary importance for the modelling of riverbank erosion problems. Critical shear stress (τ_c) is the limiting shear stress caused by flowing water, above which, soil erosion is initiated. The erosion rate is expected to be negligible if the established shear stress is less than the critical shear strength. (Hanson, 1990a; Hanson et al., 2002; Osman & Thorne, 1988). The erosion rate for the fine soils in a river bed or bank of a river is usually assumed to be proportional to the excess shear stress as shown below (Hanson, 1990b; Hanson & Cook, 1997):

$$\varepsilon = k_d(\tau_a - \tau_c)^a \tag{4.1}$$

Where ε is the rate of erosion (m s^{-1}), k_d is the erodibility co-efficient (m^{3}Ns^{-1}), τ_a the developed shear stress at the soil boundary (Pa), τ_c is the critical shear stress (Pa) and a is the exponent generally considered to be 1.

There are several approaches to the determination of soil erodibility parameters. Due to several variables' influence, the erodibility parameters are difficult to quantify (Grissinger, 1982). Based on flume testing results, Smerdon and Beasley (1961) developed relationships of τ_c to various soil index properties, as shown in equations 17-19,

$$\tau_c = 3.54 \text{ x} 10^{-28.1D}{}_{50} \tag{4.2}$$

$$\tau_c = 0.493 \text{ x } 10^{0.0182P}{}_c \tag{4.3}$$

Where τ_c is the critical shear stress (Pa), D$_{50}$ is the median particle size of soil (mm), P$_c$ is the percentage of clay content (i.e. content of soil particles less than 0.002 mm in size), and PI is the plasticity index.

Julian and Torres (2006) established an empirical equation to estimate τ_c from the percentage of silt-clay (SC),

$$\tau_c = 0.1 + 0.1779 \text{ (SC)} + 0.0028 \text{ (SC)}^2 - 2.34 \text{ x } 10^{-5(SC)^3} \tag{4.4}$$

Unlike τ_c, empirical estimates of k_d the soil properties are not available ((Hanson & Temple, 2002). However, k_d can be given empirical estimates from known τ_c. Such empirical relations

between τ_c and k_d have been developed based on submerged JET results and are often inverse power laws (Hanson & Simon, 2001; Thoman & Niezgoda, 2008; Wynn et al., 2004). Different equations developed for k_d by different researchers are given below:

$$k_d = 3.1\,\tau_c^{-0.37} \qquad \text{(Wynn et al., 2004)} \tag{4.5}$$

$$k_d = 3.16\,\tau_c^{-0.185} \quad \text{(Karmaker & Dutta, 2011)} \tag{4.6}$$

$$k_d = 19.54\,\tau_c^{-0.547} \quad \text{(Semmad & Chalermyanont, 2018)} \tag{4.7}$$

4.5 Slope stability analysis

4.5.1 General

GeoStudio 2018 SLOPE/W software is used in this study to analyze slope stability. SLOPE/W has been designed and developed to be a general software tool for stability analysis. It uses the limit equilibrium method to compute the safety factor of earth slopes. Optum G2 is used here for finite element analysis. Mainly, six scenarios with different load combination were performed here to determine the cause of instability. These scenarios are briefly described in Table 4.7.

Table 4.7: Scenarios with different load combination

Scenarios	Different load combination
1	Surcharge load, confining load of water
2	Scouring of the bank at the toe, confining load of water
3	Surcharge load, confining a load of water, scouring of the bank at the toe
4	Slope protection load, confining load of water.
5	Slope protection load, confining load of water, surcharge load
6	Slope protection load, confining load of water, surcharge load, scouring of the bank at the toe.

4.5.2 Analysis with the limit equilibrium method

The comprehensive formulation of SLOPE/W makes it possible to easily analyse slope stability problems using a variety of methods. Ordinary method of slice, Bishop's method, Bishop simplified, Janbu's generalized method, Morgenstern-price method, spencer methods are most popular among limit equilibrium methods.

4.5.3 Calculations in SLOPE/W

In SLOPE/W, the critical circular slip surface and the corresponding factor of safety are computed using Morgenstern-price method, as the method is regularly used by consultants performing slope stability analysis. The Grid and Radius method is used to generate the critical circular slip surface and the corresponding factor of safety. The search area of the grid and areas are refined until the minimum obtainable value of the factors of safety is found to ensure that the critical slip surface is obtained. The entry and exit method are used to search for specific critical slip surface. A few simulations are presented to compare the values of the factor of safety, and the shape of slip surface from different methods of calculations, including the Bishop, simplified, Janbu, generalized, and Morgenstern-price methods.

4.5.4 Building the slope model by SLOPE/W

4.5.4.1 Defining analyses

A limit equilibrium analysis was carried out using the SLOPE/W software for the slope stability of the riverbank of Jamuna near Chauhali, Sirajganj. The Morgenstern-Price method and half-sine function were selected for analysis of slope stability. Pore water pressure condition is taken as piezometric line and staged water level drawdown analysis (Duncan et al., 1990). The analysis was done from right to left. The factor of safety distribution was chosen constant. The maximum number of iterations was taken as 100. The minimum slip surface depth was 0.1m, and the number of slices was 30.

4.5.4.2 Sensitivity of slice number

In order to verify the sensitivity of number of slices to be used in the stability analysis, slice number ranging from 10 to 150 has been chosen and the corresponding factor of safety have been computed. Results of the obtained factor of safety were standardized compared to its unit value. Plotting of standardized values of factor of safety against the number of slices is shown in Figure 4.14. It is seen from the figure that, as the number of slices increases, differences in the factor of safety decreases. However, Slice number greater than 30 becomes less sensitive in computing values of factor of safety and thus not significant.
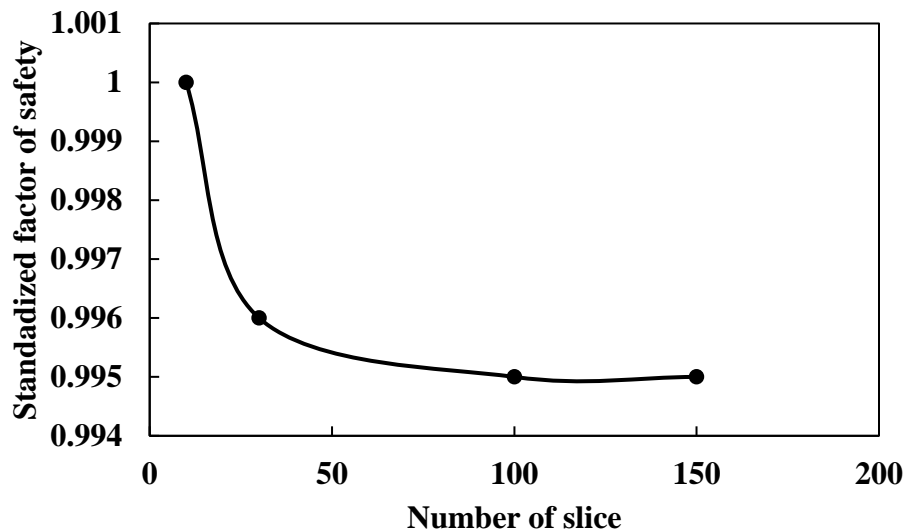
Figure 4.14: Deviation of factor of safety with change in number of slices

4.5.4.3 Defining geometry

The geometry was created by SLOPE/W software by defining the points in the software (Figure 4.15). The slope of the river bank was 3:1, which was considered for analysis. At first, the line was sketched according to the geometry of the bank to easily draw the region.
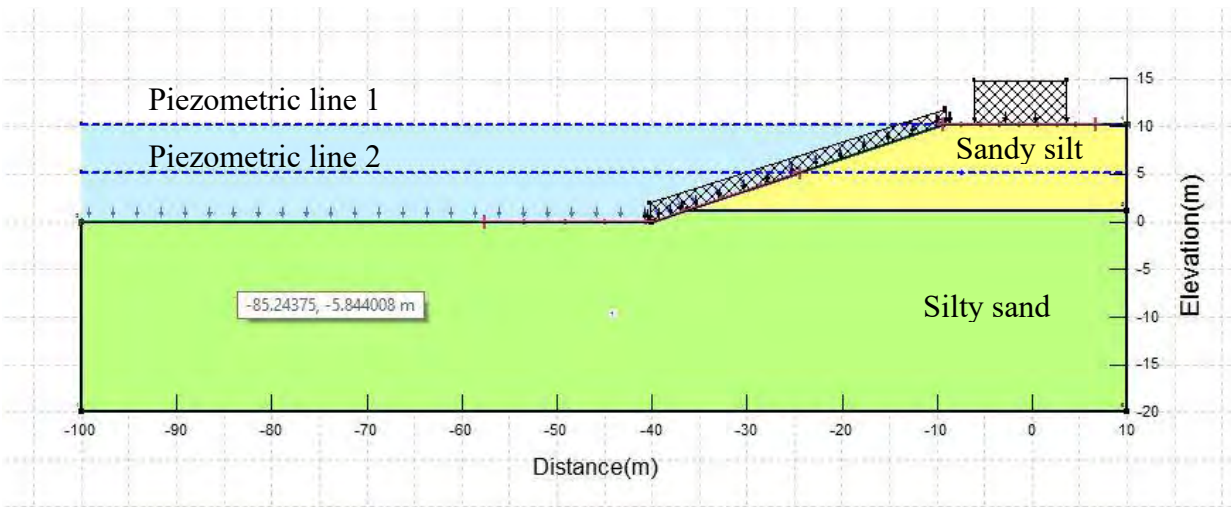
Figure 4.15: Geometry of riverbank in SLOPE/W software

4.5.4.4 Defining soil layers

The subbase soil of the Riverbank has been divided into two layers. It is considered that the upper layer consists of a sandy silt layer and lower is silty sand. These layers are considered based on Jamuna bank soil observed from borehole data. The soil layers are shown in Figure 4.15 with yellow and green colour, respectively.

4.5.4.5 Defining materials

The material properties of each bank layer were first defined and then assigned to the model. The Mohr-coulomb model was selected for each material. The input parameters needed for the Mohr-coulomb model are unit weight, the effective angle of internal friction, total angle of internal friction, total cohesion for non-freely drained material, the piezometric line before water level drawdown and the piezometric line after water level drawdown. The following Table 4.8 lists the material input values and interfaces shear strength used in the SLOPE/W analysis. Parameters in the table indicate that the values were determined by laboratory tests.

Table 4.8: Values of soil properties used in the model run

Layer	Unit weight (KN/m3)	Cohesion' (KN/m3)	Phi' (º)	Cohesion R (KN/m3)	Phi R (º)
Sandy silt	16.28	6	29	7	28
Silty Sand	16	6	27	7	25

4.5.4.6 Pore water pressure from water level

Generally, pore water pressure is developed due to the difference in water level between high and low water level condition. Measured high water level (HWL) was found as 10.2 mPWD, and low water level (LWL) was 5 mPWD. Figure 4.15 shows the high and low water levels, which indicate the piezometric line 1 and 2.

4.5.4.7 Defining surcharge load

In order to determine the external loads, the model has been carried out with various surcharge load and slope protection load. The range of the loads has been selected based on critical soil stability consideration. External load as a surcharge load was considered and defined in the model. The load values given in the model are given in the form of unit weight (KN/m3). The unit weight is converted into the pressure by multiplying with the depth of surcharge load applied. The range of surcharge and slope protection load considered in the model run are shown in Table 4.9.

Table 4.9. Range of surcharge and slope protection load considered in the model run

Surcharge load (KPa)	Slope protection load (KPa)
20	5
40	10
50	15
80	20
100	25

4.5.4.8 Slip surface for circular failure model

After the material input, pore water pressure and surcharge load were assigned, a slip surface was defined. The analyses were performed for the circular failure model. From the different method of defining the slip surface for the circular failure, the entry and exit method was selected. The problem with other methods is the visualization of the extents or the range of trial slip surface. This problem is solved by the entry and exit method because it specifies the region where the trial slip surface should enter the ground surface and where it should exit.

4.5.4.9 Verification and computation

When the slip surface has been specified, then SLOPE/W runs several checks to verify or optimize the data command in Tool's menu. When the verification is completed, and there are no errors, then SLOPE/W computes the factor of safety using the method of slices. The minimum factor of safety is obtained for that analysis, and its associated critical slip surface is displayed.

4.5.5 Analysis with finite element method

The strength reduction technique is used here for carrying out finite element analysis. Strength reduction factor/collapse multiplier less than 1 implies failure, while a value above 1 implies that the system is stable. Optum G2 is a finite element program(2D) for geotechnical applications. GUI, sequencing of operations, robust calculation core makes the software user-friendly.

4.5.6 Calculations in Optum G2

In principle, the geometry contour is first drawn, then soil layers and structural objects are added, then boundary conditions and then loading. When the geometry of the existing model is changed, the finite element mesh is regenerated. Optum G2 computes the global safety factor by the phi/c reduction technique. This method uses the progressive load number of steps. The incremental multiplier is used to denote the increment of the strength reduction of the calculation step at the beginning. The strength parameter is successively reduced automatically until all the additional steps have been conducted. The strength of interfaces is also reduced in the same manner. The last

step indicates a fully developed failure mechanism. If a failure mechanism is not fully developed, the calculation is repeated with a large number of additional steps.

4.5.7 Slope modelling by Optum G2

4.5.7.1 Defining Geometry

There are several options for drawing the geometry such as points, lines circles, arc, circle, rectangle etc. in Optum G2 software. Points can be drawn by direct input in the software. The geometry drawn was same as taken for SLOPE/W (Figure 4.16). The riverbank geometry was considered as standard.
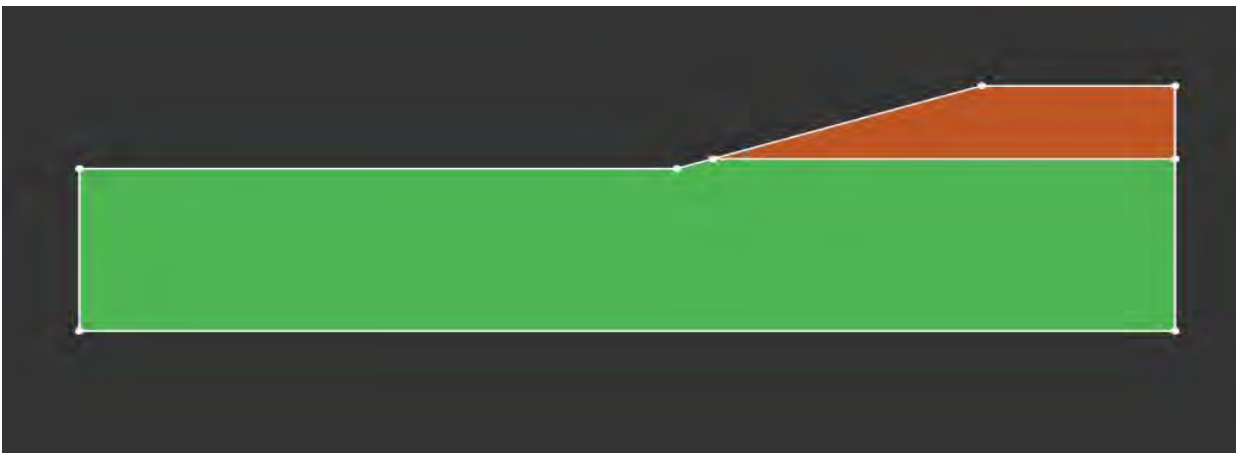
Figure 4.16: Geometry of riverbank in Optum G2

4.5.7.2 Defining material model

The basic Mohr-coulomb model was chosen. The input parameters include Young's modulus and Poisson's ratio as stiffness property of a layer, effective cohesion, effective frictional angle, unit weight, hydraulic conductivity. The associated flow was chosen during the analysis.

4.5.7.3 Assigning material

The material obtained through laboratory testing and from different literature and engineering judgement was taken as input values. These are given in following Table 4.10:

Table 4.10: Material properties for Optum G2

Material	Cohesion (KPa)	Frictional Angle (º)	Dry unit weight (γ_{dry}) (KN/m3)	Saturated Unit Weight(γ_{sat}) (KN/m3)	Hydraulic conductivity, k (m/day)
Sandy silt	6	29	16.24	16	1×10^{-5}
Silty sand	6	27	20	20	1×10^{-5}

4.5.7.4 Mesh properties

A triangular mesh element was chosen for robust analysis (Figure 4.17). It gives a very good result. The number of mesh element was taken as 1000. The iteration number was taken as three. Positive mesh adaptivity was chosen. Shear dissipation type adaptivity was taken into consideration.
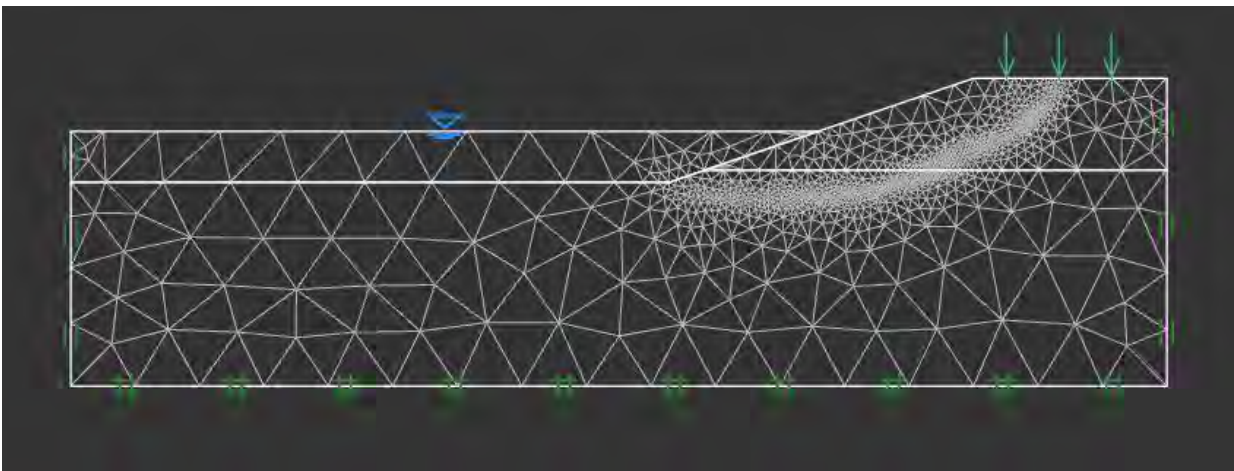
Figure 4.17: Generated mesh in Optum G2

4.5.7.5 Pore water pressure and boundary condition

Design low water level was fixed at 5 mPWD utilizing general phreatic level command. Standard fixities were given on both side and bottom so that groundwater flow does not occur at that boundary.

4.5.7.6 Analysis type

Optum G2 computes the global safety factor by the strength reduction method. The strength reduction analysis in Optum G2 proceeds by computing a strength reduction factor by which the material parameters need to be reduced in order to attain a state of incipient collapse. A factor greater than 1 implies a stable system, while a factor less than 1 implies that additional strength is required to prevent collapse. Strength reduction is only taken in solids. The analysis was run with two bands, upper and lower, to identify the range of strength reduction factor. The number of elements in the analysis was taken as 2000.

4.5.7.7 Sensitivity of element number

In order to verify the sensitivity of the number of elements to be used in the stability analysis, element number ranging from 500 to 4000 has been chosen, and the corresponding factor of safety has been computed. Results of the obtained factor of safety were standardized compared to its unit value. Plotting of standardized values of the factor of safety against the number of elements is shown in Figure 4.18. It is seen from the figure that, as the number of elements increases, differences in the factor of safety decreases. However, element number greater than 2000 becomes less sensitive in computing values of factor of safety and thus not significant.
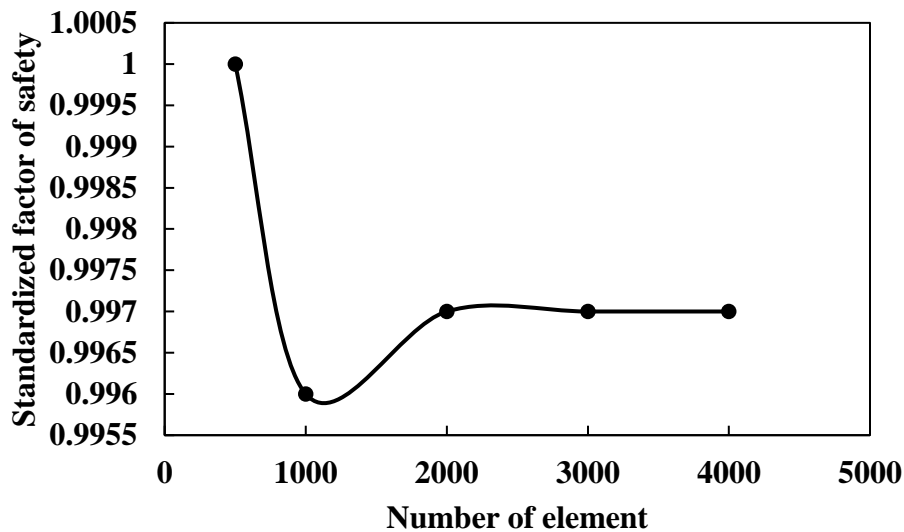

Figure 4.18: Deviation of factor of safety with change in number of elements

CHAPTER FIVE
ANALYSIS, RESULTS AND DISCUSSION

5.1 General

This chapter presents the results of the hydraulic and static load analysis on the river bank. The first part will show the flow properties and the estimate of boundary shear stress for the selected reach of the river bank using numerical modelling in SMS-SRH 2D. Then, considering the output results of hydrodynamic modelling, the correlation between flow properties and hydraulic load will be discussed. The second part demonstrates river bank stability analysis due to different hydraulic and static load conditions. There are manly six scenarios that include surcharge load, confining pressure of water, scouring and slope protection loads on the bank. SLOPE/W and Optum G2 have been used to analyze bank stability and represent different data. Based on stability analysis, specific design parameters such as cohesion, internal friction angle, the unit weight will be provided for the safe design of riverbank protection works. In the end, a case study has been done to investigate the stability of the Jamuna riverbank near Chauhali, Sirajganj.

5.2 Hydrodynamic model results

5.2.1 Model calibration

It is customary to calibrate the model before making any predictions using the model so that the reliability of the predictions can be made as much as perfect. Model calibration is the process of estimating model parameters by comparing model predictions (simulated output) for a given set of assumed conditions with observed data for the same conditions. Figure 5.1 shows the simulated water elevation on 15 August 2017. In this study, model has been calibrated by using the Chauhali site up and down boundary on August 2017 as shown in Figure 5.2 and Figure 5.3.
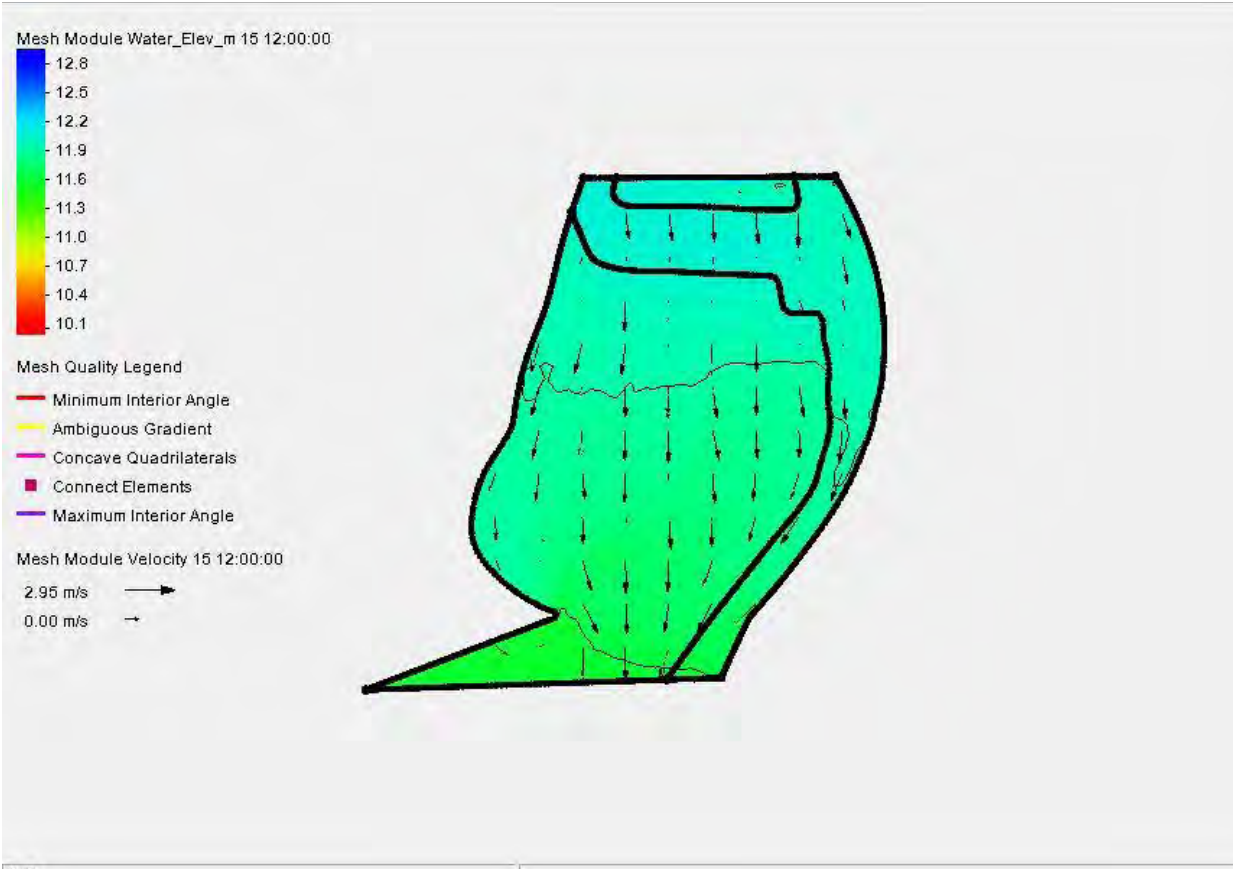
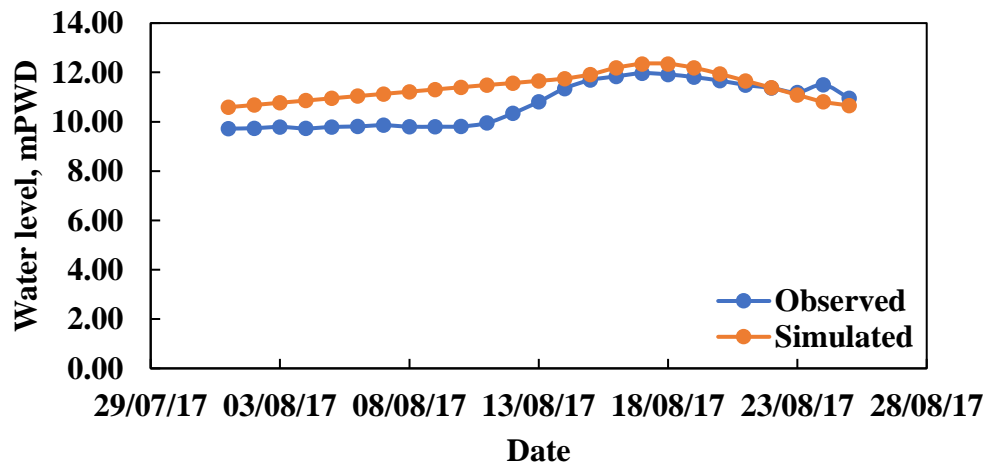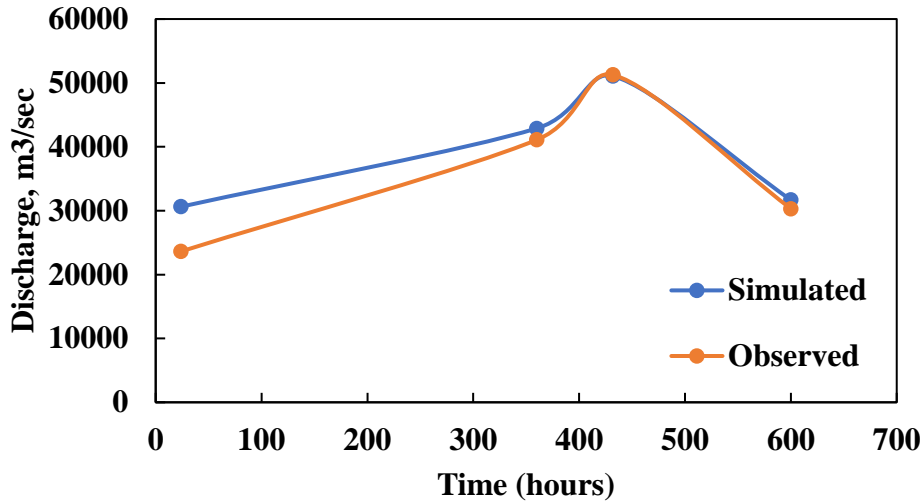**Figure 5.1: Simulated water elevation on 15/08/2017**

Figure 5.2: Water level calibration at Chauhali channel

Figure 5.3: Discharge calibration at Chauhali channel on August 2017

5.2.2 Hydrodynamic calibration

Hydrodynamic calibration is done with a rigid bed model. While calibrating a model, the goal is to calibrate the model so that computed values from the model fall within the confidence intervals of the observed field data for all measurements. At times, this is different, and personal direction is required to determine when the model has been sufficiently calibrated. The parameter which contributes to adjusting the hydrodynamic imbalance or fine-tuning the numerical models in the hydrodynamic field in SMS-SRH2D is mainly roughness (manning's n). Number of trial simulations were carried out to verify the selection of n, and finally, n=0.015 has been fixed as initial manning's value. The reason for using the limiting value of the manning's factor is to control the extreme roughness of the model domain.

5.2.3 Effect of hydraulic shear stress on riverbank stability

Hydrodynamic modelling is performed to elucidate two key concepts, flow pattern and near bank hydraulic shear stress. The flow pattern of the selected reach of Jamuna river is mainly, governed by the interchannel bar situated at the medial portion of the river, which becomes submerged during high flow event. This bar forces the flow to move along the bend of river bank, causing

72

high hydraulic load hitting on the bank. Some previous studies have highlighted, how the main flow can become separated from the channel boundary of the outer bank of sharply curving river (e.g., Rinaldi et al. (2008), Ferguson et al. (2003); Hodskinson (1996); Hodskinson and Ferguson (1998)).

Figure 5.4 shows simulated flow pattern and velocity magnitude on selected domain of Jamuna River. The velocity near the bank is higher than the other section of the channel, causing high water stress on the left bank.
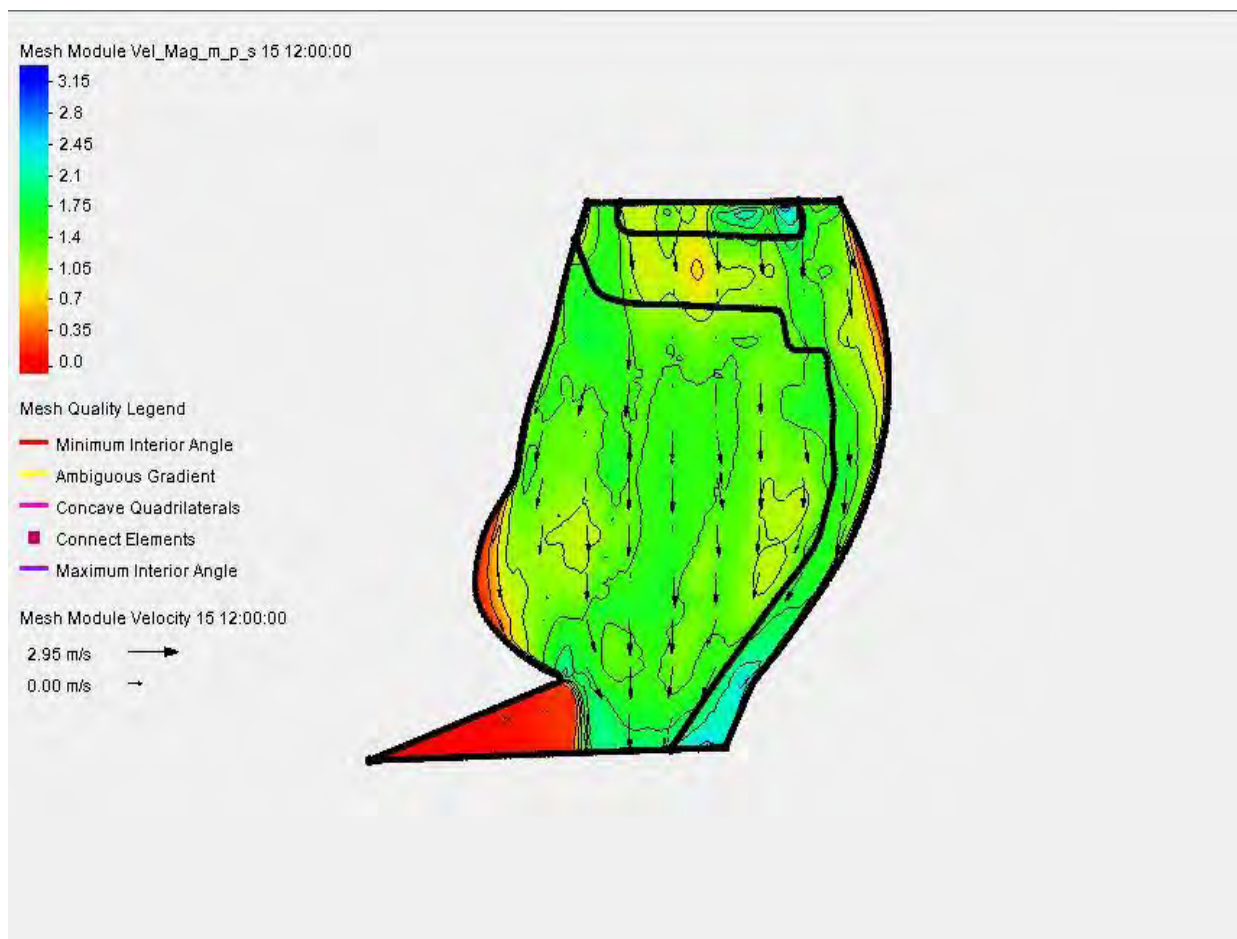

Figure 5.4: Simulated flow pattern

Figure 5.5 demonstrates the boundary shear stress distribution along the bank from the numerical analysis. It is clear from the figure that the hydraulic load in the form of bank shear stress plays an important role in bank instability.
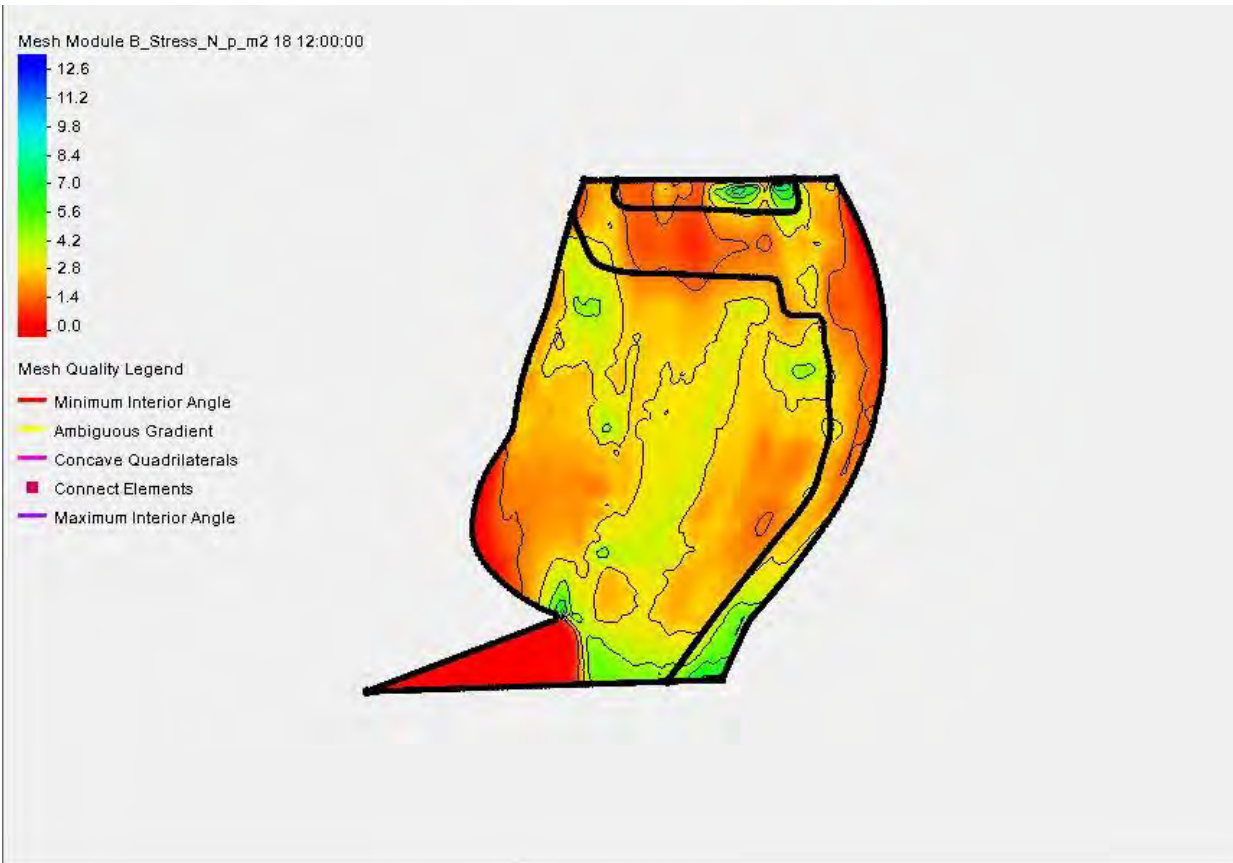

Figure 5.5: Simulated boundary shear stress indicating high flow stress near the bank.

Shear stress distribution along the river bank is shown in Figure 5.6. The result of numerical modelling shows that shear stress increases from the top of the bank to the inner part of the river and becomes maximum at the bank toe. So, evidently, shear stress is going to be the highest at the bank toe. Similar results have also been found in previous studies (Duong Thi & Do Minh, 2019; Luppi et al., 2009). They showed that relatively high shear stresses at the bank toe made the bank erodible.
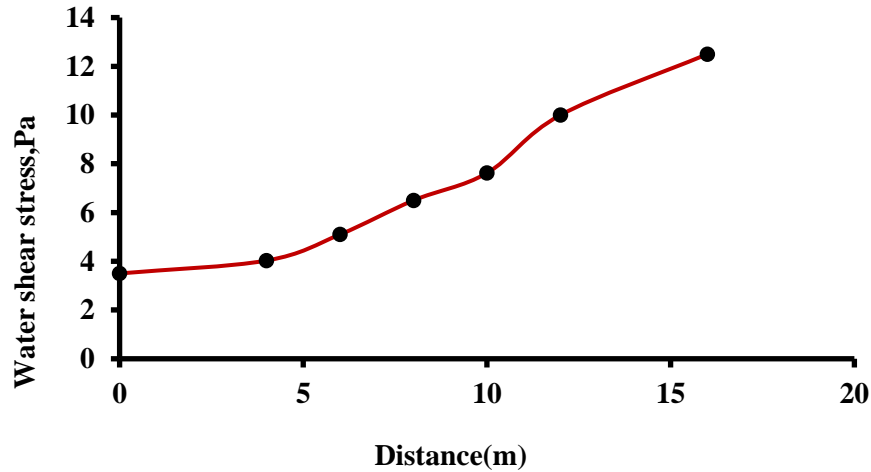
Figure 5.6: Variation of bank shear stress with distance from bank face

The riverbank consists of two layers of soil. The upper layer is made of sandy silt. The percentage of silt in the upper layer is 49.96%. The lower layer consists of silty sand, where the percentage of silt-clay is 42%. The particle size distribution curve of each layer is given in Figure 5.7 and Figure 5.8, respectively. Soil erosion is closely related to soil particle content. The silt soils found along the Jamuna river has high erodibility. Soil diameter corresponding to 50% finer, D_{50} value is 0.028 mm and soil unit weight is 16 KN/m3.
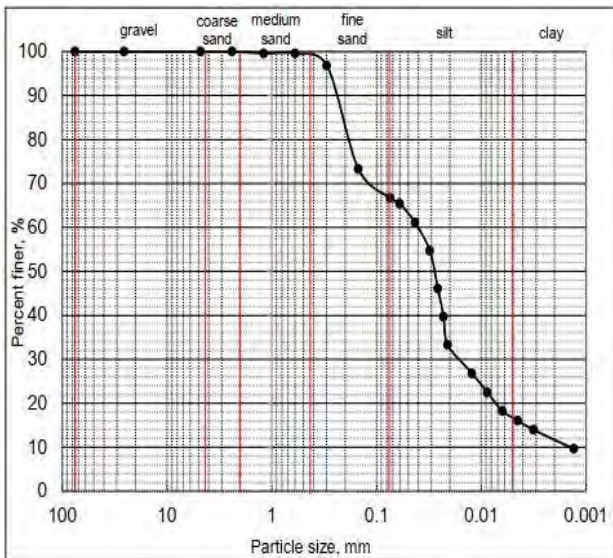
**Figure 5.7: Particle size distribution of upper layer soil**
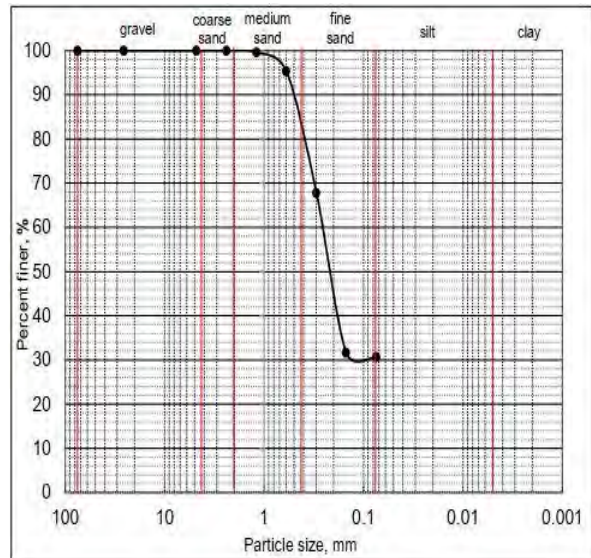
Figure 5.8: Particle size distribution of lower layer soil.

Critical shear stress, τ_c and erodibility co-efficient, k_d, in Table 5.1 are computed from (eq. 17), (eq. 18), (eq. 19) and (eq. 20), (eq. 21), (eq. 22), respectively. Then, the values of τ_c and k_d are averaged. Semmad and Chalermyanont (2018) found the range of τ_c (7.92~20.93) Pa for upper bank and (1.43~16.88) Pa for lower bank. In this study, computed τ_c value is 8.91 for upper and 6.34 for lower bank, which is within range.

Table 5.1. Estimation of erodibility parameters with empirical formulae

Layer	Computed τ_c (Pa)			Average τ_c	Computed k_d (Cm³/N-s)			Average k_d
	D$_{50}$ (Eq. 17)	P$_c$ (Eq. 18)	SC (Eq. 19)		Wynn et al. (2004) (Eq. 20)	Karmaker and Dutta (2011) (Eq. 21)	Semmad and Chalermyanont (2018) (Eq. 22)	
Upper	2.25	2.23	22.26	8.91	1.38	2.11	5.91	3.1
Lower	0.57	0.99	17.47	6.34	1.57	2.24	7.11	3.64

The variation of erosion rate with water-induced shear stress is shown in Figure 5.9. For both the upper and lower layer of the riverbank, the erosion rate increases with the increase of water-induced stress. The graph shows that the lower layer of the riverbank is more erosive than the upper layer. Therefore, fluvial erosion can be considered as one of the possible reasons for riverbank erosion.
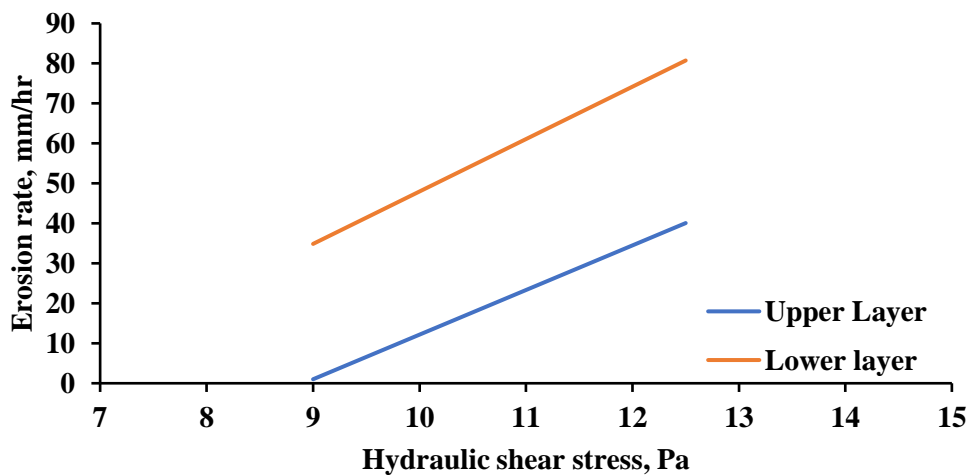
Figure 5.9: Relationship between soil erosion rate and hydraulic shear stress

To relate these erodibility parameters to the resistant or erodible nature of the river bank, a logarithmic plot between the critical shear stress and erodibility co-efficient is shown in Figure 5.10, as proposed by Hanson and Simon (2001). This indicates that riverbank soils are mostly in the category "very erodible".
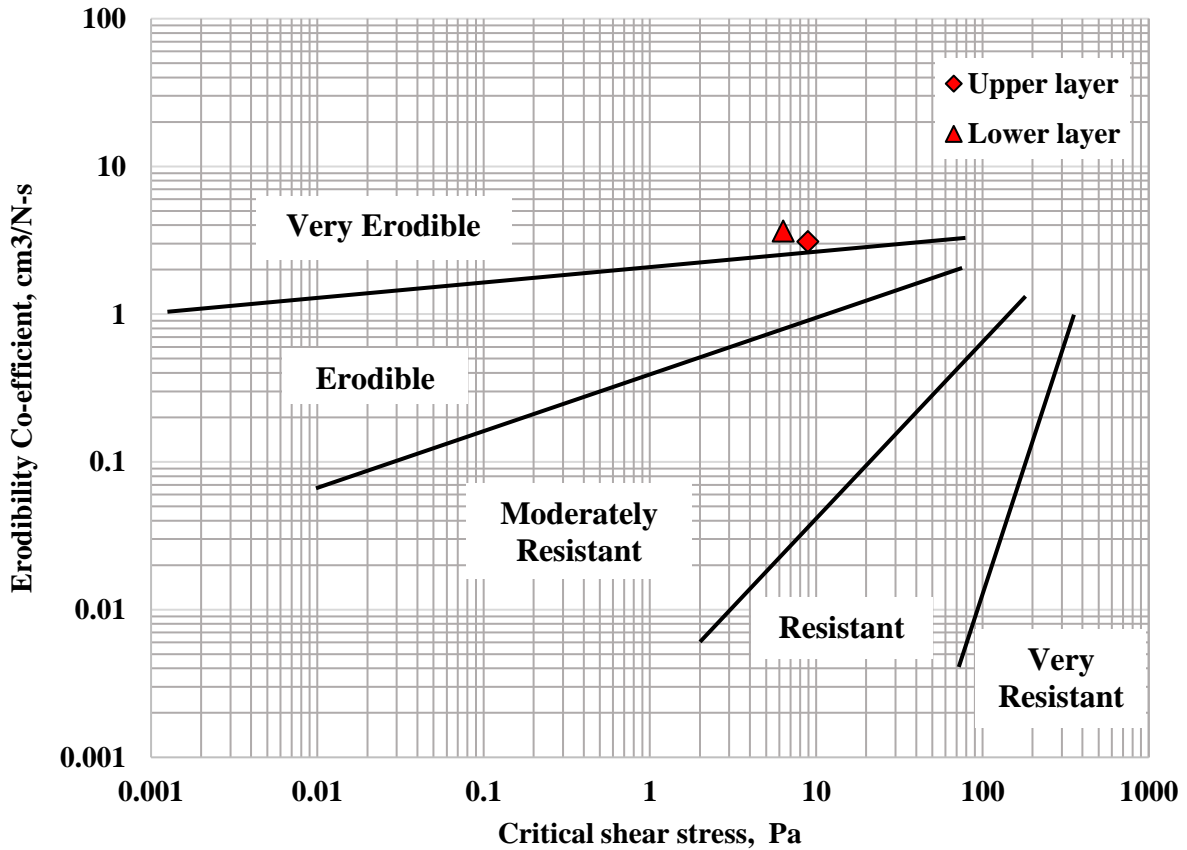

Figure 5.10: Classification of riverbank soil based on erodibility parameters (after Hanson and Simon (2001))

## 5.3   Riverbank stability analysis with limit equilibrium method

Slope stability analysis was performed, considering mainly six scenarios. Each scenario represents different load combination with undercutting at the toe, surcharge load, slope protection loads and pore water pressure. Sudden or water level drawdown can result in riverbank collapse (Liang et al., 2015). For this research, a drawdown analysis is performed from 10mPWD to 5mPWD water level after the main flow occurrence. Limit equilibrium method is used to perform the analyses by Geoslope product, SLOPE/W. Then, the result is verified by finite element method using Optum G2.

5.3.1   Scenario 1: Stability analysis with surcharge load and pore water pressure

Figure 5.11 (a) shows that the factor of safety is 1.453 when surcharge load is 20 KPa. This indicates a stable slope as FOS is above unity. Figure 5.11 (b) indicates a factor of safety below unit value when the surcharge load is 80 KPa. Hence, the slope becomes unstable. It is found that factor of safety decreases with increasing value of surcharge load. This is because the surcharge load increases the driving force, and the resistance of the soil is lower than that amount. As a result of this, the slope drives down, causing mass collapse. Before drawdown, the piezometric line is fixed at 10 mPWD. After drawdown, the line is dropped to 5 mPWD at design low water level. Effect of pore water pressure negatively influences the stability of riverbank, shown by several studies done before (Casagli et al., 1999; Fox et al., 2007; Rinaldi et al., 2004; Simon & Collison, 2001).

80 KPa

78
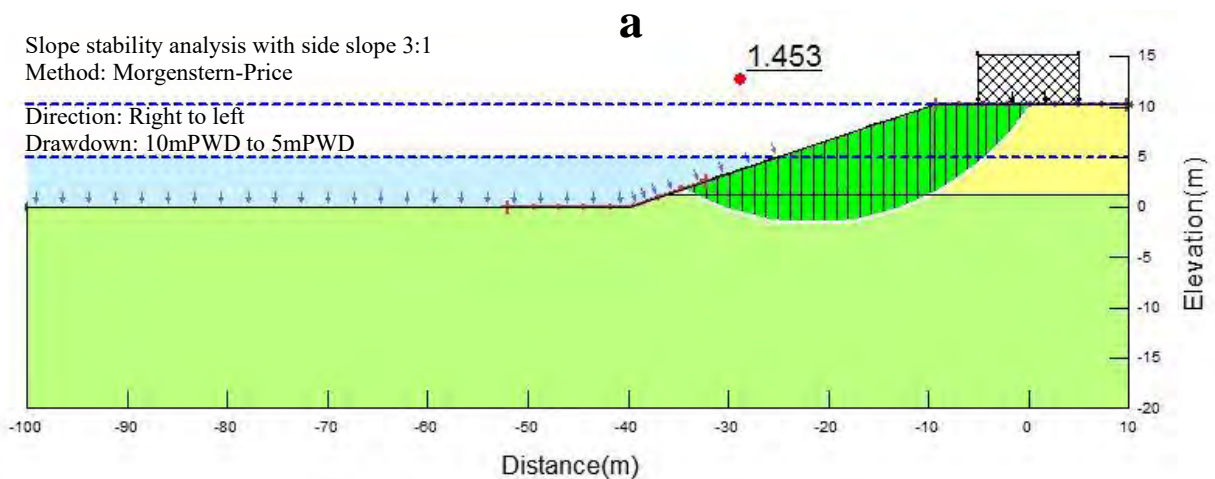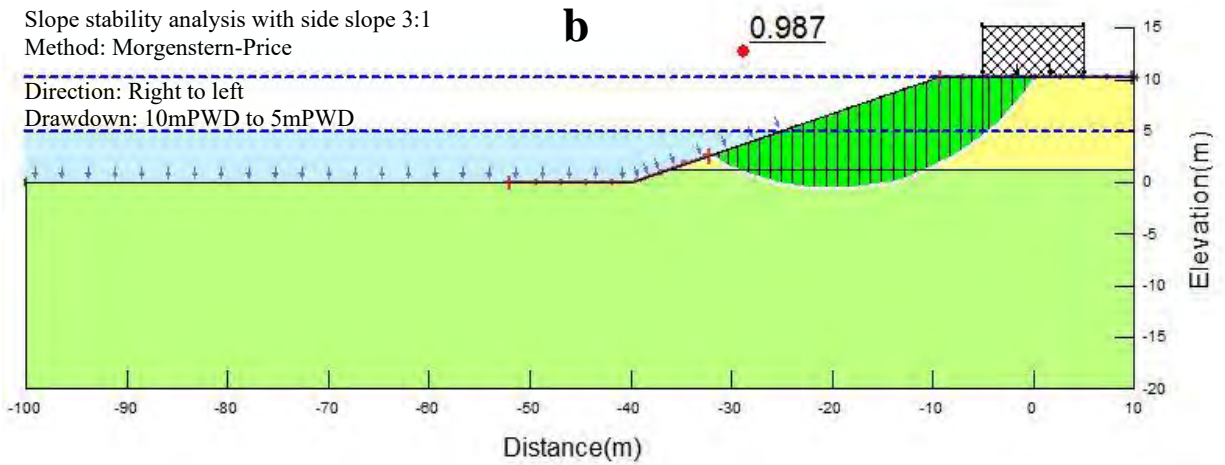
Figure 5.11: Illustration of slope stability analysis with surcharge load and pore water pressure

If different surcharge load is taken into consideration, a decreasing trend of the factor of safety is found with increasing load value. This is shown in Figure 5.12. From the figure, it is clear that when surcharge load is above 75 KPa, then the initiation of slope failure occurs.
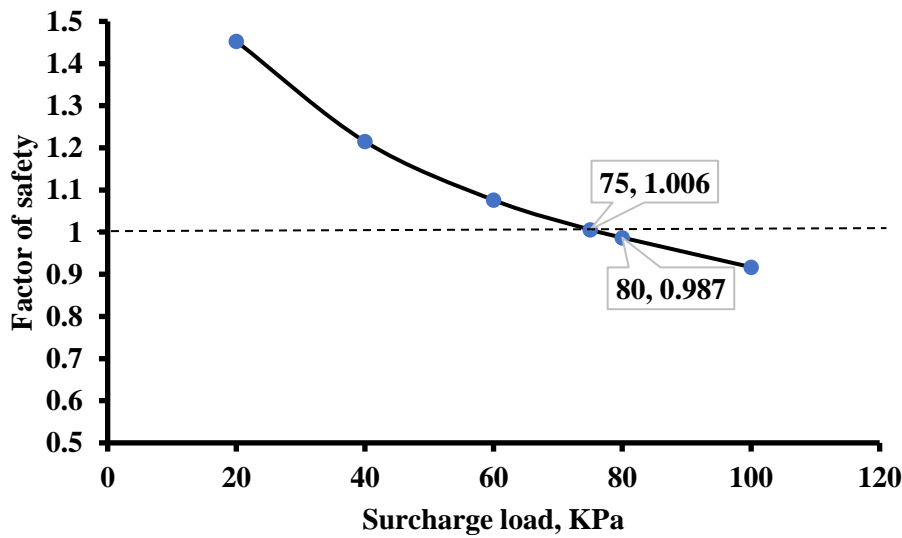
Figure 5.12: Variation of the factor of safety with a different value of surcharge load

Duong et al. (2014) performed a similar analysis with surcharge load greater than 50 KPa by building a house 50m away from the cohesive bank of Red River, Hanoi. They considered a steep slope of the riverbank (2H:1V). In the present study, the surcharge load was kept 4m distant from the bank face with 3:1 slope. From Figure 5.13, it is seen that magnitude of surcharge load causing river bank failure increases with an increase in bank slope. So, the obtained result varied with the result of the study mentioned above as bank slope and position of surcharge load was different.

Figure 5.13: Variation of surcharge load with change in slope for initiation of bank failure

5.3.2   **Scenario 2: Stability analysis with scouring at toe and pore water pressure**

Figure 5.14(a) indicates the bank of the river if no undercutting takes place. The safety factor observed was 1,790 after piezometric line drawdown from HFL 10 mPWD to LWL 5 mPWD. The safety factor decreased to 1.138 when the scour depth was considered to be 5 m, as shown in Figure 5.14(b). This is because when there is a cut below the slope, resistance to force is suddenly reduced, and failure occurs. As the soil in the bank material is very fine, it appears to collapse when there is no support behind it. The bank material is mainly sand and silt. So, the cohesion between the soil particles is very negligible. The soil grains have very little adhesive properties to prevent failure. Guo et al. (2018) found that non - cohesive soil subjected to high velocity eroded water

levelly than other types of soil. Figure 5.14(c) shows an unstable bank. The safety factor falls to 0.772 when the scour depth at the toe during the flow event is 10 m. As the factor of safety is below unity, the bank fails underwater level drawdown. The red portion in the figure is a possible failure zone where a mass failure can occur.
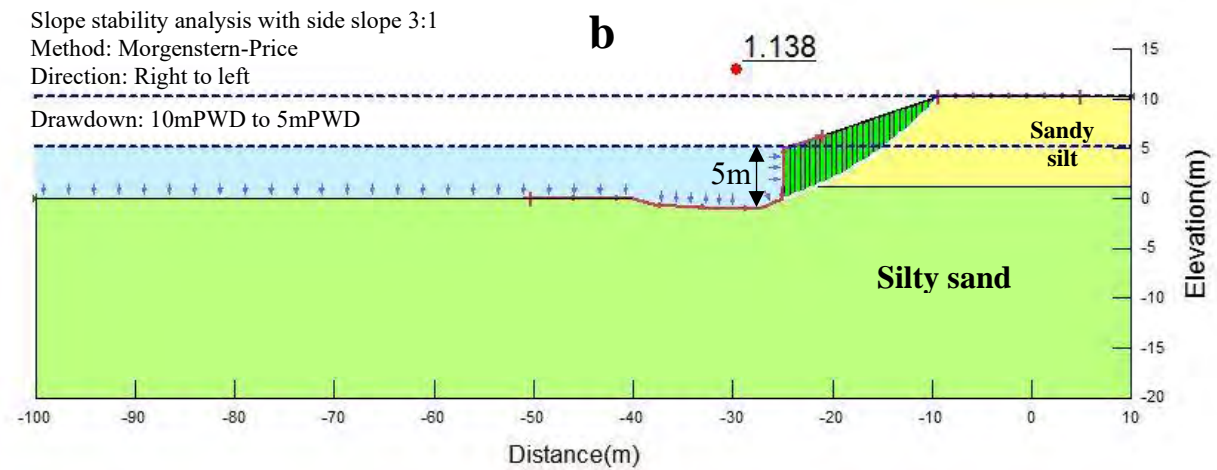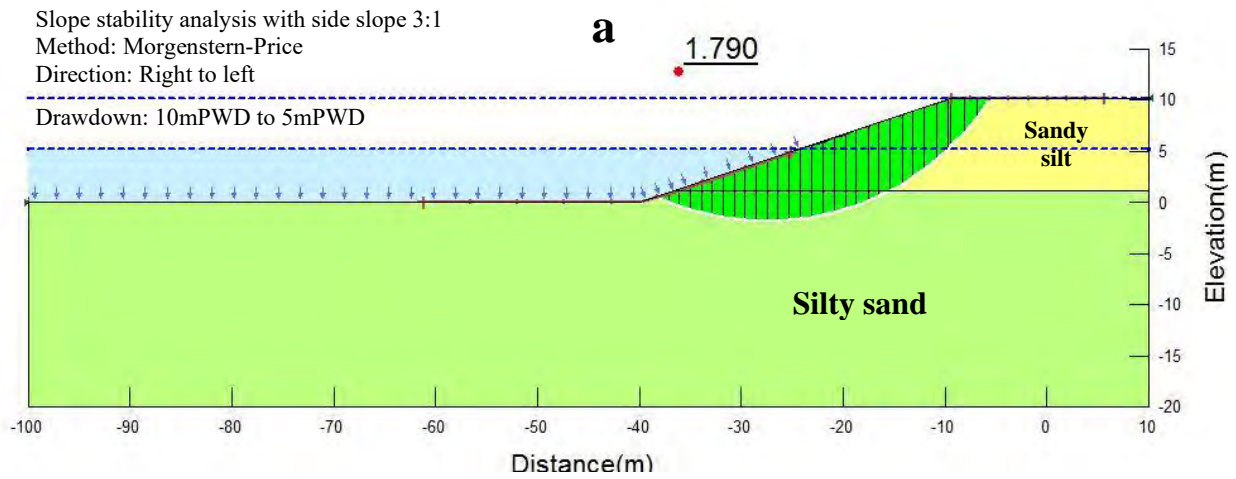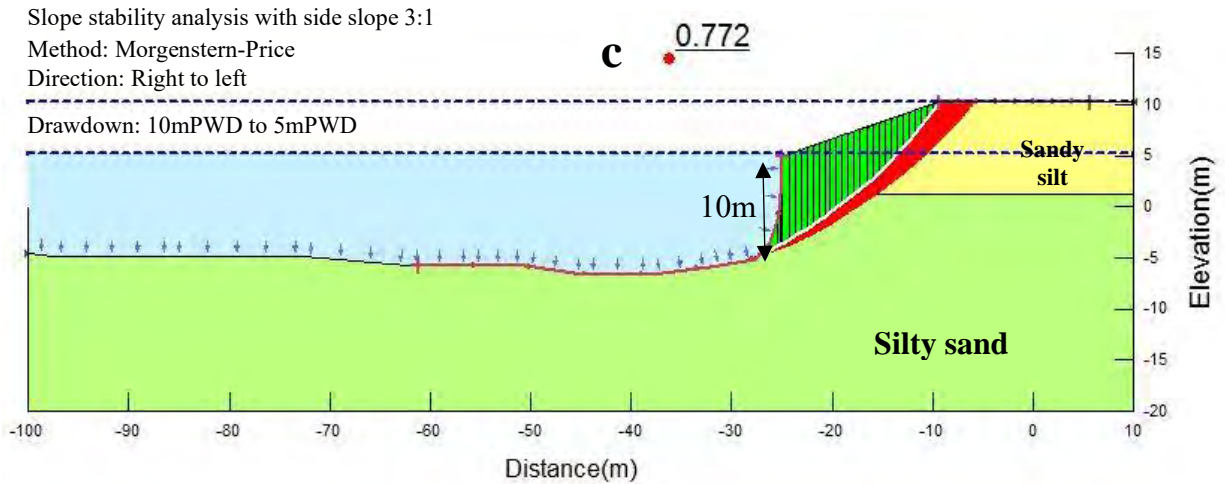
Figure 5.14: Illustration of slope stability analysis with scouring at the toe and phreatic pressure. **a**. analysis with no scouring b. analysis with scouring on the verge of failure c. scoured toe with bank failure.

Figure 5.15 shows that the safety factor decreases when the toe is scoured. As can be seen from the graph, FOS goes below the unit when the scour depth is 7 m. At this stage, fluvial erosion starts, which cannot be realized from outside (i.e., riverbank).
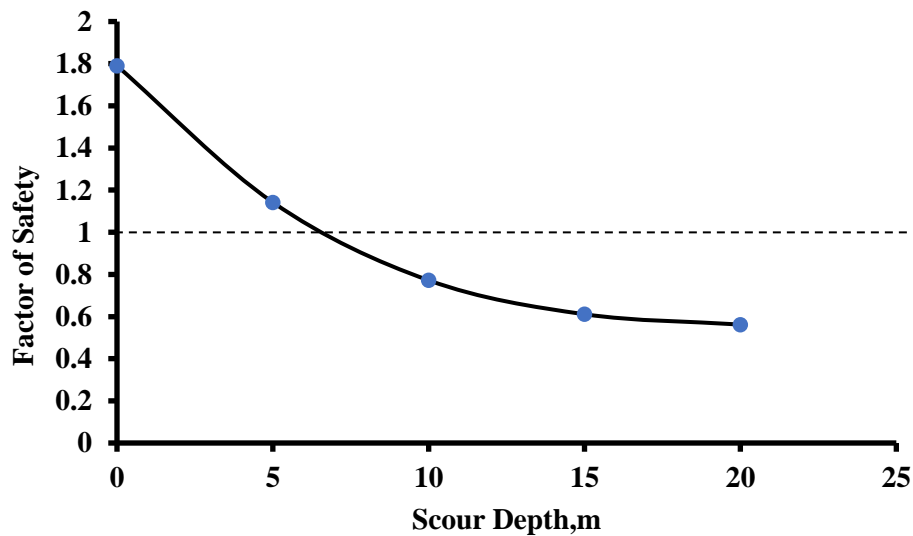

Figure 5.15: Variation of factor of safety with different scour depth.

5.3.3 Scenario 3: Stability analysis combining scoured toe and surcharge load

The analysis is carried out to determine the impact of the surcharge load on the safety factor when an established scour at the toe is present. The scour depth is increased gradually from 5m to 10m. In addition, the surcharge load is increased slowly at a specific scour depth. This is done to determine the combined effect of overload and toe scouring on FOS.

Figure 5.16 indicates that the river bank is unstable when the scour depth is 5 m, and the surcharge load is greater than 40 kPa near the bank. The safety factor observed was 0.971 for an additional load of 45 KPa, which was lower than the level. This indicates a failed bank. While the surcharge load decreased to 40 kPa, the safety factor changed to 1.001, and the failure began from 40 kPa to further increase the load. Therefore, the safety factor of 50 KPa surcharge load was 0.946. The critical load is therefore 40 KPa when the depth of the scour is 5 m. From Figure 36, v8\] KPa was seen as the critical surcharge load to fail the bank without any scouring impact. If the toe is scoured up to a depth of 5 m, the surcharge load reduces to 45 KPa. If an existing toe scour exists, less surcharge load is required to fail the bank.
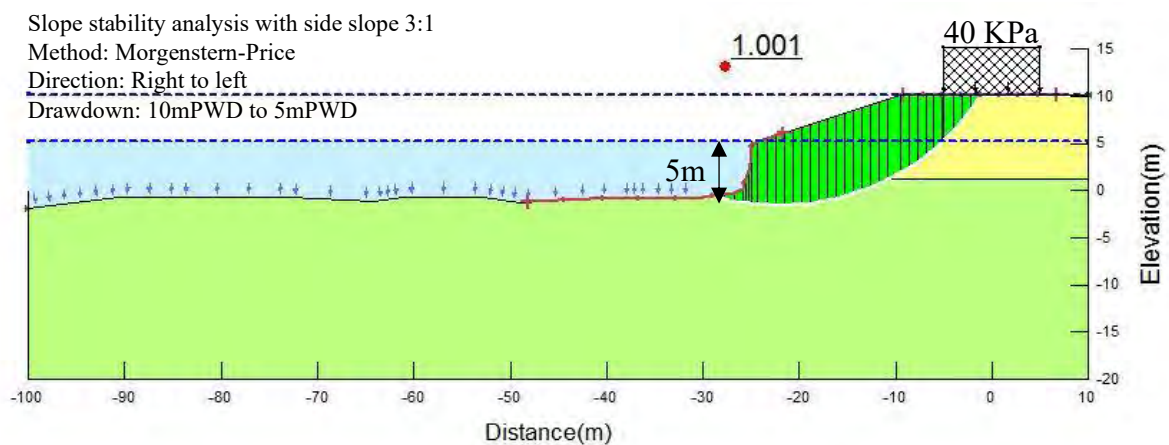
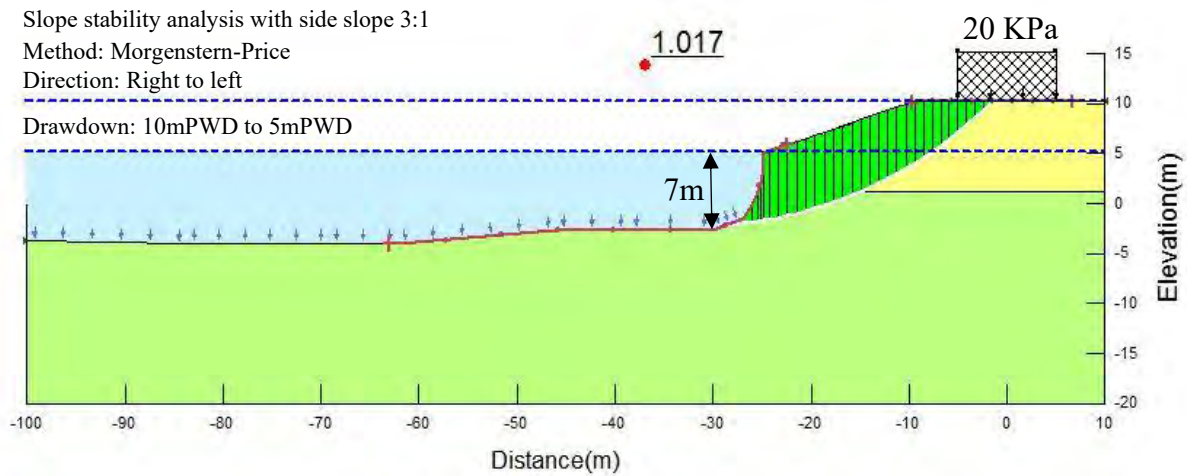**Figure 5.16: Effect of surcharge load when scour depth is 5m.**

Figure 5.17 shows a decreasing trend in the FOS value with an increase in the value of the surcharge load when the toe is cut, and the scour depth is 5 m. From the graph, it can be seen that the critical load is between 40 and 45 KPa. The Dash line indicates the safety line. All values below this line are responsible for failure.
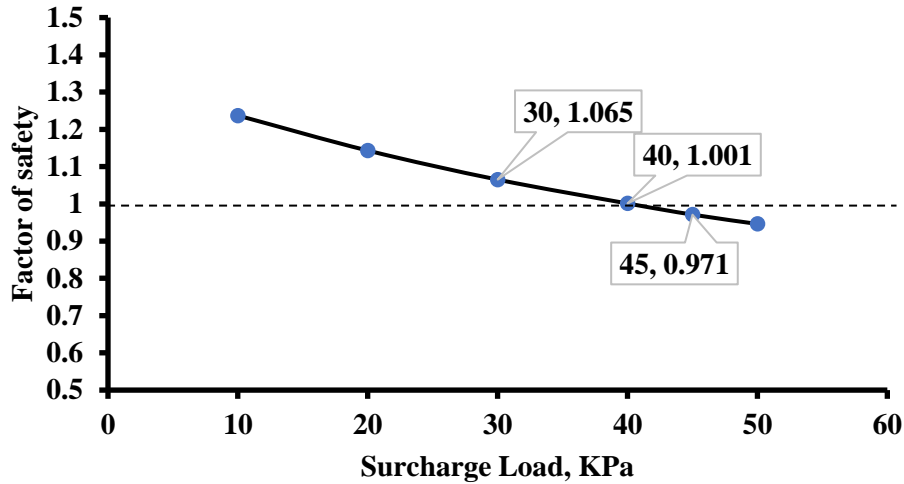
Figure 5.17: Variation of FOS with surcharge load when scour depth is 5m

Figure 5.18 indicates that when the scour depth is 7 m, 20 KPa surcharge load makes the bank at the edge of failure. This is the critical load that causes failure. As a result, when the scour depth increased from 5 m to 7 m, the critical surcharge load decreased from 40 KPa to 20 KPa causing bank failure.

Figure 5.18: Effect of surcharge load when scour depth is 7m

Figure 5.19 shows the variation of the safety factor with the increase of the surcharge load when the depth of the scour is 7 m. The graph shows that failure begins when 25 KPa load is applied. In the previous case with a depth of 5 m, the bank began to fail at a load of 45 KPa. (Figure 5.17).

84

So, it can be said that the bank fails at a lower surcharge load than before when the bank is subjected to large scour volume.
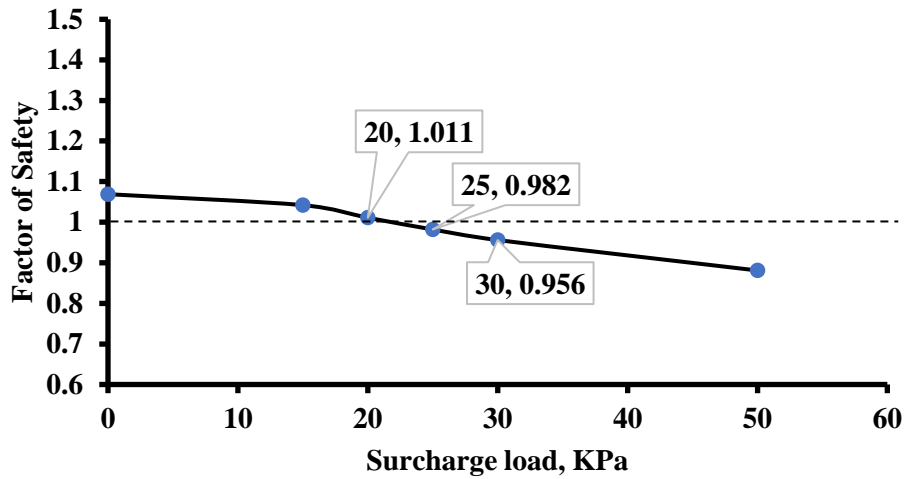
Figure 5.19: Variation of FOS with surcharge load when scour depth is 7m

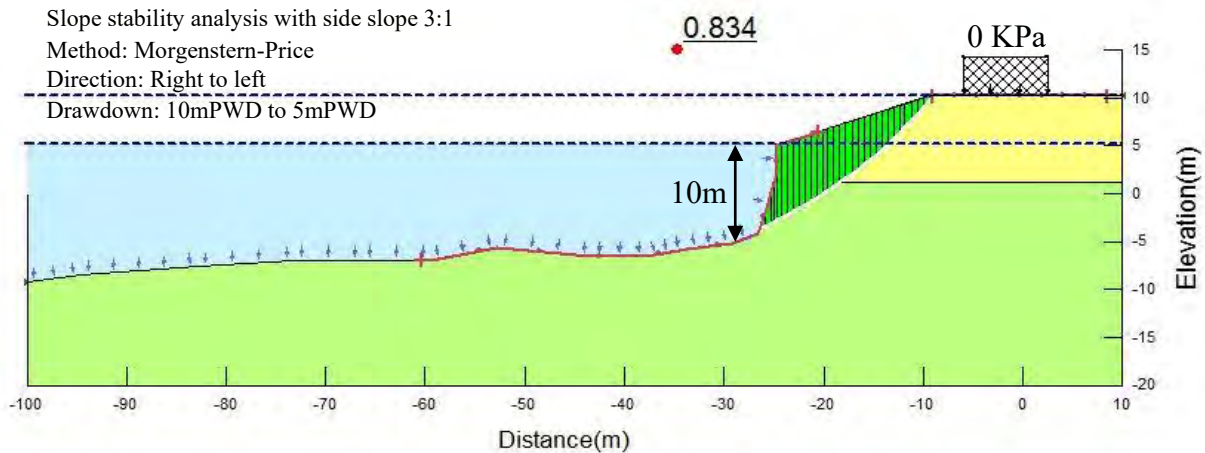In this scenario, scour depth was 10 m, and the bank began to fail with the onset of applied surcharge load. When no surcharge load was applied to the bank, FOS was found to be 0.834, and failure occurred. Therefore, this time, the bank fails with a lower load than the previous one. (Figure 5.20).

Figure 5.20: Effect of surcharge load when scour depth is 10m

Figure 5.21 indicates that bank fails when there is no surcharge load, and the only toe is scoured. FOS was 0.834 when surcharge load was 0 KPa and scour depth was 10 m. So, the bank failed when scoured depth was 10 m for all surcharge load values.

85
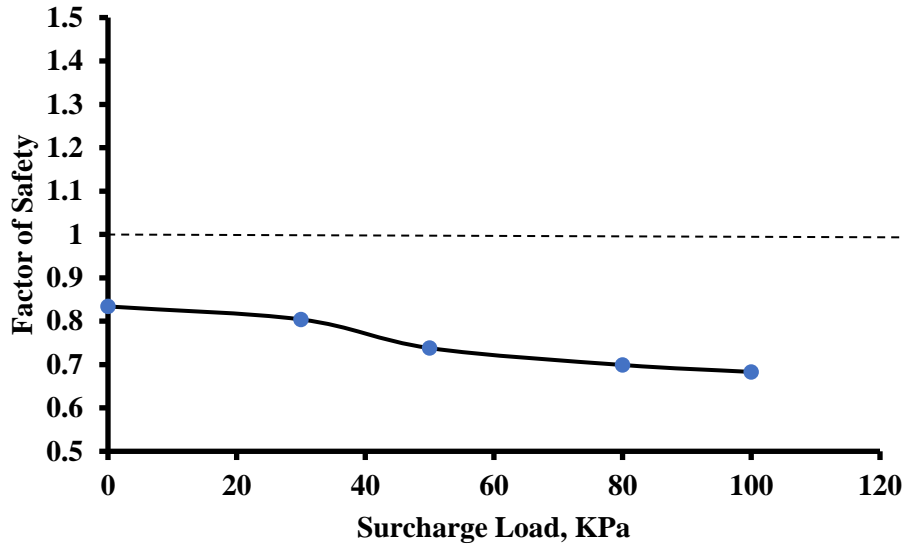
Figure 5.21: Variation of FOS with surcharge load when scour depth is 10m

5.3.4 **Scenario 4: Effect of load applied on the slope for protection work**

In Figure 5.22, load coming from slope protection works was applied along 32.4m length bank slope. The additional load applied on the bank slope was 100KPa and observed factor of safety was 1.543.
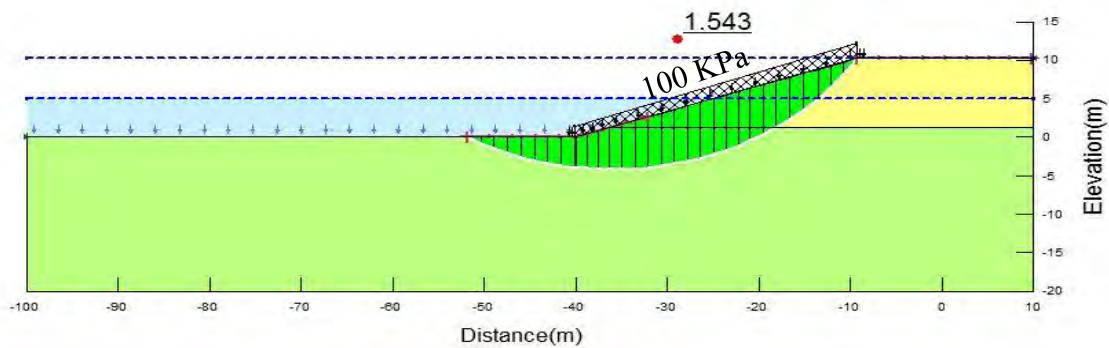
Figure 5.22: Illustration of slope stability analysis incorporating slope protective load with existing phreatic pressure

Effect of bank protective load applied on the bank surface is shown in Figure 5.23. The graph shows that the safety factor increases when the load value is low. As the load increases to a high value, the safety factor begins to decrease.
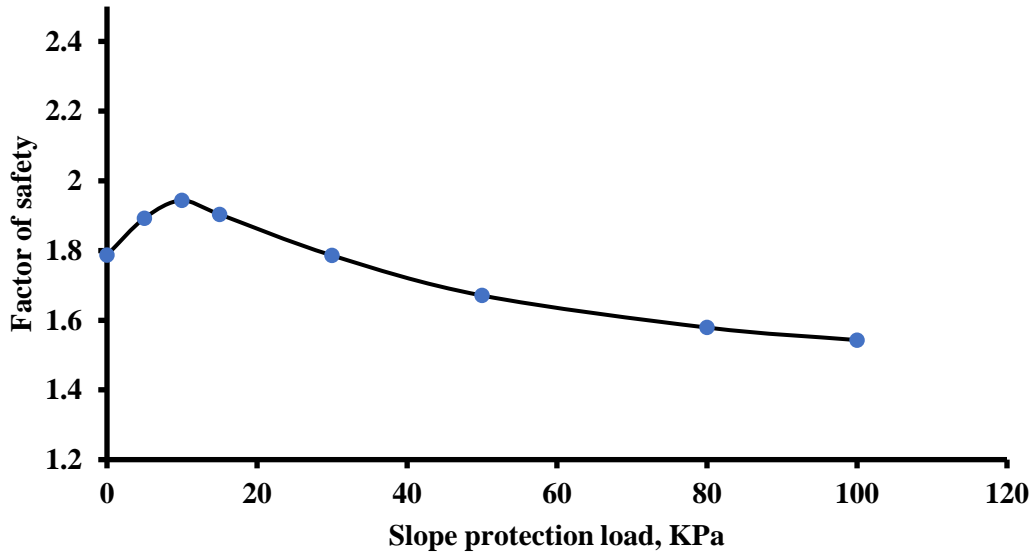
Figure 5.23: Variation of factor of safety with slope protection load

Slope protection loads have little effect on bank instability if there is no toe erosion. Bank failure initiates when there is a toe scour in presence of slope protective element. So, the effect of applied load on the bank must be checked considering scoured toe. In this scenario, the applied slope protective load on the bank was 10 kPa at 7m scour depth, and the result was 0.985, which indicates that the bank was unstable (Figure 5.24).
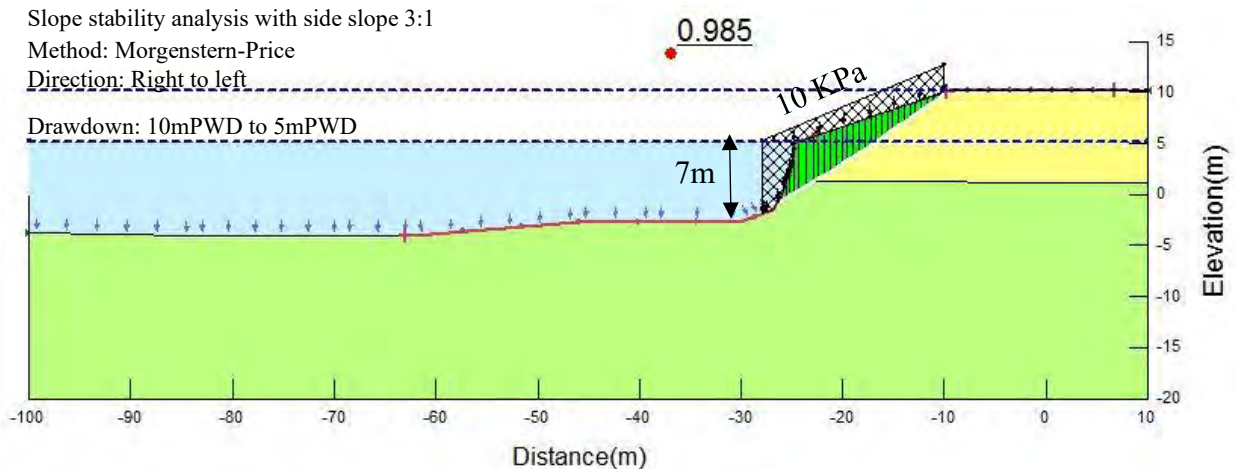
Figure 5.24: Illustration of slope stability analysis with bank protective load when there is a scour depth of 7m.

87

Figure 5.25 shows the effect of bank protection load when there is a scour at the toe. All the values below the unity FOS line indicate the failure of the bank. The graph shows that the river bank fails at a scoured depth of 7 meters with an applied load 10-15 KPa.

In previous Figure 5.23, it was seen that a large value of bank protective load was needed to fail the bank. But, from Figure 5.25, it can be seen that the bank fails under a load of 10 KPa. This means that with an existing scoured toe, the chance of a bank failure increases many times.
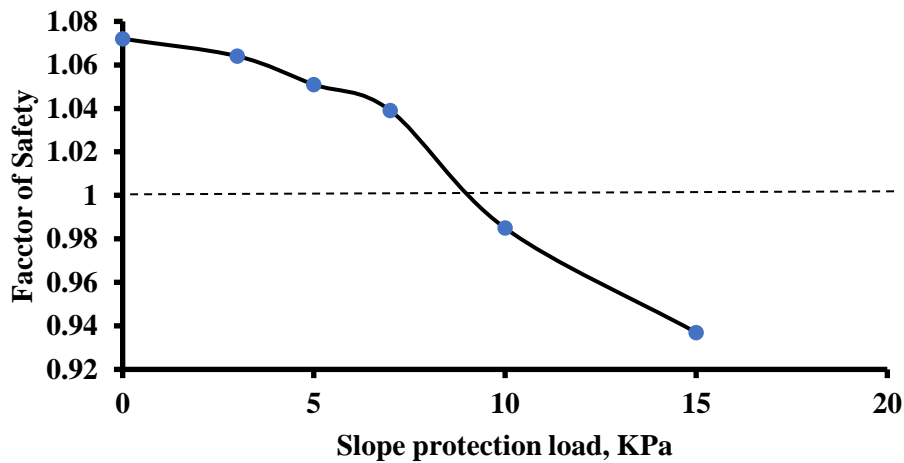
Figure 5.25: Variation of factor of safety with bank protective load when scoured depth at toe is 7m

5.3.5   Scenario 5: Stability analysis with slope protection load and surcharge load

The combined effect on bank stability of bank protection load and surcharge load is presented in Figure 5.26. With 80 KPa surcharge load and 8 KPa slope loads, FOS was 0.929. Previously, 50 KPa surcharge loads were adequate to fail the bank (Figure 5.12). In this case, surcharge combined with the load applied on a slope requires an extra 30 KPa load to make the bank unstable. This is because when the value of the bank's protective load is small, the safety factor increases (Figure 5.23). As a result, a higher value of surcharge load is required to counterbalance the increased safety factor.
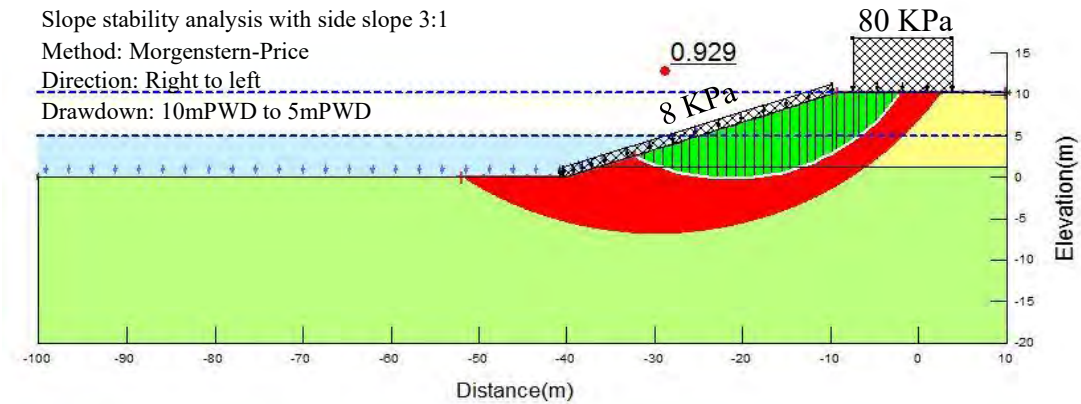
Figure 5.26: Effect of bank protective load and surcharge load on factor of safety

Figure 5.27 shows the variation of the safety factor with the combined effect of the slope protection load and the surcharge load. The left portion of unity FOS line indicates an unstable bank and right portion indicates a stable bank. The figure shows that the river bank is unstable when there are 6 KPa applied loads on the slope and 60 KPa, surcharge load.
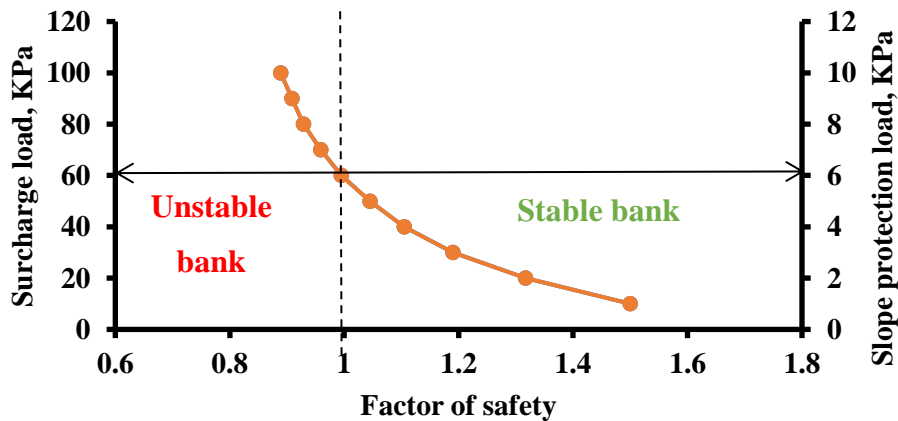
Figure 5.27: Variation of FOS with slope protection load and surcharge load

5.3.6   Scenario 6: Effect of surcharge load, slope protection load and scoured toe

The combined effect of surcharge load and slope protection load was analysed when there was an existing predetermined scoured toe. Figure 5.28 shows 60 KPa surcharge load and 6 KPa load applied to the slope at 5 m scour depth, and the observed factor of safety was 0.999, indicating bank failure. Bank failed under a surcharge load of 45 KPa at a scour depth of 5 m (Figure 5.16). And, the bank fails under applied load on slope 10 KPa, when scour depth is 7m (Figure 5.25).

89

Bank stability increased when the load on the slope was low (Figure 5.23). Therefore, in Scenario 6, a greater surcharge is required to collapse the bank than the individual load action. This is because pressure induced by surcharge load is counterbalanced in a small amount by bank protective loads, which consequently increases the load to make the bank fail.
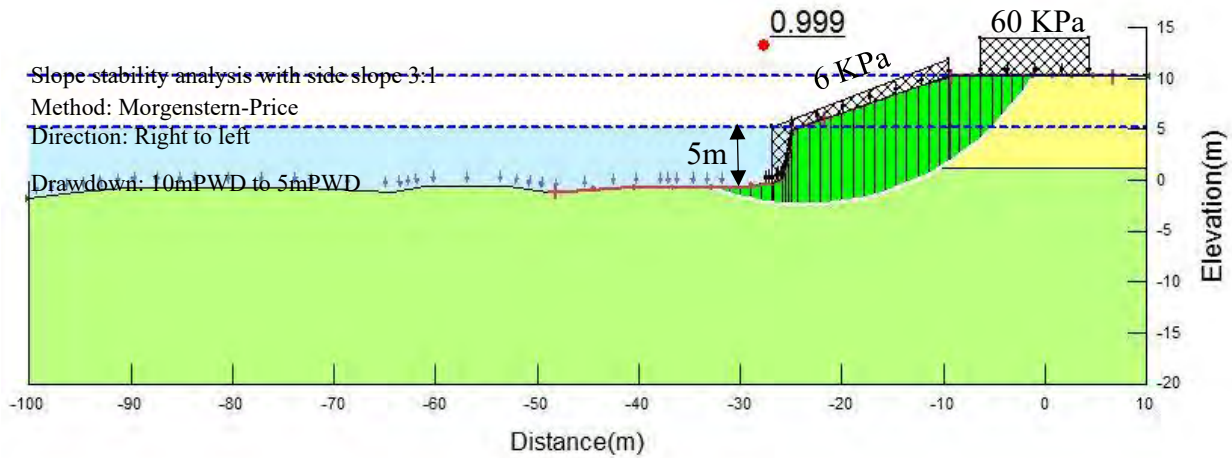
Figure 5.28: Combined effect of bank protective load and surcharge load on riverbank stability when scour depth is 5m

Figure 5.29 shows different combinations of surcharge load and load from slope protection and the corresponding factor safety value when scour depth is 5 m. Dash line indicating the unity factor of safety divides the area into two zones. The left zone corresponds to the unstable bank and the right zone to the stable bank. The graph shows the critical combination of surcharge load and bank protective load to fail the bank at safety factor 0.999 is 60 KPa and 6 KPa, respectively. As the surcharge value and bank load increased, the safety factor continued to decrease, and the bank failed. All the value left of the unity FOS line is responsible for bank failure.
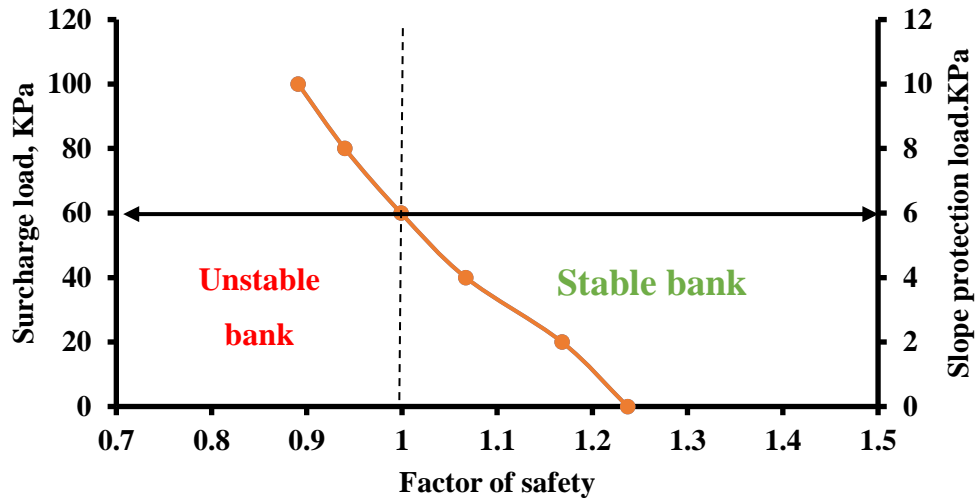
Figure 5.29: Effect of bank protective load and surcharge load on FOS at scour depth 5m

Figure 5.30 demonstrates the effect of slope protection load on the factor of safety. It was analyzed considering 5m scour depth and with a constant surcharge load of 52.5 KPa. In such a way, a close look can be given to clarify the effect of the applied load on the slope on the safety factor. When the load on the slope was 5 KPa, the factor of safety observed was 0.992. Then, applied load on the slope was increased up to a certain limit. The factor of safety also showed a similar increasing trend up to that limit. After reaching the peak point, the factor of safety continued to decrease with the increasing value of bank protective load. Again, it went below unit value when the value of the load was 145 KPa. So, the factor of safety increases with a small value of load coming from slope protection and starts decreasing when the value becomes large.
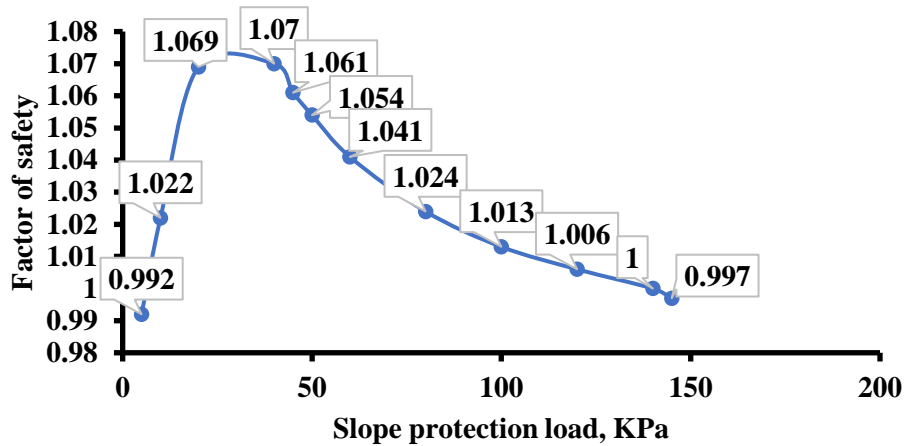
Figure 5.30: Illustration of the effect of applied load from slope protection when scour depth is 5m and surcharge load 52.5 KPa

In Figure 5.31, a combination of 30 KPa surcharge load and 3 KPa slope protective loads was applied at 7 m scour depth and a safety factor showing bank failure was 0.994. Previous analysis showed that 60 KPa overload and 6 KPa load applied on the slope made the river bank unstable. (Figure 5.27). Therefore, when scour depth is higher, less surcharge load and slope load are needed for bank failure. Without considering the protective load, the 25 kPa surcharge loads caused unstable river banks when scour depth was 7 m. (Figure 5.19). This is because the additional load applied on the slope with low value increases stability, and more surcharge is needed to make the bank of the river unstable.
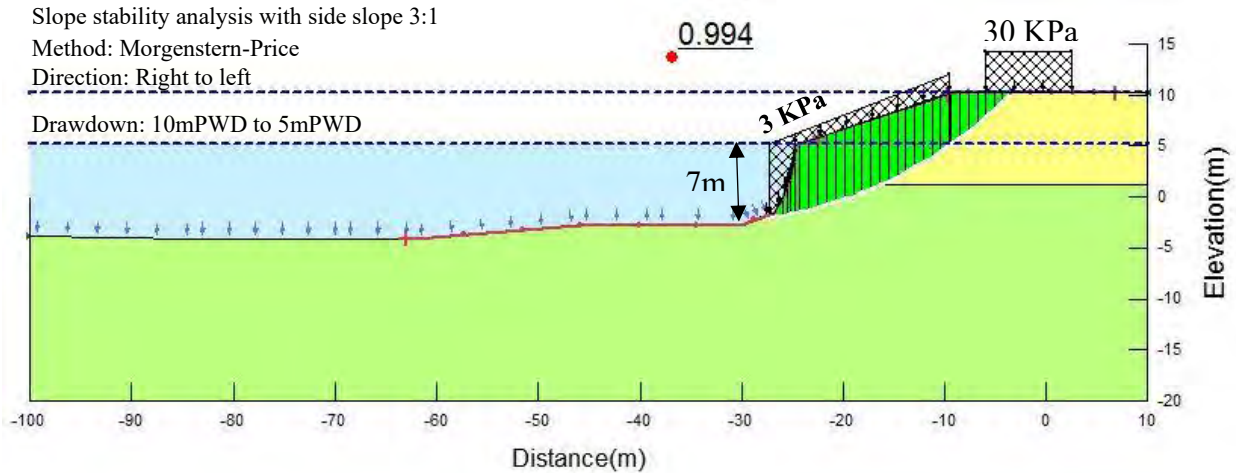
Figure 5.31: Combined effect of slope protection load and surcharge load on riverbank stability when scour depth is 7m

Figure 5.32 shows the variation of factor of safety with the load applied on slope and surcharge load when scour depth is 7m. In the beginning, when the value of surcharge load and slope protection load was small, FOS increased slightly. With the increasing value of these loads, FOS began to decline, resulting in a bank failure.
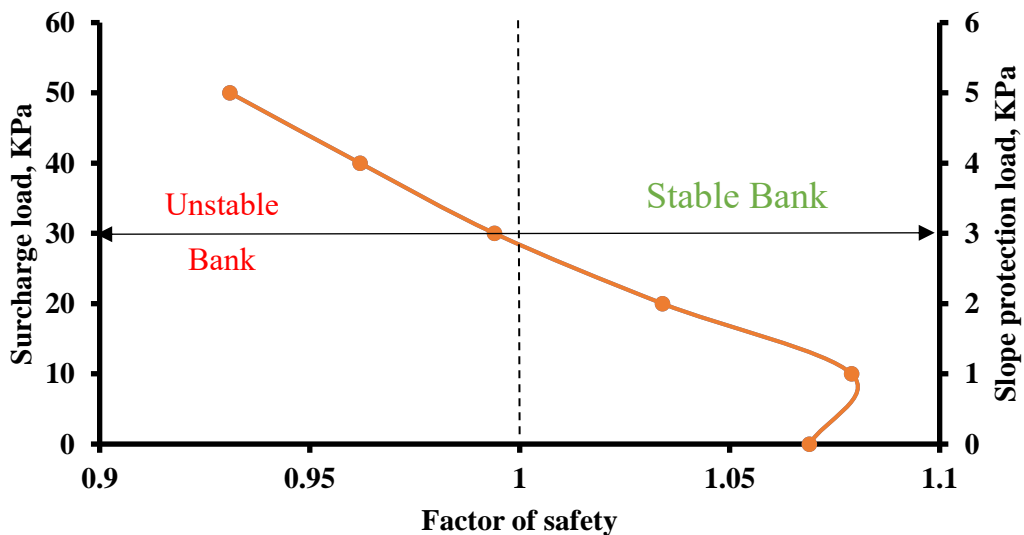
Figure 5.32: Variation of FOS with slope protective load and surcharge load when scour depth is 7m

5.3.7 Scenario 7: Effect of surcharge load, slope protective load and scoured toe when there exists clayey and mica layer at top of bank

Table 5.2 represents properties of different soil layers and interface shear strength parameters used for slope stability analysis in SLOPE/W software for this scenario. These properties are obtained from various geotechnical investigations, research papers and laboratory tests. Properties of clay loam soil are collected from ADP (2013). Mica with 30% content has the properties mentioned in the Table 5.2 obtained from Zhang et al. (2019). Parameters for sandy silt and silty sand are obtained from different laboratory test.

Table 5.2: Properties of different layers of soil

Layer	Thickness, (m)	Unit weight (KN/m3)	Cohesion' (KN/m3)	Phi' (°)	Cohesion R (KN/m3)	Phi R (°)
Clay loam	5	18	25	2	28	0
Mica (30%)	2	14.7	39.81	20.9	42	18
Sandy silt	7.2	16.28	6	29	7	28
Silty Sand	16	16	6	27	7	25

Figure 5.33 demonstrates slope stability analysis with four layers of soil such as clay loam, mica (30%), sandy silt and silty sand layer. Previously, it was analysed with only sandy silt and silty sand layer (Figure 5.14.a). FOS observed was 1.790. The factor of safety representing slope stability analysis with four layers of soil was 2.019. So, additional clay and mica (30%) layer have an increased factor of safety considerably. Riverbank with clay and mica layer at the top of the bank shows higher stability than the bank with only sandy silt and silty sand layer. As a result, the design of riverbank protection measures also changes in such a combination of bank layers. Mica is a sheet of silicates that adversely affects the shear strength of the soil. With the increase in mica content, soil shear strength decreases. But, closer packing of clay and mica induces frictional resistance and leads to high shear strength (Zhang et al., 2019).
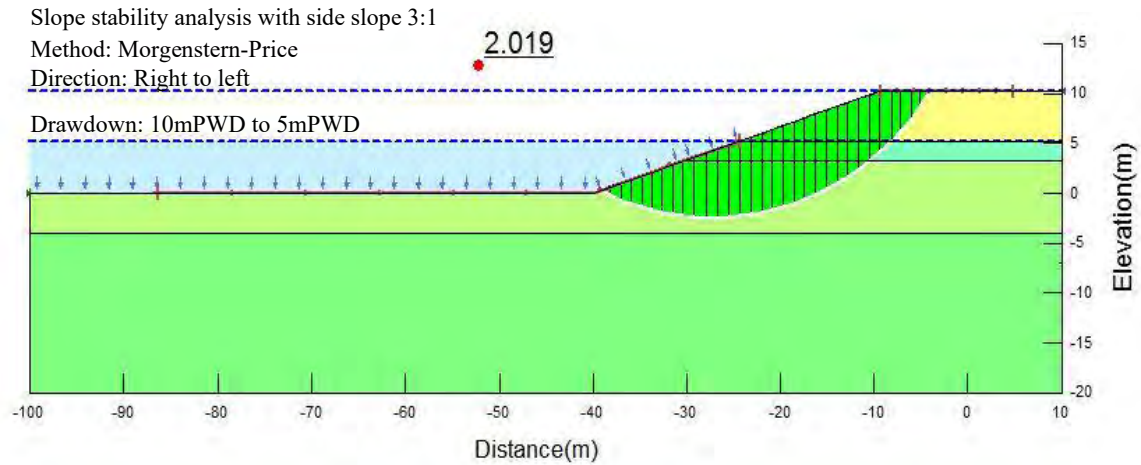
Figure 5.33: Illustration of slope stability analysis with clay, mica, sandy silt and the silty sand layer of soil

Figure 5.34 shows a comparison between two combinations of layers. It is clear from the graph that bank composition with clay, mica, sandy silt and silty sand provides more safety factor than bank layer with sandy silt and silty sand.
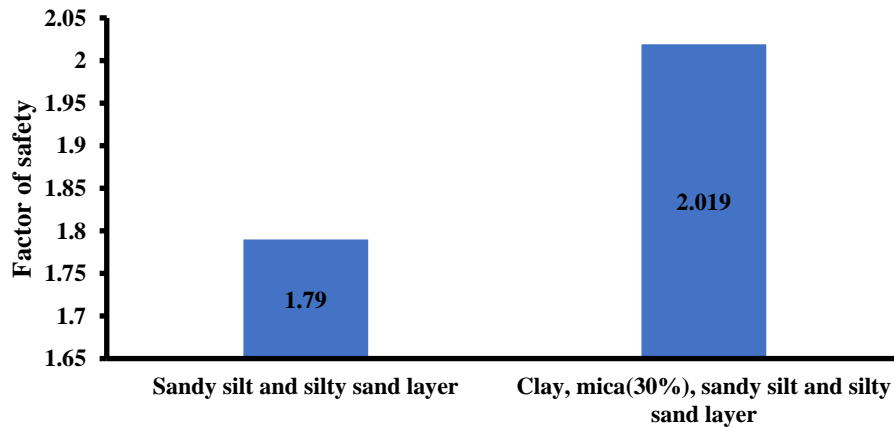
Figure 5.34: Slope stability analysis with different combination of layers

5.4   Riverbank stability analysis with finite element method

Riverbank stability analysis was performed with the finite element method in Optum G2 software. Figure 5.35-Figure 5.40 shows the comparison between the limit equilibrium method (LEM) and finite element method (FEM) for different scenarios.

Scenario 1
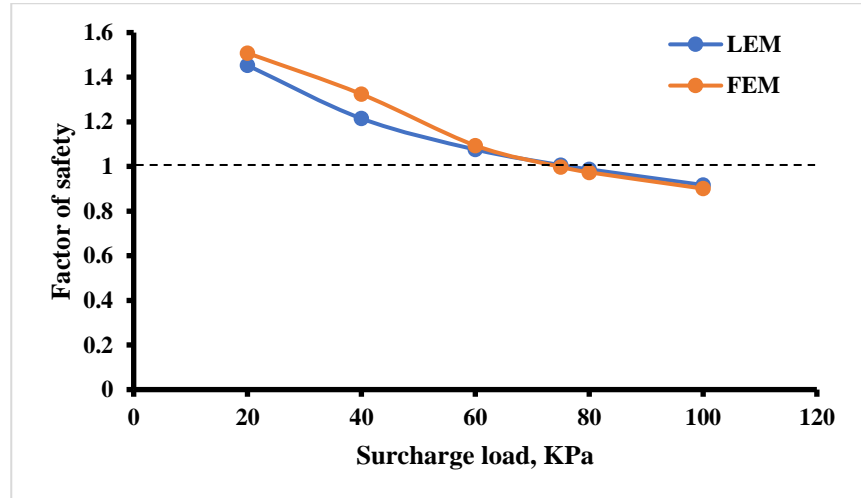
Figure 5.35: Comparison between LEM and FEM with variation in surcharge load

Scenario 2
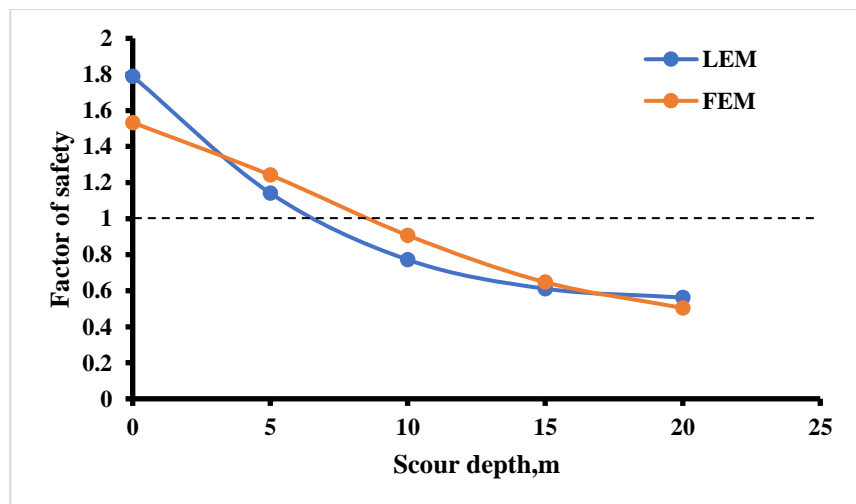
Figure 5.36: Comparison between LEM and FEM with variation in scour depth

96
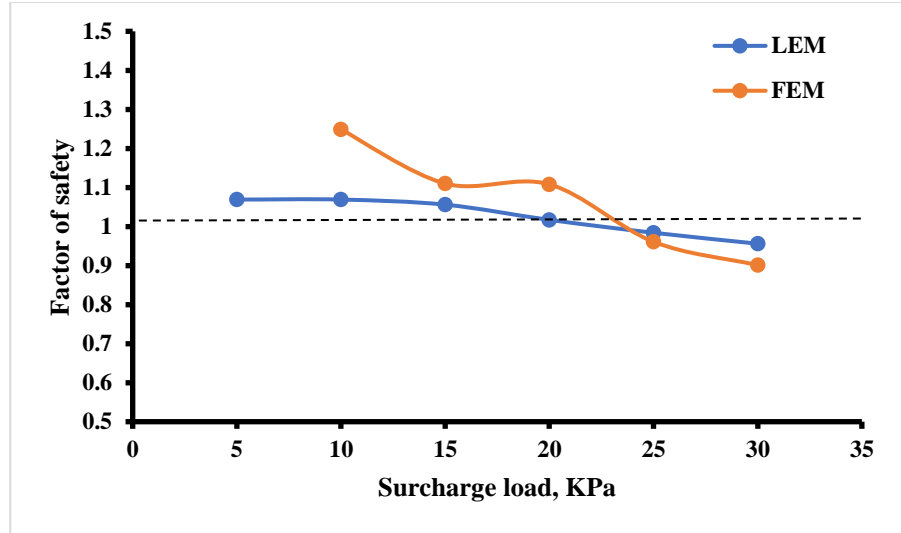
Scenario 3

Figure 5.37: Comparison between LEM and FEM with variation in surcharge load at 7m scour depth.

Scenario 4
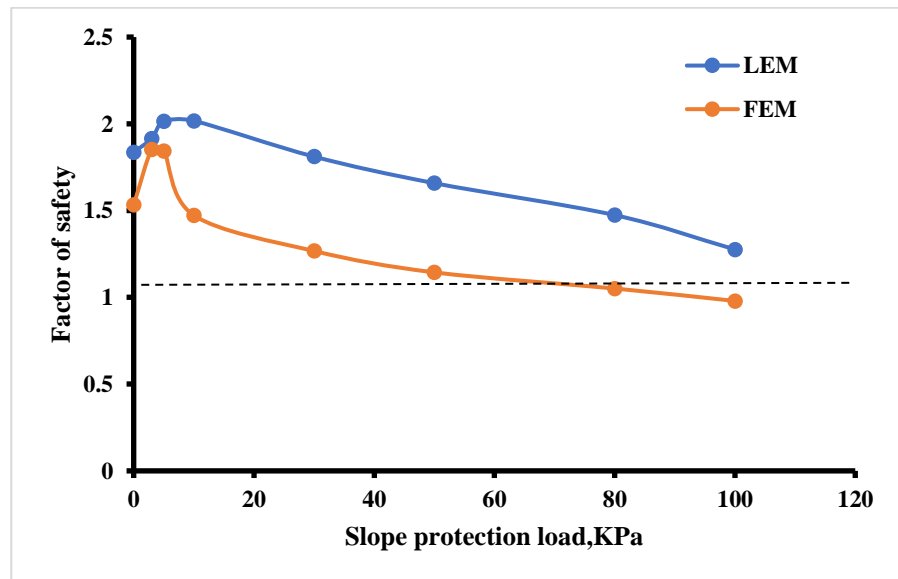
Figure 5.38: Comparison between LEM and FEM with slope protection load

Scenario 5
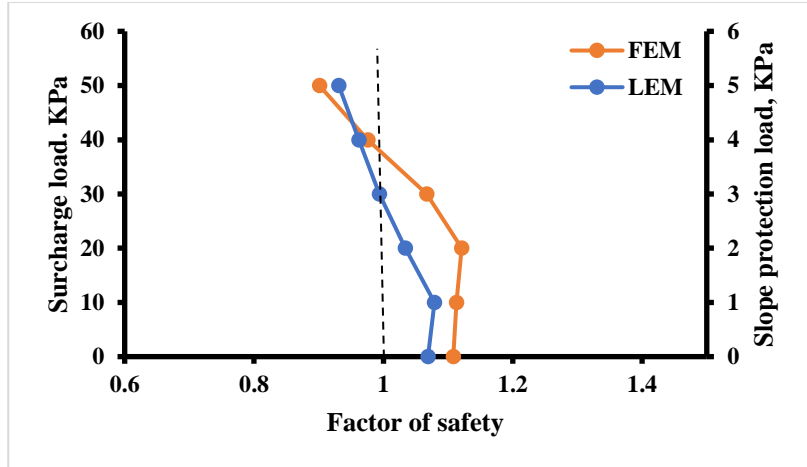
Figure 5.39: Comparison between LEM and FEM with surcharge and slope protection load

Scenario 6
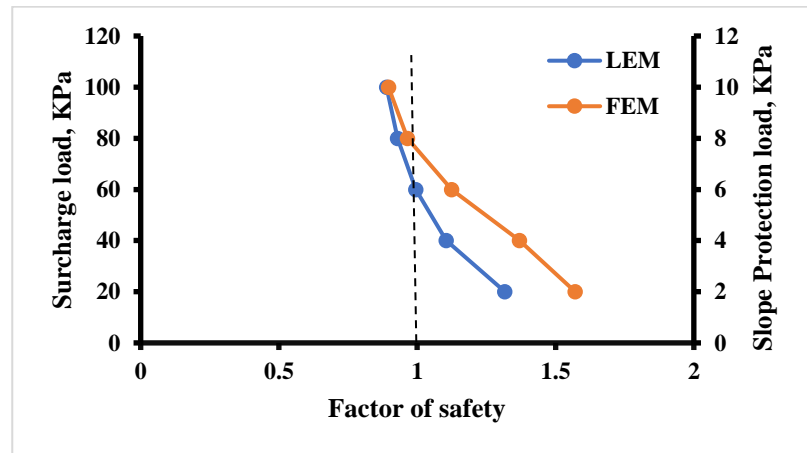
Figure 5.40: Comparison between LEM and FEM with surcharge and slope protection load at 7m scour depth

98

Table 5.3: Percentage change in factor of safety for LEM and FEM

Scenario No.	Parameters	Factor of safety		% Change
		FEM	LEM	
1	Surcharge load	1.508	1.453	+3.78
		1.324	1.215	+8.97
		1.094	1.076	+1.67
		0.998	1.006	-0.79
		0.973	0.987	-1.42
		0.901	0.917	-1.74
2	Scour depth	1.533	1.79	-14.35
		1.242	1.142	+8.75
		0.907	0.772	+17.48
		0.647	0.611	+5.89
		0.504	0.562	-10.32
3	Surcharge load and scour depth	1.249	1.069	+16.84
		1.11	1.056	+5.11
		1.108	1.017	+8.94
		0.961	0.984	-2.33
		0.901	0.956	-5.75
4	Slope protection load	1.533	1.836	-16.5
		1.853	1.916	-3.29
		1.843	2.014	-8.49
		1.473	2.017	-26.97
		1.267	1.811	-30.04
		1.144	1.658	-31
		1.051	1.474	-28.69
		0.97	1.276	-23.98

5	Surcharge and slope protection load	1.108	1.069	+3.65
		1.113	1.079	+3.15
		1.121	1.034	+8.41
		1.067	0.994	+7.34
		0.976	0.962	+1.45
		0.901	0.931	-3.22
6	Surcharge load, slope protection load and scour depth	1.571	1.317	+19.28
		1.37	1.105	+23.98
		1.125	0.995	+13.06
		0.964	0.929	+3.76
		0.896	0.889	+0.78

In scenario 1, 2, 3, 5 and 6, change in the factor of safety was found to be within $\pm15\%$, which was not very significant. For scenario 4, the change in the factor of safety of FEM from LEM was in the range of -20 to -30%. The reason behind this high percentage of change in the factor of safety is the type of input parameters used by LEM and FEM. Finite element analysis utilizes elastic modulus of soil, hydraulic conductivity, permeability, poison's ratio, dilation factors as input parameters that are not regularly measured and the accessibility of these data is generally poor. Limit equilibrium method doesn't need these parameters to run the analysis. So, in some cases, the finite element method shows a high percentage of change in the factor of safety than the limit equilibrium method.

5.5 Determination of riverbank stability parameters for safe deign of riverbank protection works

Input parameters used for riverbank stability analysis are unit weight, cohesion, angle of internal friction. If the effective range of these parameters, which make the bank stable, is known, the riverbank protection works can be designed safely. The effect of these input parameters is analyzed by means of a sensitivity analysis. The analysis was performed for the most important riverbank

combination it can undergo. The combination of different features of the riverbank in its critical condition is shown in Figure 5.41. Geo-Studio slope / w software was used to perform the analysis.
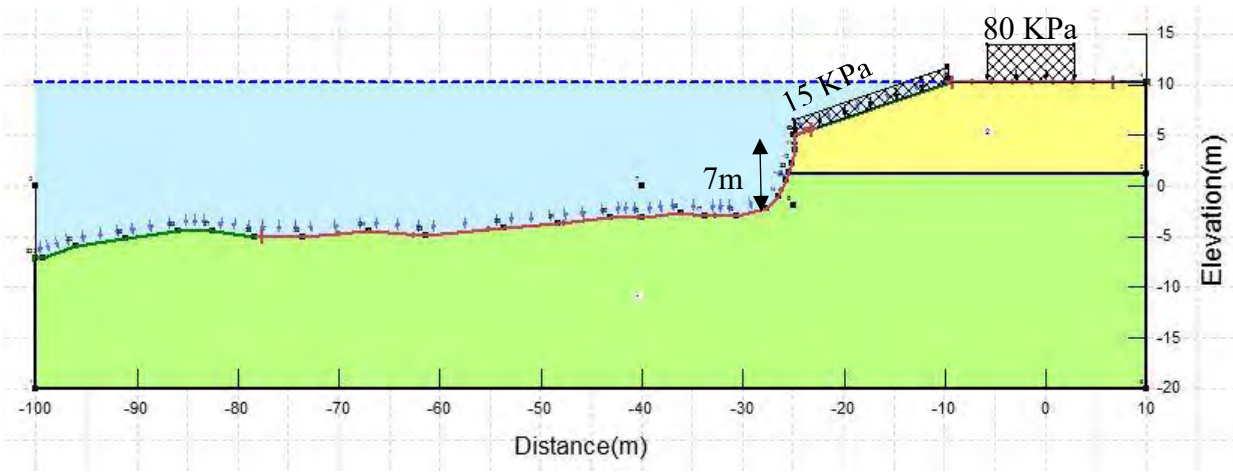
Figure 5.41: Critical condition of the riverbank with scoured toe, surcharge load and applied bank shear stress

5.5.1 Sensitivity analysis

A sensitivity analysis was performed for the parameters used in slope stability analysis for side slope 3:1. This analysis was done to study the sensitivity of the model to variation in input parameters such as unit weight, friction angle, cohesion.

5.5.1.1 Sensitivity with SLOPE/W

The SLOPE / W program provides an opportunity to specify a range of values for the material parameters and automatically calculates the safety factor when each of the parameters is used. The objective is to determine the effect of the variability of the input parameters on the safety factor. For presentation purposes, the sensitivity range is standardized (-1.0 to +1.0) so that more than one parameter can be plotted on the same graph. -1.0 is the lowest value, and 1.0 is the highest value. The point where the two-sensitivity curve cross is the deterministic factor of safety or the factor of safety at the midpoint of the ranges for each input parameters.

5.5.1.2 Effects of unit weight

The effect of varying the unit weight of the different layers on the safety factor is presented in this section. The range of unit weight values to be considered is specified in the Sensitivity Parameters

dialog box (Figure 5.42). This range is defined as an offset. The range will be 1 KN/m3 (delta) in 5 steps in both directions for unit weight in both layers. This results in a range 16.28 to 26.28 KN/m3 for sandy silt and 16 to 26 KN/m3 for silty sand.
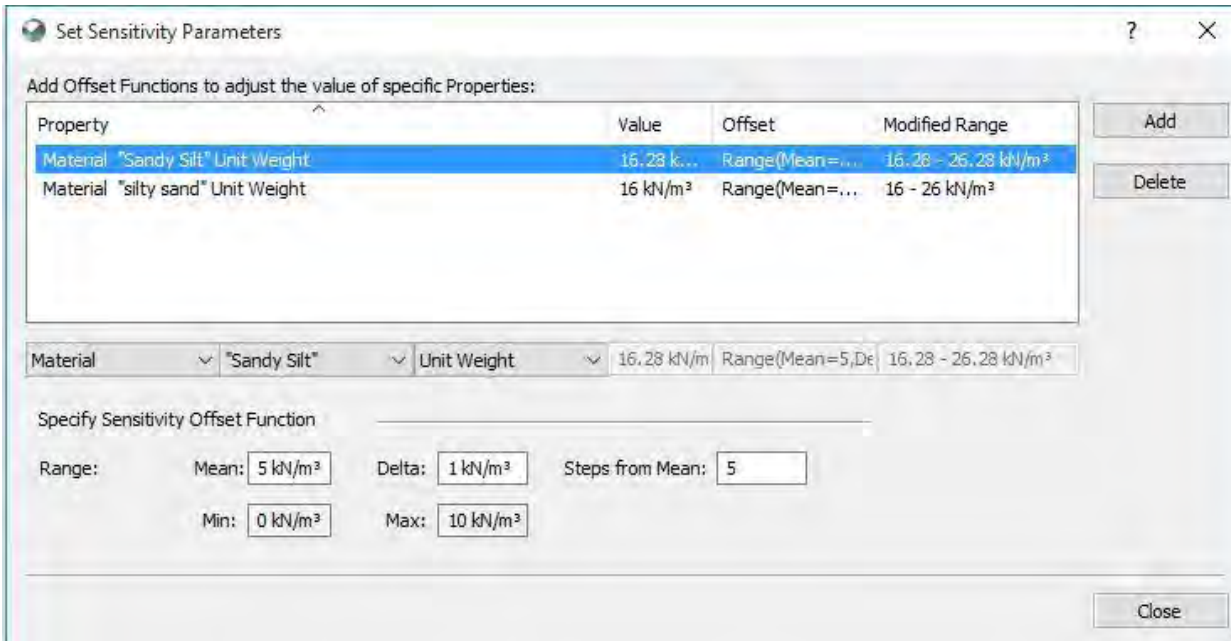
Figure 5.42: Parameters used in sensitivity analysis

Table 5.4 shows the input parameters used in the sensitivity analysis. The range of safety factor after sensitivity analysis was 1.097 to 1.117 for sandy silt and 1.090 to 1.126 for silty sand.

Table 5.4: Input parameters in sensitivity analysis and output range of FOS

Layer	Unit weight (mean), KN/m3	Delta, KN/m3	Steps from mean	Range of unit weight 0f bank material, KN/m3	Range of FOS
Sandy silt	5	1	5	16.28-26.28	1.097-1.117
Silty Sand	5	1	5	16-26	1.090-1.126

Figure 5.43 presents the variability in the factor of safety for changing unit weight in sandy silt and silty sand layer. The sensitivity graph shows that silty sand is more sensitive to unit weight than sandy silt layer. In the case of sandy silt layer, the factor of safety ranges from 1.097 when

unit weight is 16.28 KN/m3 to 1.117 when unit weight is 26.28 KN/m3. On the other hand, for silty sand, FOS ranges from 1.09 when unit weight is 16 KN/m3 to 1.126 when unit weight is 26 KN/m3. This is a significant range in the margin of safety against failure. Below the lower limit of unit weight 16 KN/m3, FOS goes below unity, and the bank becomes unstable. If the unit weight of the material can be improved to about 10 KN/m3, the factor of safety can be increased from 1.09 to 1.126.
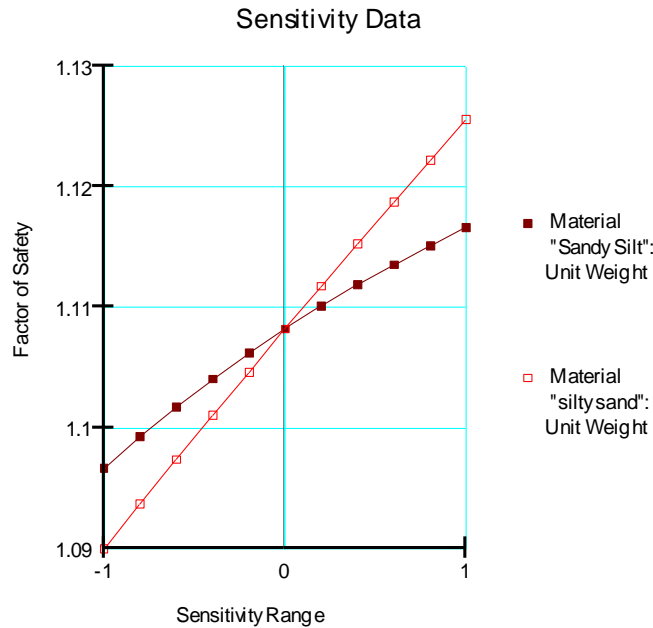
Figure 5.43: Sensitivity plot for variation in the unit weight

5.5.1.3   **Effect of friction angle**

The effect of varying the friction angle of the various layers on the factor of safety is presented in this section. The range of friction angle values to be considered is specified in the set sensitivity parameters dialog box (Figure 5.44). This range is defined as an offset. The range will be 2º (delta) in 5 steps in both directions for unit weight in both layers. This results in a range of 24º to 44º for sandy silt and 22º to 42º for silty sand.
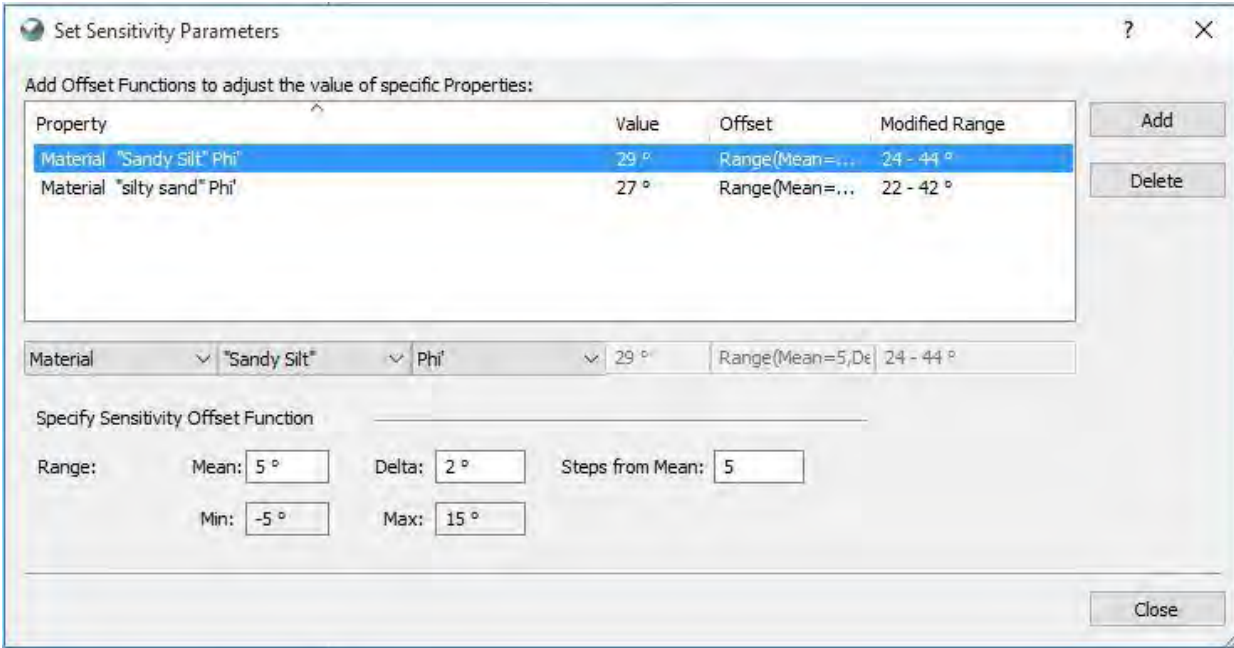
Figure 5.44: Parameters used in sensitivity analysis

Table 5.5 represents the input parameters used in sensitivity analysis when the friction angle is considered. The range of a factor of safety after sensitivity analysis was 1.084 to 1.456 in case of sandy silt and 1.012 to 1.532 in case of silty sand.

Table 5.5: Input parameters in sensitivity analysis and output range of FOS

Layer	Friction angle (mean), º	Delta, º	Steps from mean	Range of Friction angle of the bank material, º	Range of FOS
Sandy silt	5	2	5	24-44	1.084-1.456
Silty Sand	5	2	5	22-42	1.012-1.532

Figure 5.45 presents the variability in the factor of safety for changing unit weight in sandy silt and silty sand layer. The sensitivity graph shows that silty sand is more sensitive to friction angle than sandy silt layer. Both layers showed significant results as there was a varied range of a factor

of safety. In the case of the sandy silt layer, the factor of safety ranges from 1.084 when friction angle is 24º to 1.456 when friction angle is 44º. On the other hand, for silty sand, FOS ranges from 1.012 when friction angle is 22º to 1.532 when friction angle is 42º. This is a significant range in the margin of safety against failure. Below the lower limit of friction angle 24º, FOS goes below unity, and the bank becomes unstable. If the friction angles of the material can be improved to about 15º, the factor of safety can be increased from 1.012 to 1.532.

Figure 5.45: Sensitivity plot for variation in the friction angle

5.5.1.4 Effect of cohesion

The effect of varying the cohesion of the various layers on the factor of safety is presented in this section. The range of cohesion values to be considered is specified in the set sensitivity parameters dialog box (Figure 5.46). This range is specified as an offset. The range will be 2º (delta) in 5 steps in both directions for unit weight in both layers. This results in a range of 2 KPa to 22 KPa for both sandy silt and silty sand.
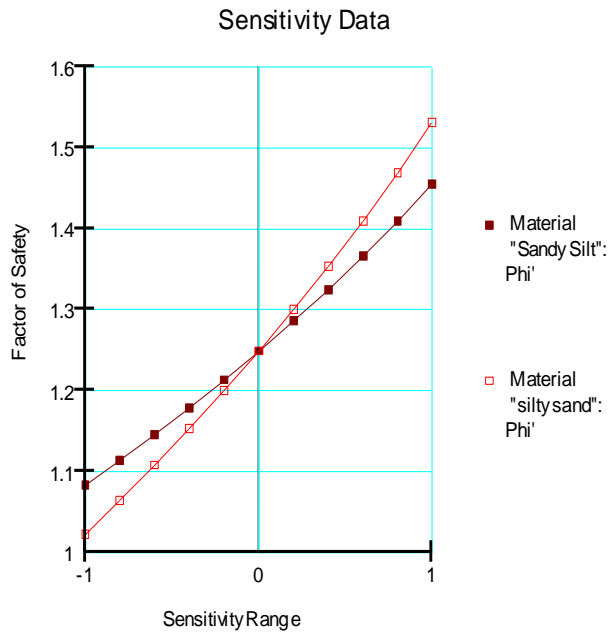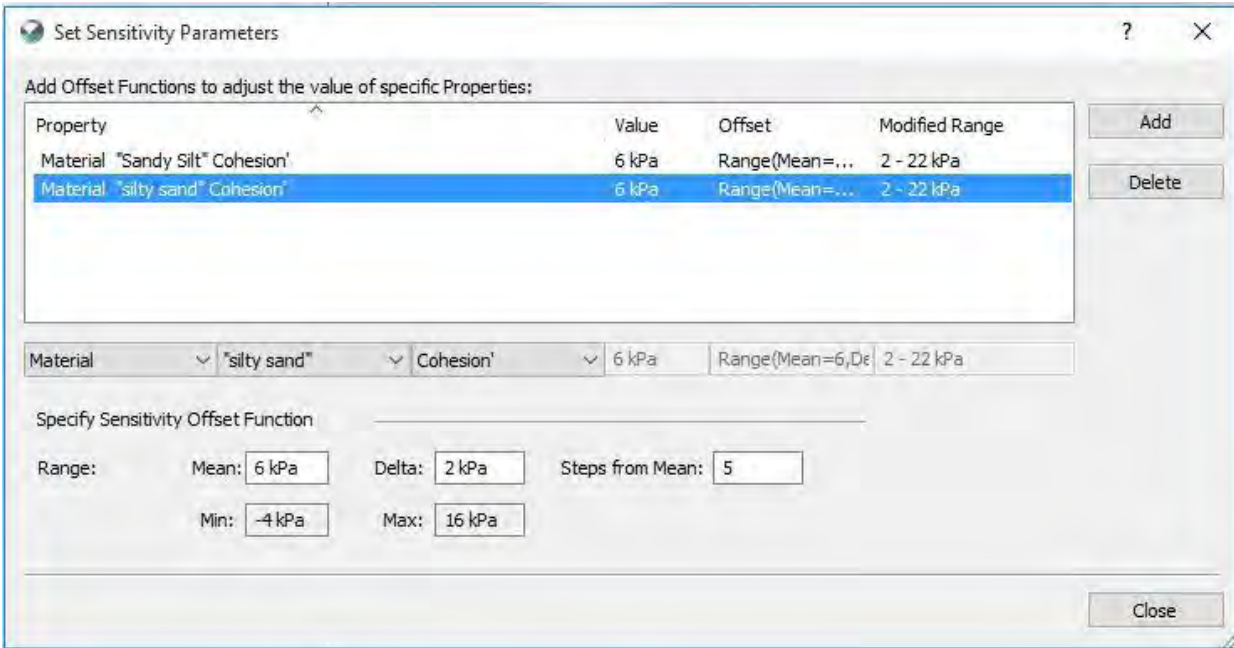
Figure 5.46: Parameters used in sensitivity analysis

Table 5.6 represents the input parameters used in sensitivity analysis when cohesion is considered. The range of a factor of safety after sensitivity analysis was 1.118 to 1.220 in case of sandy silt and 1.011 to 1.320 in the case of silty sand.

Table 5.6: Input parameters in sensitivity analysis and output range of FOS

Layer	Cohesion (mean), KPa	Delta, KPa	Steps from mean	Range of cohesion of bank material, KPa	Range of FOS
Sandy silt	6	2	5	2-22	1.118-1.220
Silty Sand	6	2	5	2-22	1.011-1.320

Figure 5.47 presents the variability in the factor of safety for changing unit weight in sandy silt and silty sand layer. The sensitivity graph shows that silty sand is more sensitive to cohesion than the sandy silt layer Sandy silt didn't show any significant effect on the factor of safety within the specified range of a factor of safety. Hence, it is less sensitive to failure with the given value of cohesion. In the case of silty sand, FOS ranges from 1.011 when cohesion is 2 KPa to 1.320 when cohesion is 22 KPa. This is a significant range in the margin of safety against failure. For silty sand, below the lower limit of cohesion 2 KPa, FOS goes below unity, and the bank becomes unstable. The typical value of cohesion for silty sand is 22 KPa (Swiss Standard, 1999). If the cohesion of the material can be improved to about 16 KPa, the factor of safety can be increased from 1.011 to 1.320.
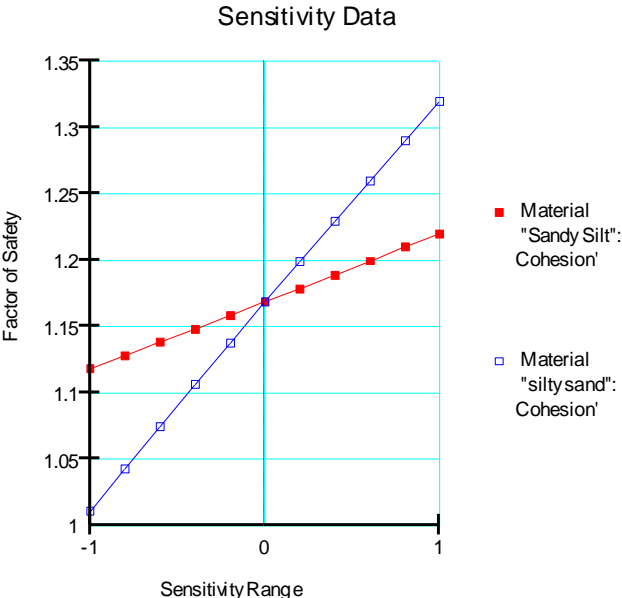
Figure 5.47: Sensitivity plot for variation in the cohesion

5.6 Post projection of design data

Sensitivity analysis shows that the safety factor can be increased by improving soil density and shear strength parameters. The soil properties used in this analysis for sandy silt soil included unit wight 22 KN/m3, cohesion 12 KPa and angle of internal friction 32°. Properties for silty sand were unit weight 20 KN/m3, cohesion 12 KPa and angle of internal friction 33°. Applied bank protection works divided into two groups: below low water protection and above low water protection. Below the low water level, three layers of the concrete block have been placed at the bottom through toe up to the middle of the slope, while two layers have been placed from the middle up to the top of the slope for the economical design of riverbank protection works. Figure 5.48 shows a necessary diagram of slope stability analysis. Dimension and density of concrete block was 45cmx45cmx45cm and 24 KN/m3, respectively. An analysis was also carried out with a surcharge load of 75 KPa to assess the effectiveness of slope protection work.
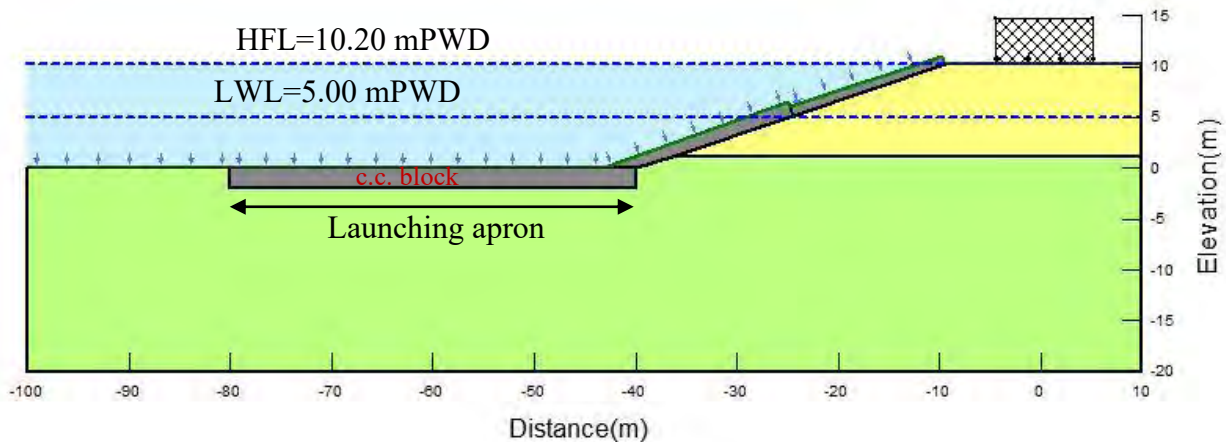
Figure 5.48: Illustration of slope stability analysis with cement concrete blocks as a protection element after modifying bank materials.

Figure 5.49 shows the variation in the safety factor with the modification of riverbank condition. The factor of safety of riverbank without any erosion was 1.790 (Figure 5.14). Safety factor increased to 2.275 with improved soil properties. After the application of slope protection, the factor of safety further increased to 2.967. At the existing condition, the surcharge load of 75 KPa was applied and found satisfactory result without any failure. Previously, this surcharge load failed the riverbank (Figure 5.12).
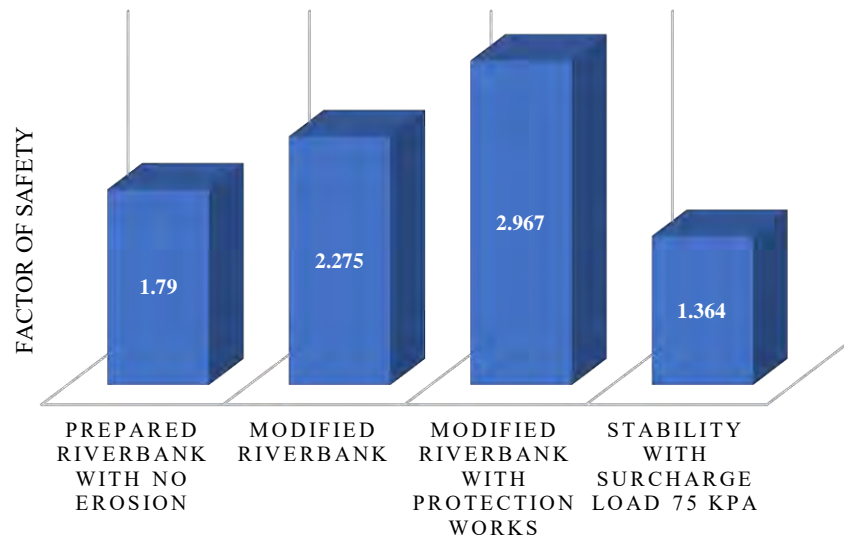
Figure 5.49: Variation in factor of safety with the modification of riverbank against erosion.

5.7 A case study: an investigation of riverbank stability along Jamuna river at Chauhali Upazila, Sirajganj.

5.7.1 Introduction

The GBM (Ganges-Brahmaputra-Meghna) basin is known for its unstable nature and harbinger of catastrophe. Instability has translated downstream into Padma and Lower Meghna rivers over time. Bangladesh covers downstream eight per cent of the GBM basin, consisting mainly of flat deltaic land. Most of the country is vulnerable to river flooding due to annual rainfall that varies from year to year. Life along the main rivers is prone to further repeated catastrophe from extreme local erosion bursts. Besides direct land losses, riverbank erosion exacerbates flooding when embankment erodes. These riverbank erosions have reduced the strength of existing flood embankments substantially, thus delaying systemic embankment lines elsewhere. Due to continuous extensive bank erosion, channel shifting and sedimentation, most of the catchment area faces serious problems. Channels frequently shift sideways due to riverbank erosion or concentrate their discharge on other channels.

Typically, riverbank failures are caused by the combined effects of gravitational forces and soil erosion associated with river water level fluctuations(Duong et al., 2014). Soil erosion is one of the main processes that have a major impact on the stability of river banks and has often been demonstrated by dynamic hydraulic erosion. (Dutta & Karmakar, 2015; Jugie et al., 2018), and seepage erosion (Al-Madhhachi et al., 2011; Chu-Agor, Fox, et al., 2008; Chu-Agor et al., 2009; Dapporto & Rinaldi, 2003; Fox & Felice, 2014; Karmaker & Dutta, 2013; Midgley et al., 2013). The failure in the riverbank deals with fluvial erosion that causes the erosion of the riverbank and its mass collapse(Darby et al., 2007; Luppi et al., 2009; Samadi et al., 2013). Soil erosion occurs when the hydraulic shear stress caused by the flow of water across the interface between soil and water exceeds critical shear stress(Semmad & Chalermyanont, 2018). The direct action of the flowing water around the interface of soil and water causes hydraulic shear stress. During the rainy season, the water level of the river increases and flows with high shear stress, raising the erosion width and causing an overhanging river bank failure.

In Bangladesh, revetments are affected by various types of problems. Devastating floods and excessive rainfall intensify the failure process, resulting in substantial annual damage to agriculture and infrastructure. One of the common failures in bank revetment work in Bangladesh is slope

failures due to faulty design, steep slope, excessive surcharge, insufficient dumping materials, lack of proper slope key, etc. This study investigates the probable cause of bank revetment failure on the left bank of Jamuna River at Chauhali Upazila, Bangladesh.

5.7.2 Study area

The Jamuna, one of Bangladesh 's largest rivers, originates at a glacier snout in the Himalayan Kailas range, south of the Gunkyud Lake in southwestern Tibet. The river rises at an altitude of about 5300 m (Goswami, 1998). It then flows 1,100 km east across the Tibetan Plateau as the Tsangpo River, before turning south to the east-west Himalayan trendy ranges (Figure 5.50). The total area of the basin is 570000 square kilometres, of which only 7% is in Bangladesh. The maximum discharge recorded at Bahadurabad is 100,000 cumec in 1988. The low flow reported in 1971 is 2860 cumec, with an average flood and low water level estimated at 19.1 and 13.6 mPWD in Bahadurabad, respectively. The average river width is 12.5 km(CEGIS, 2010).
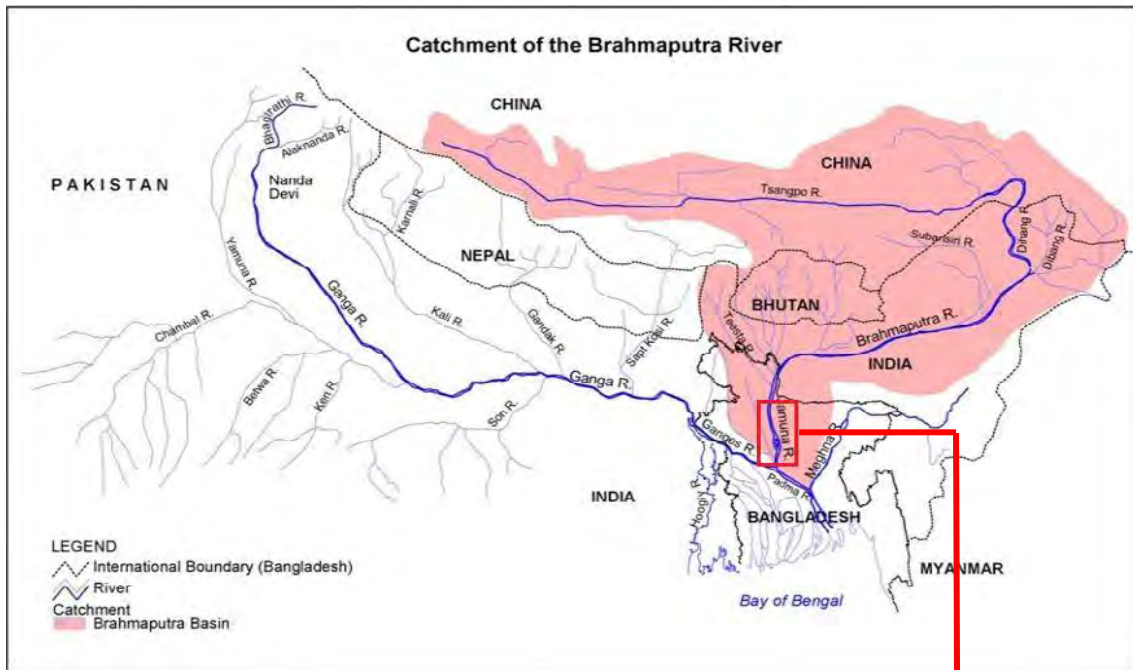
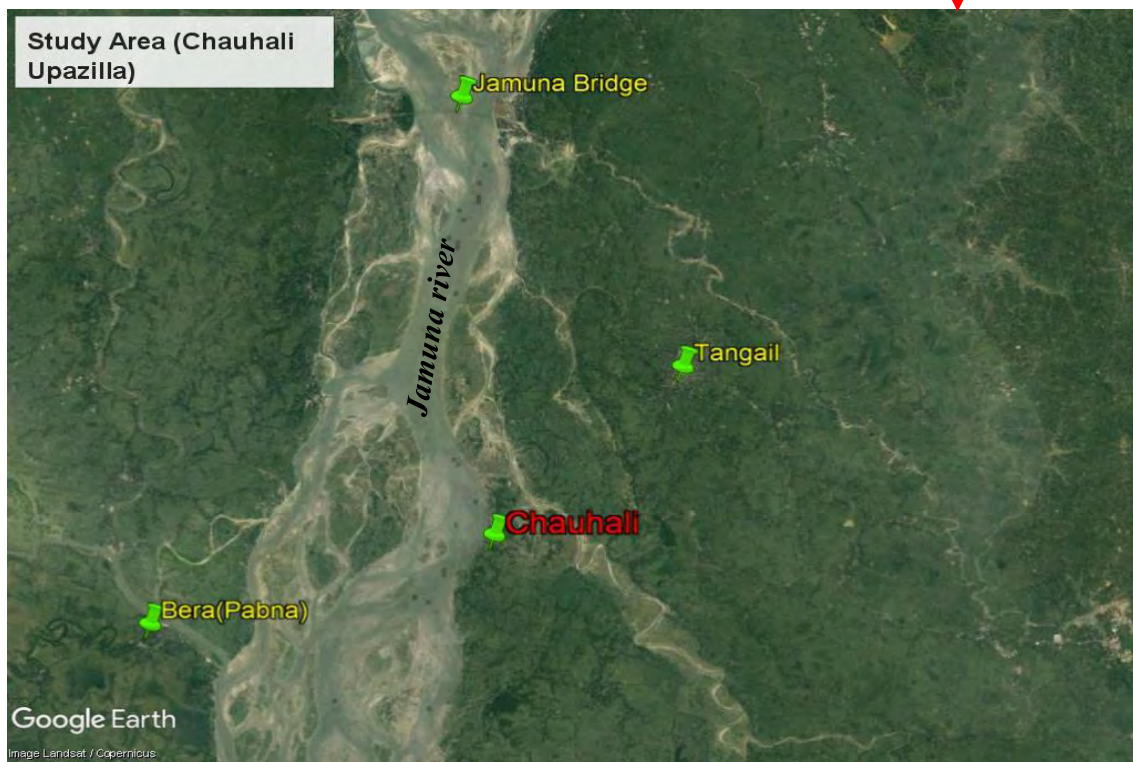**Figure 5.50: Catchment of the Brahmaputra river ((Sarker et al., 2011)**

Figure 5.51: Study locations along the Jamuna river, Chauhali, Bangladesh.

The present study is made on the left bank of braided Jamuna river, downstream of the Jamuna bridge at Chauhali under the district of Sirajganj in Bangladesh (Figure 5.51). The Jamuna river is typically braided and complex in the planform. The river is known for its high-bank erosion risks. River bed materials do not vary significantly within the study reach with average d_{50} of 0.1065mm. The bank along the left bank of Jamuna river is of composite type and composed of sand (d_{50}=0.224mm) and fine silty soils (d_{50}=0.007mm). Sand layers are sandwiched with fine silty layers. The average angle of internal friction of the soils from the banks is about 30° with very negligible cohesion. Figure 5.52 presents the configuration of different soil layers of the left bank of Jamuna river near Chauhali, Bangladesh.
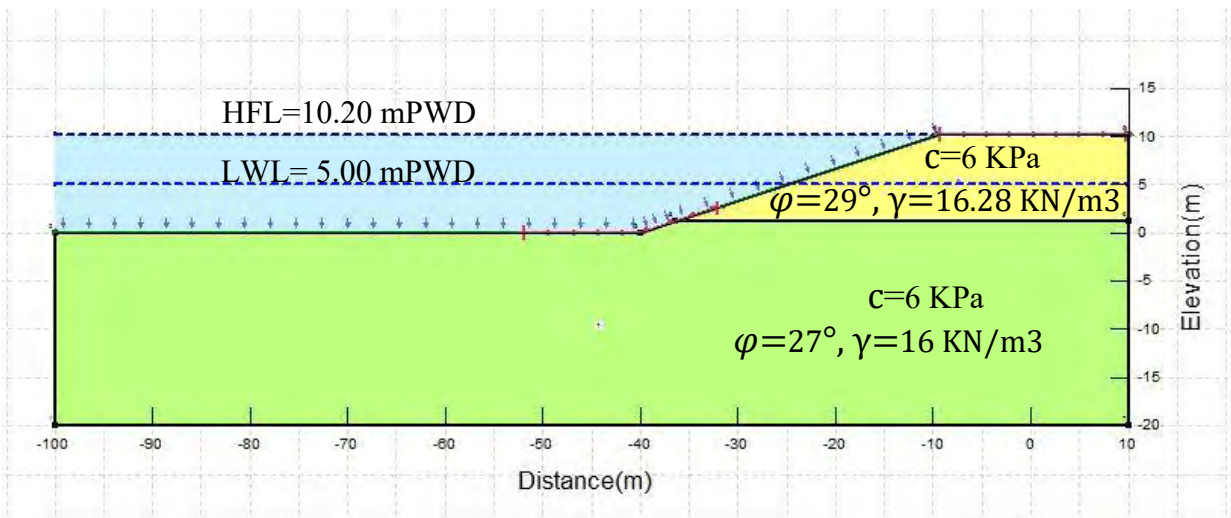
Figure 5.52: Riverbank configuration along the left bank of Jamuna river at Chauhali, Bangladesh

5.7.3 Methodology

5.7.3.1 Field investigation and data collection

The field investigation was performed during the dry season to describe the status of the riverbank and the river water level changes. Figure 5.53 shows the riverbank near Chauhali after erosion. Field data collection included bank geometry (i.e., height, slope), length of apron, type of soil. Soil borehole data are collected from the BWDB (Bangladesh Water Development Board) office. These data included particle size distribution, grain size, cohesion, angle of internal friction, unit weight. The data of hydraulic analysis such as the discharge, river water level fluctuation, satellite image, and river cross-section data were collected from the authority of BWDB.

113

Figure 5.53: Riverbank erosion scenario at Chauhali.

5.7.3.2 Hydraulic model framework

The SRH-2D (Sedimentation and River Hydraulics-two dimensional) model was used to estimate the shear stress for this study. The hydrodynamic model results were coupled with the excess shear stress approach to estimate bank erosion. SRH-2D is a two-dimensional, depth-averaged, hydraulic and sediment transport model for river systems under development at the Bureau of Reclamation. SRH-2D modelling was carried out in the following steps: i) selection of solution domain ii) mesh generation for the solution domain iii) topography and flow roughness representation on mesh iv) model calibration v) model application. The selection domain is shown in Figure 5.54(a). A 2D mesh was generated with the Surface Water Modeling System software (SMS). It consisted of a total of 33440 triangular cells and 17024 nodes (Figure 5.54.b). Once the 2D mesh was generated, the August 2017 terrain and bathymetric survey data were interpolated onto the 2D mesh. The terrain represented by 2D mesh is shown in Figure 5.54(c).
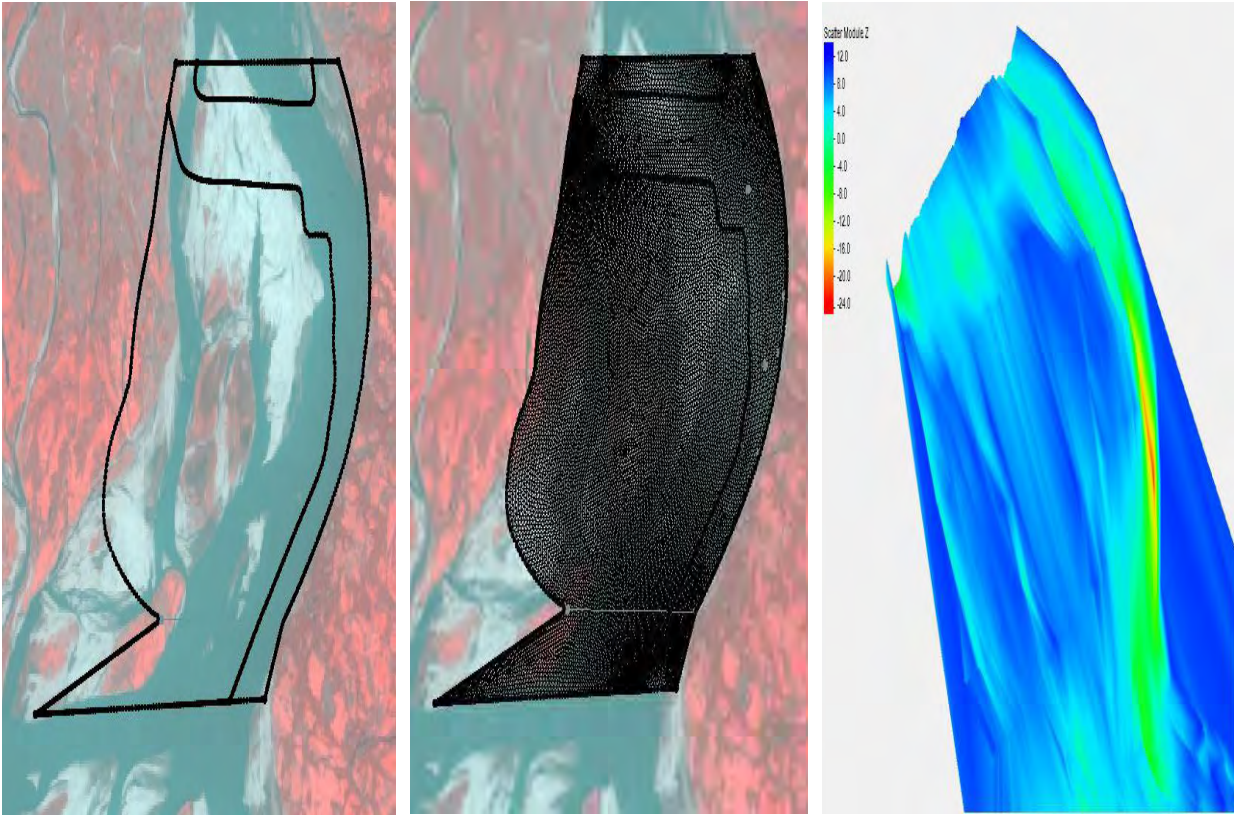
(a) Solution domain   (b) 2D mesh   (c) Bathymetry

Figure 5.54: Solution domain(left), 2D mesh (middle), bathymetry(right) at Chauhali.

The flow resistance was computed by calibrating the input data. In this study, Manning's Co-efficient of 0.013 was used in the main model, and bare bars based on the study carried out in the reach of the Jamuna river. Numerical simulations were performed for the flow event discretizing into time steps of 2 seconds. This high-resolution time step was selected as necessary and appropriate to reconstruct the temporal changes in near bank shear stress. The solution domain covers about 18.210 kilometres of the river channel. For the upstream boundary, the constant discharge was considered for the steady-state condition. At the downstream boundary, the normal water level boundary condition was applied.

5.7.3.3 Determination of near bank erosion rate

The erosion rate for the fine soils in a river bed or bank of a river is usually assumed to be proportional to the excess shear stress as shown below (Hanson, 1990b; Hanson & Cook, 1997):

$$\varepsilon = k_d(\tau_a - \tau_c)^a \tag{5.1}$$

Where ε is the rate of erosion (m s^{-1}), k_d is the erodibility co-efficient (m^{3}Ns^{-1}), τ_a the developed shear stress at the soil boundary (Pa), τ_c is the critical shear stress (Pa), and a is the exponent generally considered to be 1.

There are several approaches to the determination of soil erodibility parameters. Due to the influence of several variables, the erodibility parameters are difficult to quantify (Grissinger, 1982). Based on flume testing results, Smerdon and Beasley (1961) developed relationships of τ_c to various soil index properties, as shown in equations 17-19,

$$\tau_c = 3.54 \times 10^{-28.1D_{50}} \tag{5.2}$$

$$\tau_c = 0.493 \times 10^{0.0182P_c} \tag{5.3}$$

Where τ_c is the critical shear stress (Pa), D$_{50}$ is the median particle size of soil (mm), P$_c$ is the percentage of clay content (i.e. content of soil particles less than 0.002 mm in size).

Julian and Torres (2006) established an empirical equation to estimate τ_c from the percentage of silt-clay (SC),

$$\tau_c = 0.1 + 0.1779 \, (SC) + 0.0028 \, (SC)^2 - 2.34 \times 10^{-5} \times (SC)^3 \tag{5.4}$$

Unlike τ_c, empirical estimates of k_d the soil properties are not available ((Hanson & Temple, 2002). However, k_d can be given empirical estimates from known τ_c. Such empirical relations between τ_c and k_d have been developed based on submerged JET results and are often inverse power laws (Hanson & Simon, 2001; Thoman & Niezgoda, 2008; Wynn et al., 2004). Different equations developed for k_d by different researchers are given below:

$$k_d = 3.1 \, \tau_c^{-0.37} \qquad \text{(Wynn et al., 2004)} \tag{5.5}$$

$$k_d = 3.16 \, \tau_c^{-0.185} \quad \text{(Karmaker \& Dutta, 2011)} \tag{5.6}$$

$k_d = 19.54\tau_c^{-0.547}$ (Semmad & Chalermyanont, 2018)   **(5.7)**

5.7.3.4   Slope stability analysis

A limit equilibrium stability analysis was used to determine if the bank is liable to mass failure under gravity. GEO-STUDIO® was used to analyze the Factor of Safety (FOS) using the limit equilibrium method following Morgenstern Price principle considering fluctuation in river water level. The method of Duncan et al. (1990) was used for water level drawdown analysis. This study uses a pair of stability analyses in SLOPE/W in the Geoslope program, including surcharge load, slope protection load, scoured toe, confining pressure of water.

5.7.4   Results

5.7.4.1   Effect of hydraulic shear stress

After numerical simulation in SMS-SRH 2D, several outputs were obtained. Simulated water-induced shear stress along the wetted perimeter of the river is shown in Figure 5.55. It was seen that the magnitude of the hydraulic shear stress was higher near the left bank of the Jamuna river where Chauhali situates. The white portion in the solution domain indicates the bare bars in the river area.
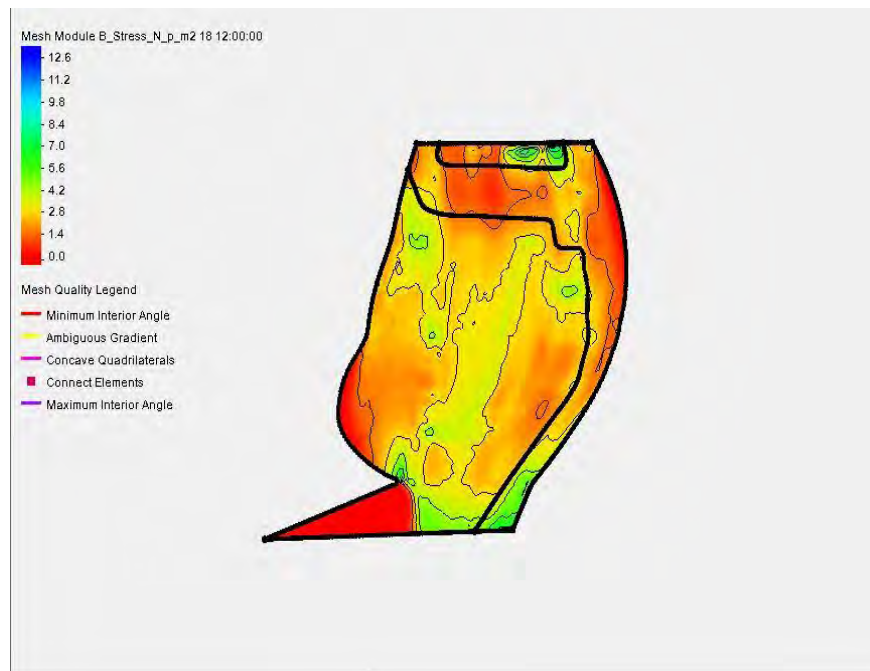
Figure 5.55: Simulated shear stress distribution along the wetted perimeter of river.

The relation of the hydraulic shear stress with the distance from the face of the left bank is shown in Figure 5.56. The graph shows that shear stress increases with the increase in distance and becomes maximum at the toe. So, the bank toe is the most erodible area of the riverbank.
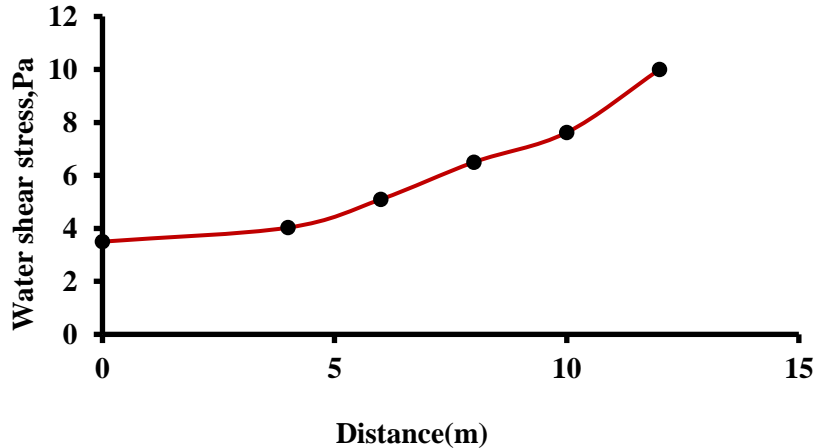
Figure 5.56: Variation of near bank shear stress with distance from the bank face

If the Shear stress applied on the bank due to the erosive power of water is higher than the critical shear stress of bank sediment, then the riverbank erodes. So, it is necessary to compute critical shear stress to know whether fluvial erosion occurs or not. Table 5.7 presents the estimation of critical shear stress, τ_c and erodibility co-efficient, k_d from different empirical formulae, which are provided in the previous section. Results of τ_c and k_d, calculated from equation, were averaged to avoid any inconvenient output for this study. The result showed that the value of τ_c was 8.55 for upper layer and 8.46 for the lower layer. The magnitude of k_d was 3.19 for upper layer and 3.20 for the lower layer.

Table 5.7: Estimation of erodibility parameters from empirical formulae

Layer	Computed τ_c(Pa)			Average	Computed k_d(Cm³/N-s)			Average
	D_{50} (Eq. 24)	P_c (Eq. 25)	SC (Eq. 26)	τ_c	Wynn et al. (2004) (Eq. 27)	Karmaker and Dutta (2011) (Eq. 28)	Semmad and Chalermyanont (2018) (Eq. 29)	k_d
Upper	2.25	2.70	20.69	8.55	1.40	2.12	6.04	3.19
Lower	0.58	4.08	20.71	8.46	1.41	2.13	6.07	3.20

Computed τ_c and k_d were compared with the values obtained from different studies. It was found that computed values were within the range of values provided in different studies. Table 5.8 presents the range of τ_c and k_d, provided in various studies and also in this study.

Table 5.8: Range of critical shear stress, τ_c and erodibility co-efficient, k_d in different studies

Study performed by different researchers	Range of τ_c (Pa)	Range of k_d(Cm³/N-s)
Hanson and Simon (2001)	0.0 to 400	0.001 to 3.75
Julian and Torres (2006)	0.95 to 17.83	Not computed
Thoman and Niezgoda (2008)	0.11 to 15.35	0.27 to 2.38
Simon et al. (2010)	>4.7	0.1 to 33.4
Karmaker and Dutta (2011)	0.1 to 100	0.519 to 11.39
Semmad and Chalermyanont (2018)	4.41 to 20.93	2.23 to 39.99
This study	8.46 to 8.55	3.19 to 3.20

Erosion rate was computed from the excess shear stress model using the equation (23). It was found that bank erosion rate increased linearly with variation in hydraulic shear stress in the upper layer (Figure 5.57) and lower layer (Figure 5.58). Duong Thi and Do Minh (2019), also found the same relationship between erosion rate and bank shear stress.
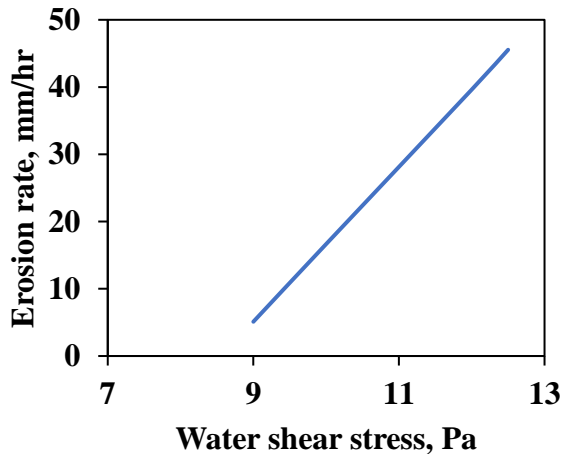

Figure 5.57: Erosion rate with hydraulic shear stress in upper layer
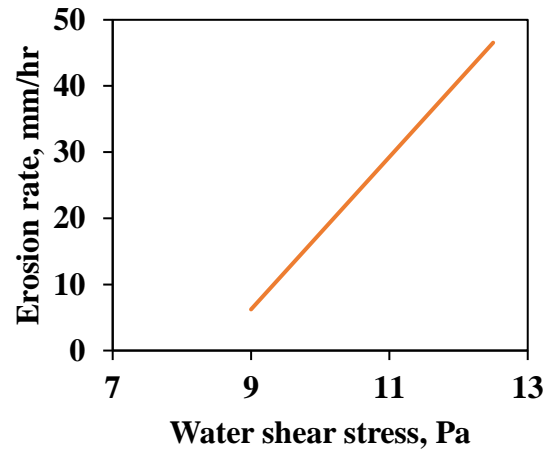
Figure 5.58: Erosion rate with hydraulic shear stress in lower layer

Figure 5.59 demonstrates different categories of riverbank soil according to their erodibility. Hanson and Simon (2001) showed the classification of riverbank soil using the test values of τ_c and k_d. To relate these erodibility parameters to the resistance or erodible nature of the riverbank, a logarithmic plot is illustrated in Figure 5.59. It was found that both layers of riverbank soil fell in the category "very erodible".
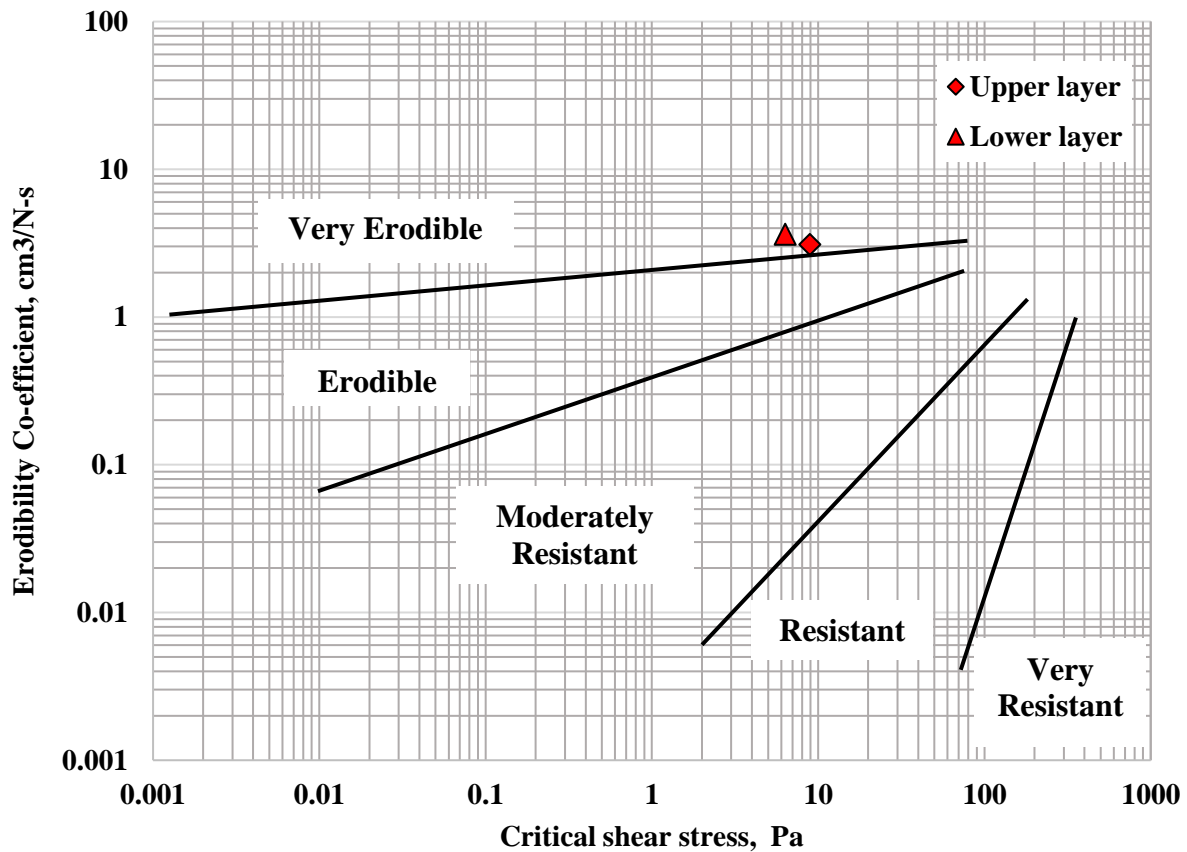
Figure 5.59: Relationship of the critical shear stress and erodibility co-efficient (after Hanson and Simon (2001))

5.7.4.2 **Effect of the scoured toe**

Basal erosion leads to mass failure, which is the failure of the overhanging portion of a bank under gravity. Figure 5.60 illustrates the variation of a factor of safety with scour depth. It was found that the riverbank started to fail when scour depth was higher than 7m. During the field investigation, scour depth was reported 18m above the calculated value of scour depth. So, the bank of Jamuna

river at Chauhali failed without giving any warning after the application of riverbank protection works.
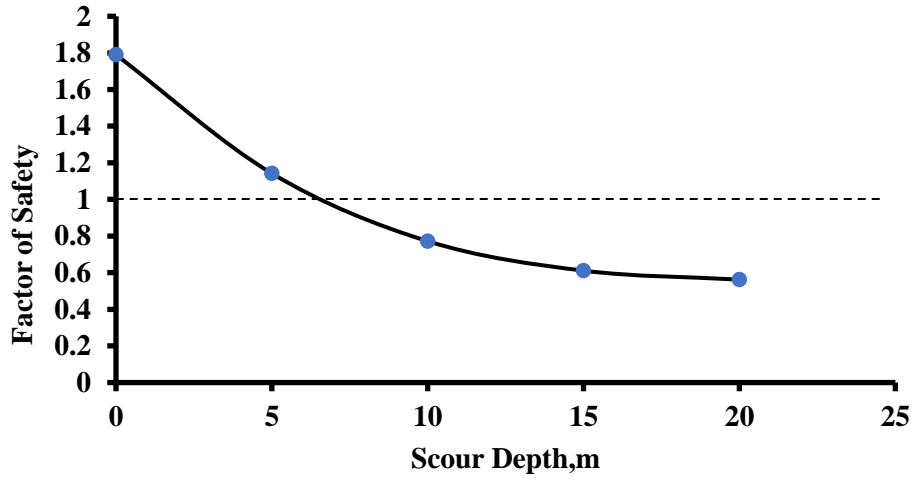

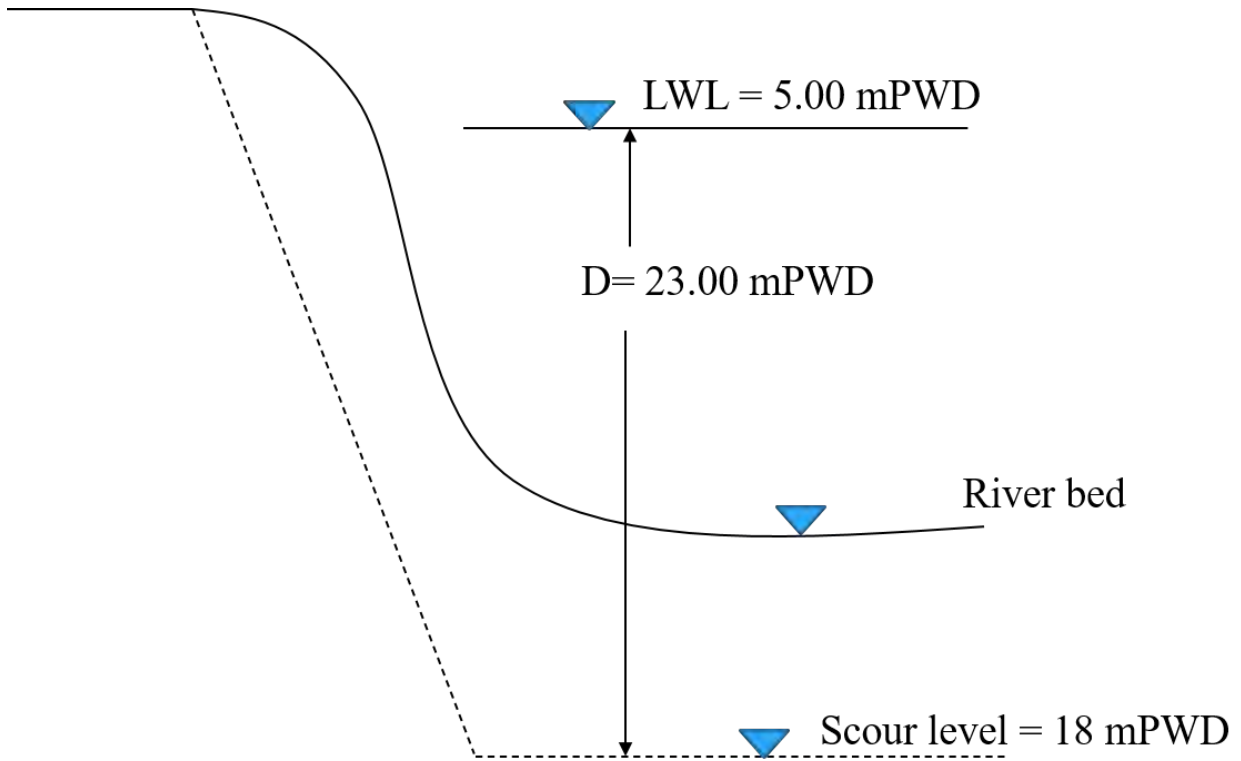**Figure 5.60: Relationship between factor of safety and scour depth**


Figure 5.61: Scour depth at Chauhali.

5.7.4.3 Effect of surcharge load

Consideration of surcharge load plays an important role in designing the riverbank protection works. The effect of the surcharge load on riverbank stability is shown in Figure 5.62. During field visits, several irregularities were identified in the implementation phase. It was observed that at some places, dredged sand was dumped on the bank. Riverbank failure was seen to have occurred in those places where dredged sand was found heaped on the bank.


Figure 5.62: Surcharge load kept over riverbank after dredging

Surcharge load is that additional load on the floodplain near the riverbank, which increases the destabilizing force. Hence, the factor of safety decreases which, eventually makes the riverbank fail. It was found that the riverbank started failing when the surcharge load was 45 KPa at 5m scour depth (Figure 5.63). Surcharge load for the failure of riverbank decreases with increasing of scour depth value. At 7m scour depth, surcharge load needed to fail the bank was 30 KPa (Figure 5.64).
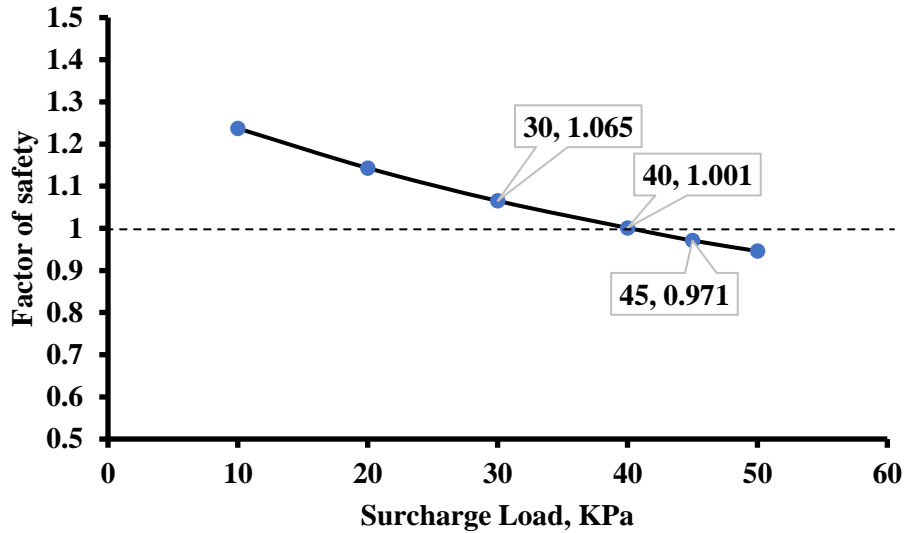
Figure 5.63: Variation of FOS with surcharge load when scour depth is 5m
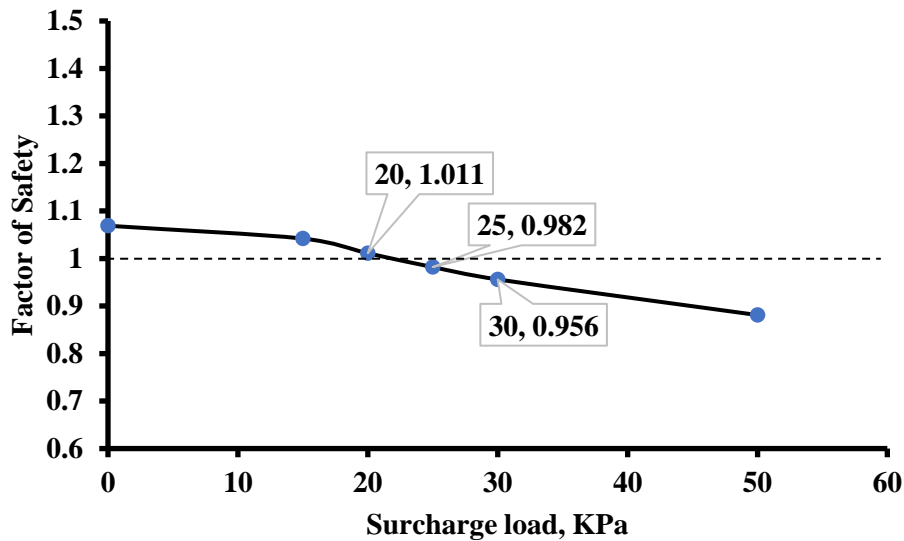
Figure 5.64: Relationship between factor of safety and surcharge load at scour depth 7m

The height of heaped soil over the riverbank was 3m, and the unit weight of that soil was 16.5 K/N/m3. So, the pressure created by this surcharge load was 50 KPa. Also, CC blocks were dumped on loose material at the bank toe. Thus, the applied load is larger than the value of the estimated surcharge load. Slope damage was noticeable in those particular locations.

5.7.4.4 Effect of slope protection load

Different slope protection measures are usually applied on the riverbank to prevent it from failure, including earthen embankment, riprap, CC blocks, sand-filled geo-bags, gabions, mattress etc. These protection measures increase the stability of the slope, preventing fluvial entrainment, piping, sapping, weathering etc. But it should be checked whether these protective elements are responsible for riverbank failure or not. At Chauhali, fluvial erosion was seen dominant as the bank soil was so erodible. During field visits, it was reported that there were at least 15m scour beneath the original river bed. Figure 5.65 shows that the second phase of riverbank protection works when the geobags on the bank slope was removed, and the riverbank was flattened to a slope of 3:1. The permanent wave protection was then constructed from January 2017 to April 2017. Figure 5.66 shows the failure of protection works after the drawdown of floodwater in 2018.

|	
Figure 5.65: Permanent wave protection	**Figure 5.66: Failure of protection works during recession time of floodwater.**

The effect of load coming from the protective element on FOS is illustrated in Figure 5.67. It was found that the safety factor increased with the increase in slope protective load at a certain limit. After that limit, it started declining, making the riverbank susceptible to failure. Therefore, the load coming from slope protective elements can cause riverbank erosion if the magnitude of loads is higher than the critical value.
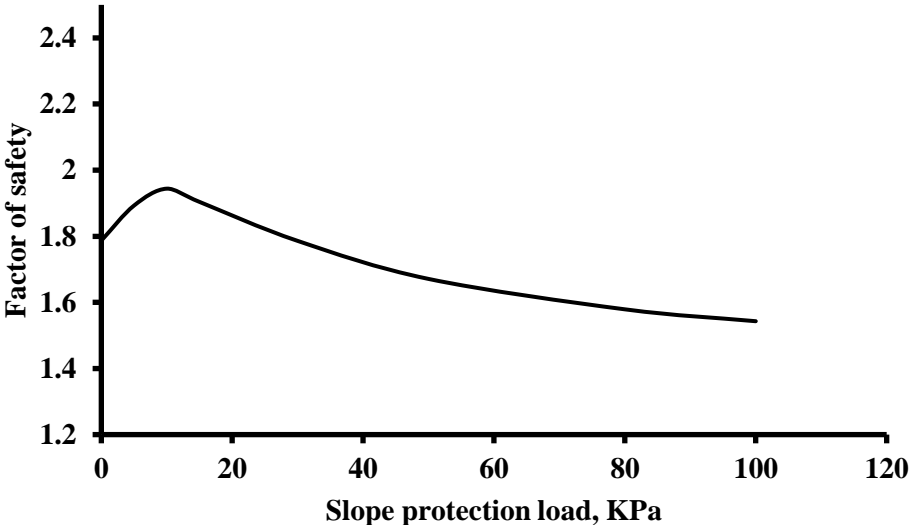
Figure 5.67: Relationship between factor of safety and slope protection load

The factor of safety was seen to decrease with the increase in slope protection load and caused the failure of the bank with the pre-existing scoured toe. During slope stability analysis, it was found that the factor of safety went below the unit value at 7m scour depth when the slope protection load was only 10 KPa (Figure 5.68).
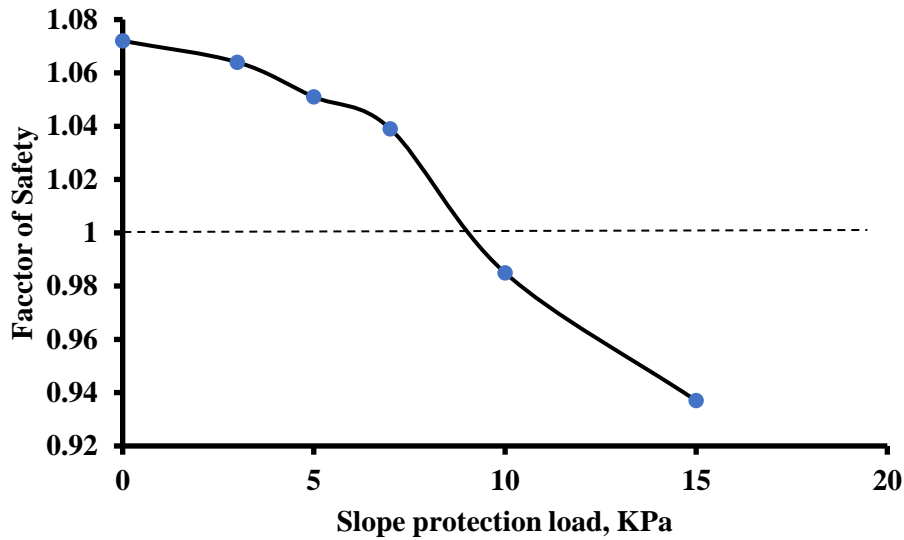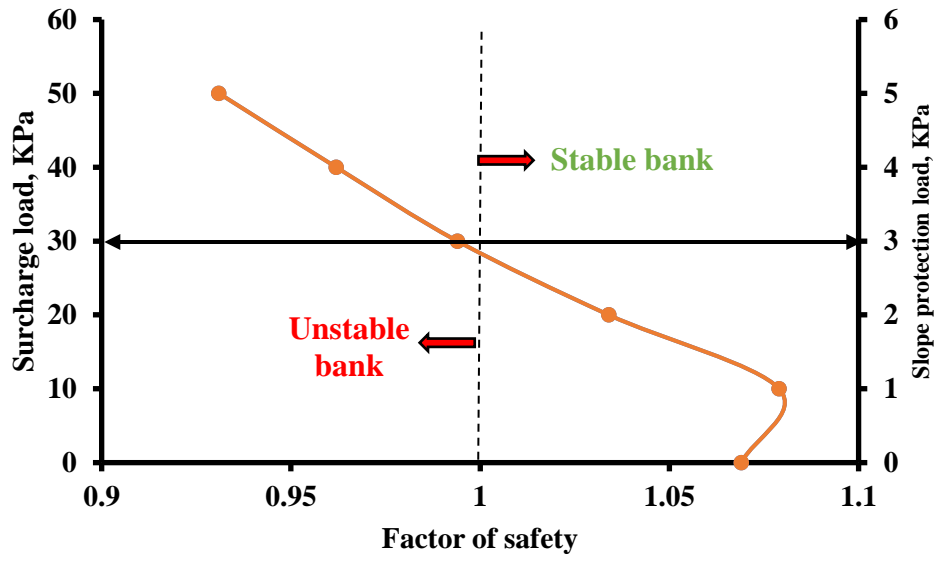
Figure 5.68: Relationship between factor of safety and bank protective load at 7m scour depth

The size of CC block used in protection work was 500 mm, and the unit weight of those blocks was 24 KN/m3. So, CC blocks created a pressure of 12 KPa on the sloping portion of the river bank. The allowable pressure was found 10 KPa with the existing 7m scour level. Hence, the applied pressure exceeded the allowable pressure; the riverbank eventually failed.

5.7.4.5 The combined effect of surcharge load, slope protection load and scoured toe

Toe erosion is a common process in alluvial type rivers due to fluvial erosion, leading to mass failure. The combined effect of surcharge load and slope protection load with a pre-existing scoured toe is shown in Figure 5.69. In the beginning, the factor of safety was seen to increase the very little amount. After that, the factor of safety began to decrease with increasing of surcharge and slope protection load. From Figure 5.69, it can be seen that a combination of 30 KPa surcharge load and 3 KPa slope protection load makes the riverbank unstable. At Chauhali, there existed a surcharge load of 50 KPa and slope protection load of 12 KPa during the implementation phase of riverbank protection works which were higher than the allowable values. So, this combination of load also causes the failure of the riverbank.

Figure 5.69: Relationship among factor of safety, surcharge load and slope protection load at 7m scour depth

5.8 Summary

The results extracted from different scenarios have been summarized in Table 5.9.

Table 5.9: Summary results of different scenarios

Serial No.	Name of parameter	Suggested value	Threshold Factor of safety
1	Surcharge load	≯ 60 KPa	1.076
2	Scour depth	≯ 7m	1.142
3	Surcharge load	≯ 40 KPa	1.001
	Scour depth	5m	
4	Surcharge load	≯ 20 KPa	1.011
	Scour depth	7m	
5	Slope protection load	≯ 10 KPa	1.944
6	Slope protection load	≯ 7 KPa	1.039
	Scour depth	7m	
7	Slope protection load	≯ 6 KPa	1.045
	Surcharge load	≯ 60 KPa	
8	Slope protection load	≯ 3 KPa	1.034
	Surcharge load	≯ 30 KPa	
	Scour depth	7m	
9	Clay, mica, sandy silt and silty sand layer	Mica-30%	2.019
	Sandy silt and silty sand layer	Silt- 50% Clay-17%	1.790
10	Unit weight of bank material	22 KN/m3	
11	Friction angle of bank material	32 °	2.275
12	Cohesion of bank material	12 KPa	

CHAPTER SIX
CONCLUSIONS AND RECOMMENDATIONS

6.1 General

Riverbank erosions are serious concerns in humid tropical climate country like Bangladesh. This study investigated riverbank stability of composite alluvial type river like the Jamuna river considering different hydraulic and static load conditions and provided some design parameters for the safe design of riverbank protection works. Riverbank erosion is closely related to the composition of bank materials. Bank sediments mostly consist of sand and silt with D_{50} range from (0.007-0.224) mm. Pore water pressure derived from water level difference has a significant effect in the riverbank failure process. Toe scouring is a common process in alluvial rivers, which leads to mass failure. Erosion rate was measured using the excess shear stress model in the upper and lower layer of the riverbank, respectively. Hydraulic shear stress was computed with the two-dimensional, depth-averaged model, SRH-2D as solver and SMS as pre-processor and post-processor. Critical shear stress, τ_c and erodibility co-efficient, k_d were calculated from an empirical formula based on Jet Erosion Tests. Results of τ_c and k_d, obtained from this study. A case study of riverbank stability at Chauhali, Bangladesh, was performed to investigate the potential reasons for slope failure.

6.2 Conclusions

The following conclusions have been drawn from the present study are given:

i) Near bank shear stress distribution along the wetted perimeter of the riverbank as resulted from the present study was found to be higher value compared to bank face. From the numerical analysis, hydraulic shear stress was found 10 to 12 Pa near the toe. Critical shear stress of bank soil was 6.34 to 8.91 Pa which was relatively lesser than the water-induced stress. Thus, fluvial erosion is considered to be responsible for bank toe undercutting.

ii) Erosion rate was found linearly varied with water-induced shear stress for both upper and lower soil layer of riverbank slope, which is consistent with the result of Duong Thi and Do Minh (2019).

iii) In Jamuna river, the lower soil layer of bank slope is composed of silty sand was more erodible than the upper layer consisting of silty soil. Based on the soil classification, a graphical relation between critical shear stress and erodibility derived in Figure 5.10. which it can be seen that the bank soil in Jamuna river cases falls into the category of "Very erodible".

iv) The stability of the riverbank was analysed considering various scour depths, i.e., 5 m, 10 m, 15 m and 20 m. It was found that the riverbank begins to erode when scour depth was greater than 7 m without any surcharge load condition.

v) Surcharge load over the riverbank played a significant role in the slope failure mechanism. From the study, it is found that surcharge load greater than 60 KPa causes riverbank failure without toe scour. When scour occurs at the toe, bank stability fails with a comparatively lesser surcharge load. For instant, about surcharge load of 45 KPa is required when scour depth is about 5m. At 7m scour depth, only 30 KPa surcharge loads were needed to destabilize the riverbank, and failure occurred at 10m scour depth without any surcharge load.

vi) With the increase in slope protection load, the factor of safety was seen to increase at certain limits. After that point, the safety factor continued to decline, showing an inverse relation with slope protection load. With pre-existing scour depth of 7m, bank failure happened when the load was only 10 KPa from slope protective elements. The critical combination between surcharge load and slope protection load was found 60 KPa and 6 KPa, respectively, with no, scour depth. When scour depth was 7m, the load combination was 30 KPa and 3 KPa, respectively.

vii) Another scenario of analysis was carried out with clay and mica (30%) underlain by sandy silt and silty sand layer. It was found that clay and mica (30%) increased the safety factor from 1.790 to 2.019.

viii) Six scenarios with different load combination were analysed using two different methods used in this study, such as the limit equilibrium method (LEM) and finite element method (FEM). Values of the factor of safety obtained from these two methods have been compared (Table 5.3). It can be seen from the comparison that the change in the factor of safety of FEM from LEM are in the range of -20 to -30% for scenario 4 indicating that LEM is giving higher factor of safety compared to FEM. The changes in a factor of safety

for other scenarios were not significant. However, finite element analysis uses number of salient input parameters (hydraulic conductivity, elastic modulus of soil etc.), which are not included in limit equilibrium analysis. Therefore, it shows a significant change in results of the factor of safety than that of limit equilibrium method in some cases.

ix) Sensitivity analysis was also performed to obtain the threshold soil properties for riverbank protection works of the Jamuna river. These are unit weight (16 KN/m^3), angle of internal friction (24°), cohesion (2 KPa).

x) For the design of riverbank protection works, it is worthwhile to suggest the values of soil properties which are unit weight (22 KN/m^3), angle of internal friction (32°) and cohesion (12 KPa), which can be considered preferable for the higher factor of safety.

xi) A case study was performed near Chauhali, Sirajganj, along the Jamuna River, which was observed to be failed during the recession period of floodwater after the application of CC blocks for riverbank protection works. During the field visit, it was observed that at some places, dredged sand was dumped on the bank, and also CC blocks were dumped on loose material at bank toe, which generated a pressure of more than 50 KPa on the bank slope. From slope stability analysis, it was found that 45 KPa surcharge pressure made the riverbank unstable when scour depth was 5m. As the applied pressure on the slope is higher than allowable pressure, the riverbank failed. From slope stability analysis, it was found that the slope protection load of 10 KPa caused riverbank failure at 7m to scour depth. At Chauhali, each CC block created a pressure of 12 KPa, which was larger than the allowable slope protection load.

6.3 Recommendations for future study

Following recommendations can be suggested for further study, these are as follows:

i) To get a rigorous understanding of riverbank failure mechanism, empirical formulae of erodibility parameters can be generated for the Jamuna river using the in-situ submerged jet test.

ii) Hydrodynamic oblique flow can be used for hydraulic load in slope stability analysis.

iii) In addition to other load considered in this study, oblique hydraulic loads of various angle can be considered and compared with the study.

iv) Laboratory scale investigation on bank stability can be carried to understand the failure process.

v) Analysis can be done with soil reinforcement by the sand hole and with geotextile.

vi) The effect of tension crack and changes in groundwater table resulting from rainwater infiltration and unsteady state flow through the unsaturated soil can be considered for further study.

vii) Riverbank stability can be assessed considering a scenario with excavation near the countryside of the protection work.

viii) A similar study can be carried out with recently available of SRH 2D which can be used for mobile bed condition.

REFERENCES

Abernethy, B., & Rutherfurd, I. D. (1998). Where along a river's length will vegetation most effectively stabilise stream banks? *Geomorphology*, *23*(1), 55-75.

Abidin, R. Z., Sulaiman, M. S., & Yusoff, N. (2017). Erosion risk assessment: A case study of the Langat River bank in Malaysia. *International Soil and Water Conservation Research*, *5*(1), 26-35.

ADP. (2013). *Bangladesh: Main River Flood and Bank Erosion Risk Management Program* (44167-012). N. H. Consultants.

Affuso, A., Casagli, N., Dapporto, S., Gabbani, G., Gargini, A., & Rinaldi, M. (2000). Monitoring and modelling of unsaturated flow and effects on stream-bank failures. Landslides in Research, Theory and Practice: Proceedings of the 8th International Symposium on Landslides held in Cardiff on 26–30 June 2000,

Al-Madhhachi, A.-S. T., Fox, G. A., Tyagi, A. K., Hanson, G. J., & Bulut, R. (2011). Measuring the erodibility of cohesive soils influenced by seepage forces using a laboratory jet erosion test device. 2011 Louisville, Kentucky, August 7-10, 2011,

Al-Madhhachi, A.-S. T., Hanson, G. J., Fox, G. A., Tyagi, A. K., & Bulut, R. (2013). Measuring soil erodibility using a laboratory "mini" JET. *Transactions of the ASABE*, *56*(3), 901-910.

Arai, R., Ota, K., Sato, T., & Toyoda, Y. (2018). Experimental investigation on cohesionless sandy bank failure resulting from water level rising. *International Journal of Sediment Research*, *33*(1), 47-56.

Arulanandan, K., Gillogley, E., & Tully, R. (1980). *Development of a Quantitative Method to Predict Critical Shear Stress and Rate of Erosion of Natural Undisturbed Cohesive Soils*.

ASCE Task Committee on Hydraul., B. M., & Adjust., M. o. R. W. (1998). River width adjustment. II: Modeling. *Journal of Hydraulic Engineering*, *124*(9), 903-917.

Ashraf, M., & Shakir, A. S. (2018). Prediction of river bank erosion and protection works in a reach of Chenab River, Pakistan. *Arabian Journal of Geosciences*, *11*(7), 145.

Bishop, A. W. (1955). The use of the slip circle in the stability analysis of slopes. *Geotechnique*, *5*(1), 7-17.

Blanckaert, K., & Graf, W. H. (2001). Mean flow and turbulence in open-channel bend. *Journal of Hydraulic Engineering*, *127*(10), 835-847.

BSTEM. (2009). *BSTEM Manual* http://www.ars.usda.gov/SP2UserFiles/Place/64080510/XLS/BSTEM-5.0.xls

Buffington, J. M., & Montgomery, D. R. (1997). A systematic analysis of eight decades of incipient motion studies, with special reference to gravel-bedded rivers. *Water Resources Research*, *33*(8), 1993-2029.

Bull, L., & Kirkby, M. (1997). Gully processes and modelling. *Progress in Physical Geography*, *21*(3), 354-374.

Cancienne, R. M., Fox, G. A., & Simon, A. (2008). Influence of seepage undercutting on the stability of root-reinforced streambanks. *Earth Surface Processes and Landforms: The Journal of the British Geomorphological Research Group*, *33*(11), 1769-1786.

Casagli, N., Rinaldi, M., Gargini, A., & Curini, A. (1999). Pore water pressure and streambank stability: results from a monitoring site on the Sieve River, Italy. *Earth Surface Processes and Landforms*, *24*(12), 1095-1114.

CEGIS. (2010). *Padma Multipurpose Bridge Design Project River Training Works Updated Scheme*

Design Report, Bangladesh Bridge Authority.

Chang, C.-H., Chen, H., Guo, W.-D., Yeh, S.-H., Chen, W.-B., Liu, C.-H., & Lee, S.-C. (2020). Predicting River Embankment Failure Caused by Toe Scour Considering 1D and 2D Hydraulic Models: A Case Study of Da-An River, Taiwan. *Water*, *12*(4), 1026.

Cheng, Y. M., & Lau, C. (2014). *Slope stability analysis and stabilization: new methods and insight*. CRC press.

Chu-Agor, M., Fox, G., Cancienne, R., & Wilson, G. (2008). Seepage caused tension failures and erosion undercutting of hillslopes. *Journal of hydrology*, *359*(3-4), 247-259.

Chu-Agor, M., Fox, G., & Wilson, G. (2009). Empirical sediment transport function predicting seepage erosion undercutting for cohesive bank failure prediction. *Journal of hydrology*, *377*(1-2), 155-164.

Chu-Agor, M., Wilson, G., & Fox, G. A. (2008). Numerical modeling of bank instability by seepage erosion undercutting of layered streambanks. *Journal of Hydrologic Engineering*, *13*(12), 1133-1145.

Clark, L., & Wynn, T. (2007). Methods for determining streambank critical shear stress and soil erodibility: Implications for erosion rate predictions. *Transactions of the ASABE*, *50*(1), 95-106.

Cossette, D., Amin, M., & Mazurek, K. Experiences in jet testing of cohesive soils.

Cossette, D., Amin, M., & Mazurek, K. (2017). Experiences in jet testing of cohesive soils.

Couper, P. R., & Maddock, I. P. (2001). Subaerial river bank erosion processes and their interaction with other bank erosion mechanisms on the River Arrow, Warwickshire, UK. *Earth Surface Processes and Landforms: The Journal of the British Geomorphological Research Group*, *26*(6), 631-646.

Crosta, G., & Prisco, C. d. (1999). On slope instability induced by seepage erosion. *Canadian Geotechnical Journal*, *36*(6), 1056-1073.

Daly, E., Fox, G., & Al-Madhhachi, A. (2013). Application of excess shear stress and mechanistic detachment rate models for the erodibility of cohesive soils. *ASABE Paper*(131596568).

Daly, E., Fox, G., Enlow, H., Storm, D., & Hunt, S. (2015). Site-scale variability of streambank fluvial erodibility parameters as measured with a jet erosion test. *Hydrological Processes*, *29*(26), 5451-5464.

Dapporto, S., & Rinaldi, M. (2003). Modelling river bank retreat by combining fluvial erosion, seepage and mass failure. EGS-AGU-EUG Joint Assembly,

Dapporto, S., Rinaldi, M., Casagli, N., & Vannocci, P. (2003). Mechanisms of riverbank failure along the Arno River, Central Italy. *Earth Surface Processes and Landforms: The Journal of the British Geomorphological Research Group*, *28*(12), 1303-1323.

Darby, S. E., Alabyan, A. M., & Van de Wiel, M. J. (2002). Numerical simulation of bank erosion and channel migration in meandering rivers. *Water Resources Research*, *38*(9), 2-1-2-21.

Darby, S. E., Rinaldi, M., & Dapporto, S. (2007). Coupled simulations of fluvial erosion and mass wasting for cohesive river banks. *Journal of Geophysical Research: Earth Surface*, *112*(F3).

Darby, S. E., & Thorne, C. R. (1996). Numerical simulation of widening and bed deformation of straight sand-bed rivers. I: Model development. *Journal of Hydraulic Engineering*, *122*(4), 184-193.

Darby, S. E., Trieu, H. Q., Carling, P. A., Sarkkula, J., Koponen, J., Kummu, M., Conlan, I., & Leyland, J. (2010). A physically based model to predict hydraulic erosion of fine-grained riverbanks: The role of form roughness in limiting erosion. *Journal of Geophysical Research: Earth Surface*, *115*(F4).

Das, V. K., Roy, S., Barman, K., Debnath, K., Chaudhuri, S., & Mazumder, B. S. (2019). Investigations on undercutting processes of cohesive river bank. *Engineering Geology*, *252*, 110-124.

Davis, L., & Harden, C. (2014). Factors contributing to bank stability in channelized, alluvial streams. *River Research and Applications*, *30*(1), 71-80.

Dietrich, W. E., & Gallinatti, J. D. (1991). Fluvial geomorphology. *Field experiments and measurement programs in geomorphology*, 169-220.

Duijsings, J. (1987). A sediment budget for a forested catchment in Luxembourg and its implications for channel development. *Earth Surface Processes and Landforms*, *12*(2), 173-184.

Duncan, J. M. (1996). State of the art: limit equilibrium and finite-element analysis of slopes. *Journal of Geotechnical engineering*, *122*(7), 577-596.

Duncan, J. M., Wright, S. G., & Wong, K. S. (1990). Slope stability during rapid drawdown. Proceedings of the H. Bolton seed memorial symposium,

Dunne, K., Arratia, P., & Jerolmack, D. (2019). A new method for in-situ measurement of the erosion threshold of river channels.

Dunne, T. (1990). Hydrology, mechanics, and geomorphic implications of erosion by subsurface flow. In *Groundwater Geomorphology: The Role of Subsurface Water in Earth-Surface Processes and Landforms* (Vol. 252, pp. 1-28).

Duong Thi, T., & Do Minh, D. (2019). Riverbank Stability Assessment under River Water Level Changes and Hydraulic Erosion. *Water*, *11*(12), 2598.

Duong, T. T., Komine, H., Do, M. D., & Murakami, S. (2014). Riverbank stability assessment under flooding conditions in the Red River of Hanoi, Vietnam. *Computers and Geotechnics*, *61*, 178-189.

Dutta, S., & Karmakar, T. (2015). Erosion Processes in Composite Riverbanks: Experiments and Modelling. *Int. J. Res. Eng. Technol*, *4*, 85-92.

Enlow, H. K., Fox, G. A., & Guertault, L. (2017). Watershed variability in streambank erodibility and implications for erosion prediction. *Water*, *9*(8), 605.

Evans, D., Gibson, C., & Rossell, R. (2006). Sediment loads and sources in heavily modified Irish catchments: A move towards informed management strategies. *Geomorphology*, *79*(1-2), 93-113.

Fellenius, W. (1936). Calculation of stability of earth dam. Transactions. 2nd Congress Large Dams, Washington, DC, 1936,

Ferguson, R. I., Parsons, D. R., Lane, S. N., & Hardy, R. J. (2003). Flow in meander bends with recirculation at the inner bank. *Water Resources Research*, *39*(11).

Flokstra, C. (1976). *Generation of two-dimensional horizontal secondary currents*. Waterloopkundig Laboratorium.

Fox, G., Wilson, G., Periketi, R., & Cullum, R. (2006). Sediment transport model for seepage erosion of streambank sediment. *Journal of Hydrologic Engineering*, *11*(6), 603-611.

Fox, G. A., & Felice, R. G. (2014). Bank undercutting and tension failure by groundwater seepage: predicting failure mechanisms. *Earth Surface Processes and Landforms*, *39*(6), 758-765.

Fox, G. A., Heeren, D. M., Wilson, G. V., Langendoen, E. J., Fox, A. K., & Chu-Agor, M. L. (2010). Numerically predicting seepage gradient forces and erosion: Sensitivity to soil hydraulic properties. *Journal of hydrology*, *389*(3-4), 354-362.

Fox, G. A., Wilson, G. V., Simon, A., Langendoen, E. J., Akay, O., & Fuchs, J. W. (2007). Measuring streambank erosion due to ground water seepage: correlation to bank pore water pressure, precipitation and stream stage. *Earth Surface Processes and Landforms: The Journal of the British Geomorphological Research Group*, *32*(10), 1558-1573.

Fredlund, D., Krahn, J., & Pufahl, D. (1981). The relationship between limit equilibrium slope stability methods. Proceedings of the International Conference on Soil Mechanics and Foundation Engineering,

Gaskin, S., Pieterse, J., Shafie, A. A., & Lepage, S. (2003). Erosion of undisturbed clay samples from the banks of the St. Lawrence River. *Canadian Journal of Civil Engineering*, *30*(3), 585-595.

Gofar, N., & Kassim, K. A. (2007). *Introduction to geotechnical engineering*. Prentice Hall/Pearson Education South Asia.

Goswami, D. C. (1998). Fluvial regime and flood hydrology of the Brahmaputra River, Assam. *Memoirs-Geological Society of India*, 53-76.

Green, T. R., Beavis, S. G., Dietrich, C. R., & Jakeman, A. J. (1999). Relating stream-bank erosion to in-stream transport of suspended sediment. *Hydrological Processes*, *13*(5), 777-787.

Griffiths, D., & Lane, P. (1999). Slope stability analysis by finite elements. *Geotechnique*, *49*(3), 387-403.

Grissinger, E. (1982). Bank erosion of cohesive materials. *Gravel-bed rivers*, 273-287.

Group, F. I. S. R. W. (1998). *Stream corridor restoration: Principles, processes, and practices*. National Technical Info Svc.

Guo, Y., Yang, Y., & Yu, X. B. (2018). Influence of particle shape on the erodibility of non-cohesive soil: Insights from coupled CFD–DEM simulations. *Particuology*, *39*, 12-24.

Hagerty, D. (1991a). Piping/sapping erosion. I: Basic considerations. *Journal of Hydraulic Engineering*, *117*(8), 991-1008.

Hagerty, D. (1991b). Piping/sapping erosion. II: Identification-diagnosis. *Journal of Hydraulic Engineering*, *117*(8), 1009-1025.

Hanson, G. (1990a). Surface erodibility of earthen channels at high stresses part I-open channel testing. *Transactions of the ASAE*, *33*(1), 127-0131.

Hanson, G. (1990b). Surface erodibility of earthen channels at high stresses part ii-developing an in situ testing device. *Transactions of the ASAE*, *33*(1), 132-0137.

Hanson, G., & Cook, K. (1997). Development of excess shear stress parameters for circular jet testing. *ASAE Paper*, *972227*.

Hanson, G., & Cook, K. (2004). Apparatus, test procedures, and analytical methods to measure soil erodibility in situ. *Applied engineering in agriculture*, *20*(4), 455.

Hanson, G., Cook, K., & Simon, A. (2002). Non-vertical jet testing of cohesive streambank materials. *ASABE Paper*, *22119*.

Hanson, G., & Simon, A. (2001). Erodibility of cohesive streambeds in the loess area of the midwestern USA. *Hydrological Processes*, *15*(1), 23-38.

Hanson, G., & Temple, D. (2002). Performance of bare–earth and vegetated steep channels under long–duration flows. *Transactions of the ASAE*, *45*(3), 695.

Hanson, G. J., & Hunt, S. L. (2007). Lessons learned using laboratory JET method to measure soil erodibility of compacted soils. *Applied engineering in agriculture*, *23*(3), 305-312.

Hemphill, R. W., & Bramley, M. E. (1989). *Protection of river and canal banks: a guide to selection and design*. Butterworth-Heinemann.

Hodskinson, A. (1996). *Flow structure and geomorphology of non-classical river bends* University of Sheffield].

Hodskinson, A., & Ferguson, R. (1998). Numerical modelling of separated flow in river bends: Model testing and experimental investigation of geometric controls on the extent of flow separation at the concave bank. *Hydrological Processes*, *12*(8), 1323-1338.

Huang, J., Hilldale, R., & Greimann, B. (2006). Cohesive sediment transport. *Erosion and sedimentation manual*, 4.1-4.54.

Janbu, N., Bjerrum, L., & Kjaernsli, B. (1956). *Soil mechanics applied to some engineering problems*. Norwegian Geotechnical Institute.

Jugie, M., Gob, F., Virmoux, C., Brunstein, D., Tamisier, V., Le Coeur, C., & Grancher, D. (2018). Characterizing and quantifying the discontinuous bank erosion of a small low energy river using Structure-from-Motion Photogrammetry and erosion pins. *Journal of hydrology*, *563*, 418-434.

Julian, J. P., & Torres, R. (2006). Hydraulic erosion of cohesive riverbanks. *Geomorphology*, *76*(1-2), 193-206.

Karamigolbaghi, M., Ghaneeizad, S. M., Atkinson, J. F., & Bennett, S. J. (2016). Experimental Design of the Submerged Jet Erosion Test for a Soil Erodibility Evaluation. World Environmental and Water Resources Congress 2016,

Karmaker, T., & Dutta, S. (2009). Predicting vulnerable bank erosion zones in a large river meander. *Proc. of Water, Environment, Energy and Society (WEES)-2009*, 1670-1676.

Karmaker, T., & Dutta, S. (2011). Erodibility of fine soil from the composite river bank of Brahmaputra in India. *Hydrological Processes*, *25*(1), 104-111.

Karmaker, T., & Dutta, S. (2013). Modeling seepage erosion and bank retreat in a composite river bank. *Journal of hydrology*, *476*, 178-187.

Karmaker, T., & Dutta, S. (2015). Stochastic erosion of composite banks in alluvial river bends. *Hydrological Processes*, *29*(6), 1324-1339.

Kim, S.-C., Friedrichs, C., Maa, J.-Y., & Wright, L. (2000). Estimating bottom stress in tidal boundary layer from acoustic Doppler velocimeter data. *Journal of Hydraulic Engineering*, *126*(6), 399-406.

Klavon, K., Fox, G., Guertault, L., Langendoen, E., Enlow, H., Miller, R., & Khanal, A. (2017). Evaluating a process-based model for use in streambank stabilization: insights on the Bank Stability and Toe Erosion Model (BSTEM). *Earth Surface Processes and Landforms*, *42*(1), 191-213.

Knighton, D. (1998). Fluvial forms and processes: a new perspective John Wiley and Sons. *New York*.

Lai, Y. G. (2008). SRH-2D version 2: Theory and User's Manual. *Sedimentation and River Hydraulics–Two-Dimensional River Flow Modeling, US Department of Interior, Bureau of Reclamation, November*.

Lai, Y. G., & Greimann, B. P. (2010). Predicting contraction scour with a two-dimensional depth-averaged model. *Journal of hydraulic research*, *48*(3), 383-387.

Lai, Y. G., Thomas, R. E., Ozeren, Y., Simon, A., Greimann, B. P., & Wu, K. (2012). Coupling a two-dimensional model with a deterministic bank stability model. World Environmental and Water Resources Congress 2012: Crossing Boundaries,

Lai, Y. G., Weber, L. J., & Patel, V. (2003). Nonhydrostatic three-dimensional method for hydraulic flow simulation. II: Validation and application. *Journal of Hydraulic Engineering*, *129*(3), 206-214.

Lai, Y. G., & Wu, K. (2013). Modeling of vertical and lateral erosion on the Chosui River, Taiwan. World Environmental and Water Resources Congress 2013: Showcasing the Future,

Lai, Y. G., & Wu, K. (2014). Combined Vertical And Lateral Channel Evolution Numerical Modeling.

Lambe, T. W., & Whitman, R. V. (1969). *Soil Mechanics*. John Wiley & Sons.

Langendoen, E. (2010). Assessing post-dam removal sediment dynamics using the CONCEPTS computer model. Proceedings of the 2 nd Joint Federal Interagency Conference, Las Vegas, NV,

Langendoen, E. J. (2000). *Concepts: Conservational channel evolution and pollutant transport system*. USDA-ARS Naitonal Sedimentation Laboratory.

Langendoen, E. J., & Simon, A. (2008). Modeling the evolution of incised streams. II: Streambank erosion. *Journal of Hydraulic Engineering*, *134*(7), 905-915.

[Record #121 is using a reference type undefined in this output style.]

Lawler, D., Grove, J., Couperthwaite, J., & Leeks, G. (1999). Downstream change in river bank erosion rates in the Swale–Ouse system, northern England. *Hydrological Processes*, *13*(7), 977-992.

Lawler, D., Thorne, C., & Hooke, J. (1997). Bank erosion and instability. Applied fluvial geomorphology for river engineering and management,

Lawler, D. M. (1993). The measurement of river bank erosion and lateral channel change: a review. *Earth Surface Processes and Landforms*, *18*(9), 777-821.

Liang, C., Jaksa, M., Ostendorf, B., & Kuo, Y. (2015). Influence of river level fluctuations and climate on riverbank stability. *Computers and Geotechnics*, *63*, 83-98.

Lindow, N., Fox, G. A., & Evans, R. O. (2009). Seepage erosion in layered stream bank material. *Earth Surface Processes and Landforms*, *34*(12), 1693-1701.

Luppi, L., Rinaldi, M., Teruggi, L. B., Darby, S. E., & Nardi, L. (2009). Monitoring and numerical modelling of riverbank erosion processes: a case study along the Cecina River (central Italy). *Earth Surface Processes and Landforms*, *34*(4), 530-546.

Matsui, T., & San, K.-C. (1992). Finite element slope stability analysis by shear strength reduction technique. *Soils and foundations*, *32*(1), 59-70.

Mazurek, K., Rajaratnam, N., & Sego, D. (1999). The characteristics of erosion of a consolidated clay. Annual Conference of the Canadian Society for Civil Engineering, June,

Midgley, T., Fox, G., Wilson, G., Heeren, D., Langendoen, E., & Simon, A. (2013). Seepage-induced streambank erosion and instability: in situ constant-head experiments. *Journal of Hydrologic Engineering*, *18*(10), 1200-1210.

Midgley, T. L., Fox, G. A., & Heeren, D. M. (2012). Evaluation of the bank stability and toe erosion model (BSTEM) for predicting lateral retreat on composite streambanks. *Geomorphology*, *145*, 107-114.

Mihn Duc, B., Wenka, T., and Rodi, E. (1996). *Depth-averaged numerical modeling of flow in curved open channels.* Proc. of 11th Conf. Computational Methods, Cancun, Mexico.

Millar, R. G., & Quick, M. C. (1998). Stable width and depth of gravel-bed rivers with cohesive banks. *Journal of Hydraulic Engineering*, *124*(10), 1005-1013.

MO, Y.-g., DING, D.-x., & XIAO, M. (2006). Application of improved back propagation neural network on stability evaluation of slopes [J]. *Mining and Metallurgy*, *2*.

Mohammed-Ali, W., Mendoza, C., & Holmes, R. R. (2020). Riverbank stability assessment during hydro-peak flow events: The lower Osage River case (Missouri, USA). *International Journal of River Basin Management*, 1-9.

Morgan, R. P. C., Collins, A., & Hann, M. (1999). *Waterway Bank Protection: A Guide to erosion assessment and management*. Stationery Office.

Morgenstern, N. u., & Price, V. E. (1965). The analysis of the stability of general slip surfaces. *Geotechnique*, *15*(1), 79-93.

Mosselman, E., Huisink, M., Koomen, E., & Seijmonsbergen, A. (1995). Morphological changes in a large braided sand-bed river. River geomorphology,

Muramoto, Y., & Fujita, Y. (1992). Recent channel processes of the major rivers in Bangladesh: centering around the bank erosion in the Meghna river. *Kyoto Daigaku Bōsai Kenkyūjo nenpō*(35), 89-114.

Musa, J. J., Abdulwaheed, S., & Saidu, M. (2010). Effect of surface runoff on Nigerian rural roads (a case study of Offa local government area). *AU J. Technol*, *13*, 242-248.

Nagata, N., Hosoda, T., & Muramoto, Y. (2000). Numerical analysis of river channel processes with bank erosion. *Journal of Hydraulic Engineering*, *126*(4), 243-252.

Osman, A. M., & Thorne, C. R. (1988). Riverbank stability analysis. I: Theory. *Journal of Hydraulic Engineering*, *114*(2), 134-150.

Papanicolaou, A. N., Elhakeem, M., & Hilldale, R. (2007). Secondary current effects on cohesive river bank erosion. *Water Resources Research*, *43*(12).

Parker, C., Simon, A., & Thorne, C. R. (2008). The effects of variability in bank material properties on riverbank stability: Goodwin Creek, Mississippi. *Geomorphology*, *101*(4), 533-543.

Partheniades, E. (1965). Erosion and deposition of cohesive soils. *Journal of the Hydraulics Division*, *91*(1), 105-139.

Patsinghasanee, S., Kimura, I., & Shimizu, Y. (2015). Experimental and numerical study on overhanging failure of river bank. *土木学会論文集 B1 (水工学)*, *71*(4), I_127-I_132.

Patsinghasanee, S., Kimura, I., Shimizu, Y., Nabi, M., & Chub-Uppakarn, T. (2017). Coupled studies of fluvial erosion and cantilever failure for cohesive riverbanks: Case studies in the experimental flumes and U-Tapao River. *Journal of Hydro-environment Research*, *16*, 13-26.

Pizzuto, J. E. (1984). Equilibrium bank geometry and the width of shallow sandbed streams. *Earth Surface Processes and Landforms*, *9*(3), 199-207.

R. Grove, J., Croke, J., & Thompson, C. (2013). Quantifying different riverbank erosion processes during an extreme flood event. *Earth Surface Processes and Landforms*, *38*(12), 1393-1406.

Ray, R., & De Smedt, F. (2009). Slope stability analysis on a regional scale using GIS: a case study from Dhading, Nepal. *Environmental geology*, *57*(7), 1603-1611.

Rinaldi, M., & Casagli, N. (1999). Stability of streambanks formed in partially saturated soils and effects of negative pore water pressures: the Sieve River (Italy). *Geomorphology*, *26*(4), 253-277.

Rinaldi, M., Casagli, N., Dapporto, S., & Gargini, A. (2004). Monitoring and modelling of pore water pressure changes and riverbank stability during flow events. *Earth Surface Processes and Landforms*, *29*(2), 237-254.

Rinaldi, M., & Darby, S. E. (2007). 9 Modelling river-bank-erosion processes and mass failure mechanisms: progress towards fully coupled simulations. *Developments in Earth Surface Processes*, *11*, 213-239.

Rinaldi, M., Mengoni, B., Luppi, L., Darby, S. E., & Mosselman, E. (2008). Numerical simulation of hydrodynamics and bank erosion in a river bend. *Water Resources Research*, *44*(9).

Rinaldi, M., & Nardi, L. (2013). Modeling interactions between riverbank hydrology and mass failures. *Journal of Hydrologic Engineering*, *18*(10), 1231-1240.

Rodi, W. (1993). *Turbulence Models and Their Application in Hydraulics*. CRC Press.

Rosgen, D. (1996). Applied river morphology. Wildland Hydrology Consultants. *Inc., Pagosa Springs, Colorado*.

Salem, H., & Rennie, C. D. (2017). Practical determination of critical shear stress in cohesive soils. *Journal of Hydraulic Engineering*, *143*(10), 04017045.

Samadi, A., Amiri-Tokaldany, E., Davoudi, M., & Darby, S. E. (2013). Experimental and numerical investigation of the stability of overhanging riverbanks. *Geomorphology*, *184*, 1-19.

Samtani, N. C., & Nowatzki, E. A. (2006). *Soils and Foundations: Reference Manual*.

Sarker, M. H., Akter, J., & Ruknul, M. (2011). River bank protection measures in the Brahmaputra-Jamuna River: Bangladesh experience. International Seminar on'River, Society and Sustainable Development, Dibrugarh University, India,

Sekely, A. C., Mulla, D., & Bauer, D. W. (2002). Streambank slumping and its contribution to the phosphorus and suspended sediment loads of the Blue Earth River, Minnesota. *Journal of Soil and Water Conservation*, *57*(5), 243-250.

Semmad, S., & Chalermyanont, T. (2018). Riverbank retreat analysis of the U-Tapao River, southern Thailand. *Arabian Journal of Geosciences*, *11*(12), 295.

Semmad, S., Chup-uppakan, T., & Chalermyanont, T. (2019). An alternative method for determining erosion parameters related to non-linear model; based on submerged jet erosion test. *International Journal*, *16*(53), 53-61.

Shields, A. (1936). Application of similarity principles and turbulence research to bed-load movement.

Simon, A., & Collison, A. J. (2001). Pore-water pressure effects on the detachment of cohesive streambeds: seepage forces and matric suction. *Earth Surface Processes and Landforms*, *26*(13), 1421-1442.

Simon, A., & Collison, A. J. (2002). Quantifying the mechanical and hydrologic effects of riparian vegetation on streambank stability. *Earth Surface Processes and Landforms*, *27*(5), 527-546.

Simon, A., Collison, A. J., & Layzell, A. (2003). Incorporating bank-toe erosion by hydraulic shear into the ARS bank-stability model: Missouri River, Eastern Montana. World Water & Environmental Resources Congress 2003,

Simon, A., Pollen-Bankhead, N., & Thomas, R. E. (2011). Development and application of a deterministic bank stability and toe erosion model for stream restoration. *Stream Restoration in Dynamic Fluvial Systems*, 453-474.

Simon, A., & Rinaldi, M. (2000). Channel instability in the loess area of the midwestern united states 1. *JAWRA Journal of the American Water Resources Association*, *36*(1), 133-150.

Simon, A., & Rinaldi, M. (2006). Disturbance, stream incision, and channel evolution: The roles of excess transport capacity and boundary materials in controlling channel response. *Geomorphology*, *79*(3-4), 361-383.

Simon, A., Thomas, R., & Klimetz, L. (2010). Comparison and experiences with field techniques to measure critical shear stress and erodibility of cohesive deposits. 2nd Joint Federal Interagency Conference, Las Vegas, NV,

Simons, D., & Li, R.-M. (1982). Bank erosion on regulated rivers. *Gravelbed Rivers*, 717-274.

Singer, M. J., & Munns, D. N. (2006). *Soils: an introduction*. Pearson Prentice Hall Upper Saddle River, NJ.

Smerdon, E. T., & Beasley, R. P. (1961). Critical tractive forces in cohesive soils. *Agricultural Engineering*, *42*(1), 26-29.

Sutarto, T. E. (2014). Bank erosion processes in streams in the US Midwest.

Swiss Standard, S. (1999). 670 010b. *Characteristic Coefficients of soils, Association of Swiss Road and Traffic Engineers*.

Taylor, D. W. (1937). Stability of earth slopes. *J. Boston Soc. Civil Engineers*, *24*(3), 197-247.

Thoman, R. W., & Niezgoda, S. L. (2008). Determining erodibility, critical shear stress, and allowable discharge estimates for cohesive channels: Case study in the Powder River basin of Wyoming. *Journal of Hydraulic Engineering*, *134*(12), 1677-1687.

Thorne, C. (1982). Processes and mechanisms of river bank erosion. *Gravel-bed rivers*, 227-271.

Thorne, C. (1992). Bend scour and bank erosion on the meandering Red River, Louisiana. Lowland floodplain rivers. Geomorphological perspectives,

THORNE, C. R. (1990). Effects of vegetation on riverbank erosion and stability. *Vegetation and erosion*.

Thorne, C. R. (1998). *Stream reconnaissance handbook: geomorphological investigation and analysis of river channels*. John Wiley & Sons Ltd.

Thorne, C. R., & Osman, A. M. (1988). Riverbank stability analysis. II: Applications. *Journal of Hydraulic Engineering*, *114*(2), 151-172.

Thorne, C. R., & Tovey, N. K. (1981). Stability of composite river banks. *Earth Surface Processes and Landforms*, *6*(5), 469-484.

Tingsanchali, T., & Chinnarasri, C. (1997). Design of Mekong river bank protection. Proc. Conf. on Mgmt. of Landscapes Distributed by Channel Incision, University of Mississippi, Miss,

Toan, D. T. (2020). Assessment Riverbank Stability of the Red Riverbank: Case Study in the Riverbank from Km 20 to km 27, Ba Vi, Hanoi. In *Geotechnics for Sustainable Infrastructure Development* (pp. 929-936). Springer.

Veihe, A., Jensen, N. H., Schiøtz, I. G., & Nielsen, S. L. (2011). Magnitude and processes of bank erosion at a small stream in Denmark. *Hydrological Processes*, *25*(10), 1597-1613.

Vermeyen, T. (1995). *Erosional and depositional characteristics of cohesive sediments found in Elephant Butte Reservoir, New Mexico*. US Department of the Interior, Bureau of Reclamation, Water Resources ….

Watson, A., & Basher, L. (2006). Stream bank erosion: a review of processes of bank failure, measurement and assessment techniques, and modelling approaches. *A report prepared for stakeholders of the Motueka Integrated Catchment Management Programme and the Raglan Fine Sediment Study. Landcare Research, Hamilton, New Zealand*.

Whitman, R. V., & Bailey, W. A. (1967). Use of computers for slope stability analysis. *Journal of Soil Mechanics & Foundations Div*.

Wilson, G., Periketi, R., Fox, G., Dabney, S., Shields, F., & Cullum, R. (2007). Soil properties controlling seepage erosion contributions to streambank failure. *Earth Surface Processes and Landforms: The Journal of the British Geomorphological Research Group*, *32*(3), 447-459.

Winterwerp, J., Van Kesteren, W., Van Prooijen, B., & Jacobs, W. (2012). A conceptual framework for shear flow–induced erosion of soft cohesive sediment beds. *Journal of Geophysical Research: Oceans*, *117*(C10).

Winterwerp, J. C., & Van Kesteren, W. G. (2004). *Introduction to the physics of cohesive sediment dynamics in the marine environment*. Elsevier.

Wolman, M. G. (1959). Factors influencing erosion of a cohesive river bank. *American Journal of Science*, *257*(3), 204-216.

Wynn, T., Henderson, M., & Vaughan, D. (2008). Changes in streambank erodibility and critical shear stress due to subaerial processes along a headwater stream, southwestern Virginia, USA. *Geomorphology*, *97*(3-4), 260-273.

Wynn, T. M., Mostaghimi, S., & Alphin, E. F. (2004). The effects of vegetation on stream bank erosion. 2004 ASAE Annual Meeting,

Yagisawa, J., van Damme, M., Pol, J., Eng, M., & Bricker, J. (2019). Verification of a Predictive Formula for Critical Shear Stress with Large Scale Levee Erosion Experiment. 11th ICOLD European Club Symposium,

Yu, M., Xie, Y., Wu, S., & Tian, H. (2019). Sidewall shear stress distribution effects on cohesive bank erosion in curved channels. Proceedings of the institution of civil engineers-water management,

Zhang, J., Soltani, A., Deng, A., & Jaksa, M. B. (2019). Mechanical behavior of micaceous clays. *Journal of Rock Mechanics and Geotechnical Engineering*, *11*(5), 1044-1054.

Zong, Q., Xia, J., Zhou, M., Deng, S., & Zhang, Y. (2017). Modelling of the retreat process of composite riverbank in the Jingjiang Reach using the improved BSTEM. *Hydrological Processes*, *31*(26), 4669-4681.

APPENDICES

Appendix A: **Hydrodynamic Analysis**

A-1 Satellite image of Jamuna river in 2018
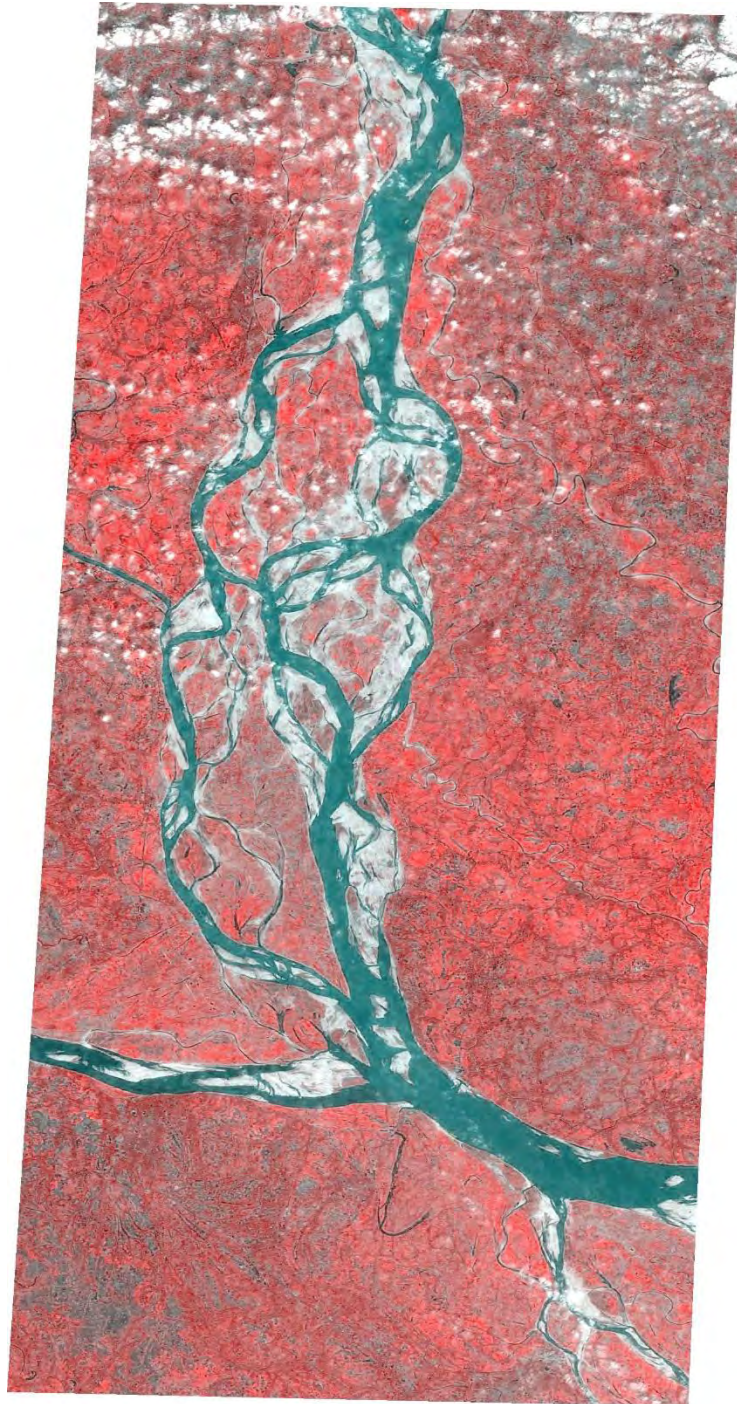
A-2 Cross section 1 of the selected reach of Jamuna river
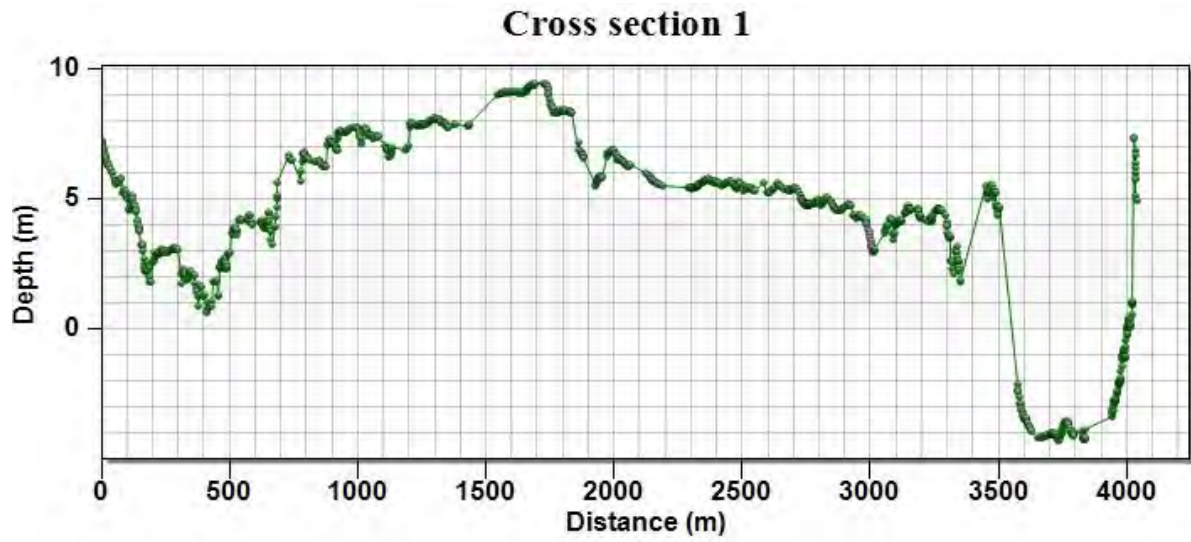
Cross section 1

A-3 Cross section 2 of the selected reach of Jamuna river
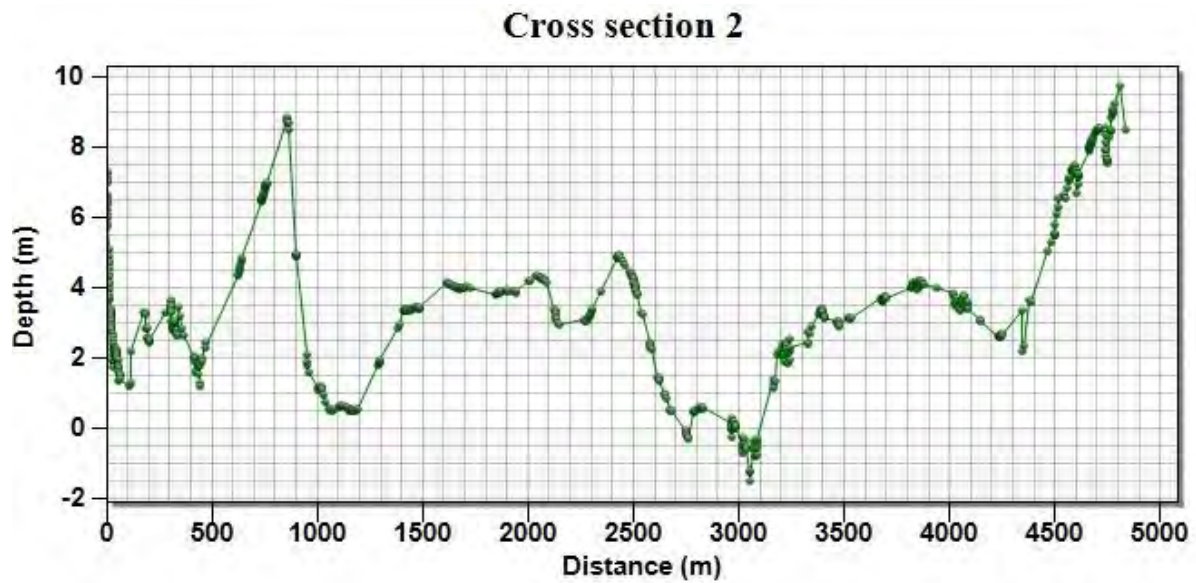
Cross section 2

A-4 Cross section 3 of the selected reach of Jamuna river
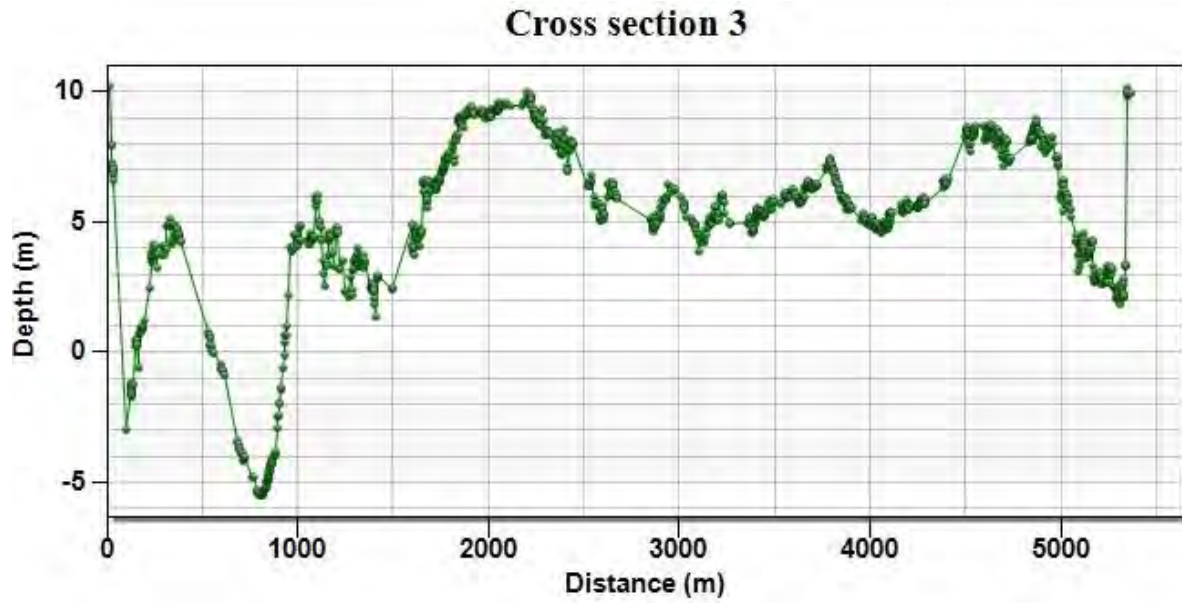
A-5 Cross section 7 of the selected reach of Jamuna river
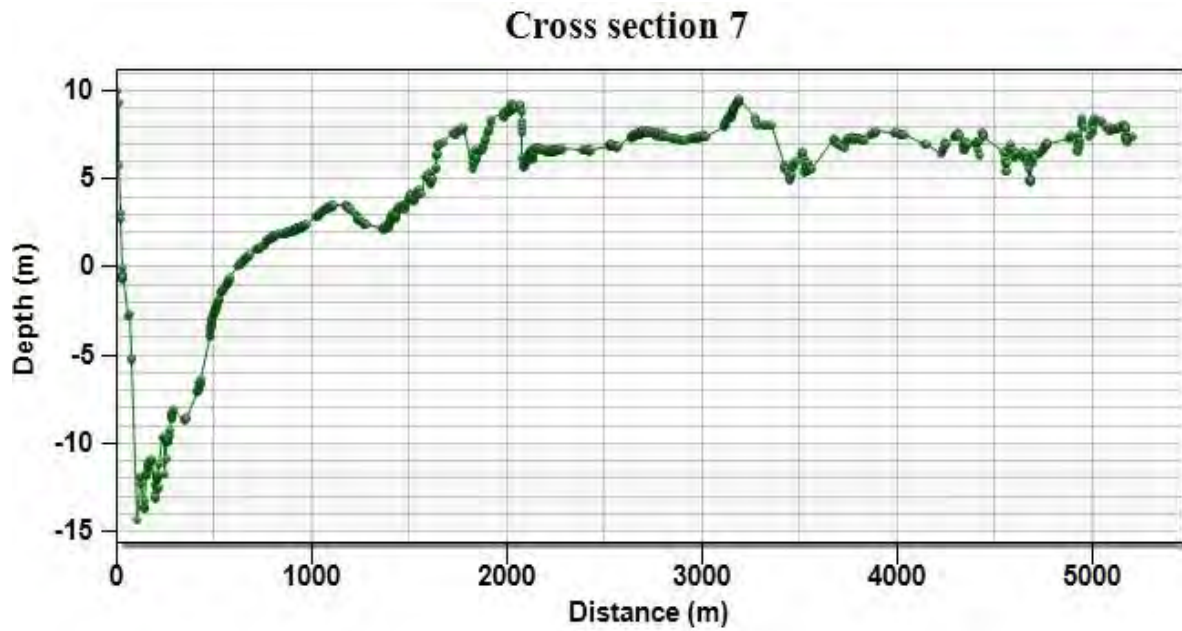
A-6 Cross section 8 of the selected reach of Jamuna river
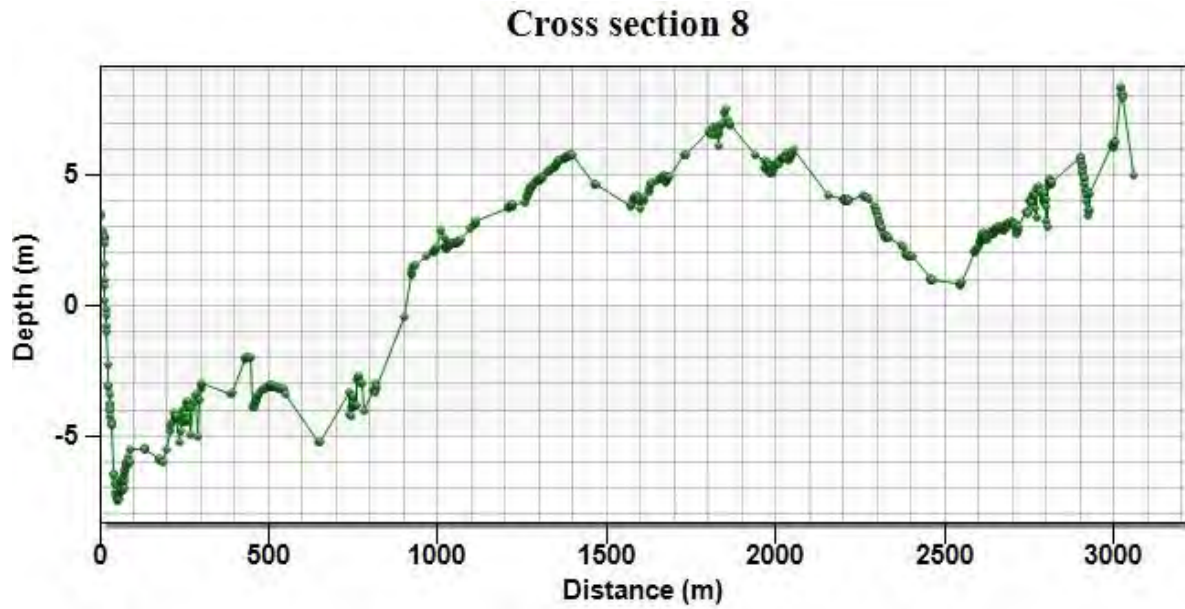
Cross section 8

A-7 Cross section 9 of the selected reach of Jamuna river

Cross section 9
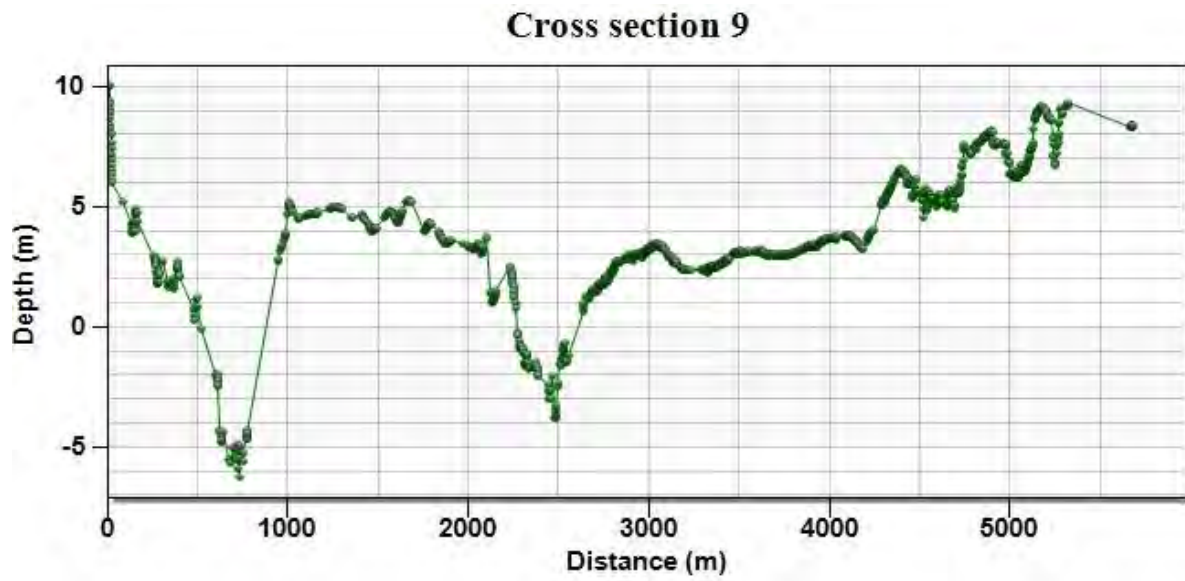
A-8 Bed elevation of the selected reach of Jamuna river.
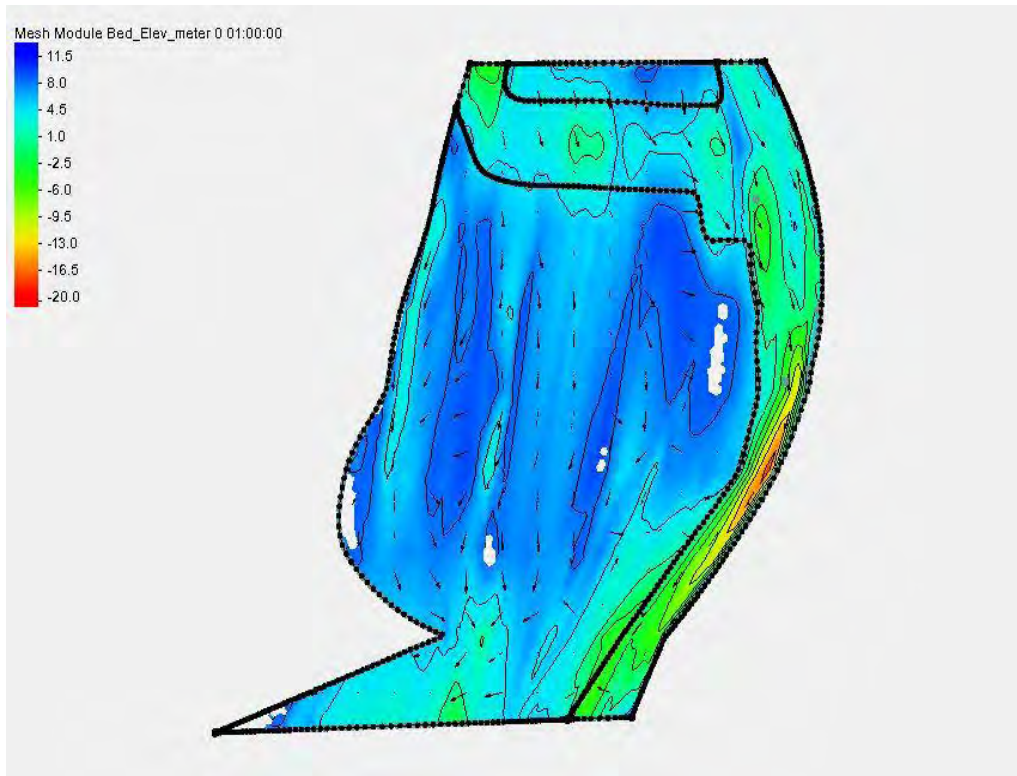
A-9 Simulated magnitude of velocity of the selected reach along Jamuna river.
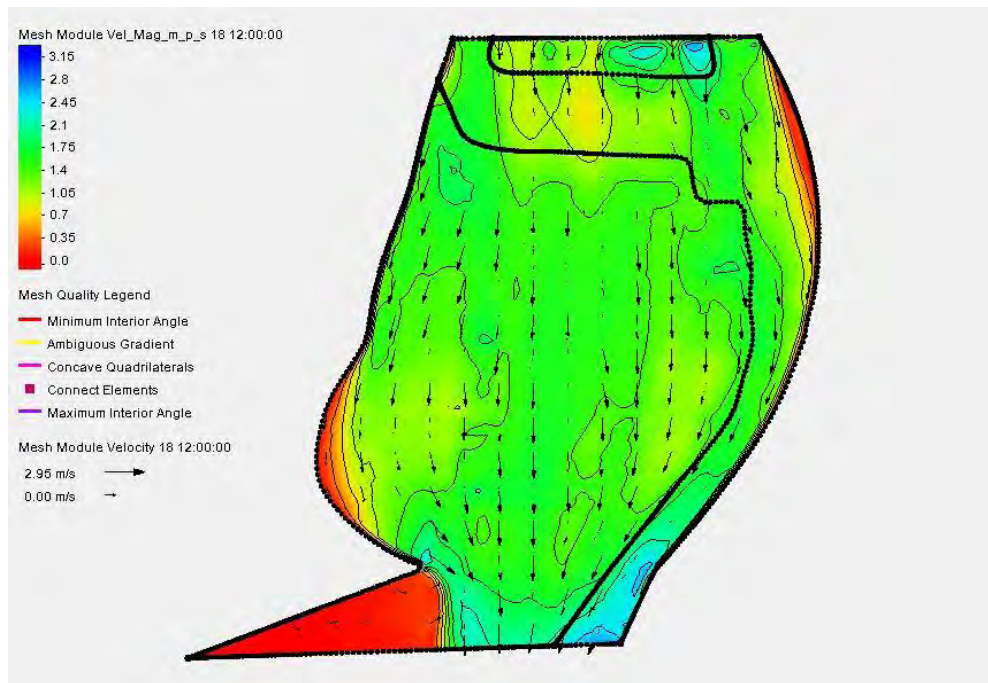
A-10 Simulated water depth of selected reach of Jamuna river
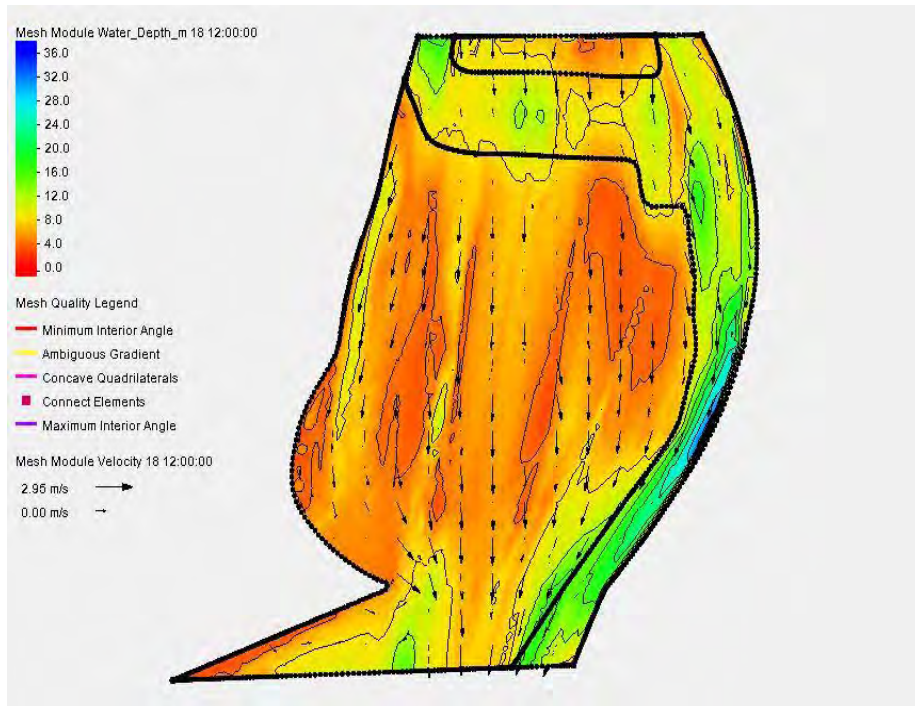
A-12 Simulated water elevation of selected reach of Jamuna river
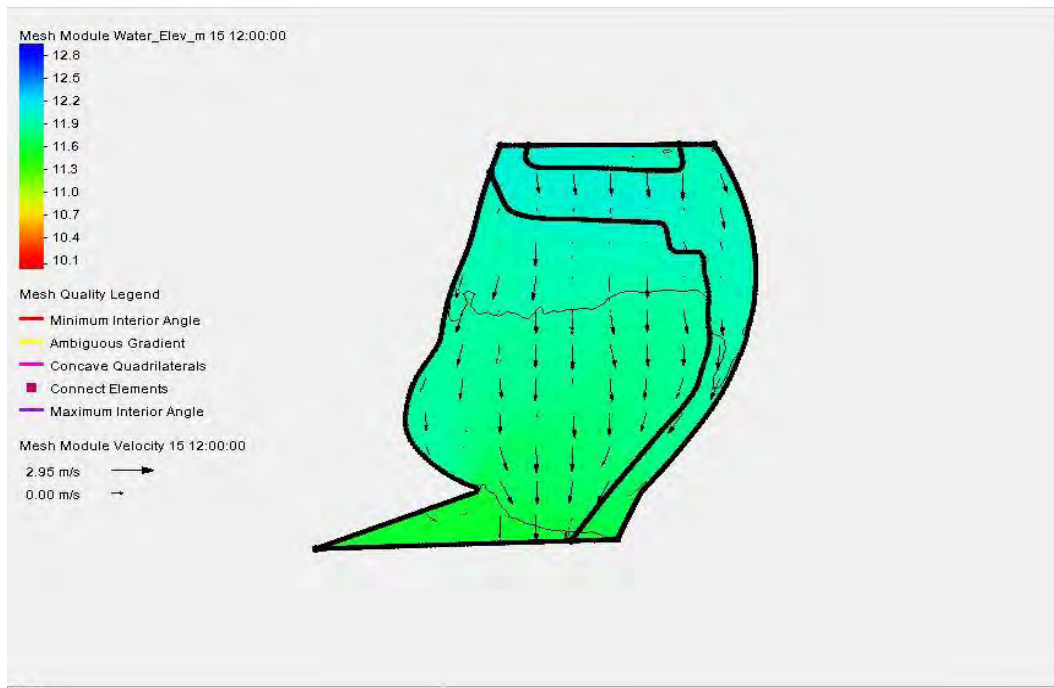
Appendix B: Slope stability analysis

Appendix B.1   : Limit equilibrium method

B.1-1 Illustration of slope stability analysis considering scour volume
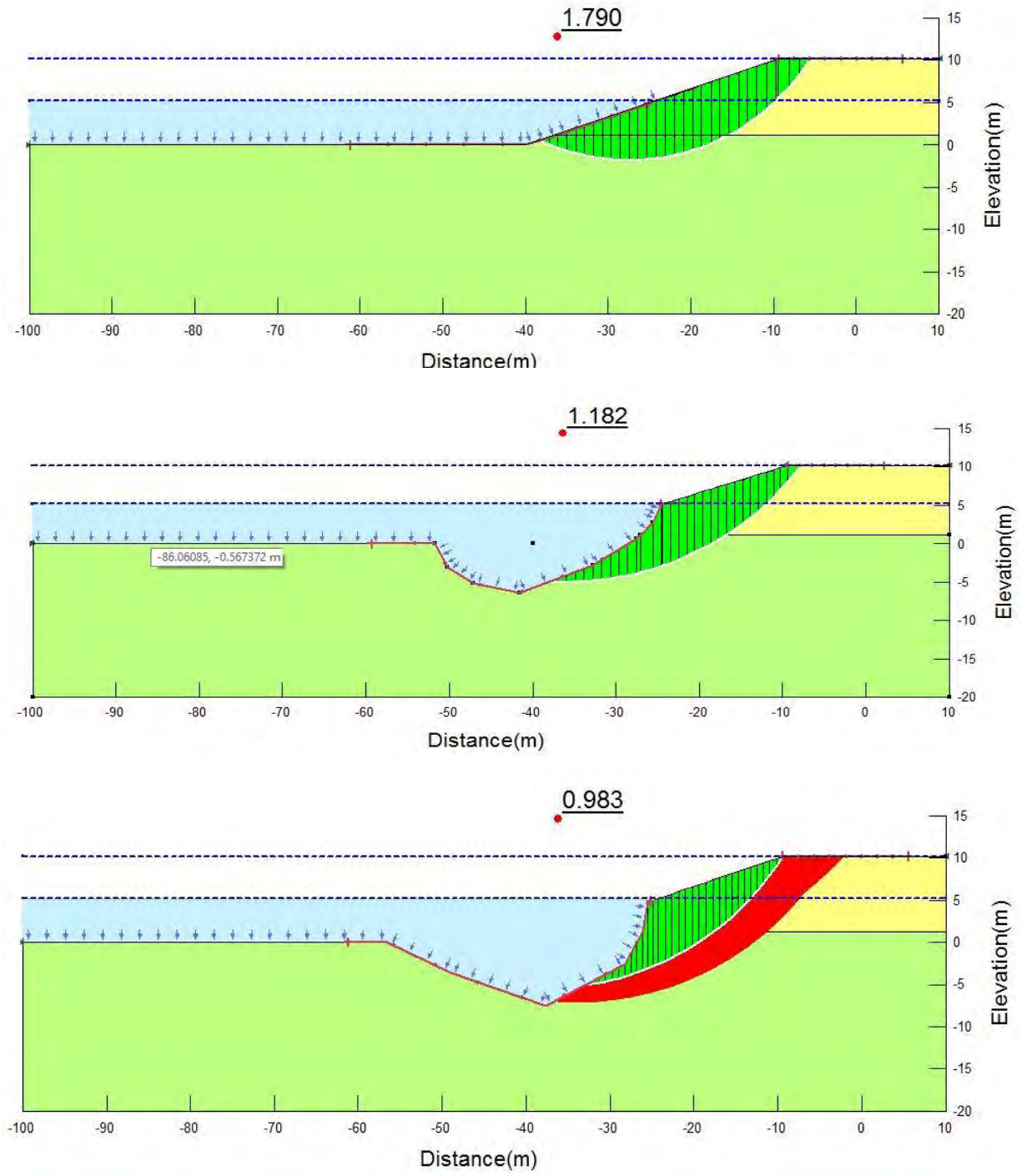
B.1-2 Variation of factor of safety with volume of soil removed from toe.
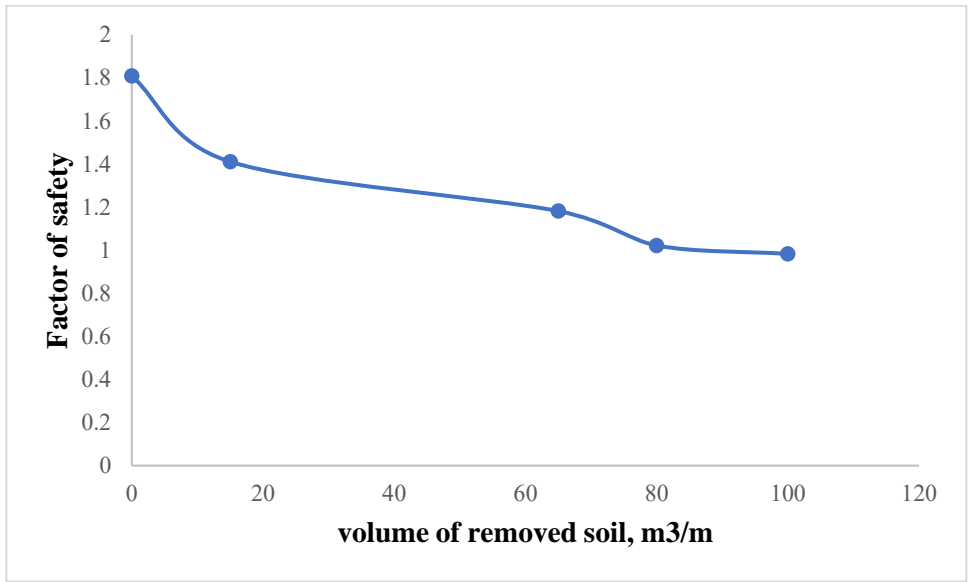
B.1-3 Effect of surcharge load when 30 m3/m width of soil is removed from bank toe.

0.971
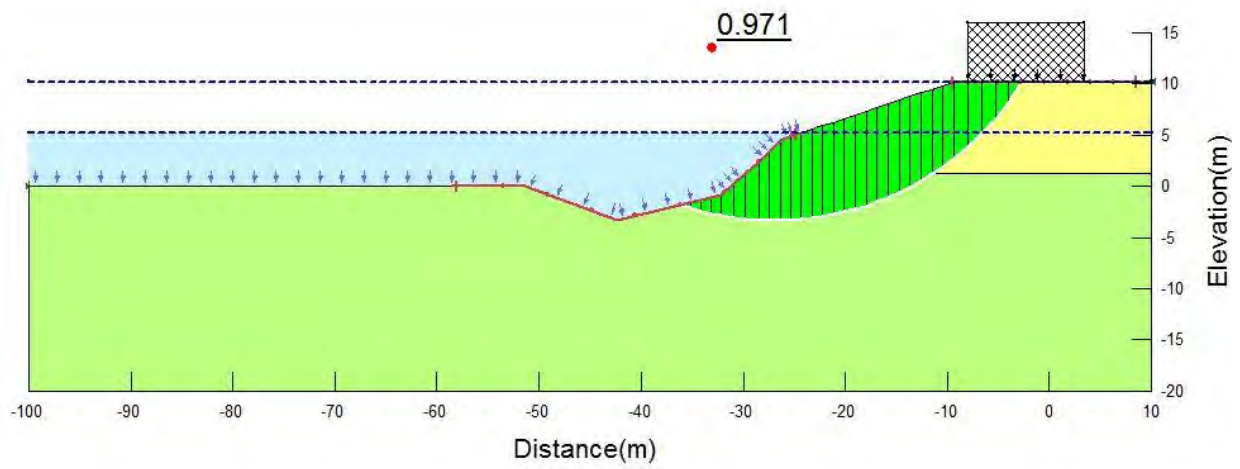
B.1-4 Variation of FOS with surcharge load when scour volume is 30 m3/m width of soil
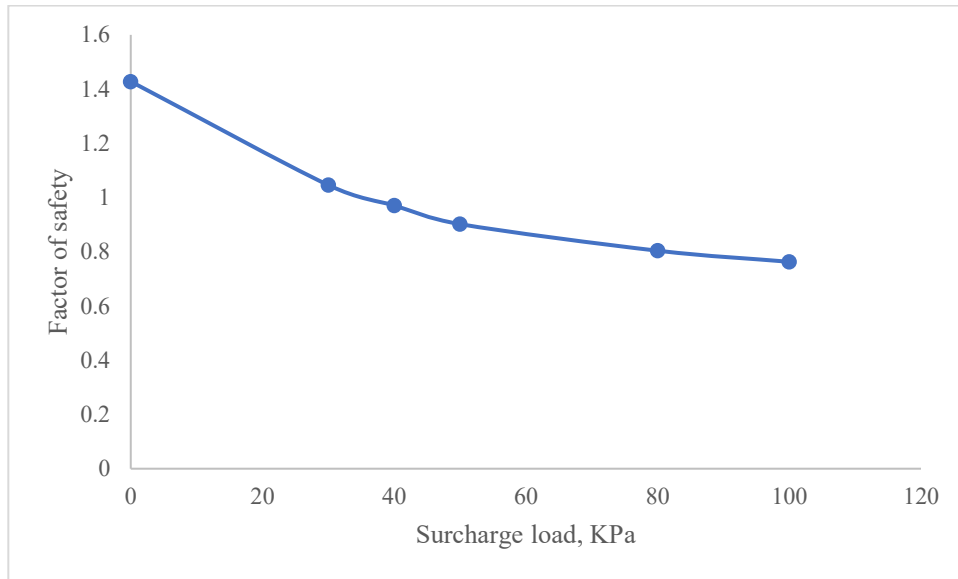
B.1-5 Effect of surcharge load when 60 m3/m width of soil is removed from bank toe
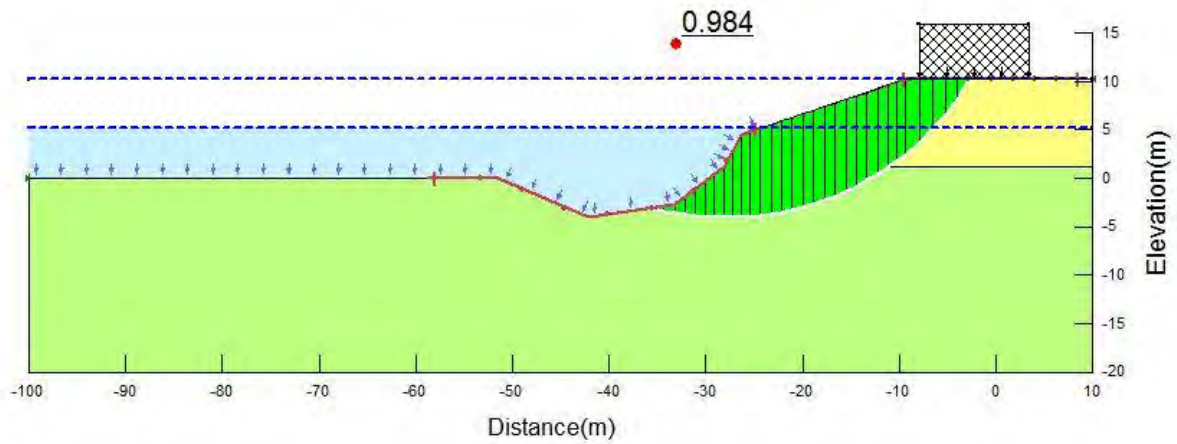
B.1-6 Variation of FOS with surcharge load when scour volume is 60 m3/m width of soil
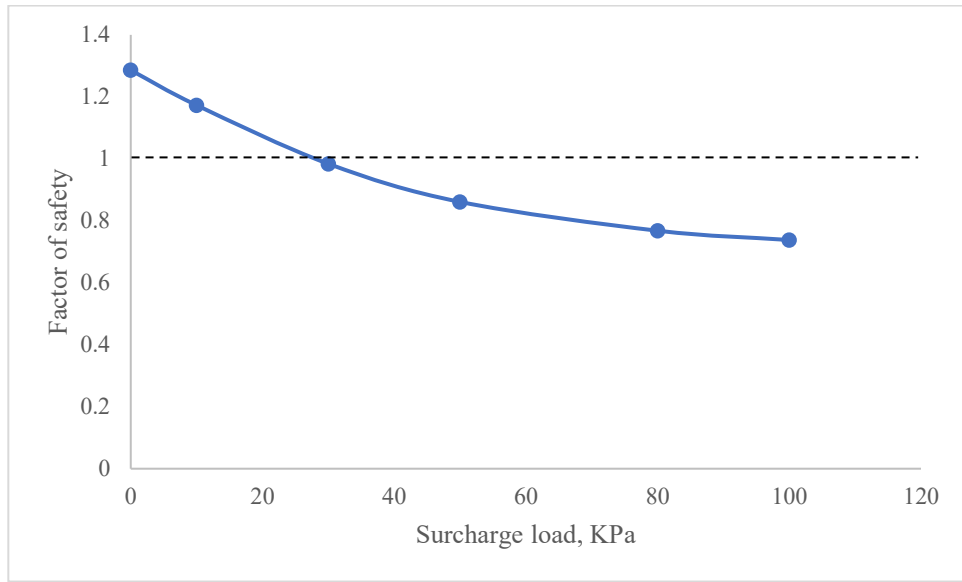
B.1-7 Effect of surcharge load when 100 m3/m width of soil is removed from bank toe
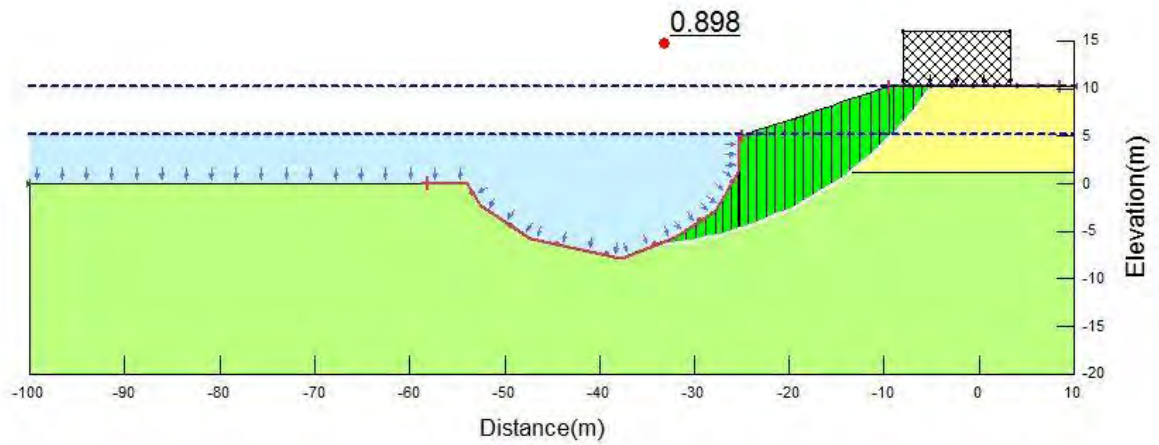
B.1-8 Variation of FOS with surcharge load when scour volume is 100 m3/m width of soil
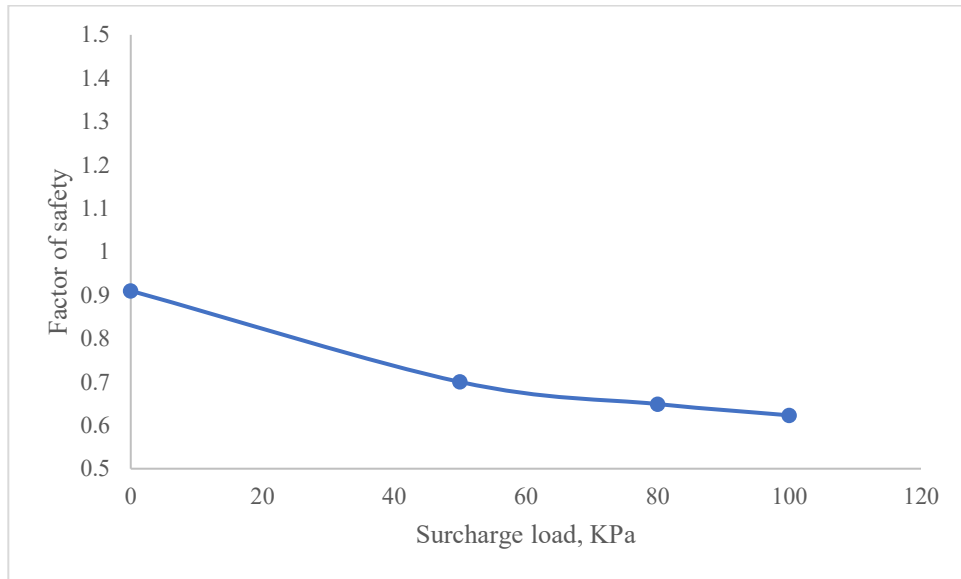
B.1-9 Illustration of slope stability analysis with slope protection load when there is 65 m3/m of soil undercutting at toe.
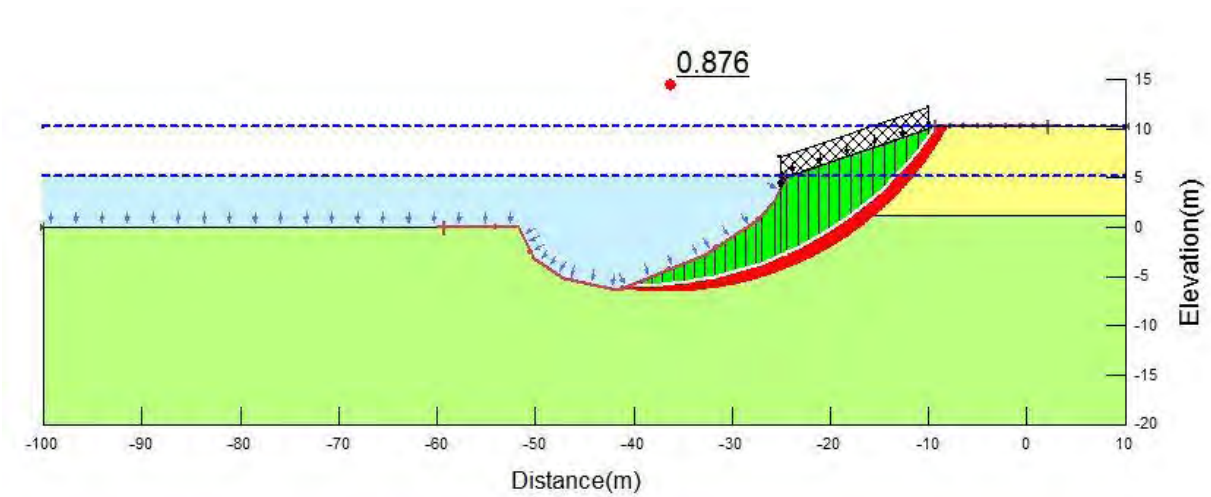
B.1-10 Variation of factor of safety with slope protection load when scoured volume of toe is 65 m3/m width of soil
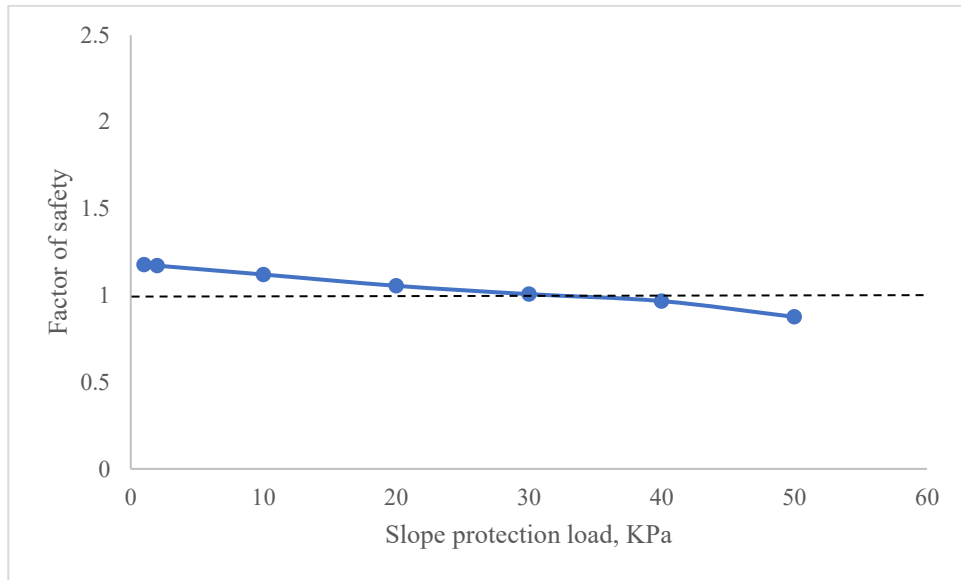
B.1-11 Illustration of slope stability analysis with slope protection load and surcharge load when there is 65 m3/m of soil undercutting at toe.
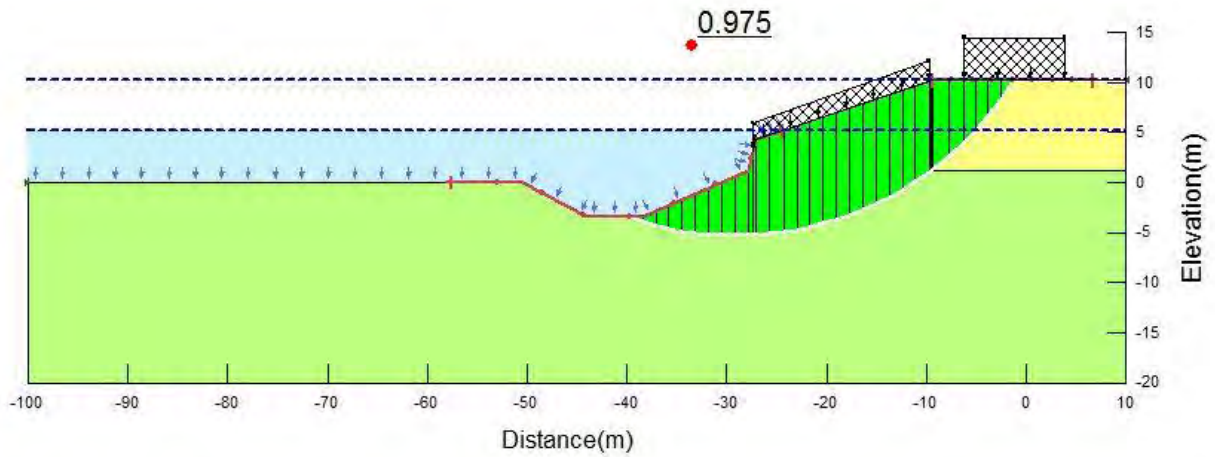
B.1-12 Variation of factor of safety with slope protection load and surcharge load when scoured volume of toe is 65 m3/m width of soil
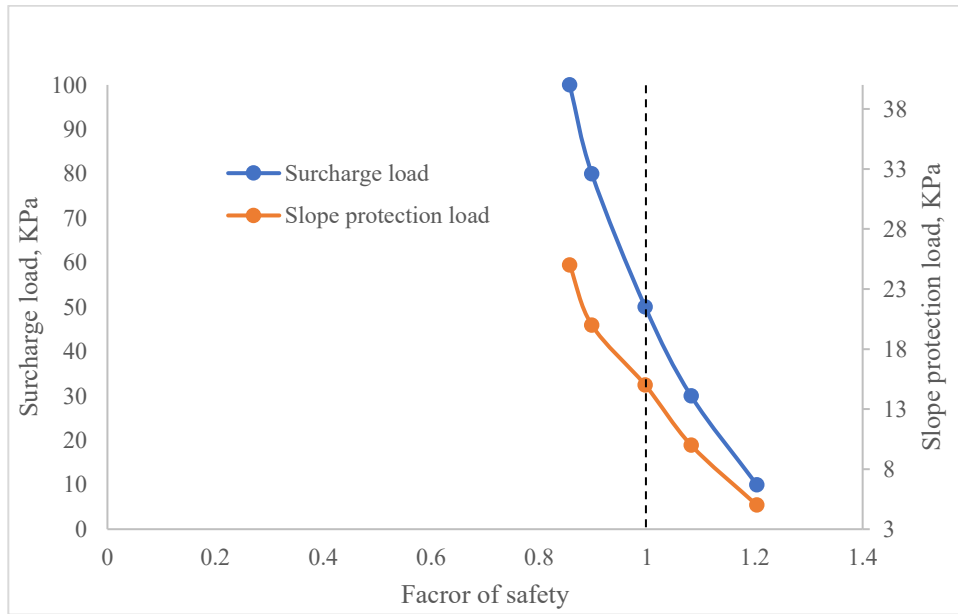
B.1-13 Illustration of slope stability analysis with surcharge load setting clay and mica as top layer
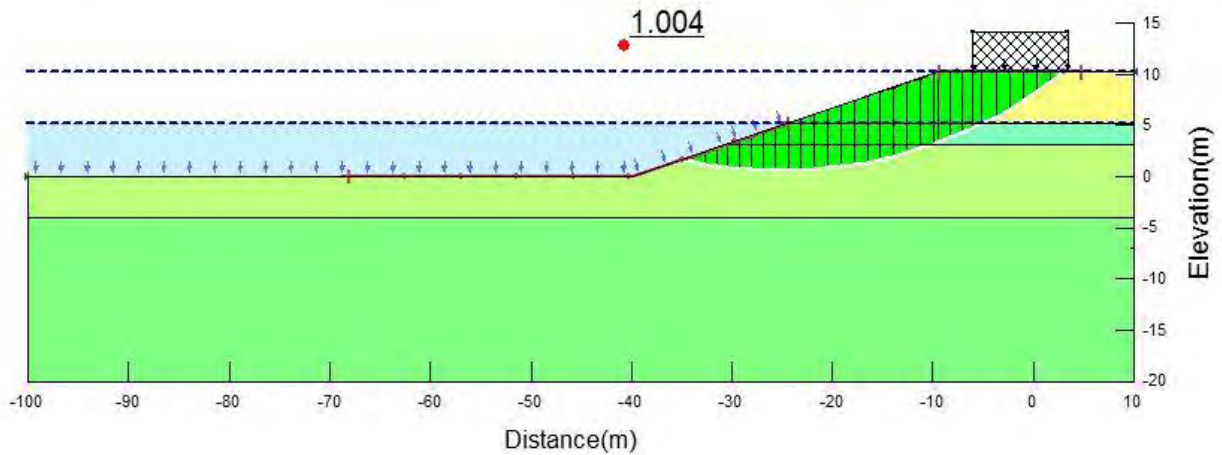
B.1-14 Variation of factor of safety with surcharge load incorporating clay and mica layer
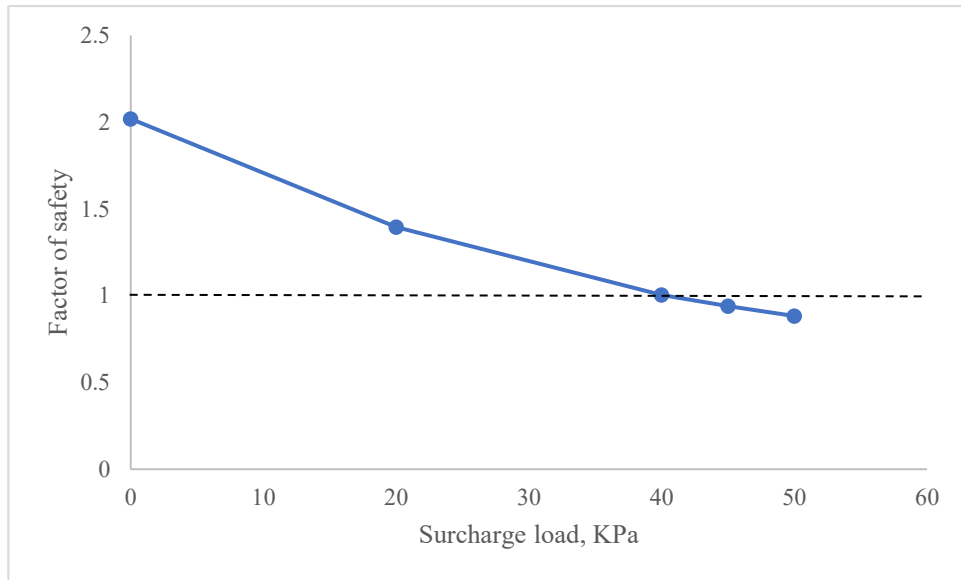
B.1-15 Illustration of slope stability analysis with surcharge load at 7m scour depth incorporating clay and mica as top layer
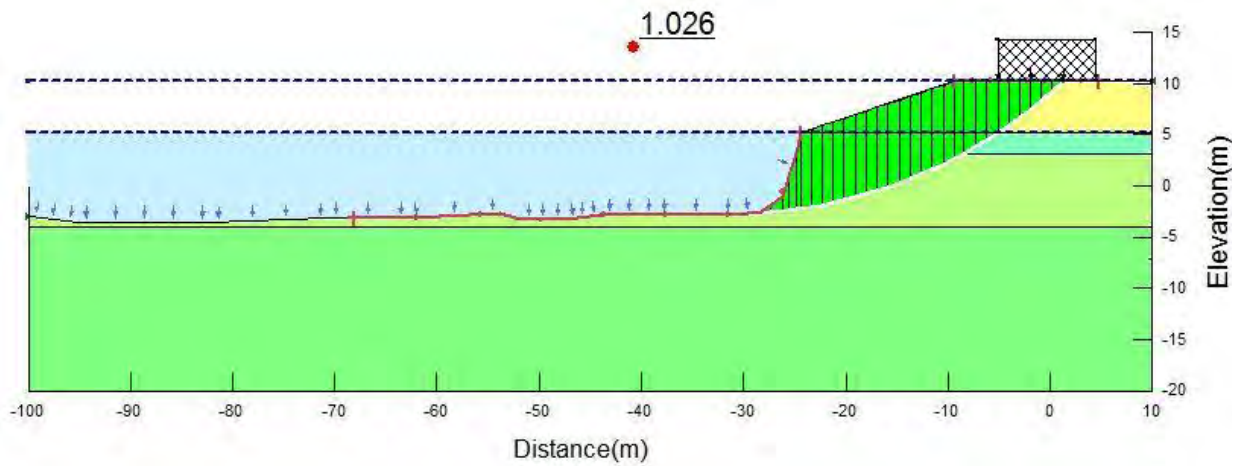
B.1-16 Variation of factor of safety with surcharge load at scour depth of 7m incorporating clay and mica layer
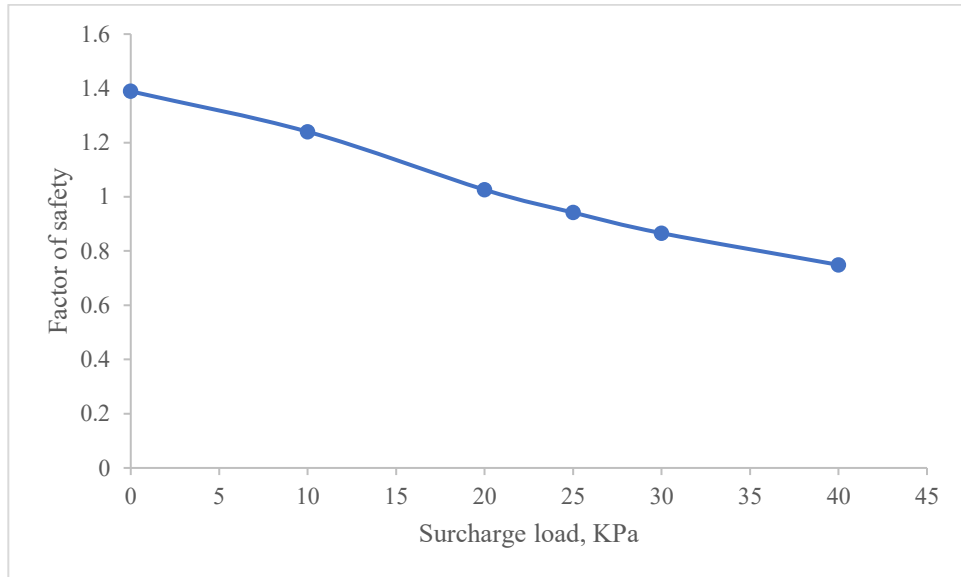
B.1-17 Illustration of slope stability analysis with surcharge load at 10m scour depth incorporating clay and mica as top layer
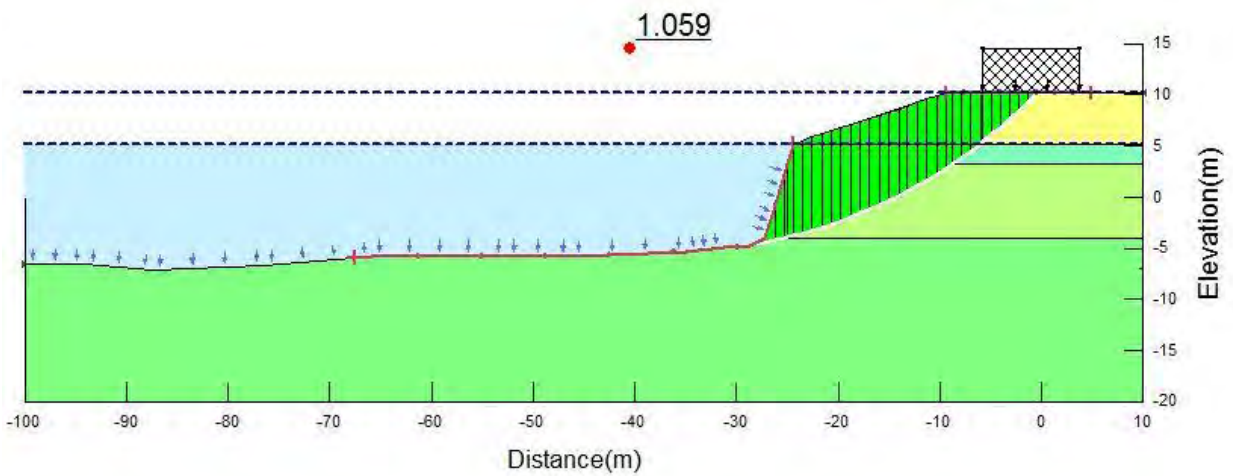
B.1-18 Variation of factor of safety with surcharge load at scour depth of 10m incorporating clay and mica layer
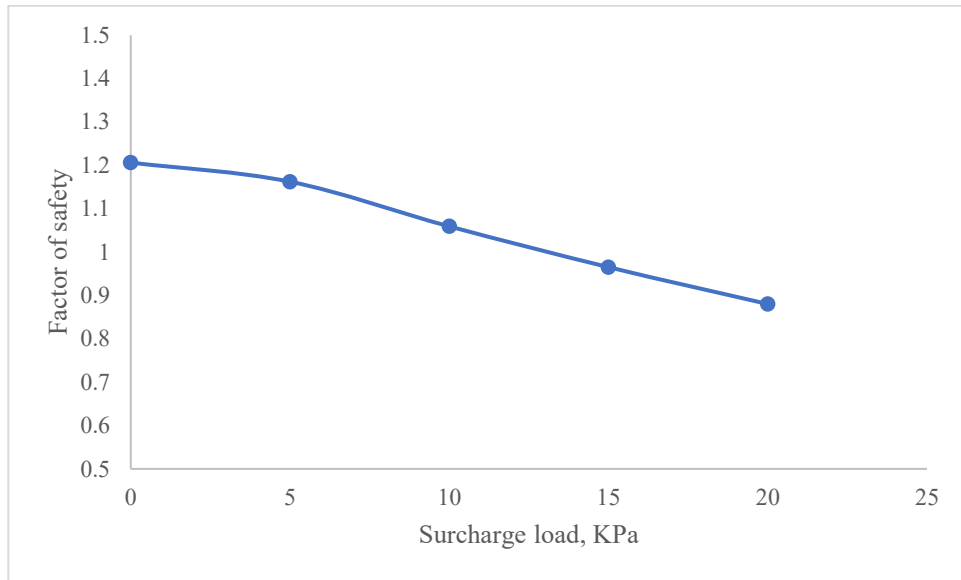
B.1-19 Illustration of slope stability analysis with surcharge load at 15m scour depth incorporating clay and mica as top layer
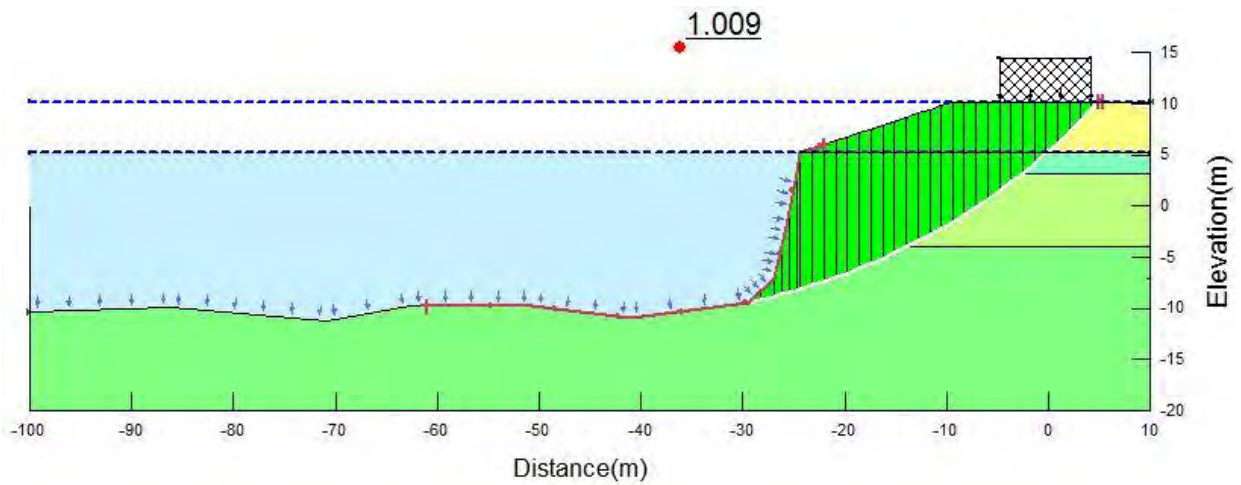
B.1-20 Variation of factor of safety with surcharge load at scour depth of 15m incorporating clay and mica layer
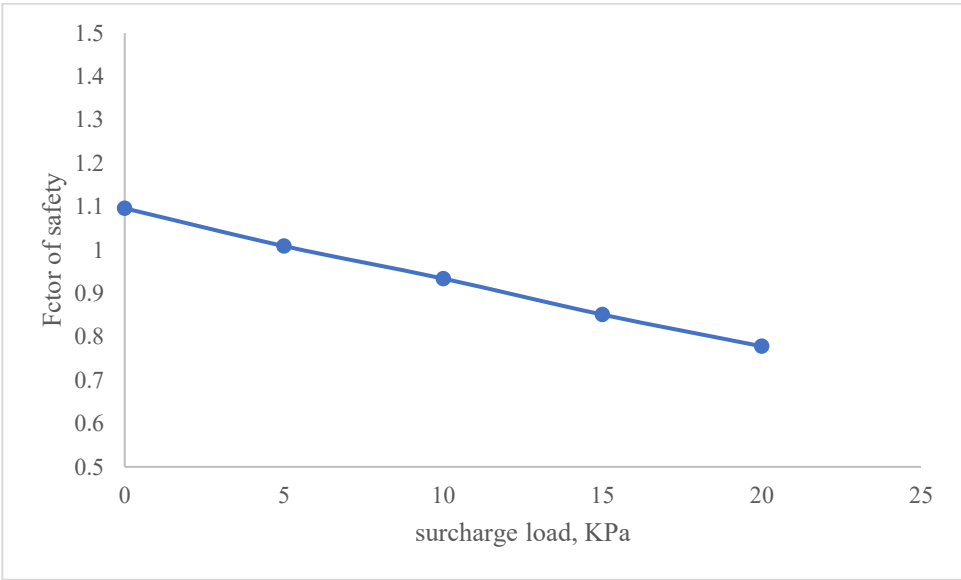
Appendix B.2 : **Finite element method**

B.2-1 Illustration of slope stability analysis with surcharge load.
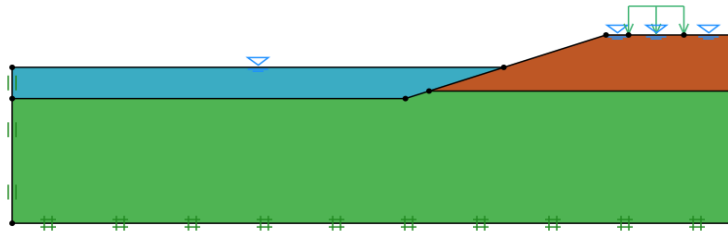
Strength Reduction Factor: 0.9008
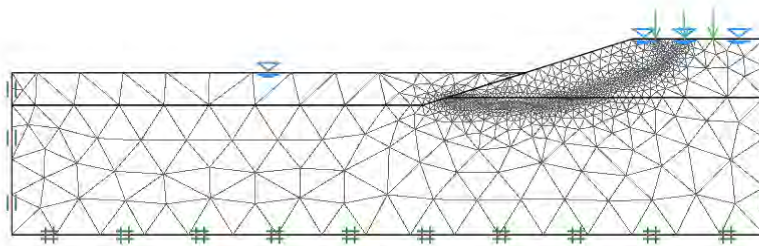
Strength Reduction Factor: 1.336
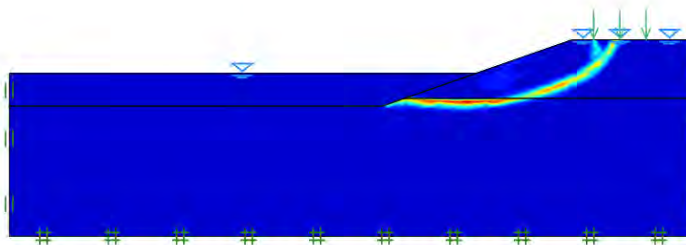
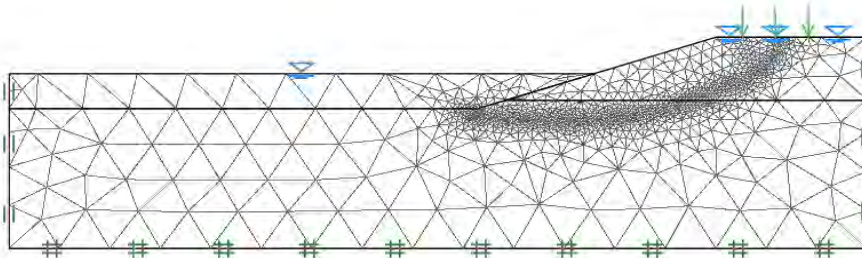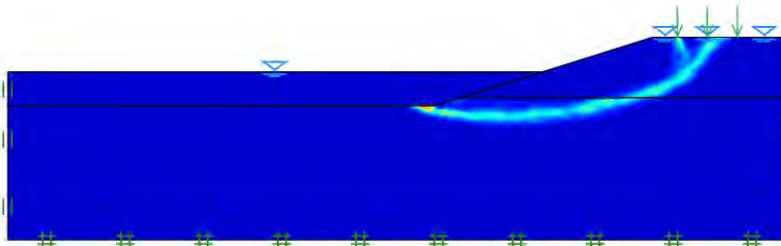Strength Reduction Factor: 1.336

B.2-2 Illustration of slope stability analysis with scoured toe
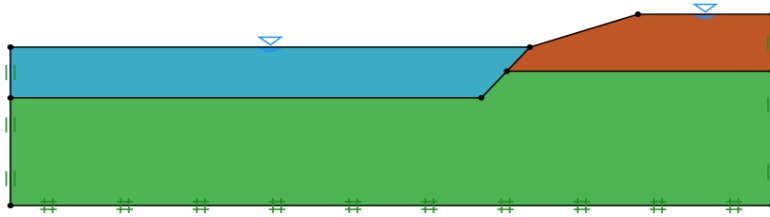
Strength Reduction Factor: 0.9321
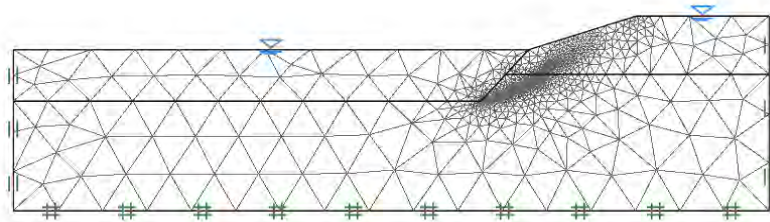
Strength Reduction Factor: 0.9321
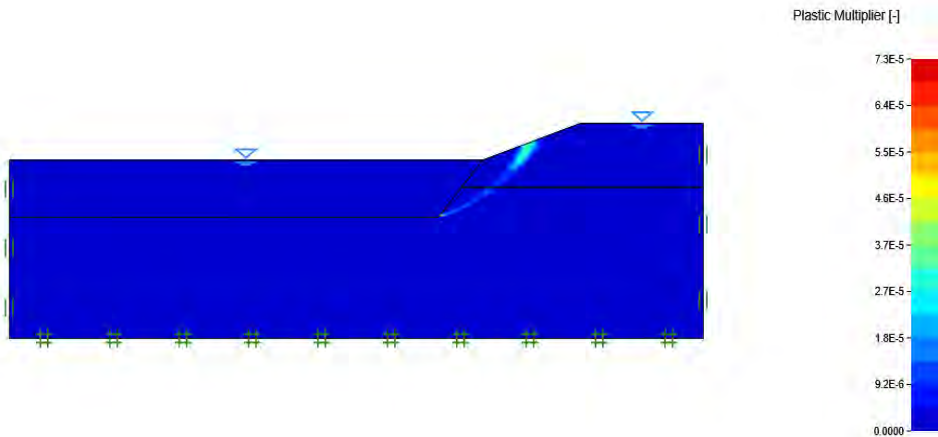
Strength Reduction Factor: 0.9321

B.2-3 Illustration of slope stability analysis with surcharge load and scoured toe.
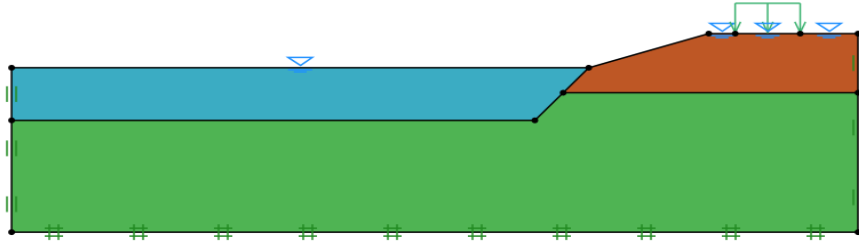
Strength Reduction Factor: 0.9321
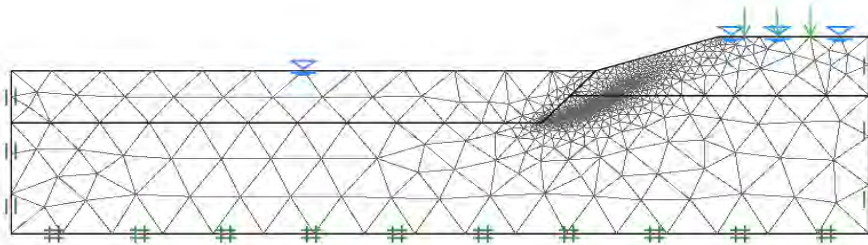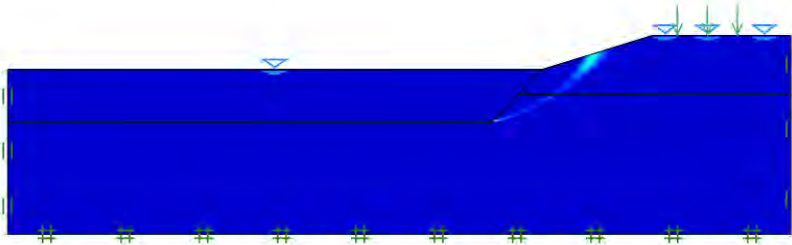
Strength Reduction Factor: 0.9321

Strength Reduction Factor: 0.9321

B.2-4 Illustration of slope stability analysis with slope protection load
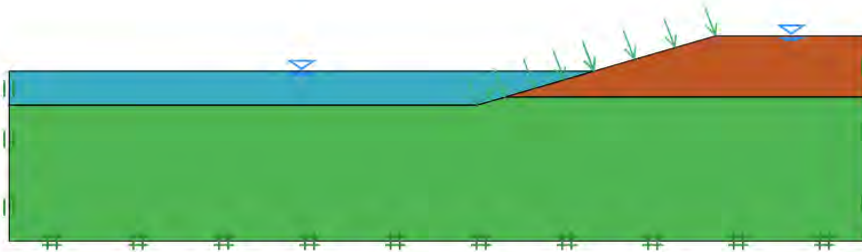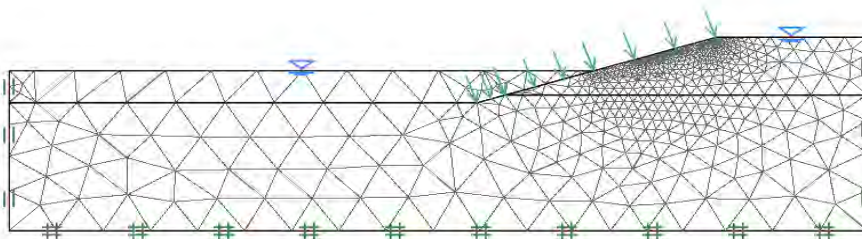
Strength Reduction Factor: 0.8448
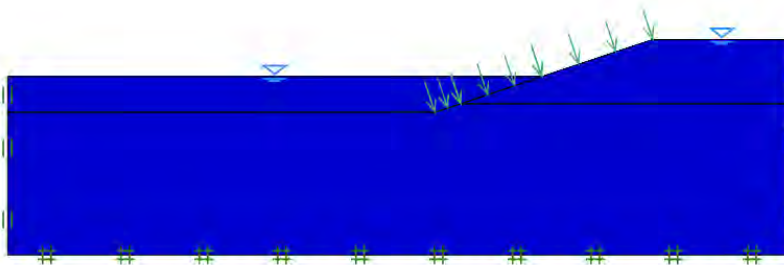
Strength Reduction Factor: 0.8448

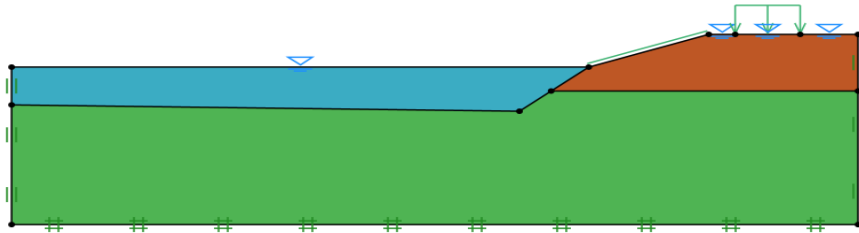Strength Reduction Factor: 0.8448

B.2-5 Illustration of slope stability analysis with surcharge and slope protection load
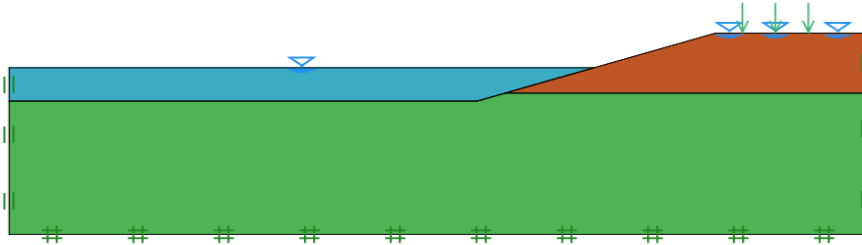
Strength Reduction Factor: 0.8955

Strength Reduction Factor: 1.565

Strength Reduction Factor: 1.565
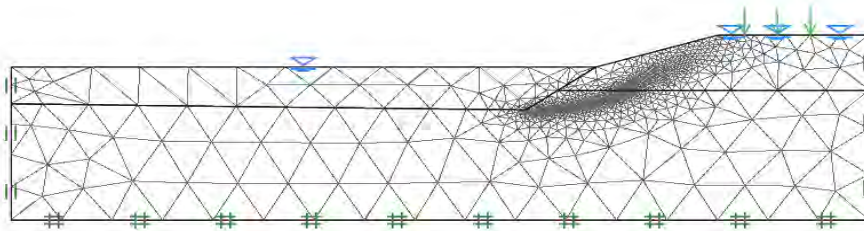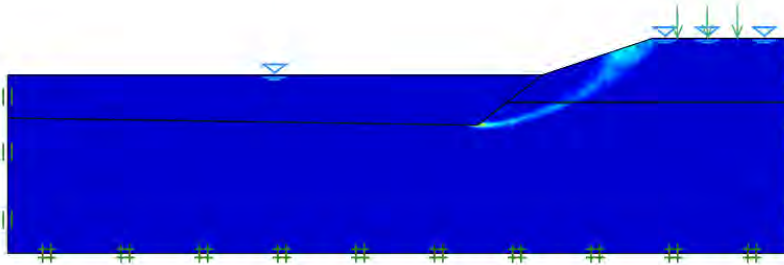
Plastic Multiplier [-]

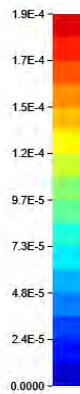B.2-6 Illustration of slope stability analysis with surcharge and slope protection load at 7m scour depth.

Strength Reduction Factor: 1.148

Strength Reduction Factor: 1.148

Strength Reduction Factor: 1.148